University of Southampton

Faculty of Environmental and Life Sciences

School of Geography and Environmental Science

The Morphology of Coastal and Fluvial Flood-Driven Sediment Deposits in Natural and Built Environments

by

Luke Taylor

ORCID ID 0000-0002-2132-4261

https://orcid.org/0000-0002-2132-4261

Thesis for the degree of Doctor of Philosophy

October 2023

University of Southampton

Abstract

Faculty of Environmental and Life Sciences

School of Geography

Doctor of Philosophy

The Morphology of Coastal and Fluvial Flood-Driven Sediment Deposits in Natural and Built Environments

by

Luke Taylor

Extreme flood events are essential for landscape creation, maintenance, and development through the unconsolidated sediment they mobilise and deposit – driving large-scale morphological change. However, hazard-prone coastal and fluvial floodplains offer socio-economically favourable conditions leading to the ubiquity of human presence. When floods extend into these built environments, they can cause widespread damage to infrastructure and pose an immediate threat to human life. Disaster damage costs include expenses associated with removing debris, including vast amounts of sediment, to allow access to stricken communities and permit an appropriate emergency response. To allow suitable disaster management plans to be implemented, there needs to be an increased understanding of sediment routing and deposition in built environments.

Therefore, this research aims to quantitatively investigate flood-driven sediment deposition on natural and built coastal and fluvial floodplains to gain physical insight into their comparative morphometry and explore how such understanding of landscape dynamics may inform risk assessment and management. It achieves this by 1) constructing morphometric scaling relationships for real-world coastal deposits, in natural and built settings, after hurricane strikes in the US, 2) using CAESAR-Lisflood to assess natural controls on fluvial deposits, 3) investigating the impact of built environments on fluvial deposits in CAESAR-Lisflood, 4) synthesising this data, combined with examples from external literature.

Storm size, grain size, and floodplain roughness impart a first-order control on deposit morphology. However, the built environment significantly impacts deposit shape and size, pertinent as many morphological landscapes depend on sediment delivery. Importantly, volume and area scale consistently regardless of the density of the built environment. The ability to derive the 3D properties from 2D metrics could help predict disaster impacts and facilitate the efficient clean-up of debris post-flood. Nevertheless, the scaling relationships depict a snapshot of deposit morphometrics, providing information concerning their morphology at one point in time, rather than the underlying dynamics of how they are formed. Consequently, future work could investigate the impact of built obstacles on flow dynamics by tracking the disturbance imparted by built environments on flow velocities and directions – and the impacts on sediment deposition. Finally, trusting models to accurately predict real-world conditions is critical. Here, CAESAR-Lisflood is quantitatively validated in its creation of deposits. Technological advances will only enable model representations of morphological systems to become more accurate and detailed – with the capability to aid policymakers and engineers in disaster impact mitigation.

Table of Contents

Table of Tables

Table of Figures

Research Thesis: Declaration of Authorship

Print name: LUKE TAYLOR

Title of thesis: The Morphology of Coastal and Fluvial Flood-Driven Sediment Deposits in Natural and Built Environments

I declare that this thesis and the work presented in it are my own and has been generated by me as the result of my own original research.

I confirm that:

1. This work was done wholly or mainly while in candidature for a research degree at this University;
2. Where any part of this thesis has previously been submitted for a degree or any other qualification at this University or any other institution, this has been clearly stated;
3. Where I have consulted the published work of others, this is always clearly attributed;
4. Where I have quoted from the work of others, the source is always given. With the exception of such quotations, this thesis is entirely my own work;
5. I have acknowledged all main sources of help;
6. Where the thesis is based on work done by myself jointly with others, I have made clear exactly what was done by others and what I have contributed myself;
7. Parts of this work have been published as:-

The results presented in chapter 3 "Comparing hurricane-induced deposit morphology in natural and built coastal environments" have been published in: Lazarus, E. D., Goldstein, E. B., **Taylor, L. A**. (**LAT**), & Williams, H. E. (2021). Comparing patterns of hurricane washover into built and unbuilt environments. *Earth's Future*, 9(3), e2020EF001818.

The work presented in chapter 3 is based on the data authored by LAT (see link below), and is written independent of the paper above. Data can be found here: **Taylor, Luke (LAT)**; Williams, Hannah; Goldstein, Evan; Lazarus, Eli (2021): Data for 'Comparing patterns of hurricane washover into built and unbuilt environments'. figshare. Dataset. https://doi.org/10.6084/m9.figshare.12608828.v1

Signature: .....Date:

Acknowledgements

Firstly, I would like to thank my supervisor, Dr Eli Lazarus, who besides providing the foundations and opportunity for me to undertake this PhD, has offered his guidance, steadfast enthusiasm and support, throughout the process. Thank you for helping sculpt the direction of this project and helping me develop my skills as a researcher. I would also like to thank the broader staff in the department, particularly, Dr Andrew Phillips, who has been a source of moral support since beginning my MSc in 2017, with his door always open.

A thank you should also be extended to the Leverhulme Trust for the funding that allowed this research to be undertaken (Grant Number: RPG-2018-282).

I am also thankful to have been able to spend the past four years within such a close-knit cohort of fellow researchers and friends who, despite the pandemic, have made the PhD process enjoyable through their moral support, humour, and weekly supply of cake on Fridays. These include and are not limited to: Laurence, Martin, Nathaniel, Rebecca, and Charlotte. A special mention goes to Chris Tomsett, who has been accessible at the drop of a hat to offer support, advice, and reassurance particularly over the final countdown towards thesis submission.

A massive thank you to my parents for their continual support and unwavering encouragement. The company of you, Oliver, and Rame, was a massive factor in remaining productive, and somewhat upbeat, during the pandemic, despite the PhD experience being so different to what was expected.

Finally, a big thank you to my best friend, Katherine, you have never ceased to make me smile, and laugh, even when we were limited to beach and park walks during lockdowns. Your endless encouragement has kept my spirits up and given me the momentum needed in times when I was struggling.

Definitions and Abbreviations

NOAA .....National Oceanic and Atmospheric Administration

OSM.....Open Street Maps

GIS .....Geographic Information System

P_m.....Measured Perimeter

P_i .....Ideal Perimeter

A_m .....Measured Area

DI .....Distortion Index

VIF .....Variance Inflation Factor

LEM.....Landscape Evolution Model

CAESAR.....The Cellular Automation Evolutionary Slope and River Model

LiDAR .....Light Detecting and Ranging

DTM .....Digital Terrain Model

Chapter 1 Introduction

The geomorphological processes of erosion, transportation, and deposition are vital in producing unconsolidated sediment and facilitating its circulation into landscapes (Blum and Roberts, 2009; Johnson *et al.*, 2009; Nickling and Neuman, 2009; Jackson and Nordstrom, 2011; Manh *et al.*, 2014). Sediment influx and movement are critical for the creation, upkeep, and development of morphological landscapes and the landforms within them and for enhancing biodiversity through enriching soils with nutrients (Heiler *et al.*, 1995).

Extreme flow-driven events, including floods, landslides, storms, and volcanic eruptions, can redistribute large volumes of sediment across landscapes (Korup, 2012). Such high-energy events can increase sediment availability in a morphological domain by instigating high rates of erosion (González-Hidalgo *et al.*, 2009; Bookhagen, 2010; Shi *et al.*, 2012) and transporting material through landscapes to be deposited elsewhere once energy levels dissipate (Lin *et al.*, 2008; Korup, 2012; Ralston *et al.*, 2013). For example, earthquakes and storms can induce landslides - vastly increasing sediment availability at affected sites (Koi *et al.*, 2008; Chuang *et al.*, 2009). Meanwhile, volcanic eruptions can produce pyroclastic flows, creating large, easily erodible deposits (Fisher, 1979; Houghton and Carey, 2015). In all these extreme scenarios, transport of the unconsolidated material to other parts of the landscape typically occurs through surface runoff, which can move the sediment into the fluvial network (Dadson *et al.*, 2004; Korup, 2012). Consequently, extreme events are morphologically essential for landscape development and maintenance, enabling the widespread mobilisation and deposition of sediment.

The research presented in this thesis examines the morphology of flood-driven sediment deposits extending onto coastal and fluvial floodplains in natural and built environments. To do this, it will examine the size and shape of washover deposits in coastal landscapes and crevasse splays in the fluvial domain. Floods, both coastal and fluvial, are likely to continue to rise in intensity and frequency because of global climate change (Lim, 2022), coupled with the urbanisation of hazard-prone low-lying floodplains (Monk *et al.*, 2019; Andreadis *et al.*, 2022). Therefore the impacts of such extreme events on high-risk landscapes must be well understood (Donnelly *et al.*, 2006; Tahvildari and Castrucci, 2021).

1.1 Flooding as a driver of geomorphic change

Flooding can be defined as the overflowing of the usual confines of a stream or other body of water, such as lakes and oceans, or the accumulation of water over areas that are generally not

submerged (Douben and Ratnayake, 2005; Field *et a*l., 2012). Fluvial floods usually occur during and after rainfall or snowmelt events – whereby the influx of water to a channel leads to the breaching of its banks and overland flow (O'Connor and Costa, 2004; Douben, 2006). Meanwhile, coastal floods are caused by water surges onto low-lying coastlines instigated by storms or strong tides (Holden, 2012; Little *et al.*, 2015). Indeed, near sea level, fluvial flooding can be concurrent with storm surges and extreme tides (Brakenridge *et al.*, 2013). Severe floods, initiated by intense storms and hurricanes, are the most devastating in terms of damage caused (Xian *et al.,* 2015) and total morphological change (Suter *et al.*, 1982; Wernette *et al.*, 2020). Aside from the power of the event itself, floods are controlled by factors such as land use, the density of drainage networks, and the characteristics of the affected catchment, i.e. shape, size and slope (Rudorff *et al.,* 2014; Zope *et al.,* 2016).

Floods are the most devastating and frequent natural disaster impacting human communities, with over 3000 extreme flood events registered in the Emergency Event Database between 1990 and 2010 (Wang *et al.*, 2011) - affecting approximately three billion people (Smith, 2013). The UNDRR (2020) estimate that between 2000 and 2019 floods caused $650 billion worth of damages worldwide. In 2016 alone, flooding triggered a global economic cost of approximately $56 billion (Wing *et al.*, 2018). These damages accrue from the destructive effect floods can have on built infrastructure, i.e. buildings, roads and bridges, and harming agriculture. As a result, floods significantly hinder the sustainable development of communities through the damage costs incurred and the impact on human life (Di Baldassarre *et al.*, 2013, Hallegatte *et al.,* 2017).

Looking to the future, a rise in flood risk by a combination of climate change (Purvis *et al.*, 2008; Bouwer and Jonkman, 2018) and socioeconomic factors (McGranahan *et al.,* 2007; Best, 2019) will increase damages and the number of people affected. By 2070 in 136 coastal cities, the population exposed to flood events is expected to increase by more than threefold, alongside economic asset exposure rising by up to tenfold (Hanson *et al.*, 2011). Furthermore, it has been suggested by Jongman *et al.* (2012) that based on population factors, economic exposure will rise from $46 trillion in 2010 to $158 trillion by 2050. Finally, under a 1.5°C rise in global temperatures, floods will affect approximately 100% more people and increase damage costs by around 120% (Best, 2019). In a stark warning - Hirabayashi *et al.* (2013) imply that without management action, total flood damages could rise by up to a factor of 20. Therefore, the impacts of flood events must be well-understood to enable effective management and recovery plans to be put in place.

1.2 Flood-driven deposition

1.2.1 Deposits in coastal and fluvial environments

Floodwaters can transport copious quantities of sediment into the affected landscapes. As the flood flows move across a floodplain, its energy dissipates, which causes the entrained material to be deposited when the transport capacity is exceeded. In the coastal domain, these post-flood relics are termed washover deposits (Morton and Sallenger, 2003; Donnelly *et al.*, 2006). Meanwhile, crevasse splays are depositional landforms produced during fluvial floods when levee breaches occur (Nienhuis *et al.,* 2018). Past work has described these two types of deposits in both coastal and fluvial landscapes as fan-like in shape (Donnelly *et al.*, 2006; Lazarus, 2016; Yuill *et al.*, 2016) - produced as the floodwater moves across a relatively unconfined terrain (Iacobucci *et al.*, 2020). However, these two depositional landforms differ in the initial transport processes that instigate landform creation. Washover typically forms when storm surges overtop a foredune (Nienhuis *et al.,* 2018), whereas, crevasse splays develop following levee breaches (natural/artificial) - instigated during periods of peak discharge in the initial flooding phase (Farrell, 2001; Toonen *et al.*, 2016). As such, washover formation is characterised by a broad overtopping of water, whilst the flood flow is more concentrated through levee breaches to create splays.

Despite this, once the initial processes have occurred and the floodwater/storm surges propagate into relatively flat floodplains, the formation of both landforms rely on similar fluid dynamics and the associated sediment transport processes – that heavily depend on the energy of floodwaters, and as such, the depositional processes are similar. As well as this, it is well-documented that the storm size, grain size, density and presence of vegetation, and landscape topography influence the morphology of deposits in both environments (Donnelly *et al.*, 2006; Matias *et al.*, 2016; Millard *et al.*, 2017). Therefore, there is a solid basis for the deposits being morphologically alike. Suppose the flood-driven sediment deposits formed in both settings can be shown to be similar in their morphology? In that case, it could provide a platform to investigate their controls in tandem, with both washover and crevasse splays being vital components within their respective floodplains.

From morphological and ecological standpoints, the importance of flood-driven sediment deposition in the natural environment is tied to the landscape's creation, development, and upkeep. For example, barrier islands can act as protection systems for coastal communities, as well as back-barrier ecosystems, which usually encompass high-value ecosystem services (Plomaritis *et al.*, 2018). Such locations rely on the repetitive sediment supply from storm surges

to sustain their height and width relative to sea level (Fitzgerald *et al.*, 2008; McCall *et al.*, 2010). Consequently, the consistent input of flood-driven sediment keeps the sediment budget of these low-lying coastlines in a dynamic equilibrium – supporting them against the threat of sea level rise (Rodriguez *et al.*, 2020). Indeed, sediment supply to fluvial floodplains plays a similar role. Fluvial flooding which instigates crevasse splay formation works to construct and regulate the elevation of floodplains (Croke *et al.,* 2013) and contribute to their evolution – controlling the creation of hillslopes, alluvial fans, and other landforms (Walling and He, 1998; Bridge, 2003).

Extreme flood events, in both coastal and fluvial settings, are vital for the ecology and productivity of these morphological landscapesas they act as vectors of nutrients and sediment. For example, coastal storm surges deliver saltwater and sediment to low-lying shorelines, crucial for the conception and upkeep of salt marshes and dune habitats – rich, biodiverse ecosystems (Seavey *et al.,* 2011; Taylor *et al.*, 2016; Goldstein and Moore, 2016). In addition, by reducing the quantity and density of sand-trapping vegetation, washover deposits increase the potential for aeolian transport across a barrier system – promoting the formation of dune fields. Also, heavy rainfall events allow fluvial floodplains to benefit from an influx of chemicals as the higher amounts of sedimentation during these extreme events positively correlate with higher quantities of organic carbon, nitrogen, and phosphorus – promoting richer biodiversity and increased vegetation growth (Baldwin and Mitchell, 2000; Steiger and Gurnell, 2003; Olde Venterink *et al.*, 2006).

1.2.2 Deposits in natural and built environments

The morphology of sediment deposits formed from extreme events is typically investigated in natural systems with minimal human presence or infrastructure, in order to minimise confounding factors that may confuse traditional theories of sediment transport. Deposits in natural settings have been studied extensively. The effect of topography and sediment size on landslide deposit morphology has been quantified using models and LiDAR (Light Detection and Ranging) (Glenn *et al.*, 2006; Frattini and Crosta, 2013). Moreover, deposits from fluvial floods have been measured (Millard *et al.,* 2017; Nienhuis *et al.,* 2018), with studies also exploring deposit morphology in natural coastal environments (Donnelly *et al.,* 2006; Donnelly *et al.,* 2009).

A key caveat to this line of research is that human domination of previously natural environments means undeveloped low-lying floodplains are rare (Foley *et al.*, 2005; Venter *et al.*, 2016). Coastal and fluvial floodplains offer favourable socio-economic development conditions, such as access to trade routes, improved agricultural productivity, guaranteed water supply, and fishing opportunities (De Stefano *et al.*, 2017; Viero *et al.*, 2019). Consequently, human presence

on low-lying floodplains is ubiquitous. Quantitatively, over 50% of the world's population lives within 3km of freshwater (Fang *et al.*, 2021), whilst over 1.4 million people inhabit barrier islands along the US Atlantic and Gulf coasts (Zhang and Leatherman, 2011).

Encompassed in the global disaster damage costs are outlays focussed on removing debris from built settings post-storm – which can include vast deposits of sediment ranging from hundreds of thousands to millions of m^3 (Brown *et al.,* 2011; Periathamby *et al.,* 2012; Lazarus and Goldstein, 2019; Montreuil *et al.*, 2020). During the immediate aftermath of these events, disaster-induced debris can block roads preventing access to emergency services and external support, causing challenges for public officials (Kobayashi, 1995; USEPA, 2008). Moreover, the clean-up of this sediment can be time-consuming and expensive (FEMA, 2007). Subsequently, to reduce damage costs associated with extreme events, it is vital to predict disaster impacts and prepare populations (Smith, 2013). Predicting the effects of floods requires knowledge and understanding of their physical consequences from measurement and modelling (Klemas, 2009; Huang *et al.,* 2021).

However, researching the sedimentary consequences of floods in the built environment can prove troublesome. Rapid clearance of debris from streets and roads to facilitate emergency response and recovery means the deposits tend to go uncaptured (Lazarus and Goldstein, 2019). Nevertheless, a growing body of research investigates how sediment deposition during extreme events interact with natural and built settings in fundamentally diverse ways. Presently, most of the work is more qualitative than quantitative and is from a range of morphological fields, including volcanic eruptions (Gurioli *et al.*, 2005; Doronzo and Dellino, 2011), landslides (Papathoma-Köhle *et al.*, 2017), tsunamis (Bricker *et al.*, 2015), and fluvial and coastal floods (Nelson and Leclair, 2006; Rogers *et al.*, 2015; Lazarus *et al.*, 2022). Indeed, it can also be thematically related to atmospheric research concerning air flows over and between buildings (Britter and Hanna, 2003). These studies have highlighted how built infrastructure can cause dispersion and turbulence in flows – which are absent in natural environments. As quantitative data concerning the makeup of built environments becomes more available, the ability to research their impact on morphological features becomes easier (Mayer-Schönberger & Cukier, 2013).

Thus far, Nelson and Leclair (2006) have undertaken the lone study into flood-driven sediment deposits entering built fluvial environments. Their study focussed on a large sandy crevasse splay deposit formed during Hurricane Katrina after a levee failure, with the resultant deposit covering approximately 54,670 m^2 (schematically shown in Figure 1-2, panel D). They qualitatively highlighted that the local street network and the layout of the built infrastructure

controlled the spatial spread of the deposit and its ensuing geometry. Their investigation suggests that channelisation of the flow and sediment down open streets was evident – with the impervious surfaces providing efficient pathways, whilst high-velocity zones were created between buildings.

An important paper by Nordstrom (1994) indicates that coastal landscapes are continuously and rapidly being altered to suit anthropogenic needs, ranging from the destruction of stabilising vegetation to the construction of buildings and roads. From this, he suggests that the presence of built environments on previously natural land disturb the historic sediment flux in the area by changing the ability for sediment to be transported unhampered, and shifting the locations of sediment sources and sinks. Such a change in sediment budgets indicates that the long-term future of low-lying barrier islands is in doubt as the repetitive influx of sediment into the landscape could be altered – pointing towards barrier drowning (Rogers *et al.*, 2015). Furthermore, this effect on the sediment budget can have knock-on impacts on nearby undeveloped areas – by instigating faster erosion and changing sediment availability. Consequently, landscapes transformed by human activity, whether it be roads, buildings, or even flood defences such as sea walls and groynes (Nordstrom, 1994), represent distinct depositional systems to the natural environment. Therefore, it can be deduced that results obtained from geomorphic research of extreme flow events impacting natural environments are not representative of extreme events affecting built-up areas. The effect of human activity highlights the need for an increased understanding of sediment routing in anthropogenically-developed settings to allow appropriate disaster management plans to be put in place. Thus, developing knowledge of the morphology of flood deposits in different depositional environments would represent a step towards understanding disaster impacts and risk whilst allowing preparation for disaster response.

1.2.3 Four depositional contexts

This thesis will study four distinct depositional environments derived from the outlines above. These are defined as coastal and fluvial floodplains – split into natural and built settings – as shown in Figure 1-1. The research will quantitatively assess the morphometrics of flood-driven sediment deposits (washover and crevasse splays) produced in these four settings, comparing coastal and fluvial deposits, natural and built.

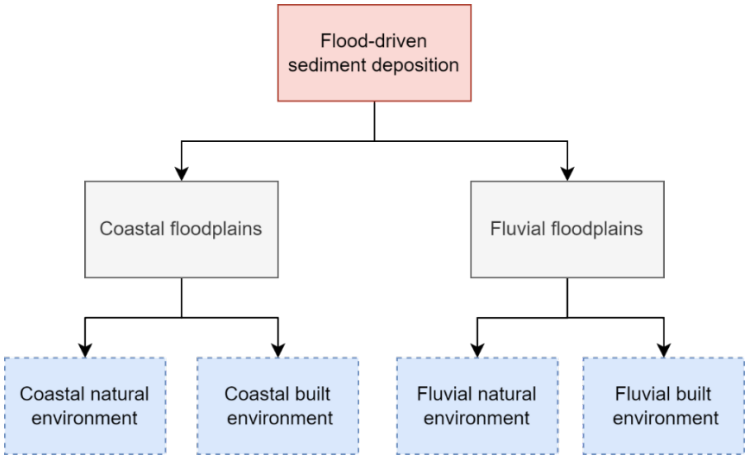

Figure 1-1 A schematic diagram comprising the four depositional environments to be investigated within this thesis: natural and built coastal and fluvial floodplains.

In addition, Figure 1-2 illustrates examples of flood-driven sediment deposition in each of the four environments. As can be seen, the natural examples in panels A (coastal – washover) and C (fluvial – crevasse splays) are semi-circular-like fans – and bear a resemblance to one another. In contrast, the built examples in panels B (coastal) and D (fluvial) show immediate distortion from the natural norms – with the flood-driven sediment deposits branching around buildings and channelling down streets (Nelson and Leclair, 2006).

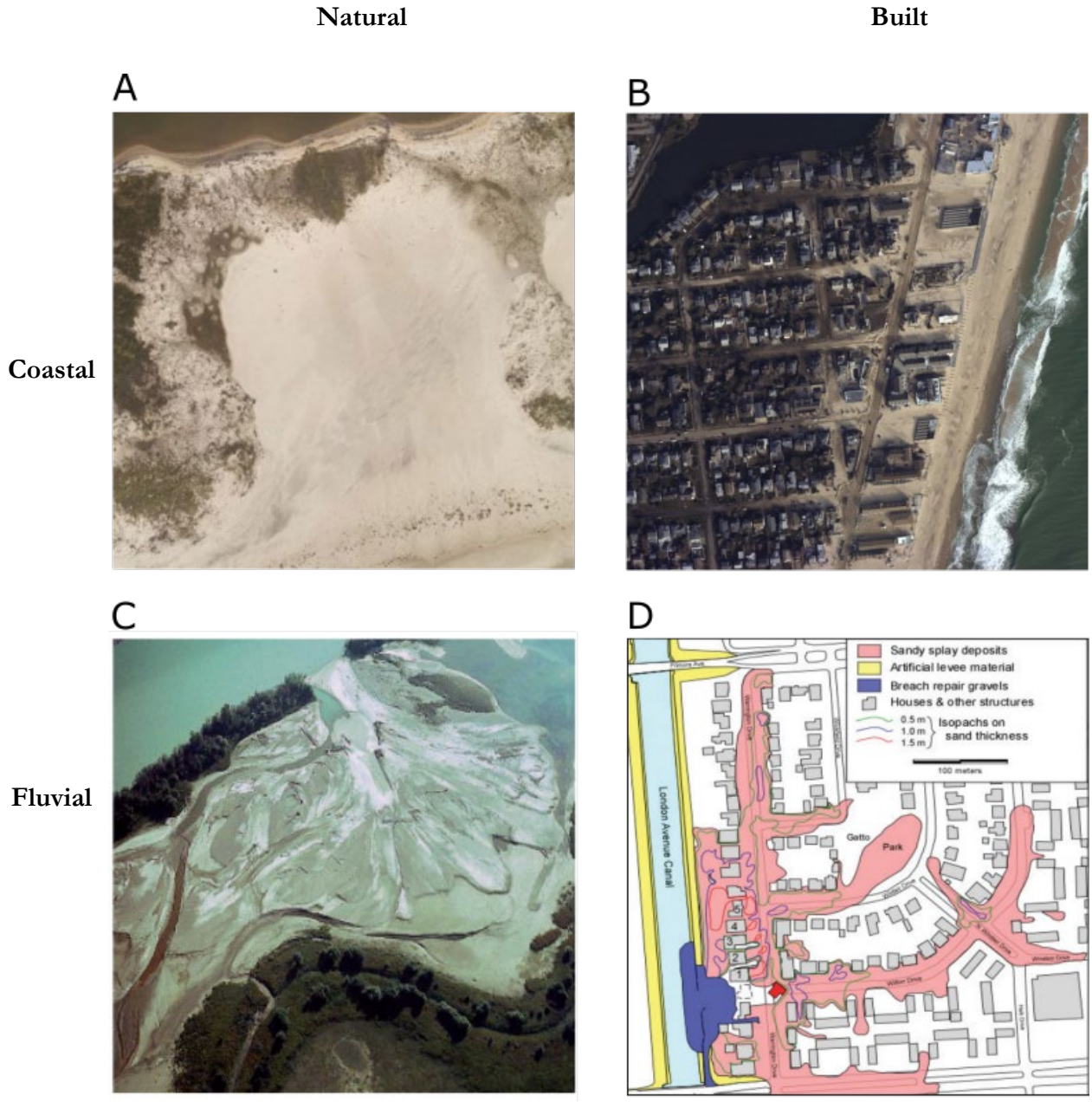

Figure 1-2 Examples of flood-driven sediment deposits in four environments. A) natural coasts (Hurricane Nate 2017, provided by NOAA), 2), B) built coasts (Hurricane Sandy, 2012, provided by NOAA), C) natural fluvial (van Dinter and van Zijverden, 2010) and D) built fluvial (Nelson and Leclair, 2006).

1.3 Morphometric scaling relationships

An appropriate methodology was sought to facilitate a quantitative comparison between the morphology of flood-driven sediment deposits in the four defined landscape environments. Therefore, scaling relationships will be constructed based on the morphometric attributes of a broad sample of the sediment landforms in each depositional environment.

Morphometric scaling relationships are formalised expressions defining consistent mathematical relationships between geometric attributes of morphological features (Dodds and Rothman, 2000; Lazarus, 2016). They are often presented as a power relationship (Lazarus *et al.*, 2020), with the size metrics in natural log form. Typically, morphometric scaling relationships are built using the empirical measurements of well-developed static landforms or a large sample of the landform at a specific moment – with the size components of landforms able to be plotted against each other. Scaling relationships are beneficial as they can provide a predictive tool to estimate one size measure from another. For example, Montgomery and Dietrich (1988) found that a drainage basin's length scales directly with its area - even over several orders of size - suggesting that if the basin's length is known, its area can be estimated. Consequently, scaling relationships can show how two physical measures can relate to one another, even when the complex mechanics driving the processes within a landscape remain unclear (Kirchner, 1993).

However, morphometric scaling relationships constructed using snapshots of landforms, i.e. static allometry, are restricted to offering quantitative information about the relationships between attributes at one point in time (Bull, 1975) and so do not address the how and why elements of landform formation and development. As such, these scaling relationships detail the terminal morphology of landforms without getting into the underpinning dynamics. Therefore, the relationships are the consequence of the physical processes rather than a direct measure of the morphodynamics during landform formation (Mackin, 1963; Lazarus *et al.,* 2020). Thus, additional study would be necessary to explore the processes governing the morphometrics of landscape features. Nonetheless, morphometric scaling relationships based on static landforms offer a quantitative signature of the intrinsic structure of landscape features in various morphological environments (Dodds and Rothman, 2000; Edmonds *et al.*, 2011).

So far, scaling relationships have been observed for natural washover deposits (Lazarus, 2016), yet there has been no visualisation of the impacts of natural environmental conditions such as storm size and grain size. In addition, there has been limited quantification of flood-driven landform morphology in the fluvial domain – although real-world examples of the landforms have been studied and measured (Millard *et al.*, 2017; Rahman *et al.*, 2022). Furthermore, scaling

relationships remain relatively unquantified where flood-driven depositional landforms intrude onto anthropogenically altered floodplains. Currently, scaling relationships derived from deposits in built environments have been studied in flume experiments by Lazarus *et al.* (2022), which extended on work by Rogers *et al.* (2015) along US coastlines post Hurricane Sandy. They demonstrated how 2D metrics could start to be scaled with 3D size measures, e.g. area and volume – opening the door for future management practices to be more informed.

Therefore, in this research, the scaling rules will comprise various size metrics, including length, perimeter, area, and volume. The morphometric components are illustrated schematically in Figure 1-3. Such scaling relationships will permit the coastal deposits to be directly compared to those in fluvial environments to evaluate whether they collapse to similar scaling relationships despite the initial transport processes differing, and will also enable the assessment of morphological differences between natural and built settings.

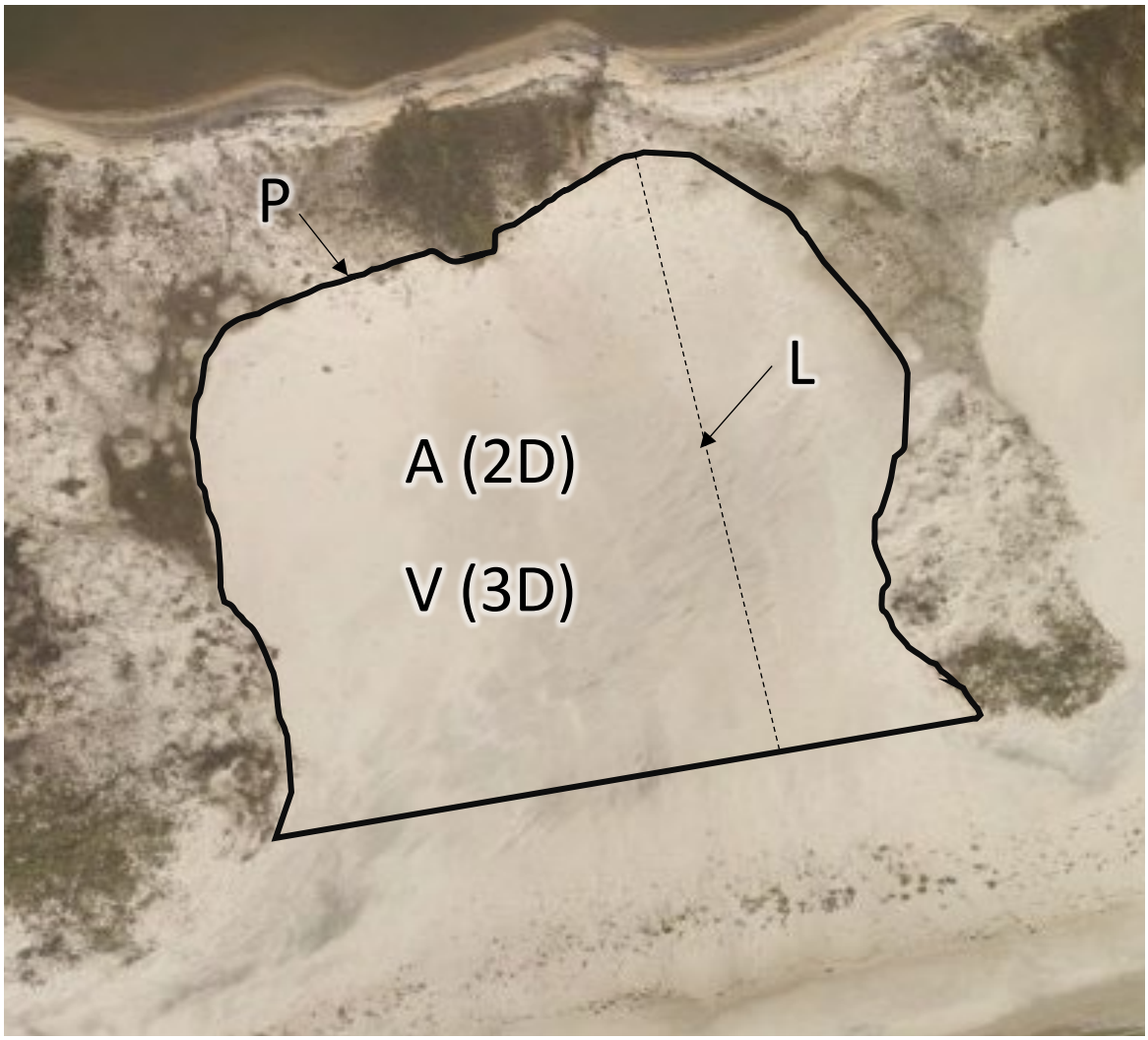

Figure 1-3 Selected morphometric characteristics of flood-driven sediment deposits. These include length (L), perimeter (P), area (A – 2D), and volume (V – 3D).

Morphometric measurements will be recorded for a series of landforms to assess the morphology of natural and built flood-driven sediment deposits. In this work, natural environments are equivalent to "unbuilt" floodplains – where built infrastructure is absent. I examine coastal examples from NOAA (National Oceanic and Atmospheric Administration) post-storm imagery and fluvial examples generated using the CAESAR-Lisflood morphological model (Coulthard *et al.*, 2013). The morphometric components of these deposits will allow the comparison of scaling relationships, alongside landform sizes, between a range of depositional settings and under various environmental conditions.

1.4 Aims and research questions

The overall aim of this thesis is to quantitatively investigate flood-driven sediment deposition on natural and built coastal (washover deposits) and fluvial (crevasse splays) floodplains to gain physical insight into their comparative morphometry and explore how such understanding of landscape dynamics may inform risk assessment and management.

I address this aim through the following research questions:

- **Research Question 1:** *What is the morphometry of flood-driven deposits in natural - coastal and fluvial floodplains? What natural environmental conditions control sediment deposit morphology?*
- **Research Question 2:** *How does the morphometry of flood-driven deposits differ between natural (unbuilt) and built floodplains? How might the spatial characteristics of built environments determine the size and distribution of flood-driven deposits?*
- **Research Question 3:** *Are flood-driven deposits in coastal and fluvial settings morphologically similar? How do they compare to depositional landforms from broader literature?*

1.5 Thesis outline

To address the aim and research questions, this thesis contains eight further chapters:

Chapter 2: Sediment deposits on coastal floodplains

This chapter reviews the literature on flood-driven coastal sediment deposits, from their formation and importance in the natural environment to controls on their morphology, and summarises the current knowledge regarding deposits in built coastal environments.

Chapter 3: Comparing hurricane-driven deposit morphology in natural and built coastal environments

This chapter examines washover deposition in natural and built coastal environments, using aerial imagery to identify real-world deposits in natural and built settings along the Atlantic and Gulf coasts of the US. Deposit morphometry is compared by generating scaling relationships differentiated by natural and built environments.

Chapter 4: Sediment deposits on fluvial floodplains

This chapter reviews the literature on the morphology of fluvial flood-driven sediment deposits, surveying morphological models and validating the model chosen in this thesis.

Chapter 5: Modelling controls on crevasse splay morphology on a deliberately simplified floodplain

This chapter delivers quantitative evidence of the impact of various environmental conditions on crevasse splay morphology. The effects of storm size, grain size, and floodplain roughness are observed by developing scaling relationships and investigating size parameters. This analysis uses CAESAR-Lisflood, a numerical process-based model, to generate a series of flood-driven sediment deposits on a simplified floodplain.

Chapter 6: Modelling impacts of the built environment on crevasse splay morphology

This chapter focuses on the influence of the built environment on flood-driven sediment deposition on a fluvial floodplain. Morphometric scaling laws demonstrate the effects of built infrastructure on crevasse splay deposits modelled with CAESAR-Lisflood, as well as examining the effect of the built environment on deposit size metrics.

Chapter 7: Synthesis of coastal and fluvial analyses

This synthesis combines the results from the coastal and fluvial depositional environments to compare the morphometry of flood-driven deposits in natural and built settings, and compares the data collected for this thesis with data reported in the existing literature.

Chapter 8: Implications

This chapter addresses the three core research questions and discusses the broader implications of this work, focusing on its relevance to predicting and managing hazard impacts. Given anthropogenic changes to sediment budgets, this chapter also considers the long-term survivability of hazard-prone low-lying floodplains. Finally, this chapter frames future research avenues that may provide further insight into flood-driven sediment deposits on coastal and fluvial floodplains in natural and built environments.

Chapter 2 Sediment deposits on coastal floodplains

In this background chapter, I explore the current understanding of overwash occurrence and processes, the subsequent morphological impacts, and the potential effect of built environments on natural coastal sediment dynamics. I begin with a brief introduction to coastal flooding and explain the need to study its impacts. I then define overwash with respect to four distinct processes and highlight its importance to low-lying coastlines. In the third section, I focus on the sediment deposits formed during overwash events, the natural controls on their morphology, and the effect built environments have on these deposits and sediment budgets in general. Lastly, I summarise the gaps existing in the research relating to the sediment deposit morphology along low-lying coasts.

2.1 Coastal floods

Coastal floods usually occur due to powerful waves instigated by storms and/or high tides (Kirkpatrick and Olbert, 2020). Cyclones and hurricanes can cause storm surges and high waves which intrude over a beach and onto natural and human-altered landscapes. Coastal regions most susceptible to flooding include barrier islands, low-lying shores, atoll islands, and deltas. During recent decades, coastal populations have grown faster than the mean global population (McGranahan *et al.*, 2007), with this disparity driven by favourable socio-economic conditions, including the desire to access trade routes and fishing opportunities (De Stefano *et al.*, 2017; Viero *et al.*, 2019).

Over 600 million people inhabit these coastal flood-prone landscapes (<10 m elevation), with Merkens *et al.* (2016) predicting a rise to over 1 billion by 2050. Climate change is expected to increase the coastal flood hazard globally – driven by rises in sea level (thermal expansion and ice sheet/glacier melting), precipitation, and storm winds (Purvis *et al.*, 2008; Bouwer and Jonkman, 2018). In addition, a warmer atmosphere will have a higher carrying capacity promoting increased moisture content, potentially leading to more intense precipitation extremes (Pfahl *et al.*, 2017; Bevacqua *et al.*, 2020). These factors will increase coastal flood damage. The global costs under current protection measures could reach US$1 trillion, and even with infrastructure adaptations, global costs are expected to top US$60 billion annually by 2050, a rise from US$6 billion in 2005 (Hallegatte *et al.*, 2013). Therefore, accurate and thorough predictions of the amount and distribution of storm damage are vital for coastal planners, giving them a greater chance to mitigate impacts on human life and economic cost (Donnelly *et al.,* 2006).

2.2 Overwash

2.2.1 Storm classifications

The impacts of coastal storms have been classified by Sallenger (2000) into four distinct regimes: swash, collision, overwash, and inundation, with each classification uniquely affecting landscape morphology by having different effects on the sediment budget of the coastlines affected. These sediment budget differences are caused by the range in magnitudes of erosion and accretion occurring in each storm regime. Swash occurs when the dunes restrict the stormwaters to the foreshore of the beach. Here, the erosion becomes replenished post-storm; consequently, there is no net change within the sediment budget. The collision regime typically involves a net loss in sediment budget caused by erosion when the storm run-up strikes the base of the foredune, with a lack of subsequent replenishment (Ruggiero *et al.*, 2001). The third regime is overwash which arises when the run-up exceeds the height of the dune/berm crest (D_{high}). Lastly, inundation, the fourth regime, occurs when the sea level rise caused by a storm is enough to submerge a barrier island/low-lying coast. Both 'overwash' and 'inundation' regimes are morphologically significant as they lead to the erosion of the dune system with the sediment produced subsequently transported inland. The storm's power and the foreshore's dune morphology govern the type of regime that occurs (Figure 2-1). Notably, the more substantial the storm, the more likely overwash and inundation will occur regardless of the initialbarrier morphology (Matias *et al.*, 2008) e.g. dune topography, habitats i.e. salt marshes and mangroves, and anthropogenic structures such as seawalls.

<table>
<tr><td></td><td colspan="5">Dune morphology</td></tr>
<tr><td>Oceanographic conditions</td><td>Depression in stable foredune</td><td>Seaward end of washout channel</td><td>Backdune depression</td><td>Inlet associated dune depression</td><td>Human associated dune depression</td></tr>
<tr><td>Exceptional conditions
Extreme storm</td><td colspan="5">Overwash + Inundation</td></tr>
<tr><td>Infrequent conditions
Severe storm</td><td>Overwash</td><td colspan="4">Overwash + Inundation</td></tr>
<tr><td>Regular storm conditions
Weak to moderate storm</td><td colspan="2">No overwash</td><td colspan="3">Overwash</td></tr>
<tr><td>Typical winter conditions
Non-storm</td><td colspan="3">No overwash</td><td colspan="2">Overwash</td></tr>
<tr><td>Fair-weather conditions
Non-storm</td><td colspan="5">No overwash</td></tr>
<tr><td></td><td>No overwash-prone morphology</td><td colspan="3">Overwash-prone natural morphology</td><td>Overwash-prone artificial morphology</td></tr>
<tr><td></td><td>EXCEPTIONAL TO INFREQUENT OCEANOGRAPHIC CONDITIONS</td><td>WASHOUT PROCESSES</td><td>STRUCTURAL EROSION</td><td>INLET DYNAMICS</td><td>HUMAN INTERVENTIONS</td><td>FORMATION MECHANISMS</td></tr>
</table>

Figure 2-1 The impact of storm size and dune morphology on the chance of overwash and inundation taking place (Matias *et al.,* 2008).

2.2.2 Occurrence and types of overwash

Overwash is caused by a combination of wave run-up, storm surge and wave setup (Carruthers *et al.*, 2013). An episode of overwash can occur over timeframes of minutes to days, during which several individual overwash events can occur for under a minute each (Leatherman, 1976). Overwash frequency is the number of overwash events per second, and the return period is the average time between two events (Matias and Masselink, 2017). Overwash occurrence, frequency, and magnitude are controlled by a variety of factors, including shoreline orientation (Fletcher *et al.*, 1995), marine conditions, i.e. bathymetry and wave height (Houser, 2012), and the topography of the beach, the back-barrier, and the dune system (Donnelly and Sallenger, 2007). The water level during storms is fundamental in inducing overwash, with episodes generally associated with a range of wave heights offshore, e.g. up to 4m (Leatherman, 1976) and 9m (FitzGerald *et al.*, 1994). Overwash events unrelated to storms can be triggered by extreme tides, lagoon floods (Nguyen *et al.,* 2006) and even El Niño events (Morton *et al.*, 2000).

Overwash morphology can be separated into four processes: crest accumulation, crest lowering, minor inundation, and complete inundation, which fall into two distinct categories: run-up and inundation (Donnelly *et al.*, 2004; Blenkinsopp *et al.*, 2016). The four processes can sometimes occur during the same storm event either in synchronisation due to local differences in beach crest height or chronologically on account of variations in water level during a storm event. Donnelly *et al.* (2004) used a series of cross-sectional diagrams depicting the respective wave setups and barrier morphologies to classify the overwash regimes. Run-up overwash, illustrated in Figure 2-2, happens when the wave run-up overtops the fore dune (Carruthers *et al.,* 2013). The excess wave run-up, ΔR, is calculated as the sum of wave run-up height (R) and storm surge height (S), with dune height (d_c) then subtracted.

Run-up overwash is associated with smaller storms and high tides (Leatherman *et al.,* 1977). The two types of run-up overwash, crest accumulation and crest lowering, differ due to dissimilarities in the relative magnitudes of R, S, and d_c. Crest accumulation (Orford *et al.,* 2003) occurs when $R + S$ is slightly above the d_c value, where the wave run-up reaches the beach crest but lacks the energy to carry sediment further. In this scenario, a few infrequent waves, characterised by a low ΔR, overtop the dune. As a result, a limited amount of sediment is transported inland, with the sand deposited predominantly on the dune crest (Leatherman, 1976). When this process recurs several times at the same water level, crest height progressively increases, potentially preventing future overtopping of the dune system (Orford *et al.,* 2003).

In crest lowering, the other regime of run-up overwash (Donnelly *et al.,* 2006), the value of S is higher than in the crest accumulation regime but remains lower than d_c. This leads to a higher

frequency of waves characterised by an R and ΔR, sufficient to overtop the dune. Regarding the morphological impact, crest lowering causes erosion from the dune face or the crest, thus lowering the elevation. The eroded sediment is transported inland and deposited in the back-barrier (Zhu and Kobayashi, 2021).

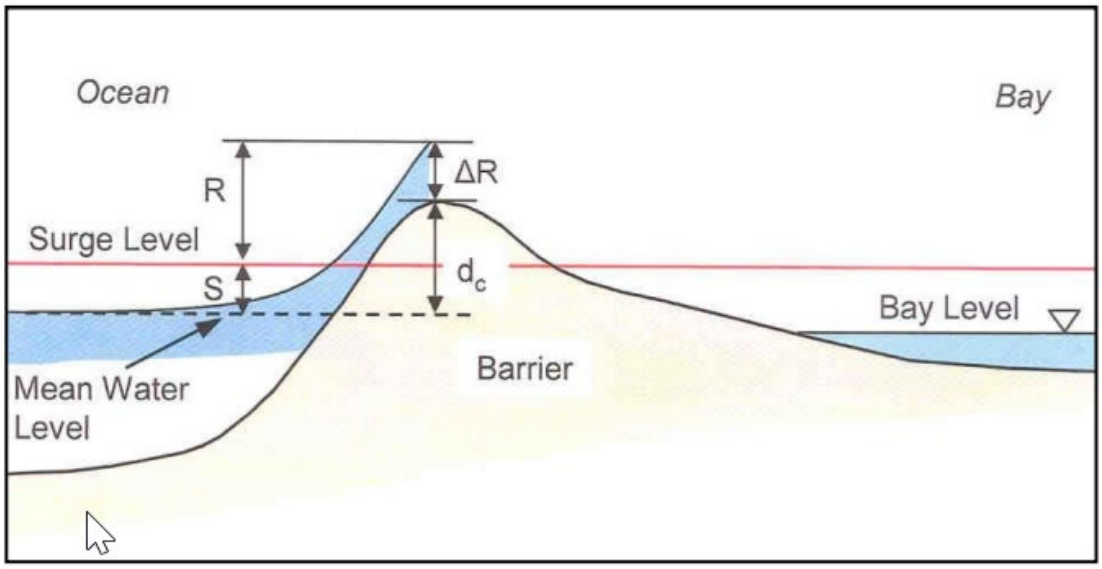

Figure 2-2 Cross-section schematic of a barrier experiencing run-up overwash (Donnelly *et al.,* 2004). ΔR = excess wave run-up, R = wave run-up height, S = storm surge height, d_c = dune height with respect to mean water level.

The other overwash mechanisms fit into the inundation overwash category and occur when S exceeds d_c – with the mean water level (derived from figures including storm surge) surpassing the crest elevation (Sherwood *et al.*, 2014; VanDusen *et al.*, 2016). Inundation overwash can lead to the water levels of the ocean and the bay behind the barrier becoming linked when water from the ocean flows continuously over the barrier system. As a result, a gradient can be created due to the elevation difference between the bay and ocean water levels, acting as a primary driver of morphological change (Engelstad *et al.*, 2017). Within the inundation overwash classification, water easily overtops a beach, and the dune system, and two regimes can occur based on the inundation magnitude.

Inundation overwash can be split into minor and complete inundation (Donnelly *et al.,* 2006). Minor inundation, referred to as "constant flow over the beach crest" (Donnelly *et al.*, 2004; Figlus *et al.*, 2011), is described in Figure 2-3. In this case, S constantly exceeds d_c either during extreme storms or where the beach crest is of low elevation and, therefore, susceptible to flooding. Sediment is usually removed from the face of the beach and occasionally also from the back-barrier. However, one or more of the barrier width, topography (e.g. rear dunes), porosity, and/or surface friction prevent the overwash from reaching the bay. Surface friction,

often increased by the presence of vegetation, can cause the overwash to deposit sediment. The local wave height at the beach crest (H_c) can influence the quantity of water and sediment transported into the back-barrier through mass flux and sediment mixing.

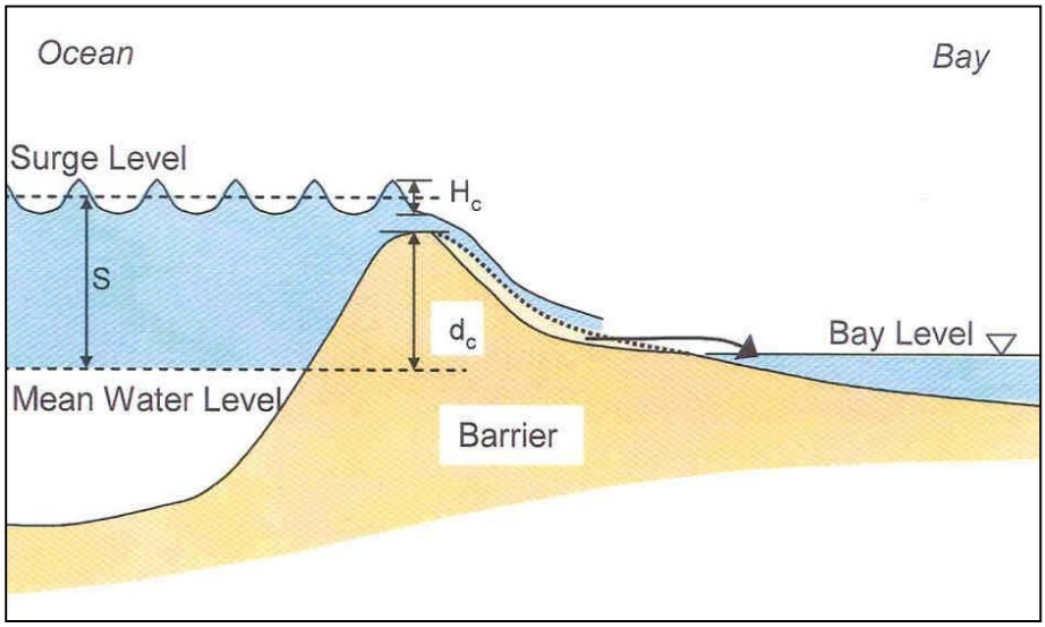

Figure 2-3 Schematic of the overwash regime of minor inundation (Donnelly *et al.,* 2004).

Complete inundation (Figure 2-4) is "constant flow over a prominent dune feature", and where S significantly exceeds d_c during extreme storms, leading to inundation of the whole barrier or beach system (Donnelly *et al.,* 2004). As stated above, when overwash flows reach the bay behind the barrier, then the ocean and bay water levels may become coupled, and a water gradient can form. The elevation difference between the mean ocean water level and bay water levels is referred to as d_b. In this regime, if coupling happens, the magnitude of the water gradient can be defined as $S - d_b$, and this can control the quantity of overwash flow and sediment entrained.

Complete inundation causes widespread erosion of the shoreline and reduces the height of the dune crest, with the sediment deposited inland. This regime has the highest likelihood of causing breaches in the dune/beach crest (Kraus and Wamsley, 2003). During these events, the localised inundation through beach crest gaps can form temporary breaches, which then close post-storm when the water level returns to normal. Sheet overwash, where the water overtops a vast lateral extent of the beach, usually occurs when the crest is uniformly low (Orford *et al.,* 2003) or during extreme storms (Fisher and Stauble, 1977).

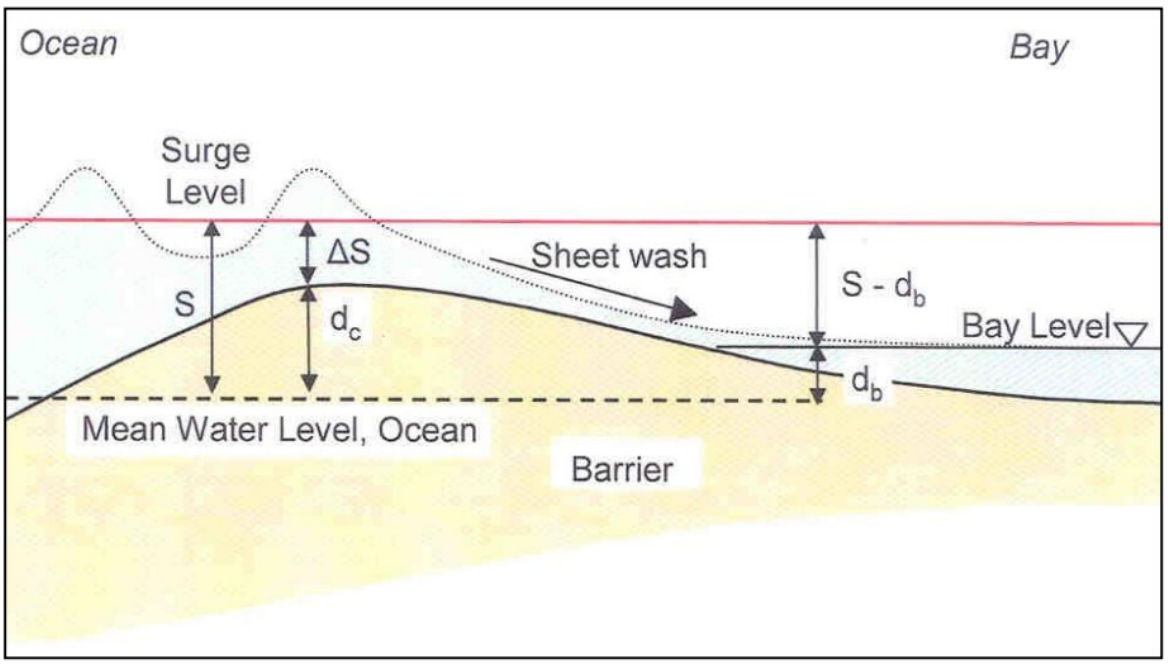

Figure 2-4 Schematic of complete inundation overwash (Donnelly *et al.,* 2004).

2.2.3 The importance of overwash

The overwash process is vital for the morphology and ecology of many natural landscapes. Over 100s to 1000s years, the sediment delivery by overwash is constructive, allowing barrier islands and low-lying coasts to retain their height and width relative to sea level, acting as a quasi-continuous process to shape shorelines (Leatherman, 1988, Nienhuis and Lorenzo-Trueba, 2019). Barrier islands can protect coastal communities and back-barrier ecosystems, which usually encompass high-value ecosystem services (Plomaritis *et al.*, 2018). Rising sea levels cause barrier islands and shorelines to migrate landwards (Davis, 1985). Therefore, repetitive overwash is necessary to sustain sandy barrier islands as it maintains the net volume of the barrier system whilst the landscape migrates (Dolan and Godfrey, 1973).

Overwash transports sediment from the nearshore and foreshore to the back-barrier to be deposited as elevated landforms in a process termed "rollover" (Matias *et al.*, 2016; Plomaritis *et al.*, 2018). Overwash and the ensuing rollover help a barrier system to survive by preventing barrier drowning (Lorenzo-Trueba and Ashton, 2014). This highlights the morphological importance of episodic overwash for keeping the sediment budget in a dynamic equilibrium and supporting the response of transgressive barrier islands to the threat of sea level rise (Kraft *et al.,* 1973, Rodriguez *et al.*, 2020).

Overwash plays a crucial ecological role in creating and developing unique habitats. Here, one such unique habitat, the salt marsh, will be detailed with respect to the overwash process.

Initially, new sediment deposits provide a base for the growth of salt marshes which are coastal wetlands regularly flooded and drained by tidal seawaters (Walters *et al.*, 2014; Schuerch *et al.*, 2018). Overwash deposition reduces the quantity and density of sand-trapping vegetation, increasing the potential for aeolian transport of sand across a barrier system. Consequently, dune fields are formed alongside the re-establishment of grasses (Rodriguez et al., 2020). If minimal disruption exists, the new dune system and sand flats will offer a substrate suitable for salt marshes. Once the ecosystems are in place, the sediment movement by overwash helps protect these ecosystems from sea level rise whilst adding a vast quantity of nutrients, and enhancing productivity (Mendelssohn and Kuhn, 2003). These salt marshes and tidal wetlands provide essential ecosystem services (Eisma, 1998, Kennish, 2001; Fagherazzi *et al.*, 2020), e.g. they offer a rich biodiverse habitat for animals and plants by stimulating vegetation growth (Costanza *et al.*, 1997; McKee and Cherry, 2009). In addition, salt marshes lower the potential for storm surges flowing inland. The halophytic vegetation present can add friction to the environment – attenuating waves and slowing flows (Bendoni *et al.*, 2019). Consequently, salt marshes and barrier systems can be seen as natural flood defences (Langley *et al.*, 2009; Leonardi *et al.*, 2018). However, there is a balance between overwash and salt marshes' upkeep - as thick sediment deposition can bury vegetation and lead to widespread plant mortality (Wang and Horwitz, 2007). Therefore, the thickness of overwash deposits, which is likely to increase due to more powerful storms and sea level rise, has the potential to make salt marshes less resilient (Kirwan *et al.*, 2016).

2.3 Washover

Washovers are depositional sedimentary landforms created by overwash events. Washover is predominantly active during extreme storm events and can appear as post-flood relics (Galloway and Hobday, 1996). This landform is produced when the energy of overwash carrying sediment across a beach crest dissipates, such that it deposits the entrained material. Schwartz (1982) suggested that washover is more likely to occur in storm-inflicted regions characterised by < 2m tidal ranges (micro-tidal) than those in 2-4m tidal range (meso-tidal) settings. This is because strong tidal currents can redistribute sandy sediment from within the washover and its margins to elsewhere (Leatherman and Zaremba, 1986). The thickness of deposits formed by a single overwash episode can rangefrom 2 cm to 2 m (Sedgwick and Davis, 2003, Hudock *et al.,* 2014).

The sediment deposits' overarching morphology is primarily due to the overwash regime occurring during flooding. Each regime exhibits different energy levels, affecting both the quantity of sediment that can be transported and the amount of erosion of the beach and dune

crest. Figure 2-5 illustrates the three types of washover deposits: fans, terraces, and sheetwash, which can form under specific overwash regimes.

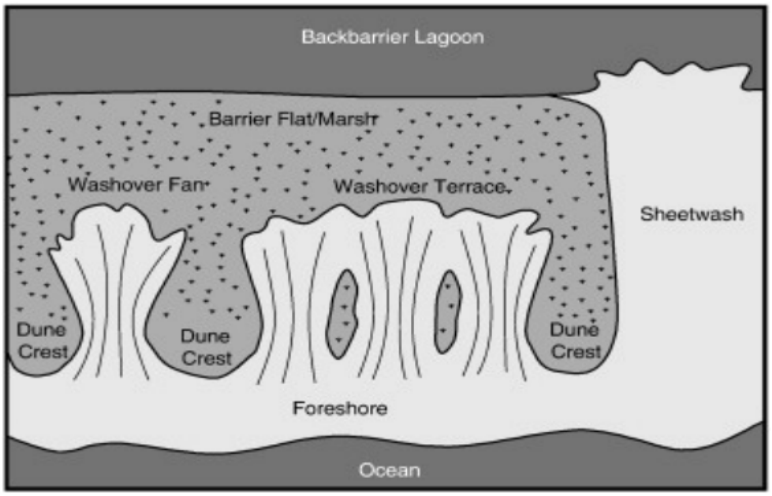

Figure 2-5 The three types of washover deposits: fans, terraces and sheetwash (Donnelly *et al.,* 2006).

When run-up overwash occurs, washover morphology is primarily governed by the topography of the barrier landscape and the excess wave run-up (ΔR). Washover fans are distinctive artefacts of run-up overwash, formed where the dunes are relatively high compared to the wave run-up, but where dune topography is uneven along the shoreline. They can appear as singular, isolated deposits or are regularly spaced along the shoreline (Lazarus, 2016). Distinct washover fans are created where the storm surge surpasses the elevation of the minor dunes but is blocked by neighbouring dunes of higher elevation. The run-up overwash is constricted by the openings and then funnelled through the beach crest/foredune, with the overwash spreading once on the back-barrier. Depositional fans are created when water on the back-barrier is affected by friction and percolation, which cause the water mass to decelerate, losing the energy required to transport its sediment load. Therefore, washover fans are commonly described as shaped like a teardrop oriented perpendicular from the shore with a drainage "throat" feature channelling through the dune breach from the ocean into the fan (Lazarus, 2016).

During run-up overwash episodes, washover terraces can also be formed. Washover terraces are "elongated deposits oriented parallel to the shore" (Schwartz, 1982, Morton and Paine, 1985, Morton and Sallenger, 2003). The morphological conditions associated with terrace landform development include a narrow barrier island, low-elevation dunes, and small distances alongshore between crests and breaches (Morton and Sallenger, 2003). When these criteria are fulfilled, it can lead to washover fans occurring more frequently along a stretch of shoreline. The borders between the washover fans can then become blurred, and a series of fans may

merge into a "terrace". Terraces may also form on coastlines where the foredune or beach crest elevation is uniform alongshore and is exceeded by the maximum storm surge. Consequently, washover terraces can either appear as a deposit with a similar intrusion length along its entire width or highly irregular intrusion lengths and has the potential to reach any existing back-barrier bays/lagoons. This variety of intrusion length is determined by the local topography of the land, the presence of vegetation, and the interactions between the currents during sediment deposition (Morton and Sallenger, 2003).

In contrast, inundation overwash has the potential to produce sheetwash which are widespread washover extending 100s to 1000s metres in width across an alongshore segment of the beach (Morton and Sallenger, 2003; Donnelly *et al.*, 2006; Rogers *et al.*, 2015; Lazarus, 2016). These deposits occur where dunes are lower than the storm surge – either from beach conditions existing pre-storm or following the reduction of crest height by persistent wave action and overwash. During the formation of sheetwash deposits, the sediment transport is continuous across the dune system with no lateral confinement of the water and sediment flow, resulting in sediment deposits reaching and extending into any existing back-barrier bay/lagoon (Morton and Sallenger, 2003, Donnelly *et al.,* 2006). The duration of the flooding drives the amount of morphological change caused by inundation overwash. Bedforms associated with sheetwash deposits include thin zones of erosion and deposition forming outlines parallel to the flow direction from the shore to the back-barrier.

The extent and planform of the washover deposits formed during overwash can be shaped by: the topography encountered on the foredune and the back-barrier; the barrier island width; vegetation presence and type (Donnelly *et al.,* 2006); the size of the sediment deposited, and the size of the waves and storm (Liu and Fearn, 2000). Morton and Sallenger (2003) imply that the classification of washover is directly linked to the deposit volume, with sheetwash and washover fans having the largest and lowest volumes, respectively.

2.3.1 Natural controls on washover morphology

Washover deposits form in different shapes and sizes. However, when formed in an undisturbed, relatively flat coastal environment, they are typically teardrop in shape once they have extended beyond the foredune (Lazarus, 2016). The type of overwash regime (run-up and inundation) that occurs during flood events, together with the duration of the overwash episode, are the primary determinants of the morphometric components of washover deposits.

Early field studies demonstrated that storm surge height is a major factor controlling overwash magnitude and, thus, washover deposit size (Fisher and Stauble, 1977; Leatherman and

Zaremba, 1986). These field studies have subsequently been corroborated by laboratory experiments at small (Donnelly *et al.*, 2004, Larson *et al.,* 2004) and large scales (Matias *et al.*, 2016) found discharge to directly correlate with the amount of sediment transport during overwash. In addition to dictating the distance that washover can extend onto low-lying floodplains, the increased energy associated with more intense storms can erode, entrain, and transport more sand - increasing sediment availability and creating more extensive washover deposits (Matias *et al.*, 2016).

The washover sizes and shapes generated by a given overwash event are also influenced by landscape characteristics of the barrier or low-lying coastlines, e.g. topography and vegetation, which can alter the morphology of washover deposits by disrupting overwash flow patterns and speeds (Donnelly *et al.,* 2006). The topography of foredunes and the barrier can play a significant role during the development of coastal sediment deposits (Fisher and Stauble, 1977; Morton and Sallenger, 2003). Morton and Sallenger (2003) used aerial photographs of historic hurricane events – ranging from Hurricane Carla (1961) to Hurricane Hugo (1989) - to investigate controlling factors on washover penetration distance and morphology, primarily focusing on land elevations and nearshore bathymetry. They found topography to be an essential factor in shaping washover deposits, with low and uniformly shaped barrier systems promoting the formation of terraces or sheetwash. Whereas dune systems with irregular topographies typically encourage overwash flows to be constrained and washover to be assembled as fans or a series of terraces.

The presence of vegetation in areas that experience overwash can impose increased friction on the flowing water and alter the terminal morphology of sediment deposits (Donnelly *et al.,* 2006). For example, early qualitative studies by Godfrey and Godfrey (1974) and Dahl *et al.* (1983) suggested that more material is transported and deposited on non-vegetated dunes during hurricanes than on those that are vegetated. Wang and Horwitz (2007) used coring and GPR (Ground Penetrating Radar) to compare the effects of dune vegetation on washover deposits created by the 2004 Hurricanes Frances and Jeanne on South Florida barrier islands with those caused by the Hurricanes Ivan (2004) and Dennis (2005) along the North Florida coast. They indicated that vegetation such as marsh grass could reduce the amount of erosion on dunes by acting as a barrier above the surface and reducing wave-overtopping frequency. In addition, Kobayashi *et al.* (2013) conducted a laboratory experiment to assess the influence of woody plants' presence on low and high dunes on overwash morphology and found similar patterns. Usually, erosion on the foredune provides overwash with more sediment to transport and deposit on land further from the sea. Consequently, a band of vegetation on a foredune can decrease the amount of sediment delivered to the back-barrier – where deposits are typically

thickest (Wang and Horwitz, 2007). Therefore, it can be seen from these effects on sediment availability and overwash flows that vegetation affects both the volume and the extent of washover deposits formed during an episode of overwash (Kobayashi *et al.*, 2013).

2.3.2 The impact of built environments on washover morphology

Human activity alters the coastal landscape (Walker, 1984), with built infrastructure affecting the formation and evolution of landforms (Nordstrom and McCluskey, 1984; Morton *et al.*, 1994; Nordstrom, 1994, 2004). In addition, anthropogenic changes to coastlines, including flood defences, building development, and road production, modify the landscape's natural sedimentary sources, pathways, and sinks (Nordstrom, 1994).

Hard engineering structures substantially affect sediment movement and the sediment budgets of coastal landscapes. Groins, built to maintain beaches, capture sediment as it moves alongshore, yet they can cause high shoreline retreatment rates downdrift of their location due to the reduction in sediment supply, e.g. at Westhampton Beach, New York, there was 6.5 m/a of downdrift erosion over 14 years due to the placement of groins (Nersesian *et al.,* 1992). Seawalls can reduce the overwash potential along coastlines by acting as shore-parallel barriers. They affect swash velocities and elevations, leading to increased erosion through deflecting waves during peak energy events, causing stronger backwash and increased turbulence (Plant and Griggs, 1992). In preventing overwash occurrence, seawalls can stop washover deposits from being produced. This can have long-term impacts on barrier morphology, with the occurrence of fewer overwash events resulting in a reduced sediment supply, which may cause barrier drowning (Magliocca *et al.*, 2011). Thus, hard engineering structures can significantly impact the sediment budget of coasts by inducing new depositional and erosional patterns.

Despite the presence of hard engineering structures, overwash on developed coastlines is common during extreme flood events. Built environments constructed on low-lying coasts and barrier islands inherently involve placing buildings on landscapes susceptible to overwash events (Nordstrom and McCluskey, 1984). Buildings replace the back beach and dune system (Morton *et al.*, 1994) and can alter the overwashing flow's magnitude and direction, disrupting natural depositional patterns. The impact on flows is minimal where buildings are raised off the ground, potentially by stilts (Nordstrom, 2004). However, where buildings are not elevated, they provide obstacles to overwash flows which can act in two different ways: localised scouring where flows are channelled, or accretion where the flow velocity is reduced. Moreover, buildings can block overwash on barrier islands – negatively affecting the sediment budget (Donnelly *et al.,* 2009; Rogers *et al.,* 2015).

Impervious surfaces such as paths, roads, and car parks can alter natural washover morphology. Such surfaces provide unconstrained pathways for coastal floods during large storms as they prevent percolation and lack the friction to slow flow down (Fletcher *et al.,* 1995). Consequently, overwash infiltrates longer distances onto low-lying coasts along corridors provided by roads perpendicular to the shore (Nordstrom, 2004). This leads to washover forming as narrow, elongated, channelised deposition (Rogers *et al.,* 2015).

The complex real-time interactions between elements of the built environment and overwash are unknown because of the danger associated with attaining velocity and morphological data during powerful debris-loaded floods. Nevertheless, the anthropogenic impact on overwash and its accompanying sediment deposits are evident by investigating the morphological changes post-storm. A study by Hall and Halsey (1991) provided the first qualitative assessment of overwash penetration in natural and built environments. From aerial photography during the aftermath of Hurricane Hugo (September 1990), they visually estimated the distance overwash extended onto the different landscapes. They suggested that a factor increasing overwash extent was the impermeable smooth surfaces of the street network and car parks oriented perpendicular to the sea.

Rogers *et al.* (2015) analysed the quantitative impact of built environments on washover deposit morphology. They utilised LiDAR (Light Detection and Ranging) survey data taken before and after Hurricane Sandy (2012) along the New Jersey coast to generate washover extents and volumes in natural and built settings. Buildings and vegetation were filtered out of the LiDAR data, with the pre-storm elevation layer subtracted from the post-storm raster to depict the thickness of the washover (Figure 2-6). Washover extent was digitised in natural settings using aerial imagery, which informed an elevation threshold to classify overwash extents in built environments. The deposition was defined to begin where elevation change along each transect became positive and continued until the outer extent of the washover. To calculate deposit extent and volume, they generated a series of transects extending perpendicular from the shoreline at 10m intervals alongshore. Washover volume was calculated as the area under the elevation change profile at each transect – in units of m^3/m representing a width-averaged volume. This analysis confirmed a positive linear relationship between washover extent and volume. However, as the washover extent increased, its correlation with volume became less constrained to a dominant trend line. This result was attributed to lateral spreading and increases in infiltration as the washover deposit extends further onto land (Donnelly *et al.*, 2009). In addition, they suggested that the built environments reduced the volume of sediment deposited compared to that delivered to natural settings. This was quantified as a 40% and 90% reduction in sediment deposited in the residential and commercial settings, respectively, relative to the

natural deposits studied. Therefore, they suggest that the built infrastructure on barrier islands results in a net loss within the sediment budget – even before the impact of post-storm cleanup is included. It is worth noting that the commercial setting had a 4.5 m high continuous boardwalk at the back of the beach, which limited the amount of overwash that could occur (Rogers *et al.,* 2015).

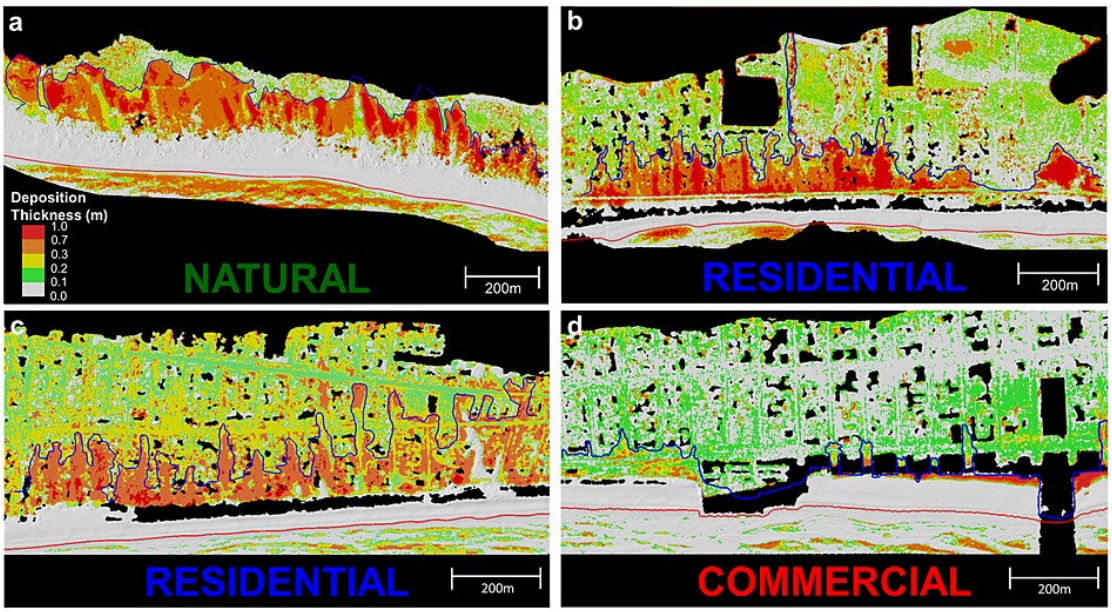

Figure 2-6 Visualisation of elevation change models from Rogers *et al.* (2015). This highlights washover thicknesses and extents (blue line), created using LiDAR and split by shore environment a) natural, b) residential, c) residential and d) commercial.

The detrimental effect of built settings on sediment supply was also shown during a study by Donnelly *et al.* (2009), which used the SBeach model to investigate overwash. The model was used to predict overwash at six locations along the Atlantic coast of the US, with 26 sets of beach profiles. They concluded that the model performed well at predicting qualitative and quantitative profile changes for all of the study sites, except for highly urbanised settings where volumes of washover were overestimated compared to validation data. This reduction in sediment volumes highlights the impact that a built environment can have on the terminal morphology of washover deposits and coastal morphological systems by reducing sediment availability.

This research on the human impact on coastal depositional landforms implies differences between natural washover morphology and those deposited in built environments. Although some studies have started to investigate overwash extent and volumes, there has been no quantification of the extent of areas affected and the influence different built environments can have on deposit shape and size. Furthermore, the results have been limited to a few specific

storms (primarily Hurricane Sandy) and provide little information concerning the impact of storm size/location on deposit morphology. Indeed, it is known that where coastlines are developed, overwash and the entrained sediment can be a hazard. Therefore the morphological interactions between overwash and the built environment must be understood to provide planners and engineers with detailed information (Donnelly *et al.,* 2009).

2.3.3 An overview of research methods

Various techniques can be utilised to investigate washover morphology. Initial studies of overwash and washover took place in the field using hand-held current meters to examine flow patterns during a storm (Fisher *et al.*, 1974). However, due to the danger associated with being present on a stretch of beach experiencing storm conditions, they quickly became unfeasible – being replaced by remote instruments (Leatherman, 1976; Fisher and Stauble, 1977; Kochel and Wampfler, 1989;), and post-storm analyses of sediment distribution (Carruthers *et al.*, 2013; Hodge and Williams, 2016). As technology advances, the ability to investigate overwash processes and morphology during storm events is enhanced. With the aim of providing a method to create datasets of high-frequency, in situ recordings of overwash - of which very few exist - Reeves *et al.* (2021) developed a novel sensor platform called MeOw (Measuring Overwash). MeOw stations are described as weather resistant – able to withstand high winds and powerful waves, characteristic of storms and overwash – and can be left independent for a period of months to years. A caveat of these studies is that by the time access to washover is available after the storm, the deposit will have changed due to aeolian processes – particularly if the deposition is minor (Leatherman and Zaremba, 1986). Consequently, it is difficult to attain accurate information on the physical morphometric parameters of washover deposits in the field environment.

Alternatively, laboratory research can be undertaken on various scales, from small to large flume experiments. They offer advantages over in situ field studies, such as the absence of danger alongside the capability to control the hydrodynamic conditions that a) ensure overwash occurrence (Matias *et al.*, 2016) and b) can test different storm surge sizes with a range of sediment grain sizes. These experiments typically measure the barrier topography before and after overwash trials allowing the quantification of morphological changes and volumes of sedimentation (Matias and Masselink, 2017). However, at times there can be scale and applicability limitations associated with laboratory experiments (Matias *et al.*, 2019).

Numerical process-based models, e.g. XBeach (Roelvink *et al.*, 2009), assess the natural response of the coast during storm conditions and are often used to validate field data and can act as

predictive tools. The input of topography and bathymetry, water levels, and wave characteristics allow models to predict the distribution of washover deposits, dune erosion and breaching (Jamal *et al.,* 2014). XBeach was calibrated and validated during model creation against field surveys and large-scale flume experiments. Although XBeach has been used in settings with constructed seawalls (Silveira *et al.*, 2016), numerical models are yet to be used where sediment extends into the built environment. These experiments typically measure the barrier topography before and after overwash trials allowing the quantification of morphological changes and volumes of sedimentation (Park and Edge, 2010; Matias and Masselink, 2017).

Finally, empirical techniques can use remotely sensed imagery and field observations to derive statistical morphological models (Schumann *et al.*, 2009). Data from remote sensing sources, such as high-resolution aerial and satellite imagery, offer a mechanism to study flood-driven sediment deposits without needing to access the sites – permitting many landforms to be sampled efficiently, as shown by Hudock *et al.* (2014), who utilised Google Earth imagery to study 118 washover fans in natural environments. Furthermore, the availability of this data source in high-resolutions is only on the rise, both freely and commercially (Notti *et al.*, 2018), providing the opportunity to study events in detail. For example, a repository of post-storm aerial imagery is provided by NOAA, with the data captured in the days following hurricanes affecting the US. Such imagery presents a chance to gain an insight into landform morphology in the immediate aftermath of a flood event and, in the case of built environments, can portray the sediment deposits before removal during post-storm clean-up efforts.

2.4 Gaps in coastal research

1) Natural washover deposits

Examining the existing literature has identified a distinct lack of empirical evidence concerning the morphology of real-world washover deposits, i.e. their size and shape. A study that quantified a range of morphological attributes (i.e. length, perimeter, area) of recently deposited washover in a natural context was conducted in a laboratory environment (Lazarus, 2016). Although Hudock *et al.* (2014) examined 118 washover fans using Google Earth – they acknowledge that it was a snapshot of historically deposited washovers during their evolution (deposits can change dramatically due to aeolian processes) rather than an investigation into the morphology of coastal sediment deposits immediately after formation. Therefore, there remains a significant gap in the quantitative research into the morphology of real-world natural coastal sediment deposits, particularly in the immediate aftermath of extreme overwash events.

2) Washover deposits in built environments

At present, there is little understanding of the impact built environments have on overwash events and the washover deposits they produce on barrier islands and low-lying coasts. As explained above, the quantitative investigations into the impact of anthropogenic development on the morphology of washover deposits are limited. One reason for this is the fast removal of sediment post-storms to allow access to stricken inhabitants and reopen key routes (Overbeck *et al.*, 2015). Although Rogers *et al.* (2015) investigated overwash extent and volume, this was for a small subset study area where the built environment was universally similar. Consequently, there has been little assessment of how a range of built settings, i.e. different building densities and street lengths, affects the shape and size of washover deposits and distorts them from the natural norms.

Chapter 3 Comparing hurricane-induced deposit morphology in natural and built coastal environments

Nota bene – The results presented in this chapter contributed to and were published in: Lazarus, E. D., Goldstein, E. B., **Taylor, L. A.**, & Williams, H. E. (2021). Comparing patterns of hurricane washover into built and unbuilt environments. *Earth's Future*, 9(3), e2020EF001818.

3.1 Chapter objectives

This chapter seeks to address the research gap identified in Chapter 2. The research gap outlined a need for more morphometric data of real-world natural washover deposits immediately after overwash occurrence and the lack of quantitative understanding concerning the built environment's impact on washover deposits.

To do this, it will:

1. Expand on the existing shortage of empirical measurements of real-world washover deposits in natural and built settings, determining if a morphological difference exists between the two environments.
2. Explore the impact of components of the built environments on the morphology of coastal washover.
3. Investigate whether sediment deposits generated using a simple numerical model with a range of "built fabrics" align with the morphometric data from real-world examples.

3.2 Introduction

Overwash is the landward movement of water and sediment over a sand or gravel beach crest that does not directly return to its original water body source (Donnelly *et al.*, 2004). Overwash occurs when the water level is elevated, usually caused by a combination of tide, wave set-up and storm surge, and is a typical process on barrier islands and low-lying coastlines (Donnelly *et al.*, 2006; Lazarus and Armstrong, 2015; Matias and Masselink, 2017). The overwash process is a vital contribution to the sediment budget of many low-lying coastlines and can help to regulate the height and width of barrier coasts relative to sea level – ensuring the long-term survival of these landscapes (Dolan and Godfrey, 1973; McCall *et al.*, 2010; Lorenzo-Trueba and Ashton, 2014). In addition, through the delivery of saltwater and sediment, overwash is vital for

establishing and maintaining salt marsh and dune habitats (Mendelssohn and Kuhn, 2003; Seavey *et al.*, 2011; Goldstein and Moore, 2016).

The sedimentary features produced during overwash are termed washover (Sallenger, 2000; McCall *et al.*, 2010). Washover deposits formed in undisturbed natural environments are typically in a regular semi-circular-like shape. However, the land's topography can alter their shape, whilst surface roughness facets such as vegetation presence can stunt their inland growth (Kobayashi *et al.*, 2013). When overwash during intense storms exceeds a continuous length of foredune along the coast, deposits can form as terraces or sheetwash, which are usually wide and can extend to the back-barrier lagoon of some barrier islands (Donnelly *et al.*, 2006).

Meanwhile, little is known regarding the morphology of washover that extends into built environments – which are now ubiquitous along vulnerable low-lying coasts. Gaining an understanding of the impacts that different built environments have on the sediment budget of low-lying coasts is a priority given the necessity of regular sediment supply to maintain these landscapes, particularly as the importance of this supply is being amplified under current and projected sea level rise (Viles and Spencer, 1995; Carruthers *et al.*, 2013). Therefore, an accurate understanding of coastal overwash, particularly in built-up barrier island settings, is vital (Donnelly *et al.*, 2006).

Here, aerial imagery is sourced from the NOAA (National Oceanic and Atmospheric Administration) post-storm repository (National Geodetic Survey, 2020) for five hurricane events impacting the low-lying and well-populated Atlantic and Gulf coasts of the US: Irene (2011), Sandy (2012), Matthew (2016), Nate (2017), and Michael (2018). The morphological characteristics of the washover deposits from these extreme events are quantified, with physical attributes including length, perimeter, and area measured in natural (n = 115) and built (n= 167) environments (figure 3-2B). Morphometric scaling laws are defined from these dimensions, allowing the geometry of the washover between natural and built settings to be compared. Combined with the calculation of a novel metric termed "Distortion Index" (DI), these allow the impact of built environments on deposit morphology to be explored. Here, the built fraction (a non-dimensional measure of building density) and street length represent spatial components of the built environment. The simple numerical model produces washover deposits for a range of built fractions, with the same physical parameters measured as the real-world examples.

3.2.1 Background

On a short timescale, overwash during intense storms and hurricanes has the highest potential to induce significant natural morphological change. However, when overwash extends into built environments on these susceptible low-lying shorelines, it often constitutes a natural hazard (Jongman *et al.*, 2012). Low-lying coasts with sandy beaches are attractive for human inhabitation and, as such, have become densely populated with widespread anthropogenic development and infrastructure (Stutz and Pilkey, 2011). For example, in the US, over 1.4 million people live on barrier islands along the Atlantic and Gulf coasts, based on the 2000 census (Zhang and Leatherman, 2011). In these hazard-prone regions, populations continue to grow at higher rates than the US national average (Culliton, 1998; Stutz and Pilkey, 2011; McNamara and Lazarus, 2018). Moreover, climate change is predicted to increase the intensity and frequency of storms and cause rising sea levels (Vermeer and Rahmstorf, 2009; Visser *et al.*, 2014). For example, areas of the US east coast near southeast Virginia are experiencing a high relative sea level rise rate, leading to a higher risk of extreme flooding (Ezer and Atkinson, 2014). This, together with the ongoing urbanisation of low-lying coastlines (Nirupama & Simonovic, 2007), points to an increase in population and economic asset exposure in these zones, with severe consequences aligned with this growth (Smith and Matthews, 2015).

When overwash occurs along anthropogenically developed low-lying coastlines, the vulnerable inhabited zones are subject to seawater flowing into urban areas and posing an immediate threat to the population (Takagi *et al.*, 2016). These overwash flows can cause extensive damage to the built environment, with the resulting debris adding to the volume of the final washover deposits (Izumida *et al.*, 2017). Indeed, the occurrence of overwash transports and deposits 10,000-100,000s cubic metres of sediment and debris in built environments annually (Nordstrom, 2004; Rogers *et al.*, 2015). Such washover often blocks roads restricting access and disturbing the response of emergency services to aid isolated and injured inhabitants, as well as hindering the ability to repair damaged utilities (Environment Agency, 2018; Johansen and Tien, 2018).

A lack of real-world examples of built washover deposits has led to their morphology remaining relatively unknown. One reason for this is the 'bulldozer effect' (Lazarus and Goldstein, 2019), whereby bulldozers are used to clear the roads for settlements to be reconnected, disrupting these built deposits (Nordstrom, 2004, Figure 3-1). Until repeat satellite imagery has the return times capable of capturing deposits in built environments before clearing has started, it remains challenging to collect widespread data on these landforms. To permit appropriate planning mechanisms to be put in place to improve the resilience of coastal settlements, the impacts of storm surges on humans need to be assessed and understood (Tahvildari and Castrucci, 2021).

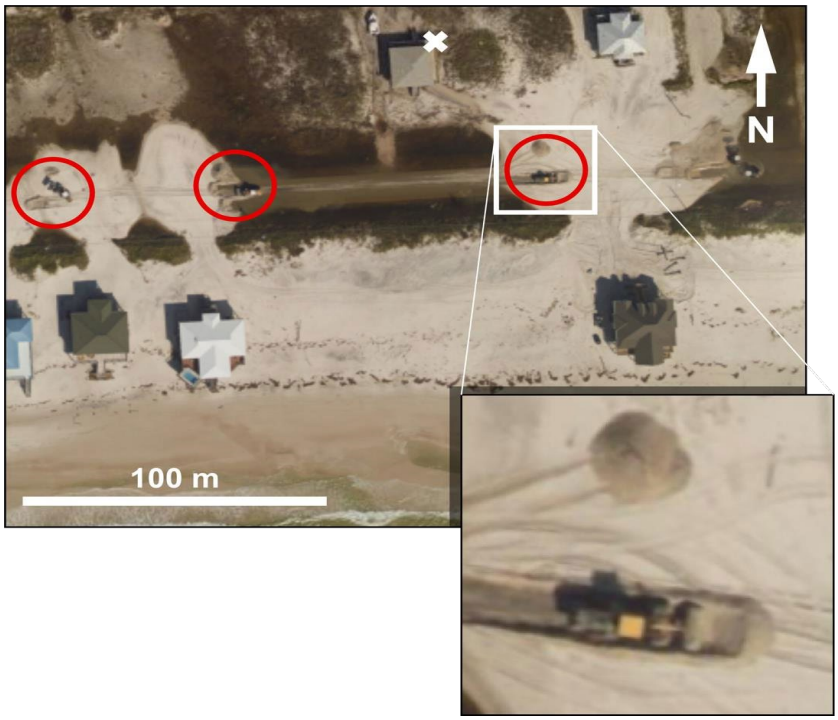

Figure 3-1 The "bulldozer" effect in action. Excavators, as circled, removing sand deposited during Hurricane Nate on Dauphin Island, Alabama, 10/10/2017 – two days after hurricane landfall (Location X: 30°15'03"N, 88°10'77"W.) Image courtesy of NOAA.

Anthropogenic changes to coastlines, including coastal defences, building development, and road production, alter the landscape's natural sources, pathways, and sediment sinks (Nordstrom, 1994). As such, natural and built settings must be viewed as separate entities when formulating scaling laws due to the impact of built infrastructure upon overwash flow and deposition (Nordstrom, 1994; Mignot *et al.*, 2006). Overwash flow in built settings is thematically related to research on tsunamis (Park *et al.*, 2013; Bricker *et al.*, 2015) and volcanic hazard (Gurioli *et al.*, 2005; Doronzo & Dellino, 2011) impacts on populated areas, as well as to atmospheric research into air flows over and between city buildings (Britter and Hanna, 2003). These studies have highlighted the dispersion and turbulence caused by building presence. In addition, increased available quantitative data regarding built environments (Mayer-Schönberger and Cukier, 2013) has enabled researchers to study built settlements with greater efficiency and efficacy. These can include measures of street networks, i.e., length/density, and the built infrastructure, i.e., building density/total area (Boeing, 2017).

Morphometric scaling laws can define consistent mathematical relationships between physical attributes and are a simple yet powerful predictive tool even when encapsulating complex morphological processes (Dodds and Rothman, 2000). Such relationships are derived using the size components extracted during the study of washover deposits. Morphometric attributes for

globally distributed natural washover deposits have previously been attained for width, length, and area (Hudock *et al.*, 2014), yet these deposits ranged in age - so aeolian processes may have altered them post-deposition (Leatherman and Zaremba, 1986). Further, experimental washover deposits for natural coastal floodplains conformed to Hudock's results and deposit fans on Mars (Lazarus, 2016). However, comparative scaling laws for deposits in built settings still need to be constructed to observe the human impact on natural norms.

Therefore, this chapter will develop morphometric scaling laws using flood-driven sediment deposits digitised from post-storm aerial imagery on US coastlines in various natural and built environments.

3.2.2 Hurricane events

Barrier islands and low-lying coasts on the Atlantic and Gulf coasts of the US regularly experience overwash caused by hurricanes and intense storms. Washover deposits along these coasts are ubiquitous and remnants of recent and historical extreme weather events. Therefore, this chapter focuses on examples of hurricane-induced washover in this region. Below is a brief outline of the selected hurricanes and the areas affected by washover where examples will be sourced.

1) *Hurricane Irene (2011)*

Hurricane Irene started on the 15th of August 2011 off the Atlantic coast of Africa as a tropical wave before moving across the ocean and making landfall as a category three hurricane in the Bahamas (Avila and Cangialosi, 2012). From here, it weakened whilst moving north and hit North Carolina as a category one storm, with 38 ms^{-1} winds causing surges up to 3.4 m in height (Muis *et al.*, 2019). All washover deposits (natural and built) sampled from Hurricane Irene are located in North Carolina.

2) *Hurricane Sandy (2012)*

Hurricane Sandy began as an intense Category three hurricane just south of Cuba but weakened to Category 1 as it passed over high-elevation land in Cuba. However, the storm then grew to have a diameter of more than 1100 miles – the biggest in the history of the Atlantic basin and re-strengthened to Category 3 once more. Before landfall in the US, it developed weather fronts, becoming a hybrid hurricane and winter nor'easter (Halverson and Rabenhorst, 2013). It made landfall on the 29th of October 2012 and lasted three days. It affected an area spanning much of the Atlantic coast of the US and Canada from Florida to Newfoundland, including major cities such as New York, Atlantic City and Ontario. Winds of over 30 m/s (Martínez *et al.*, 2021)

instigated observed sea heights of up to 2.9 m along the coast of New York state (Muis *et al.,* 2019). Hurricane Sandy caused 233 deaths, with economic costs exceeding US$70 billion (Blake *et al.,* 2013). All the sampled washover deposits from Hurricane Sandy are in New Jersey.

3) Hurricane Matthew (2016)

Hurricane Matthew affected the Atlantic coast of the US between the 6th and the 9th of October 2016 (Thomas *et al.*, 2019). It reached Category 5 strength during its shore-parallel path along 1900 km of the US coastline (Stewart, 2017), with wind speeds over 70 m/s (Thomas *et al.,* 2019), causing surges of 2.3 m. As a result, hurricane Matthew became the deadliest Atlantic hurricane since 2005, triggering 603 fatalities in Haiti and the US. Several washover deposits were sourced from North Carolina, South Carolina, and Florida.

4) Hurricane Nate (2017)

Hurricane Nate began as a tropical depression near Central America. It moved through the Gulf of Mexico after strengthening to a Category 1 storm – with winds reaching ~41 m/s. It made landfall during the evening of the 7th of October 2017 in Mississippi. It has been estimated that 500 km of low-lying coastlines experienced storm surges over 0.6m in height over mean higher high water (Beven and Berg, 2018) – the average water level of the highest tide. Nevertheless, some areas experienced surges of over 2 m (Beven and Berg, 2018). Hurricane Nate's natural and built washover deposits were all sourced from Dauphin Island in southwest Alabama.

5) Hurricane Michael (2018)

Hurricane Michael was a Category 5 storm with sustained winds of 72 m/s that made landfall along the coast of Florida on the 9th of October 2018 (Kennedy *et al.*, 2020). Starting as a large area of low pressure in the Caribbean Sea, it rapidly intensified over the Gulf of Mexico. Beven *et al.* (2019) indicated that it became one of the most powerful storms on record to hit the continental US, with winds over 71 m/s observed. The storm surge of 4 m upwards (Beven *et al.,* 2019) caused flooding further inland than expected for a 1-100 year storm – suggesting the previous estimates of potential inundation extents of such an event were inaccurate. The washover deposits sourced from this storm were all located along the northwest coast of Florida, just Southeast of Panama City.

3.3 Methods

The methods section is split into four parts. It begins by detailing the data sources, including acquiring the necessary post-storm imagery data, with information provided regarding its temporal and spatial resolution. The method then describes the extraction of physical measurement of real-world washover deposits, followed by the generation of sediment deposits using a simple numerical model – and the background to this model. Finally, it specifies the analytic steps, encompassing a novel physical metric used to explore the data in depth.

3.3.1 Data sources

Storm imagery

Post-storm aerial imagery was sourced from the National Oceanic and Atmospheric Administration (NOAA) using their online database many of storm events (available online at: https://storms.ngs.noaa.gov/). This dataset has been compiled to aid emergency response by providing a resource for coastal managers to assess the visual damage to affected regions (National Geodetic Survey, 2020). The NOAA Remote Sensing team captured the aerial photos at various altitudes using a Trimble Digital Sensor System (DSS). Imagery for Hurricanes Matthew, Nate, and Michael was obtained from altitudes of 2500 - 5000 feet, Hurricane Irene from heights of 5000 - 7500 feet and Hurricane Sandy from 7500 feet. Regarding image resolution, the Ground Sample Distances (GSD) are provided. The lowest GSDs are available for Hurricanes Michael and Nate at 25 cm, 35 cm for Irene and Sandy, and 50 cm for Matthew.

Following data collection for each storm event, the images were subject to pre-processing by NOAA. Firstly, the raw photos were orthorectified through OSSIM software using GPS-Aided Inertial Navigation parameters powered by elevation data. Subsequently, the individual images were collated into a seamless mosaic.

Built fabric parameters

Buildings and streets were sourced to quantify the "built fabric" of different environments affected by washover. Buildings were extracted from an open-access database consisting of US building footprints published by Microsoft – using the version available in January 2020 (**https://github.com/microsoft/USBuildingFootprints**). The data comprises 129,591,852 building footprints created from satellite imagery using computer algorithms. The building footprints are downloadable at the state level in a GeoJSON format which is helpful for encrypting geographic data structures. Due to the Hurricanes sourced, the GeoJSON files downloaded were from Alabama, Florida, North Carolina, South Carolina, and New Jersey.

Street networks were sourced from Open Street Maps (OSM) – downloaded from Geofabrik (https://download.geofabrik.de/). Geofabrik is an open-source data service allowing street networks and other OSM data to be downloaded free of charge for a specific region – here, they were extracted for the necessary US states. Contributors ensure that the data within OSM is kept up-to-date and of high accuracy. The street network downloaded was provided as a shapefile in the polyline data format.

3.3.2 Real-world washover deposits

3.3.2.1 Digitisation

Data visualisation and analysis were undertaken in ArcGIS Pro 10.2.5. Once loaded into the GIS software, all data was projected into their relevant NAD 1983 coordinate system zone – in this case, zones 16N and 18N as needed.

The NOAA post-storm database was used to find storms that induced several washover deposits in natural and built environments. The georeferenced orthorectified post-hurricane aerial imagery was manually filtered through. This process narrowed the dataset down to five hurricanes: Irene, Matthew, Michael, Nate, and Sandy. Where a GIS server address was available in WPS (Web Processing Service) format, the hurricane imagery could be opened in the GIS software without downloading data or loading individual aerial images. The specific swath for the correct date and location (with the least amount of cloud cover) was downloaded in GeoTIFF format when this function was unavailable.

For each hurricane, separate shapefiles were created for the natural and built washover deposits, with each deposit saved as an individual polygon. A natural washover deposit example was observed when the sediment extent was absent of anthropogenic development. Whereas a deposit in a built setting was defined as washover that interacts with the presence of any buildings or human infrastructure; for example, one building interacting with the deposit edge. The deposits, captured within days of the hurricane strike, were digitised manually. For consistency, the process was undertaken by one individual using the scale derived from the spatial resolution of the imagery. The number of natural and built washover deposits for each storm is shown in Table 3-1.

Table 3-1 Information regarding the hurricane events sampled – dates of landfall and aerial imagery capture. The number of built and natural washover deposits per storm event is provided.

Hurricane	Landfall	Imagery Dates	Built Deposits	Natural Deposits
Sandy	29th of October 2012	31st of October and 1st of November 2012	83	56
Nate	7th of October 2017	10th of October 2017	21	20
Michael	10th of October 2018	11th and 14th of October 2018	7	12
Matthew (FL)	7th of October 2016	9th of October 2016	10	-
Matthew (NC)	7th of October 2016	10th of October 2016	4	-
Matthew (SC)	7th of October 2016	9th of October 2016	-	9
Irene	27th of August 2011	28th of August 2011	42	18
total			**167**	**115**
Corresponds to the locations shown in Figure 3-2B.				

Where areas of sediment inside a deposit's extent had already been cleared from the street network, the deposit limit was distinguished using ridges of sand palpable at the edge of roads. Three physical parameters: length, perimeter, and area, were collected from these deposits and added as fields in the attribute tables. Example deposits, with the morphometric components labelled, are presented in Figure 3-2, along with the distribution of washover sampled along the Atlantic and Gulf coasts of the US. First, the measure tool manually quantified the length (intrusion distance). The length was defined as the distance from the seaward deposit edge to the most inland extent, perpendicular to the shoreline. Then, the software calculated the perimeter (m) and area (m^2) using the calculate geometry tool. In the built environment, a separate perimeter shapefile was created for each storm to capture only the outer perimeter of a deposit rather than any interior geometry caused by building presence. Therefore, this data management method required fifteen shapefiles, three for each hurricane event: 1) natural deposits, 2) outer perimeter extents for built examples, and 3) the washover deposit area for built examples.

3.3.2.2 Built fabric analysis

The 'built fabric' effect was assessed using the building footprints sourced from Microsoft and the street networks from OpenStreetMaps. First, the GeoJSON files for each state were converted into a shapefile format using the JSON-to-Feature-Class geoprocessing tool in ArcGIS to make the building footprints usable. To ensure that the buildings interacting with a built deposit edge are captured during analysis, convex-hull bounding boxes around each deposit were created using the Minimum-Bounding-Geometry tool (Figure 3-2). Next, the area of each convex hull was calculated. The Intersect tool allowed the buildings to be clipped to the extent of the convex hulls. This retained the parts of buildings interacting with the deposit edge alongside those entirely encapsulated within the deposit, e.g. where the convex hull passes through the middle of a building, the portion inside the bounding box will be extracted. In the attribute table of the resulting "interacting buildings" shapefiles, each building polygon was automatically labelled with the ID of the built deposit they interact with. These were then merged based on their deposit ID to create one building polygon per deposit. Finally, the total building area could be calculated within each convex hull bounding box. These processes allowed the built fraction to be calculated by dividing the total building area within a convex hull by the convex hull bounding box area.

The intersect tool was also utilised to clip the street network, yet this used the original deposit extents as the spatial limit rather than the convex hulls. The street length was taken as the total length of streets within the footprint of a deposit – calculated by merging the street polylines for each respective deposit ID and generating their total length.

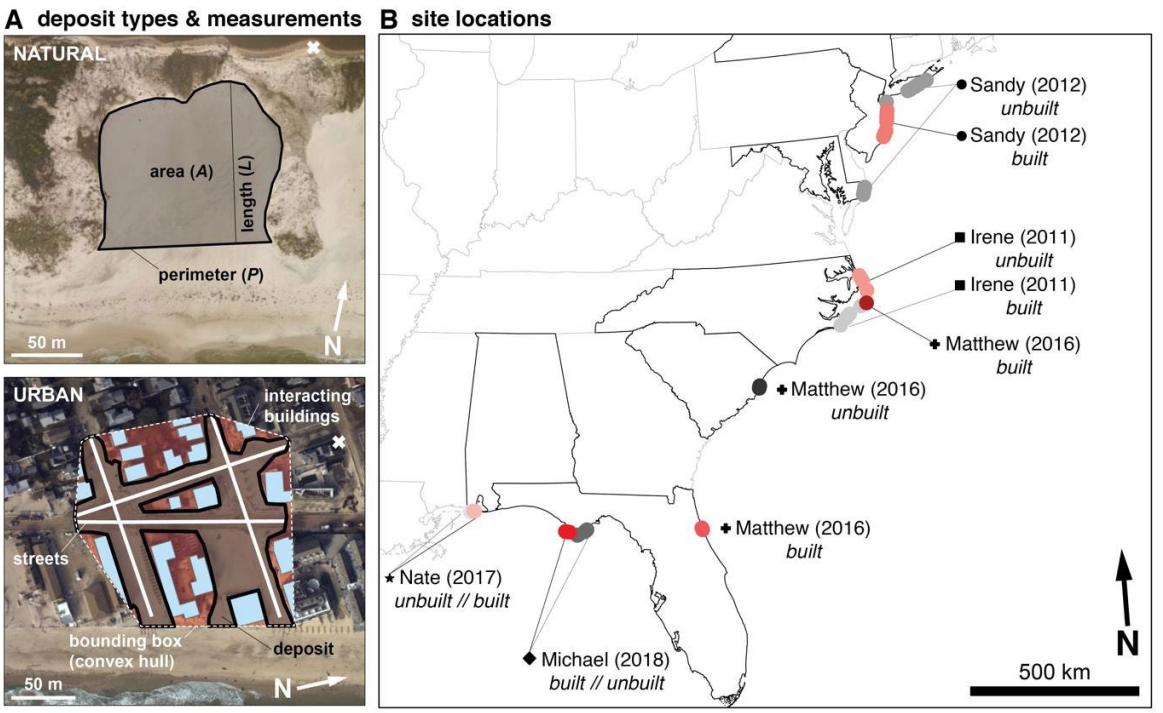

Figure 3-2 Washover deposition in natural and built settings examples and sampled locations A) An example of both a natural (location marker x: 30°14'5"N, 88°16'55" W) and built (location marker x: 40°5'19"N, 74°2'22" W) deposit with the measured physical metrics (length, perimeter, and area) and the built variables sampled in this research – buildings and streets. The natural deposit in the upper panel was created by overwash induced by Hurricane Nate (2017) on Dauphin Island, Alabama. The built washover deposit in the lower panel is from Hurricane Sandy (2012) and is located on Point Pleasant Beach, New Jersey. B) Map of the washover deposits sourced, labelled by hurricane name, and coloured by deposit type. Deposits from built environments are shaded red according to their relative built fraction, and natural deposits are greyscale.

3.3.3 Simple numerical model

3.3.3.1 Model background

To accompany the real-world washover deposit dataset, a simple numerical model was sourced to generate deposits. The model used in this study is an adaption of the simple numerical model for generating washover deposition created by Lazarus and Armstrong (2015), coded in Matlab (available at https://github.com/envidynxlab/Model-World). Previously, this model has been utilised to analyse deposits formed in natural environments and the spacing of washover deposits along a barrier island (Lazarus and Armstrong, 2015). In their work, Lazarus and Armstrong (2015) highlighted that washover deposits along a barrier are self-organised i.e. they

form as a function of the interactions between sediment flux, overwash flow routing, and the topography of barriers. Here it is instead used exclusively to produce deposits in artificially built environments to allow their morphology to be assessed. Although other numerical hydrodynamic models are available at higher levels of complexity wherein they resolve overwash processes in four dimensions (Roelvink *et al.,* 2009), the use of this simplified cellular model within an exploratory context enables an observation of whether a comparatively constrained set of processes can produce results comparable to that found in the real-world work. Further, a model of relatively low complexity provides the capability to undertake a substantial number of experiments efficiently – allowing a wide range of building densities to be investigated.

The model itself is based on a flat, grid-cell domain comprised of rows (i) and columns (j) (i and j signifying alongshore and cross-shore position, respectively). The principle force powering the function of the model is the height of the water (H) on the seaward side of the barrier. The erodible barrier, of single column width, is placed along the left hand edge of the grid and given a starting height of $Z_b = 1$. At the beginning of the model runs (t = 0), the barrier and water heights are in equilibrium – at even levels. In order to create water flow across the shore (from left to right), two incisions are generated at random locations in the barrier column of the domain. The depth of each incision is defined as $d_i = bA_i$, wherein A_i refers to the disparity between the height of the first and second columns of cells, whilst *b* represents a sustained proportion of the barrier height, in that, d_i always remains much less than Z_b. The flow of water across the barrier column takes place when the water height exceeds that of the barrier (initially in the incision locations). The water along the barrier is considered a conserved quantity – with the water height reducing after each time step based on the volumetric amount of water being discharged through the barrier from the sea.

The discharge (q_b) through the breach in the barrier column is governed by the proportion (p) of cells along the length of the column nearer to the particular breach than to the other breach generated – as proposed by McNamara and Werner (2008). Consequently, the discharge though a specific breach is dependent on its location alongshore compared to the other barrier incisions.

$$q_i = p_i(H_i - Z_{bi})$$

Equation 3-1

After entering the barrier column, the flux of water further into the domain is driven by proportional distribution to the nearest downslope cells, with sediment movement from cell to cell defined as a proportion of the total water flux: $q = cq$, where c is a constant between 0 and

1. Sediment movement is prohibited where the slope between cells is positive. Additionally, a threshold parameter is included (q_{wmin}) which sets out the minimum water depth necessary to transport sediment between cells. Using the above processes, the topography of the model domain evolves at each timestep as flow is propagated across the surface behind the barrier column. Flow propagation ends when the water depth is insufficient to advance further downslope. At this point, a topographic contour is utilised to capture the terminal position of the washover deposit.

The model also incorporates a periodic boundary location which allows the domain to diffuse in the alongshore dimension – occurring at the start of each time step. Although this process is not critical to model dynamics, it allows two assumptions to be carried through the model runs. Firstly, it enables the erodible barrier column to be seen as non-cohesive and unarmoured by vegetation, and secondly, that flow into the throats from on top of the barrier leads to the widening of an incision.

3.3.3.2 Model runs

The model setting used was a grid of 100 x 100 cells with the seaward edge having an artificial erodible barrier of the height z = 1 and the area inland comprising constant flat elevation. The sea's water level was initially set at the same height as the erodible barrier island (z = 1). Buildings were added as a grid of blocks, with their length increased by one cell after each trial, with streets being kept at a constant width of 4 cells to test a range of building set-ups. The buildings were defined as square in shape, non-erodible, and z = 2 in height to prevent overtopping. This model set-up aimed to capture a series of artificial built fractions, not to test specific real-world built environment scenarios. An example of the model set up is provided in Figure 3-3.

Each built fabric set-up was tested 25 times – using a different breach location in every model run and a new breach size. The cell representing the location of the breach was randomly selected from within the 60 most central cells along the barrier to prevent the deposit from reaching the edge of the domain. Moreover, this random allocation allows the chance that in some of the trials, the washover was blocked immediately by building presence and could not penetrate further into the setting. In others, the washover flowed straight into the street network, diverging through the gaps between buildings and subsequently through the built environment. The likelihood of the washover being blocked was raised when the built fraction was increased.

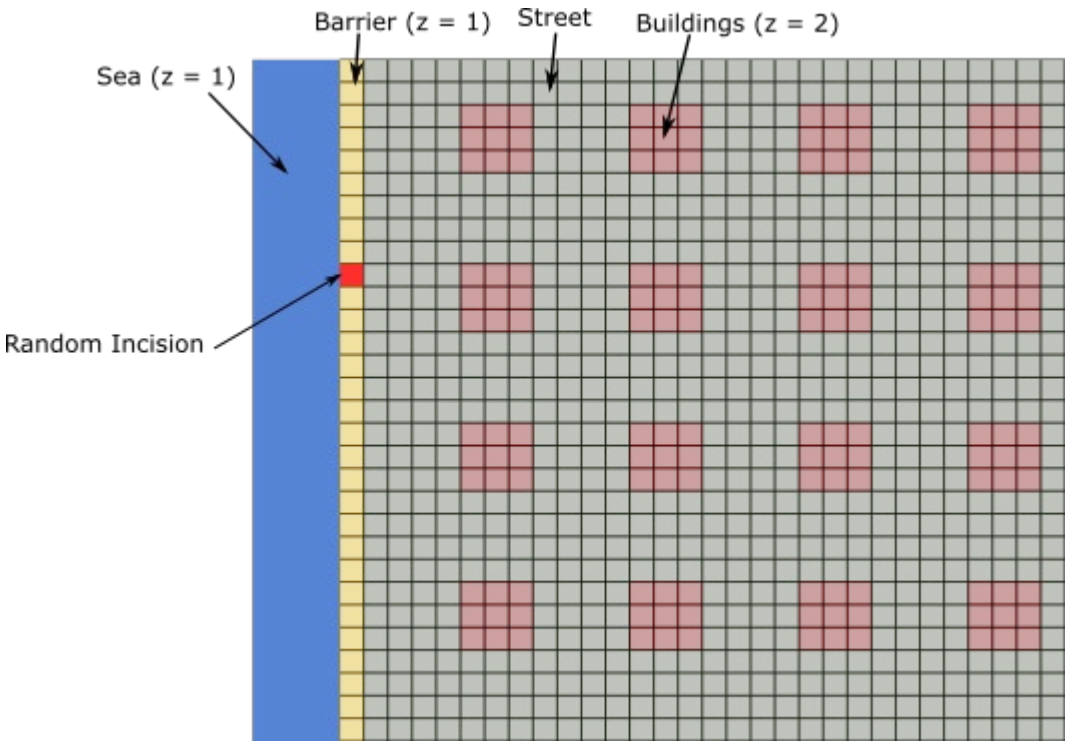

Figure 3-3 An example of the model set up (actual set up was 100 x 100 cells). Here, two random incisions are shown in the barrier, with the sea and barrier characterised by height z =1, and the buildings incorporated at a height of z = 2 with street widths of 4 cells.

Changing the breach height with each model run allowed an assortment of deposit sizes to be created for a given built environment. The heights used were randomly selected from between 0.1 - 0.7 as a proportion of barrier height (z = 1). Where a low built fraction characterised the built environment, the washover size produced in a trial was correlated with the breach size. These chosen configurations of the range of breach sizes and locations allow various washover deposits to be created and the built environment's impact to be assessed.

Overwash flow into the built domain occurred when the water height exceeded the barrier height at the breach location. As the water moved through the barrier breach as overwash flow, the seaward water level decreased due to the volumetric loss over time. In this model, sediment was transported through the domain and deposited elsewhere as a function of the flow depth in each cell. A threshold depth must be defined to provide the basis for sediment movement – where flow depths drop below this threshold, deposition occurs. Regarding the flow direction through the model domain, the flow depth of a particular cell was proportionally dispersed to its adjoining cells with a lower elevation. This has the effect of overwash and washover fanning into the built environment from the barrier breach.

Each model was run for a specified duration of 20 iterations. After this time, the deposits had typically stopped growing as most of the washover was formed quickly within the first few iterations. Therefore, this period is set for convenience and efficiency. The washover deposit ceased to grow when the flow depths were too shallow to transport any additional sediment. Further, restricting the model runs to this duration meant that when the built fraction was low or null, the washover deposits did not reach the most landward edge of the setting, removing the effects of boundary conditions.

3.3.4 Analysis

Morphometric scaling laws were created to examine how the physical attributes of washover deposits relate to each other in natural and built environments. These relationships can simplify complex physical geomorphic processes and thus provide a useful predictive tool even when there is little understanding of the mechanisms underpinning them (Dodds and Rothman, 2000). Here, the scaling laws examined were length vs area, and perimeter vs area, with a comparison of the relationships between the settings. These relationships were constructed in linear space using $y = Cx^b$ as a nonlinear regression (c being the coefficient and b being a scaling component). The results were then plotted in natural log space.

In addition to these morphometric laws, this research defined a novel dimensionless metric named the "Distortion Index" (DI) – formulas are provided below (Equations 3-1 to 3-5). This measure aims to analyse the relationship between perimeter and area by comparing the perimeter measured (p_m) to the perimeter of a "perfect" idealised semi-circle (p_i) calculated using the same area value as the measured washover. DI allows the complexity of the deposit perimeter to be simplified to a planform path and how much it deviates from an ideal, non-disrupted deposit perimeter. In this case, the ideal non-distorted shape was chosen to be a semi-circle as it is a typical depositional fan shape in various morphological landscapes (Menard Jr, 1955; Donnelly *et al.*, 2006; Hoyal and Sheets, 2009). Consequently, DI can illustrate the impact of the depositional environment on a sediment deposit's "ideal" shape.

The idealised perimeter was calculated by rearranging the formula for the area (measured area = A_m) of a semi-circle (Equation 3-2) to make the radius (r) the subject (Equation 3-3):

$$A = \frac{1}{2}\pi r^2$$

Equation 3-2

$$r = \sqrt{\frac{2A_m}{\pi}}$$

Equation 3-3

This definition of a semi-circles radius was then substituted for r in the circumference formula for a semi-circle (Equation 3-4):

$$Circumference\ of\ Semi\ Circle = \pi r + 2r$$

Equation 3-4

The ideal perimeter (P_i) was defined as the circumference of a semi-circle (which includes the outer arc of the shape added to the diameter – 2 x the radius). The final form of this formula is presented below (Equation 3-5):

$$P_i = (\pi + 2)\sqrt{\frac{2A_m}{\pi}}$$

Equation 3-5

Distortion Index (DI) was then calculated by dividing the measured perimeter (P_m) by the derived idealised perimeter (P_i) for a semi-circle of the same area (Equation 3-6):

$$DI = \frac{P_m}{P_i}$$

Equation 3-6

A multiple linear regression model was utilised to assess whether deposit area, built fraction, and street length could be used to predict the morphological structure of the real-world washover deposits. This provided the opportunity to see to what extent deposit distortion (response variable) can be accurately estimated from the combination of these three explanatory variables. The analysis highlighted that the dependent variable was not normally distributed, so the values were converted to logarithmic equivalents to make them suitable for the regression model. The linear model function was utilised in R, which provides the significance of each variable and the adjusted R-squared value for the prediction of distortion from the three variables. Before accepting the results from the regression model, it was necessary to ensure the variables used conformed to the assumptions needed to validate the results. This involved ensuring that there was no multicollinearity between the independent variables, the residuals were normally distributed with constant variance (homoscedasticity), the variables used were

normally distributed, and the residuals were uncorrelated (Uyanık and Güler, 2013). The multicollinearity was tested using the variance inflation factor (VIF), which produced values ~2 for each independent variable – lower than the threshold of 10, wherein the variable should be removed from the model (Mason and Perreault, 1991). Once these assumptions were confirmed, the results could be analysed.

Following this, the same linear regression methodology was utilised for the data produced by the numerical model, with the absence of street length as a predicting variable – just built fraction and deposit area. In this case, the distortion index values were not subject to a logarithmic transformation, as the raw values were normally distributed.

3.4 Results

This section presents the results from the empirical real-world washover alongside the numerical model findings. These results provide quantified measures of the morphology of washover and their differences between unbuilt and built environments.

3.4.1 Scaling laws

The empirical methodology undertaken permitted morphometric scaling relationships to be constructed between length and area and perimeter and area, using real-world measurements of washover. These geomorphic laws can demonstrate mathematical relationships between morphological measures of a landscape feature. Observing the scaling laws developed here (Figure 3-4, panels A and B), there are clear positive correlations between length and area, and perimeter and area, in both natural and built settings. All these relationships are shown as significant ($p < 0.001$) with minimal standard errors (SE) present – 0.03 and 0.02 in both environments, for length vs area and perimeter vs area, respectively.

Panel A (Figure 3-4) indicates no discernible difference between the two depositional environments' length vs area scaling relationship. The scatterplot visually shows a slight variation between natural and built domains, with an even spread of data points on either side of the trend lines for each environment. Indeed, the gradients of the lines of best fit - $h = 0.35$ and 0.36 - imply that as deposit area increases, length increases at a similar rate in both depositional settings. Furthermore, the inset histogram in panel A suggests a considerable overlap in the distributions of L/A between natural and built settings – suggesting that, for a given area, the distance a deposit extends onto a barrier island is not significantly impacted by the environment it interacts with. However, there is a higher frequency of L/A values above ~0.6 within the built sample compared to the natural dataset – suggesting that in some

situations, the built environment causes washover to be longer for a given area than that observed in a natural context. It could be noted that the channelling effect imparted by buildings and streets results in greater washover intrusion lengths.

Meanwhile, panel B (Figure 3-4) suggests that perimeter is a more sensitive metric when differentiating washover morphology between natural floodplains and built environments of varying building densities. In general, sediment deposits extending onto developed floodplains have the potential to have longer perimeters than those in natural settings for a given area. This finding is emphasised by the relative gradients of the lines of best fit, whereby built has an h value of 0.59, whilst natural has an h value of 0.46. Therefore, as the washover area increases, the perimeter of deposits in built environments rises faster than natural deposits. Using perimeter as a metric against area prevents the data from collapsing to a single relationship, as shown in length vs area configurations. Although some washover in built environments exhibit similar morphologies to natural landforms using this metric - highlighted by the areas of overlap in the P/A histogram and the positions of the dark blue data points in the scatterplot – many built washover diverge from the scaling norms existing in the natural domain. The inset histogram in panel B shows a vast deviation between the two environments, with a substantial proportion of the built P/A values over 0.72. In contrast, most of the natural washover deposits lie beneath this threshold.

Distortion Index (DI) is utilised to examine the structure of the relationships between the perimeter and area in each depositional environment. In panel B of Figure 3-4, the built data points have been coloured by DI values. By doing so, a gradient in DI demonstrates that deposits with more extensive areas in the built environment have the potential to be more distorted than smaller washover deposits. In the more extensive built examples, DI can regularly exceed a value of 2, whereas the DI for their smaller counterparts rarely breach 1.6. The DI values of the built washover, which overlap with the unbuilt examples, remain below 1.2 - 1.3, suggesting their perimeter is 20/30% higher than a semi-circle with the same area. However, it is also evident that several smaller deposits exhibit elevated distortion levels in that high DI values are not limited to large deposits.

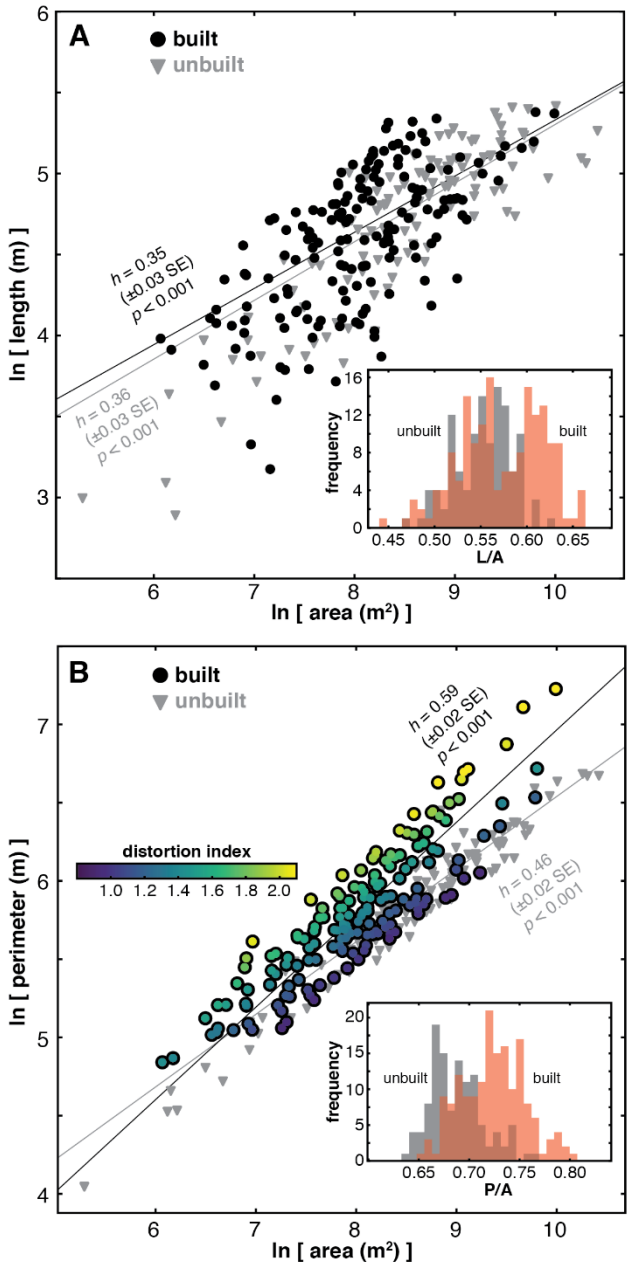

Figure 3-4 Scaling laws for hurricane deposits in unbuilt and built environments. **A)** Relationship between washover length and area (black circles = built and grey triangles = unbuilt). **B)** Relationship between washover perimeter and area from built (circles with black outline) and unbuilt (grey triangles) environments. Each panel includes a histogram displaying the distribution of the L/A and P/A ratios, unbuilt (grey bars) and built (orange bars) settings are depicted. The colour gradient added to the built deposits shows the DI of each washover. The trend lines were derived using nonlinear regression ($y = Cx^b$) in linear space and then plotted in log space – provided are the gradient, standard error, and p values.

3.4.2 Distortion Index

3.4.2.1 Real world

DI is used to explore the impact of the "built fabric" of built environments on washover morphology in the coastal zone, with the distributions demonstrated in Figure 3-5. This plot highlights that built washover can exhibit substantially higher DI values than deposits in unbuilt settings. However, a wide range of distortions can occur in each environment. DI has been plotted against the area, with the points coloured by a built fraction (Figure 3-6:empirical and modelled) and street length (Figure 3-7 empirical) - providing an additional dimension to the relationship between DI and area. Before looking at the deposits in built environments, it is evident that a range of distortions are present in the natural, real-world dataset. DI values of close to 1 characterise most natural washover, i.e., semi-circle with the same area. However, some natural deposits exhibit higher distortion values of around 1.5, independent of the storm event (Figure 3-5).

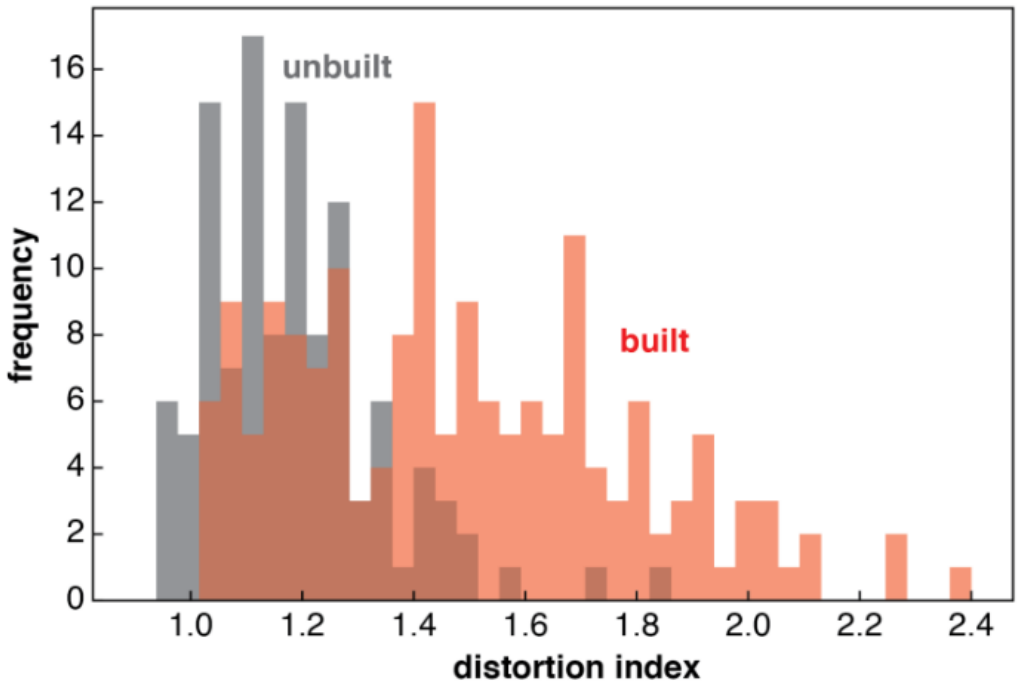

Figure 3-5 The distribution of the Distortion Index of washover sampled in unbuilt and built environments.

In analysing the washover in built settings, a positive relationship exists between built fraction and DI (Figure 3-66, Figure 3-8, Figure 3-9). However, when looking closely at the empirical dataset, washover in built environments display a vast range of DI values, from low distortion, where they overlap with natural deposits (Figure 3-6), to heavily distorted, dependent on the built fabric and washover size. The mean DI values of deposits found in unbuilt and built

environments are provided for each hurricane in Table 3-2, with the mean built fraction shown for the built washover.

Table 3-2 Summary statistics of DI values within each hurricane event. The mean built fraction for each hurricane is provided for the deposits extending onto anthropogenically-altered floodplains.

Setting	**Built**		**Unbuilt**
Hurricane	**Mean BF**	**Mean DI**	**Mean DI**
Sandy	0.13	1.65	1.2
Nate	0.04	1.14	1.18
Michael	0.14	1.45	1.17
Matthew (FL)	0.14	1.31	-
Matthew (NC)	0.15	1.46	-
Matthew (SC)	-	-	1.04
Irene	0.1	1.37	1.23

The overlap of washover in built settings with the deposits sampled from natural conditions exists where the distortion index ranges from 1 – 1.5, which occurs under two circumstances. Firstly, much overlap transpires when the deposits extend into urban areas with low building density. However, it can also happen when the deposit size is small, regardless of the built fraction. In this scenario, small deposits in a densely constructed built environment can have a similar shape to small deposits in open, unbuilt settings. An example of the former situation is provided in Example 1 in panel A of Figure 3-6. This deposit was created by Hurricane Nate and is located on Dauphin Island, Alabama – a low-density built environment (shown in Table 3-2) – with this sedimentary feature experiencing a built fraction of 0.01 and having a DI of 1. Several other deposits interacting with sparsely built environments also occurred during Hurricane Nate on the same barrier island - as shown by the number of start symbols in this section of the plot – where morphologically, these deposits are similar in shape to natural washover. Here, the built fabric of affected areas at Dauphin Island has a low mean built fraction of 0.038 m^2/m^2, leading to a mean DI of 1.14, similar to the natural deposits.

Washover deposits that intrude into developed coastlines with built fractions between 0.1 - 0.2 can show DI values over 1.6, dependent on their size. Example 2 in Figure 3-6 was found in Seaside Park, New Jersey, following Hurricane Sandy, with a DI of 1.7 caused by a moderately high built fraction of 0.18. This deposit is an elongated splay extending down a street perpendicular to the shoreline from the fronting dune, diverging into driveways and spaces between houses. Finally, when the built fraction of an urban environment exceeds 0.2 in the empirical dataset, it can cause DI values above 2. Example 3 in Figure 3-6, again from Hurricane Sandy but located at Bay Head to the North of example 2, is a large washover deposit (area = 9.655 ln[m^2]) which interacts with a dense urban fabric (built fraction = 0.22) and is consequently heavily distorted (DI = 2.4). This deposit first interacts with a dense urban fabric close to the shorefront. Then it extends into two streets perpendicular to the beach further inland once portions of the deposits have joined together on a road parallel to the beach, midway along the intrusion length. All the buildings in the initial deposition segment are encapsulated by the convex hull bounding box and the structures between the two furthermost inland streets.

The other built environment metric investigated was the length of the street network within a washover deposits footprint. The scatterplot in Figure 3-7 is presented similarly to Figure 3-6 but coloured by street length instead. The street length provides qualitatively comparable results but is more scattered than the built fraction metric. The plot has a clear lateral colour gradient whereby, as the deposit area increases, the street length the sediment interacts with rises. However, there is a slight vertical colour gradient from low distortion to higher distortion, particularly for the deposits with a larger area – where the largest deposit, which interacts with the most extended street network, is the most distorted.

3.4.2.2 Numerical model

In the case of the numerical modelling results in Figure 3-6B, the general pattern reflects that of the empirical dataset, even though the model-run domains were set up to capture double the range of the built fraction. For a given deposit area, an increase in built fraction leads to deposits becoming increasingly distorted – shown by the vertical colour gradient from blue (low built fraction) to yellow (high built fraction). In addition, when separating the data points by a built fraction, there are strong positive correlations between deposit area and distortion index. This implies that DI values also rise for similar building densities as the deposit area increases. Some deposits generated by the numerical model are situated in the lower left of the plot, particularly from high-built fraction domains, where deposit area and DI are both low.

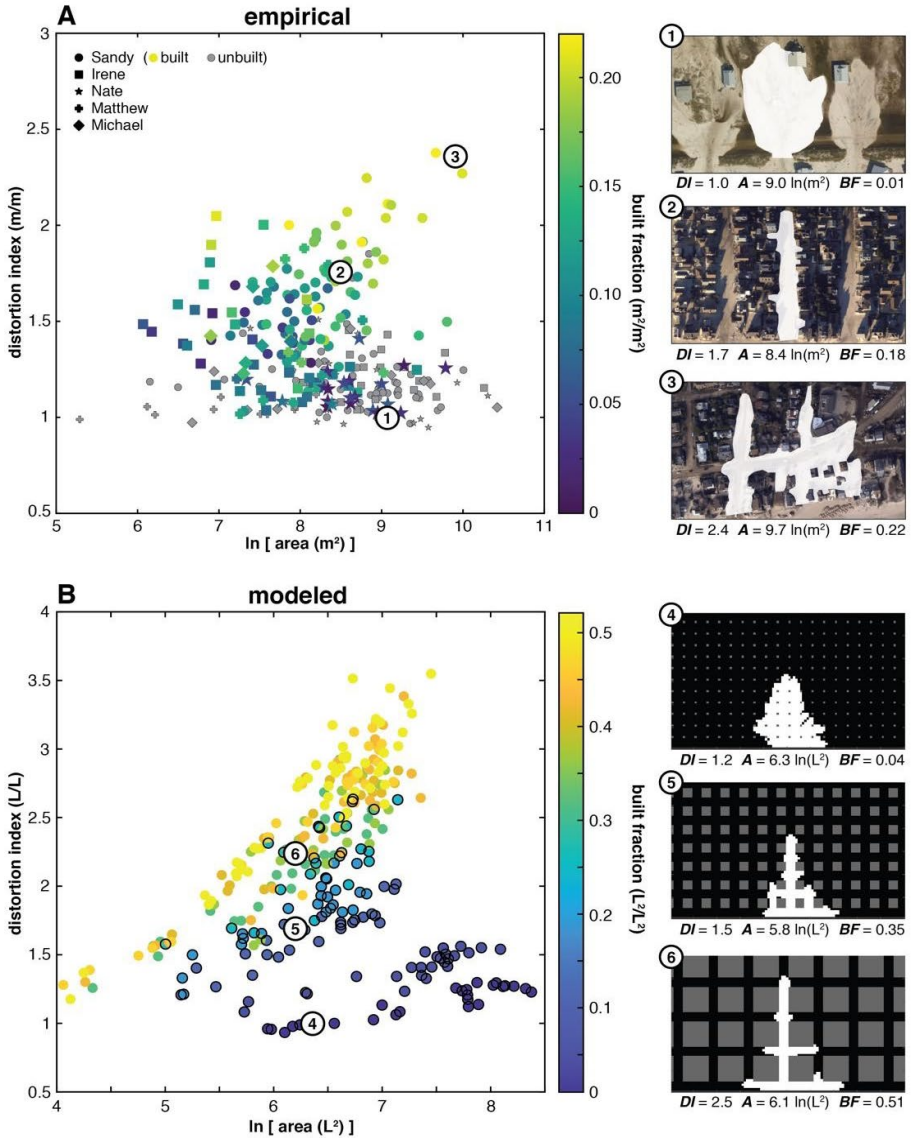

Figure 3-6 Scatterplots depicting DI of the washover, as a function of area, coloured by built fraction. (**A)** Scatterplot for the empirical data – symbols depicting the hurricane event that induced deposit formation. Grey symbols represent washover deposits extending onto natural settings. To the right of the plot are three examples from the empirical samples – with white outlines and DI, area, and Built Fraction labelled. 1) A low DI example created by Hurricane Nate on Dauphin Island, Alabama. 2) A medium DI example created by Hurricane Sandy at Seaside Park, New Jersey. 3) A high DI example created by Hurricane Sandy at Bay Head, New Jersey. Imagery sourced from NOAA. **(B)** Scatterplot for the numerical model data. The built fractions tested were on a larger scale than the empirical methodology – the circled points highlight data points where the built fractions were within the real-world samples. The examples provided to the right of the graph illustrate a (4) low, (5) medium and (6) high DI.

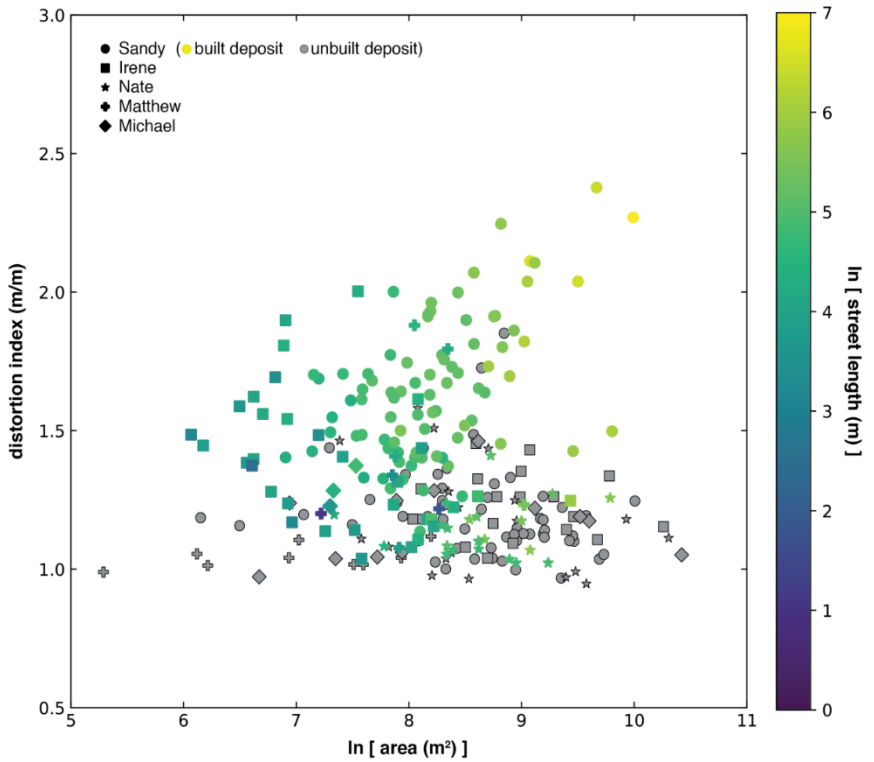

Figure 3-7 DI of washover deposits as a function of area, coloured by street length for the empirical, real-world washover deposits. Symbol shape depicts the hurricane event that has created deposition, and grey symbols represent the occurrence of natural washover – with no streets present.

3.4.2.3 The response of the Distortion Index to various built fabrics

To assess the relationships between the built fabric of the coastal environment and the distortion index of individual deposits, the distortion index values of washover in built environments were plotted against both built fraction and street length for the empirical dataset (Figure 3-8, panels A and B, Figure 3-9), and built fraction for the model examples (Figure 3-9). Focusing on built fraction, there is a clear overlap between the data points from the real-world deposits and the washover generated by the model. Although a range of distortion values can occur for any built fraction, taking the maximum DI value at each built fraction shows a strong positive relationship between the two variables using both methodologies. Using the real-world data as an example (Figure 3-8A), the maximum distortion at a built fraction of approximately 0.05 is 1.6, which increases to 1.9 at a built fraction of ~0.17, whilst a built fraction of 0.2 has the potential to create deposits with a DI reaching 2.3. In the real-world dataset, the minimum DI increases as the built fraction increases – for the range of built fractions observed. This same pattern is shown in the model dataset until a built fraction of 0.25. After that, however, the model creates deposits intruding into built environments double the density of the highest built fraction observed in the real-world examples. When the built fraction rises beyond 0.25, the minimum DI decreases as the urban environment's density increases. Therefore, this highlights that a similar density of built environment can induce a variety of deposit morphologies, potentially through channelling and blocking effects.

Regarding the relationship between street length and DI, there is a steep positive linear relationship for many deposits. This trend indicates that the longer the size of the street network that the deposit interacts with, the more the washover can be distorted. Although this pattern appears to be independent of the depositional event, many of the deposits in the upper right corner of the plot were created in urban environments along the coast of New Jersey during Hurricane Sandy. However, some deposits do not conform to this trend whereby they have interacted with a small amount of street length, i.e., the two leftmost points from Hurricane Matthew. As a result, these two deposits have higher distortion index values (approximately 1.2) than many deposits interacting with a greater total length of street networks.

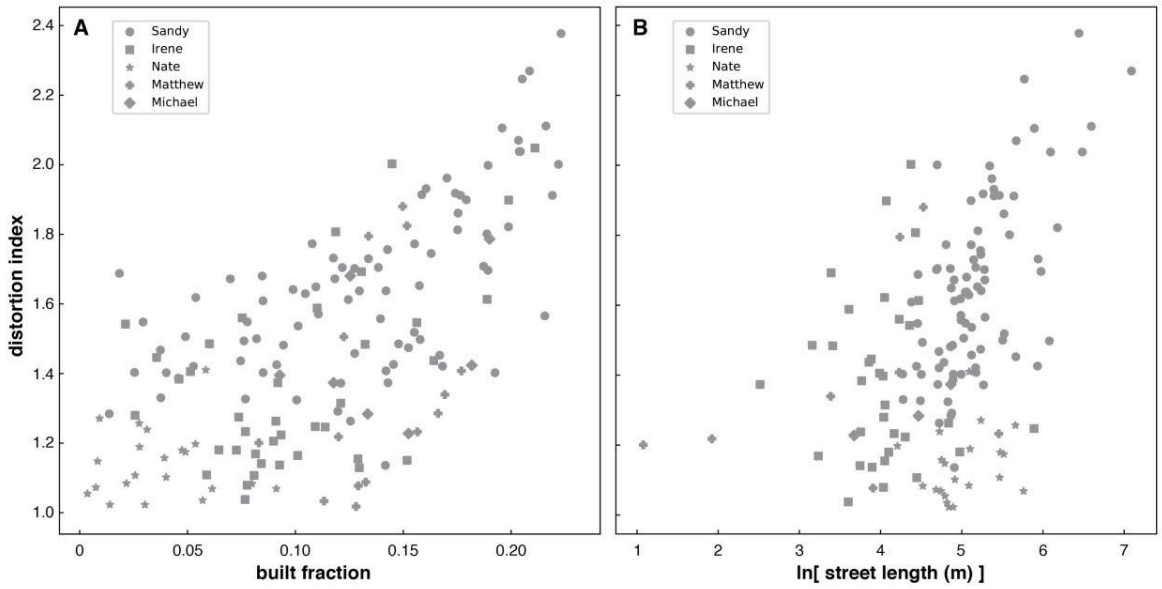

Figure 3-8 DI of washover deposits plotted as a function of a) built fraction and b) street length for the empirical data. Hurricane events are indicated by symbol shape.

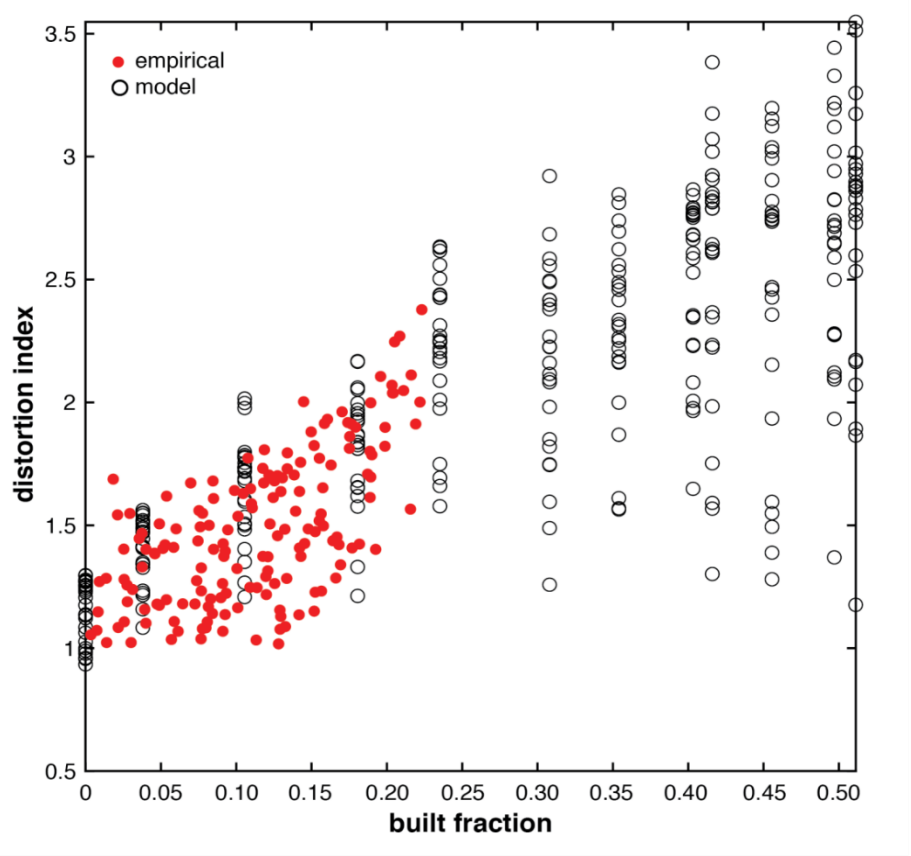

Figure 3-9 DI of the washover, plotted as a function of the built fraction. Red dots represent empirical deposits from figure 3-7A, and open black circles depict modelled results. The simple numerical model tests hypothetical scenarios with built fractions extending to double those observed in the real-world dataset.

To further investigate the impact of the built environment on real-world washover morphology, a multiple linear regression model was used to observe how deposit area, built fraction and street length can combine to predict deposit distortion. After ensuring that the assumptions of linear regression models were fulfilled, the adjusted R-squared value and p-values can be reported (Table 3-3). These statistics indicate that the amalgamation of deposit area, built fraction and street length can account for approximately 51% of the variance in distortion index values, as implied by the adjusted R-squared output. Moreover, the p-values generated for the individual predictors indicate that the influence of each explanatory variable was significant in predicting the distortion index to the 99.99% confidence level. Lastly, it was found that the residuals were normally distributed and symmetrical around zero, implying that the model fits the data well. This is substantiated by the overall p-value (99.99% confidence level), suggesting that the combination of explanatory variables in the whole model fits well with the observed distortion index values.

Meanwhile, the linear regression utilised for the morphometric data generated by the numerical model produced a very close-fitting model using deposit area and built fraction to predict distortion. From figure 3-4B, an interaction between the built fraction and deposit area exists to influence subsequent deposit distortion, given the positive gradients of DI within each built fraction tested, as the area increases. As such, when the explanatory variables were incorporated into an exploratory model in R, the best-fitting model included the interaction between area and built fraction. The statistical results of this linear regression model are included in Table 3-3. The model created using the numerical model dataset has a better fit than the results from the real world, with the explanatory variables explaining 84% of the variance in distortion values, demonstrated by the R-squared value. Moreover, each input variable significantly impacts DI, using the p-values generated at over a 99.9% confidence level. The overall p-value ($p < 0.001$) of each model suggests that the combination of explanatory variables provides a very well-fitting model in predicting the distortion index values produced.

Table 3-3 Multiple linear regression model summary statistics predicting DI of washover deposits from built fraction, deposit area, and street length (only in real-world deposits).

Dataset	R-squared	Model p-value
Real-World	0.556	$p < 0.001$
Simple Model	0.846	$p < 0.001$

3.5 Discussion

The results above have extended upon the previous body of research into washover morphology in natural coast environments and provided novel morphometric information concerning washover in various built environments. The results attained from exemplar washover deposits are derived from the Atlantic and Gulf coasts of the US. Nevertheless, the method can be extended to other settings affected by overwash processes, with emerging sources of open-source, high-resolution satellite imagery permitting access to new study sites. Through the real-world empirical and numerical model results, this study has demonstrated that the scaling relationships associated with washover in natural and built settings do not depend on the storm event. Instead, it is highlighted that the spatial conditions set by the built environment impart a fundamental control on deposit morphology through governing sediment pathways and sinks – as suggested by Nordstrom (2004).

3.5.1 Is there a morphological difference between washover deposits in unbuilt and built environments?

Previously, geometric scaling laws for washover were representative of deposits in natural environments (Hudock *et al.*, 2014; Lazarus, 2016; Lazarus *et al.*, 2020). Within natural settings, this research sampled 115 sedimentary deposits induced by five hurricane events, whilst in built environments, a dataset comprising 167 examples of washover was created. Initially, it was shown that there is a minor difference in the length vs area scaling relationship between the two depositional settings. In the scatterplot and histogram provided in figure 3-4A, there is substantial overlap between the two datasets, with the trend line having a similar gradient. The primary reason for this is the variety of washover deposit shapes that can be produced in built environments – governed by the layout of the built infrastructure. In some densely built settings, blocking pre-existing sediment pathways is commonly induced by built obstacles. Here, deposit length is low relative to the area, and data points are located beneath the line of best fit, with these deposits being broader than they are long, i.e. shaped like a washover terrace (Morton and Sallenger, 2003). Thus, they intrude less distance inshore for a given area than many deposits formed in a natural setting.

Meanwhile, in anthropogenically-developed settings with low built fractions, the deposits experience little disturbance to their lengths. However, the inset histogram in Figure 3-4A does suggest a portion of the built washover has a higher L/A ratio than that commonly found in the natural environment – illustrated by the black data points furthest above the trendlines in the scatterplot. A potential explanation is that although built obstacles can limit the lateral spread

of a deposit, sediment is often channelised down streets with low friction and no barriers (Nordstrom, 1994). This results in washover deposits which are narrow and elongated in shape, meaning the intrusion length will be higher relative to the area. Therefore, although the built environment can influence the respective length and area of individual deposits across a range of built fabrics and locations, the morphology averages out to create a similar trendline as that of natural sediment deposits. As such, the use of the trendline alone is limited, and instead, the relationship is more nuanced.

On the other hand, the difference between washover deposited in natural and built environments is more evident when considering their scaling relationships of perimeter vs area. In this case, the morphological relationships of the deposits in built environments diverge from the scaling norms set out in the natural domain. It is evident that longer perimeters typically characterise deposits in built settings for a given area. Furthermore, the steeper gradient of the trendline for the built deposits indicates that as the deposit area increases, the gap between deposit perimeters in both environments widens. Applying the distortion index values to the scaling relationship of perimeter vs area Figure 3-5 demonstrates that deposits encroaching on built coastlines are likely to be more distorted than smaller urban deposits relative to their unbuilt counterparts. Thus, it can be deduced that the greater the washover area in each built environment, the more it can differ morphologically from natural washover.

A consequence of this disparity between deposit morphology in unbuilt and built settings is that landforms in each environment must be viewed as separate entities when formulating scaling laws, given the effect of built infrastructure on overwash flow and sediment deposition. The data generated here is the most in-depth quantitative evidence concerning the disturbance effect that human-altered coastlines have on the natural norms of sediment deposition. As initially suggested by Nordstorm (1994), it is evident that built environments have a profound impact on coastal sediment processes and the resulting landform morphology. However, this only becomes clear when looking at scale-dependent effects on specific morphological scaling laws or by utilising newer indices, such as the presented distortion index, to differentiate between unbuilt and built environments.

3.5.2 To what degree do elements of the built environment impact deposit morphology?

The morphology of washover can be split into deposit size and shape, with human infrastructure influencing both. So far, it has been shown that washover deposits that extend into built environments are morphologically different to natural deposits. Therefore, this chapter has

incorporated measurable elements of the built environment that differ between the sampled built washover, i.e. the dimensionless built fraction and street length, which have previously been determined as useful spatial metrics concerning urban development (Boeing, 2017). Different built infrastructural elements of developed coastlines provide the conditions within which the complex processes governing flood-driven sediment deposition must operate. As such, the built fabric exerts a first-order control on sediment landform morphology regarding size and distortion.

3.5.2.1 Deposit size

Several factors can define the extent of land covered by sediment following the occurrence of overwash – irrespective of the built environment. Naturally, a fundamental aspect is the size and duration of the storm event triggering overwash. These features drive the storm's energy, which directly governs the sediment supply from the water to the shoreline by controlling the storm surge's transport capacity (Liu and Fearn, 2000; Matias *et al.*, 2016). Aside from this, various environmental conditions can influence deposit size within a given storm. These include sediment characteristics (grain size) and its local availability, the surface roughness of the affected landscape, fronting dune characteristics, i.e. spatial heterogeneity, height, and volume, and whether the primary facet of overtopping water onto the back-barrier is wave action or storm surge (Donnelly and Sallenger, 2007; Houser, 2009).

The built infrastructure on barrier islands significantly impacts the sediment delivered during overwash events (Rogers *et al.,* 2015). The data created in this chapter does indicate that deposits typically have a smaller area in built settings relative to those in unbuilt locations (Figure 3-6). However, comparing washover size between the two depositional environments is challenging as storm size is not necessarily constant within and between storms. As detailed in the hurricane events section of the background, the strength of the five hurricanes sampled ranged from category 1 to 5 when they made landfall on the US coastline. The grain size will also differ by hurricane landfall location and concurrent changes in sediment availability.

Moreover, various locations within storm events along the shore could involve the wave set-up varying spatially, causing the storm size to not be uniform, potentially due to variances in topography and front dune set-up (Nott, 2006), as well as the direction the shoreline faces relative to the storm front (Fletcher *et al.*, 1995). This is highlighted by natural deposits in this work, created during the same storm, differing in size even though they are nearby. Consequently, it is tricky to isolate the built environment's impact on deposit size unless storm size and sediment supply can be controlled or monitored. However, given that the smallest deposits form under the high built fractions in the modelling work (Figure 3-6), it is evident that

high-density obstacles can block and prevent the growth of washover - highlighting the control built infrastructure can impart on deposit.

Although from different storm events and locations along the US coast, this study's findings regarding deposit area corroborate the results from Rogers *et al.* (2015). Using topographic surveys of LiDAR (Light Detection and Ranging) before and after Hurricane Sandy, Rogers et al. (2015) found 40% and 90% reductions in sediment quantity delivered in residential and commercial built settings, respectively, when compared to natural washover deposits. Indeed, they also suggest that dense commercial-built environments prevented overwash from occurring along ~50% of the reach studied. It has been demonstrated in this work that the built environment can block and disturb pre-existing sediment pathways and sinks. The presence of human development on coastlines provides obstacles to overwash that can directly affect sediment supply to the landscape, which impacts landform morphology (Hoyt, 1968; Stutz and Pilkey, 2001). Buildings and seawalls, amongst other built infrastructure, can completely block storm surge flows (Rogers *et al.,* 2015), reducing sediment supply. Furthermore, they can dissipate the energy within overwash, causing the flows to have a lower transport capacity meaning the entrained sediment cannot be carried as far onto the shore, leading to smaller washover deposits.

3.5.2.2 Deposit shape

Previously, it would have been necessary to analyse washover shape qualitatively. However, the definition of the Distortion Index provides a quantitative tool to investigate how the environment manipulates a deposit's shape by looking at how far its shape diverges from that of a semi-circle. From the analysis undertaken, it has been shown that the planform shape of coastal sediment deposits is independent of the storm the washover is produced by and instead is fundamentally governed by the spatial components of the built environment the overwash interacts with – namely the set-up of buildings and the geometry of the street network available to facilitate sediment movement.

A range of washover deposit shapes have been observed and recorded within the real-world built environment dataset, with three key examples in the panels of Figure 3-6. Panel 1 portrays a low-density built environment where the DI of the deposit is low. The anthropogenic development on this barrier setting, with one building present, has negligible impact on the morphology of the washover deposit compared to if it was completely unoccupied. Meanwhile, the deposit shown in Panel 2 is restricted in its distribution as it enters a narrow road perpendicular to the coastline and does not reach any intersections in the street network. Instead, it forms an elongated lobe with limited width yet has a medium DI as it branches onto

driveways and into the gaps between buildings. Finally, the landform presented in Panel 3 indicates a large washover deposit interacting with a sprawling, dense built environment characterised by widespread infrastructure. In this instance, the overwash intrudes into two parallel streets running perpendicularly to the shoreline, with the deposit then merging and branching further into the built domain. These three deposits were chosen as examples as they provide a vivid visualisation and quantification of how different urban footprints can affect the shape of sedimentary features.

To further examine the relationships between the built fabric and their respective impacts on deposit morphology, two multiple linear regression models were utilised to see how variables could predict distortion index. The model used for the real-world data incorporated three explanatory variables: built fraction, street length and deposit area, whilst the regression for the numerical model used built fraction and deposit area as predictors. The r-squared and p-values values obtained for both regressions indicate that the predictor variables impart a first-order control on washover deposit shape. However, a clear discrepancy exists between the real-world empirical data and the numerical model dataset. The r-squared value of 0.51 in the real-world regression differs from that of the model (0.84). This implies that extraneous variables affecting sediment deposition patterns in the real world are not encapsulated in the simple model – which focuses solely on the impact of built obstacles on deposit morphology, so other factors remain unaccounted for. To highlight this, the results from the model in Figure 3-6B show clustering by building density, whereas the data in the real world in Figure 3-6A shows far more substantial variation – with some deposits exhibiting high DI values despite extending into moderately dense urban environments.

Factors affecting the sediment supply and subsequent routing and deposition on the barrier islands and low-lying coasts should first be considered, as they can directly impact landform morphology (Hoyt, 1968; Stutz and Pilkey, 2011). Along the shoreline, the fronting dunes can be a range of sizes, and in some areas – they may not even exist. In such places, the sediment supply will be minimised. Whereas, along coastlines with large fronting dunes – sediment supply during overwash is increased due to the increased erosion that can occur, which generates mobile material (Nott, 2006). Furthermore, more potent storms with a longer duration can increase the sediment supply to an inland environment if all other environmental conditions are the same (Donnelly *et al.,* 2006). In relation to this research, differences in sediment availability, which can be governed by natural factors such as fronting dune morphology and storm size/duration, can alter the distance hurricane deposits can intrude into a given built environment. Indeed, the findings here indicate that where deposits extend further into a built environment, they exhibit higher DI values due to interacting with a greater area of the built

fabric. Therefore, when sediment supply is maximised, the distortion will be highest – within the same urban setting, suggesting natural factors influencing the initial sediment availability play a substantial role.

Once the initial sediment availability has been determined, there are also natural features inland from the fronting dune within built settings, which can act to shape deposits through altering sediment pathways and sinks, separate from the built structures present. Firstly, variations in topography can work to channel and disrupt overwash flows (Morton and Sallenger, 2003), whereby elevation change can change the speed of storm surges and thus its energy – directly impacting the water's capacity to transport sediment and/or change the direction of flows by diverting the course of the overwash (Kain *et al.*, 2014; Soria *et al.*, 2017). Moreover, variations in elevation can create areas of slow-moving sediment-laden water in surface depressions where deposition occurs due to the reduction in the flow's energy – leading to overwash fans being restricted by local topography (Donnelly *et al.,* 2006).

Aside from this, the presence of vegetation and the density of such fauna can contribute to the surface roughness of coastal floodplains. Increased roughness leads to greater flow resistance and can change the sedimentary landforms' morphology (Donnelly *et al.,* 2006). In this context, vegetation can act as sediment traps, capturing material from the overwash flows and instigating deposition earlier than expected (Nepf and Koch, 1999; Feagin *et al.*, 2015). Within this research, many of the washover deposits in the real-world dataset would have interacted with front lawns/gardens and local parks/shrubs. These influences are unaccounted for as factors controlling deposit morphology. Nevertheless, they may provide some guidance as to why the explanatory power of the built fabric to predict deposit distortion was so different between the real-world dataset and that of the simple model.

Finally, elements of anthropogenic developed coastlines - that are not encapsulated in the built fraction or street length parameters - can play a substantial role in shaping washover deposits. For example, human-made flood defences, such as groins and seawalls, can disrupt storm surges by affecting swash velocity and deflecting waves – manipulating the energy and direction of the flow (Plant and Griggs, 1992) and, consequently, natural sediment movement and budgets. Furthermore, these structures can capture sediment and create new sinks for the material (Nordstrom, 1994) – altering the morphology of the final washover deposits. Another facet of the urban environment affecting the terminal shape of coastal sediment deposits that are not accounted for in the simple model are fences, driveways and other anthropogenic structures that block and divert flows. Driveways provide smooth, low-friction routes for storm surges to move through and onto. This study highlights this primarily by the elongated deposits down

one street in the real-world dataset, with no interactions with road intersections. Here, several deposits (e.g., in Figure 3-6 Panel 2) branch into driveways as they intrude into the built domain. As a result, these washover deposit examples exhibit low built fraction values relative to their distortion index as they interact with few buildings and are instead shaped by factors not quantified in this study.

Additionally, on many low-lying coasts, buildings are often elevated on stilts to make them less susceptible to damage from overwash as a hurricane-proofing measure (Givoni, 1994; Abdelfatah *et al.*, 2022). In regions with this typical building style, the impact on flow direction and speeds will be negligible, as water can remain undisturbed (Nordstrom, 2004). Therefore, this research approaches all buildings as the same – which may not necessarily be true – and instead, the washover deposit may continue under the buildings.

3.6 Chapter Summary

This chapter, using washover data generated by a combination of post-storm aerial imagery and a simple numerical model, has provided new information regarding the morphology of coastal deposits in unbuilt and built environments and, consequently, has achieved the three objectives defined in this chapter's introduction.

1. Expand on the existing shortage of empirical measurements of real-world washover deposits in both natural and built settings, determining if a morphological difference exists between the two environments.

In total, 282 washover deposits were sampled from post-storm aerial imagery, 115 and 167 from unbuilt and built environments, respectively. The results extended on previous research (Hudock *et al.*, 2014; Lazarus *et al.,* 2016), which focussed on deposits formed in natural domains, showing how different built fabrics disrupt the scaling norms constructed in unbuilt settings, with patterns of channelising and blocking being prevalent. In addition, a novel metric, termed Distortion Index, has demonstrated that the shape of the deposits differs between depositional environments, with deposits in built settings typically exhibiting higher DI values, yet with some crossover between settings.

2. Explore the impact of components of the built fabric on the morphology of coastal washover.

It has been established that the higher the built fraction – the higher the potential for the deposit to be distorted more from a natural deposit shape with the same area, whilst the street network provides pathways for sediment distribution. The findings of a linear regression model suggest

that built fraction and street length are significant explanatory variables in predicting DI, with over 51% of variance explained.

3. Investigate whether sediment deposits generated using a numerical model with a range of "built fabrics" align with the morphometric data from real-world examples.

The data obtained from the numerical model illustrated that built fraction again had a substantial impact on deposit shape, with the built fractions tested here exceeding the real world by double. However, the linear regression model run for the numerical model shows a disparity between the predictive power of variables from the real-world dataset (built fraction, street length and deposit area) and the numerical model (built fraction and deposit area) in explaining variance in distortion. Furthermore, as the model data regression exhibited a higher r-squared value than the empirical, it indicates that extraneous variables such as vegetation, fences and surface roughness can influence the real-world deposits – which are not picked up in the model domain.

The next section of this research will investigate flood-driven sediment deposition in natural and built fluvial environments. The first step is a review of the literature, which will focus on the existing knowledge of deposit morphology and models able to generate them.

Chapter 4 Sediment deposits on fluvial floodplains

This background chapter is separated into four parts exploring the current understanding of crevasse splays. This will include an outline of the formation of crevasse splay deposits and the factors influencing their terminal morphology, such as flood size and human activity. I begin with a brief introduction to fluvial flooding will highlight its importance to floodplains and also its potential detrimental effects. The second section examines the formation of crevasse splay deposits and the controls on their morphology. I will assess existing numeric morphological models applicable to investigating crevasse splays in natural and built environments. Lastly, I will identify and outline an appropriate numerical model to utilise in studying crevasse splays.

4.1 Fluvial floods: importance and impacts

Fluvial flooding occurs when the water level within a river channel is increased to cause overbank flow, leading to the neighbouring floodplains becoming inundated. Such a change in water level primarily occurs due to heavy and/or prolonged rainfall (Douben, 2006). However, it may also result from breakages of natural or human-built dams, and snowmelt events (Hancox *et al.*, 2005; Feyen *et al.*, 2012; Tariq and van de Giesen, 2012). These floods can either be a rapid response as rain falls directly into the channel – typically in small, upstream catchments, or on a longer timescale where rainfall runs through a larger catchment and into the channel. Characteristics of the drainage basin: topography; presence and type of vegetation; and network density, shape the timing, duration, and size of fluvial floods (Samela *et al.*, 2017).

Frequent fluvial floods are essential for many floodplains – promoting connectivity between the river channel and local terrains (Heiler *et al.*, 1995). Indeed, fluvial floodplains cover approximately 2 x 10^6 km^2 of the Earth's land surface and, as such, represent substantial sedimentary reservoirs (Mitsch and Gosselink, 2015). Junk et al. (1989) proposed the flood pulse concept whereby flood events control the ecological and morphological systems encompassing the river corridor and adjacent floodplains. These floods allow the exchange of water, sediment, nutrients, and biota to and from the channel (Heiler *et al.*, 1995). River corridors and the surrounding floodplains are ecologically essential facets of a landscape. The movement of river-borne sediment and nutrients to nearby low-lying land is vital for productivity and biodiversity (Walling and He, 1998; Noe and Hupp, 2005). Morphologically, the sediment movement from the river channel to the floodplain plays a vital role in the construction and evolution of floodplains (Wolman and Leopold, 1957, Kooistra *et al.*, 2003). The fine sediment deposited on the typically flat terrain surrounding channels results in the vertical accretion and maintenance

of the floodplain surface, allowing the subsistence of the landscape (Middelkoop and Van der Perk, 1998; Walling and He, 1998).

Fluvial floods may threaten human life and property when they interact with human infrastructure (Koks and Thissen, 2016). River floods have directly inflicted more than 200,000 deaths since 1980 (Dottori *et al.*, 2018) and have induced economic costs of over US$1 trillion between 1980 and 2013 (Kundzewicz *et al.*, 2019). The threat of dangerous fluvial floods to humans is expected to rise due to socioeconomic development and climate change (Feyen *et al.*, 2012; Hirabayashi *et al.*, 2021).

Land use change on floodplains and in catchments can alter the time taken for fluvial floods to occur and can also affect their duration and size. The urbanisation of flood-prone landscapes with the addition of tarmac and concrete surfaces decreases the permeability of previously natural areas (Hu *et al.*, 2018; Li *et al.*, 2020), increasing both the speed at which surface runoff can reach river channels and the volume of precipitation reaching the channel (Kjeldsen, 2009). These factors can significantly impact peak discharges, influencing the timing, duration, and amount of overbank flow (Verbeiren *et al.*, 2013). The conversion of land for agricultural purposes through deforestation or the removal of smaller vegetation can have an impact. For example, in a model focussing on deforestation in the Upper Chao Phraya River Basin, Thailand, it was found that a 1% decrease in forest cover leads to an increase in annual discharge by 1.9% for the entire basin and a 2.5 - 5.4% increase in the upstream sub-basins (Zhao *et al.*, 2022). This study also highlighted that a 1% decrease in forest cover could cause the annual sediment load to rise by 8.7%.

Global warming is expected to increase heavy precipitation events – potentially leading to more frequent, high-magnitude floods. Indeed, Wright *et al.* (2019) indicated that these heavy rainfall events have already become more common in the contiguous US, and Du *et al.* (2019) found such precipitation patterns to be occurring globally. Using climate attribution frameworks, these local and worldwide trends in precipitation have been linked to human-induced global warming (Diffenbaugh, 2020). It has been projected that extreme rainfall could rise between 5 - 10% per degree of global warming (Pendergrass *et al.*, 2017). A combination of a high-resolution flood model and a climate model has indicated that a high warming scenario – whereby a 100-year rainfall event is increased by 20% in magnitude and ~200% in frequency – would cause a 30 - 127% rise in population exposure to flooding (Swain *et al.*, 2020).

The ongoing rise in flood occurrence and magnitude highlights a necessity to properly account for the risk that natural hazards pose to human life and safety in order to implement land management planning to mitigate disaster impacts correctly and reduce costs (Petak, 1985;

Manfreda *et al.*, 2011; Brunner *et al.*, 2021).The outlays directed on removing debris from built environments post-flood event, which can include substantial deposits of sediment (Nelson and Leclair, 2006; Brown *et al.*, 2011), are encapsulated within the costs associated with extreme disasters. Such debris can block access routes restricting the ability of emergency services to provide aid (USEPA, 2008), as well as damage vital infrastructure. Furthermore, the monetary cost involved in removing the debris can be expensive, as well as time consuming (FEMA, 2007). As a result, it is imperative that the effects of floods are understood through measurement and modelling, in order to reduce damage costs associated with extreme flood events (Smith, 2013; Huang *et al.*, 2021). Therefore, there is a need to increase the understanding of the morphological impacts of fluvial inundation events because linking components, including sediment, morphology, and built infrastructure, is vital for successfully coordinating flood risk mitigation measures and reducing disaster costs (Lane and Thorne, 2007).

4.2 Crevasse splay deposits

4.2.1 Crevasse splay definition and formation

During fluvial floods, sediment can be transported by high energy flows out of a river channel and deposited on the floodplain when the floodwater energy dissipates (Walling and He, 1998). For rivers characterised by levees that rarely breach or flat banks without levees, floodplain deposition is predominantly from flows going directly over the river bank – with fine washloads being transferred onto the floodplain (Pizzuto, 1987; Smith *et al.*, 1998; Adams *et al.*, 2004). This fine sediment can be transferred to inundated areas on the floodplain far from the channel due to the small amount of energy needed to transport these small grains (Syvitski *et al.*, 2012).

However, for other rivers which commonly breach their bankside levees, water with its sediment load is driven onto the local floodplain environments through these gaps (Smith and Perez-Arlucea, 1994; Nienhuis *et al.*, 2018). In addition, natural levees of low-gradient river systems often breach during periods of peak discharge in the initial flooding phase (Farrell, 2001; Toonen *et al.*, 2016; Chomiak, 2020), leading to the creation of landforms known as crevasse splays - common in alluvial and deltaic environments (Toonen *et al.*, 2016). Crevasse splays are described as overbank sediment deposits produced by the material being advected through levee breaches onto surrounding floodplains during the diversion of river water and sediment from the channel (Bristow *et al.*, 1999; Aslan *et al.*, 2005; Yuill *et al.*, 2016; Millard *et al.*, 2017). These materials can then form patches of high sedimentation near the channel belt on low-elevation areas of the adjacent floodplain (Shen *et al.*, 2015; Toonen *et al.*, 2016). Deposition typically

occurs in fan shapes as the floodwaters decelerate when they move out of a confined channel into a less confined environment (Iacobucci *et al.*, 2020).

Typically, the deposits are comprised of bedload material close to the breach, with suspended sediment dominating the deposition in the medial and distal portions of the splays (Burns *et al.,* 2017). As sediment is delivered and deposited in the splay, it decreases the crevasse bed slope causing the splay deposit to accrete vertically and backfills upstream into the levee breach (Yuill *et al.*, 2016). The deposit's growth subsequently tails off because transport capacity reduces as the splay grows, resulting in the crevasse splay being closed off from additional sediment supply (Roberts, 1997).

The understanding of crevasse splay formation and morphology is necessary as they are a significant component of land building (Nienhuis *et al.*, 2018) – contributing to levee growth (Bridge, 1984), floodplain elevation upkeep, and channel avulsion processes (Stouthamer, 2001). A crevasse splay located in the Mississippi River Delta (Figure 4-1), approximately 60 km^2 in size, could store over 75% of available sediment delivered to it – contributing significantly to the landscape (Esposito *et al.*, 2017). Given that they are standard morphological features, remarkably little is understood about how the shape and size of crevasse splays are affected by landscape controls (Millard *et al.*, 2017).

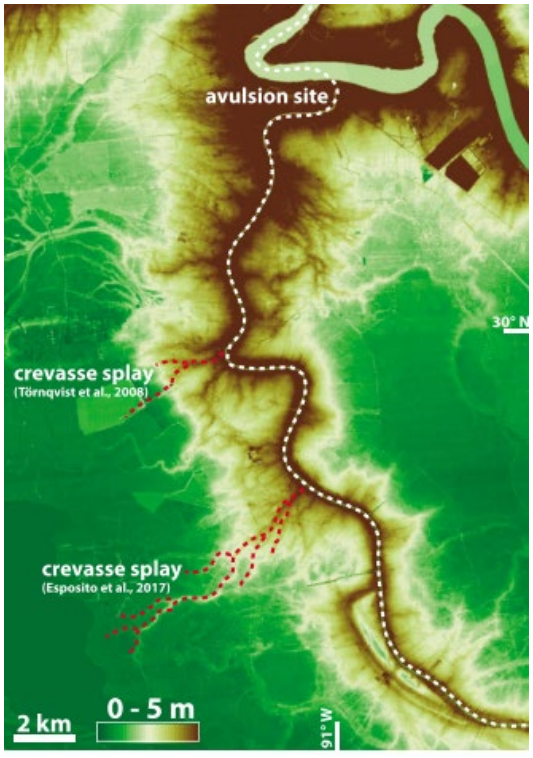

Figure 4-1 Elevation layer depicting two crevasse splay locations and their networks in the Mississippi River Delta (Nienhuis et al., 2018). The red dashed lines represent the

splays networks and the white dashed line the historic channel course of the Bayou Lafourche.

4.2.2 Crevasse splay morphology

4.2.2.1 Natural controls

Crevasse splays have been generated in diverse fluvial environments with various shapes and sizes between the domains (Millard *et al.*, 2017; Rahman *et al.*, 2022). Splay deposits are distributed worldwide; many are current features of landscapes, whilst others are retained in the stratigraphic record. Contemporary sedimentary environment examples can be found along the north bank of the Colorado River (Aslan and Blum, 2009), on the east and west banks of the Niobrara River, Nebraska (Bristow *et al.,* 1999), and 14 splays on the north slope of the Colville River Delta (Tye, 2004). These splay deposits range from 240 m to 4500 m in length and from 170 m to 1300 m in width. The morphology of crevasse splays is controlled by various factors, which can affect the amount of sediment transported onto the floodplain, and/or shape the formation and growth of splay deposits. These factors influence deposition patterns through three main processes: a reduction in flow energy, a reduction in flow depth, and an increase in floodplain roughness (Yuill *et al.*, 2016). Flow conditions, sediment characteristics, and floodplain features affect the size of splay deposits (area and volume) and their planform shape (Millard *et al.*, 2017).

The discharge of a river channel should impact the size of the splay deposit that can be generated, as it governs the energy present and, in turn, the quantity of sediment that can be entrained in the floodwaters funnelling onto the floodplain (Millard *et al.*, 2017). Furthermore, the initial discharge of floodwater - laden with sediment - dictates how far a splay deposit can extend into a given floodplain environment before energy is lost and deposition of all the material has occurred (Yuill *et al.*, 2016).

Crevasse splay and shape can also be affected by sediment size. The D50 of a river channel can govern the amount of sediment made available to the crevasse splay (Slingerland and Smith, 1998), and influence sediment deposition patterns (Park and Chu, 1991; Fedele and Paola, 2007). It was suggested by Millard *et al.* (2017) that larger grain size distributions lead to more extensive crevasse splay deposits. They posited that this is primarily due to finer sediment, such as silts and clays, being able to be transported out of the nearby floodplain zone in suspension. However, they did not explore the relationship between grain size and deposit size for the sediment that did not get washed away – with the silt results potentially skewing their findings.

This is especially pertinent as they only used three grain size distributions in their models to make their conclusions, including the silt distribution. However, it was still clear that the combination of discharge and grain size fundamentally controlled the mass balance of sediment provided to the floodplain and how effectively the material could be transported (Millard *et al.*, 2017).

Various external factors can influence the size and shape of crevasse splay deposits for a given discharge and grain size distribution. Firstly, riparian vegetation's presence, quantity and type can directly impact splays' formation, development, and terminal morphology (Esposito *et al.*, 2017; Nienhuis *et al.*, 2018). The presence of vegetation markedly affects floodplain roughness (Darby, 1999; Straatsma and Baptist, 2008; Tomsett and Leyland, 2019), which can considerably impact depositional patterns. The roughness of a floodplain dictates the amount of friction exercised by the surface on floodwater (Baptist *et al.*, 2007). Riparian vegetation on floodplain surfaces promotes sediment entrapment, concomitant with a reduction in the amount of erosion able to occur (Schumm and Lichty, 1963; Esposito *et al.*, 2017). The floodplain roughness is influenced by the structure of the vegetation, such as: the height and density; leaf presence, and the rigidity of the stems (Dawson, 1988; Straatsma and Baptist, 2008; Tomsett and Leyland, 2022). In high flow situations, vegetation can become the primary control of floodplain roughness, with the potential to substantially affect flood wave dynamics (Forzieri *et al.*, 2011) and, thus, influence sediment deposition. Indeed, research has indicated that the largest crevasse splays and highest land growth rates occur on floodplains with intermediate vegetation density (Nardin and Edmonds, 2014; Nienhuis *et al.*, 2018). This indicates that in floodplains comprising of higher density vegetation, sediment is trapped and a greater amount becomes deposited closer to the floodplain, whereas where vegetation is sparse, friction is low, so the flows are not slowed enough to induce widespread deposition.

Another control on crevasse splay morphology is the drainage conditions of the floodplain. The flood basin slope can alter sediment deposition rates once the flows extend through the levee breach (Pizzuto, 1987; Hajek and Wolinsky, 2012). The gradient of the slope impacts the floodplains efficiency in advecting sediment away from the breach. Millard *et al.* (2017) utilised two floodplain types: ponded and drained, with three models run for each environment in Delft 3D. The ponded floodplain replicated water entering a lake-like floodplain with a constant water level and reduced runoff. This floodplain was given water-surface levels 20 cm lower than the crest of the levee. Whereas the water level for the drained floodplain scenario was specified as 1.45 m lower than the levee crest, defined as 5 cm above the floodplain bed elevation in order to create a slope from the exit of the breach towards the edge of the model's domain. In running their models, the drained floodplain received 4 - 5x more floodwater and 5 - 8 x more sediment

than the ponded floodplains. Consequently, the crevasse splay deposits were more widespread in the drained environments, with channels commonly forming on the floodplain. The splays generated in the ponded set-ups were small, but thick, semi-circular deposits, because the floodplain runoff was slow and lacked the energy to transport substantial amounts of sediment from the river channel. As a result, the sediment that could be carried onto the ponded floodplain was deposited close to the levee breach.

The extent to which the soil is consolidated can impact splay morphology. For example, Nienhuis *et al.* (2018) highlighted that floodplains with more significant soil consolidation, e.g. thicker peats under the top surface, allow the formation of larger crevasse splays which can then stay active for longer. They put this down to a reduction in floodplain erodibility, with a more erodible surface leading to greater avulsion and scouring.

4.2.2.2 Impact of human activity on crevasse splays

The study of the quantitative impact of human activity on the natural morphology of landforms is an emerging field. Anthropogenic developments can alter the sources, pathways, and sinks of sediment - having the potential to disturb sediment budgets and change the morphology of the landscapes impacted (Nordstrom, 1994).

Despite this, the only research focussing on the morphology of crevasse spays in a built setting was undertaken in New Orleans following Hurricane Katrina (2005) (Nelson and Leclair, 2006). These sandy splay deposits are thought to have occurred because of a blowout of hydraulic piping, leading to levees' failure along the London Avenue Canal. The crevasse splays, which formed at the southern breach of the channel (illustrated in figure 4-2), covered an area of approximately 54,670 m^2 (excluding buildings) with an estimated volume of 26,380 m^3. The map shows that sand was deposited throughout the local street network and between built structures, with deposit thickness exceeding 1 m in places. Nelson and Leclair (2006) discuss how the streets and buildings within the urban environment spatially controlled the geometry of the splay. They suggested that there was channelisation of the flow and sediment down open streets, with the impervious surfaces providing efficient pathways. Consequently, splays were often thicker down one side of a road and where the accessible network widened, e.g. at intersections. In addition, high-velocity flood flow zones created between buildings provided the energy to transport the available sediment. Once the water had receded, recovery efforts quickly removed the deposit, and this explains why there are so few descriptions within the literature of splay morphology in built environments.

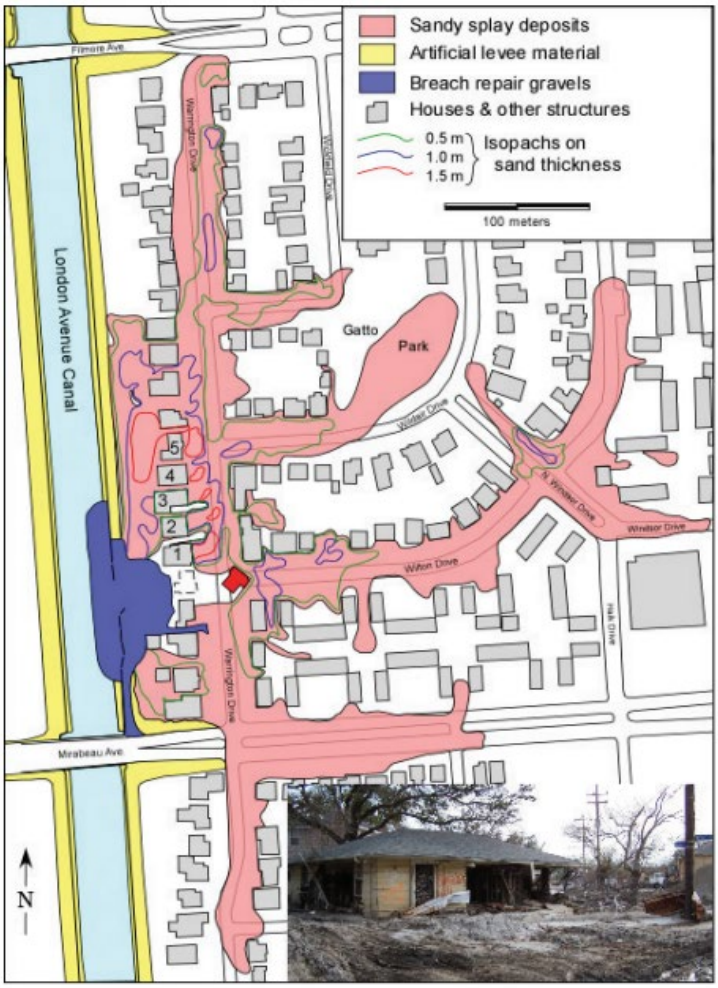

Figure 4-2 The spatial extent of a crevasse splay deposit created in New Orleans during Hurricane Katrina (Nelson and Leclair, 2006).

4.2.2.3 Overview of the gaps in research

It is evident that although there is some degree of understanding of the controls on crevasse splay morphology (size and shape), there is a lack of quantitative data in this research area. The two studies, which used Delft 3D software, used a limited sample of data to develop their conclusions. Millard *et al.* (2017) used three distinct sediment sizes (silt, fine sand, and coarse sand) across two floodplain set-ups. Nienhuis *et al.* (2018) used five variants of vegetation with a constant discharge and one set sediment size distribution. Therefore, the relative impacts of sediment size, discharge, and vegetation's presence and density, on natural splay morphology remain limited.

Furthermore, the only study of crevasse splays in the built environment is qualitative (Nelson and Leclair, 2006). There are no studies showing how buildings and streets quantitatively impact the morphology of splay deposits. The next section will explore various modelling software and

their suitability to study sediment movement during flood events and to select the most appropriate for this investigation.

4.3 Numerical models

4.3.1 Criteria for model selection

A suitable numerical model must be sourced to study crevasse splays in natural and built settings due to a lack of available high-resolution imagery depicting real-world examples. An appropriate model would allow the morphological impacts of various environmental conditions to be investigated as an extension of what imagery offers. Several models exist with different complexities that can transport and deposit during flood-driven events; therefore, to identify which model best fulfils the needs of this research, the following selection criteria were defined:

a) the model must be able to operate on a high temporal resolution (minutes) and on a small spatial scale (1 m to 10s m) to enable many individual flood events to be run efficiently without being too computationally intensive;
b) the model must permit a variety of environmental conditions, e.g. storm size, grain size and floodplain roughness, to be user-defined and altered quickly between model runs;
c) the model must allow the incorporation of built obstacles on the floodplain to test the effect of anthropogenic infrastructure on landform morphology;
d) the model results should be able to be seamlessly integrated into GIS (Geographical Information Systems) software for analysis and extraction of the morphometric components of the crevasse splay deposits.

By fulfilling these criteria, the chosen numerical model will allow the generation of appropriate data able to address the research gap.

4.3.2 Overview of numerical models

Computer-based numerical models have assessed general fluvial morphology and specific landforms driven by flood events over various timescales. Such models can help investigate the impacts of different environmental conditions on morphological landscapes (Martin *et al.*, 2000; Van De Wiel *et al.*, 2007; Gurnell *et al.*, 2012; Millard *et al.*, 2017). Computer models, which began to emerge in the 1970s and were labelled Landscape Evolution Models (LEMs), can portray the movement of sediment as a function of surface and channel flow (Coulthard *et al.*, 2013). Such models are primarily contingent on the input and manipulation of grids and meshes, with the spatial resolution and underlying processes governing the complexity of the model at

hand. However, models have become more advanced, refined, and realistic, with technological developments providing more powerful, innovative computer systems. Subsequently, numerical models can simulate high-resolution morphological changes in a fluvial environment over various timescales. For example, Zhang *et al.* (2021) used a large-scale 3D hydrodynamic model called SCHISM (Zhang *et al.*, 2016) to accurately replicate a 2013 flood event and associated sediment transport along a 280 km reach of the Three Gorges Reservoir, China. This study highlights the vast capabilities of current numerical models and their potential to produce realistic morphological outcomes.

Morphological numerical models can be grouped into three main categories: system-based, physics-based, and cellular automata, which all lie along a continuum from reduced complexity models to reductionist physics-based models (Schuurman *et al.*, 2013). System-based morphological models are developed for a specific study area where they can firmly apply to the particular landscapes and underlying processes. Such models are often used to observe long-term responses of particular systems by operating in reduced-complexity conditions – making them run efficiently in simulations over extended time frames. For example, the Mississippi Delta Model (MDM), developed by Martin *et al.* (2000), can deliver multidecadal landscape and ecological projections at high degrees of confidence yet requires a 1 km^2 gridded input of elevation for the hydrodynamic models to undertake the modelling of river channels (Martin *et al.*, 2002). Further, the MDM model operates over timesteps which range from 20 – 1200 seconds, comparable to other system-based models (Costanza *et al.*, 1990; Reyes *et al.*, 2000). However, due to many system-based models requiring coarse spatial resolution inputs and the associated lengthy timesteps, they are inappropriate for studying small-scale landscape changes during individual flood events – one of the vital model selection criteria. Also, because these models are developed for a specific area of interest, they are not necessarily transferable to other morphological landscapes.

Alternatively, physics-based models show more promise for capturing comprehensive morphological change. Physics-based numerical models often split morphodynamics into three separate components: flow modelling; sediment erosion, transport, and deposition; and making subsequent alterations to the elevation grid (Spasojevic and Holly, 2008; Williams *et al.*, 2016). These models are often seen as reductionist as they break morphological processes down to as many small-scale physics-defined equations as possible to reproduce larger-scale landscape changes accurately (Schuurman *et al.*, 2013). Complex physics-based processes, e.g. shallow water equations, are integrated and solved by the models when simulating morphological changes and allow the mass and momentum of flows to be conserved. As such, they have been well-used in various morphological studies, including investigating changes in braided river

channels over time, and assessing bank erosion and floodplain accretion (Crosato and Saleh, 2011; Nicholas, 2013). Consequently, physics-based models are often viewed as capable tools for undertaking detailed morphological analysis because of their aptitude to reflect realistic outcomes, ability to integrate various environmental conditions, and flexibility across spatial scales. However, the numerical complexity of these models, which is an artefact of their ability to integrate many complex process equations, makes them computationally intensive and thus may only be applicable at coarse resolutions across short timescales (Vaz *et al.*, 2009). Despite this, the strengths associated with physics-based models mean they would be applicable in studying natural and anthropogenic impacts on crevasse splay morphology, and so should be an option that is progressed to the next stage.

Finally, two-dimensional cellular automata models are a form of reduced complexity models. These models attempt to reflect and capture complex morphological system behaviour using a minimal ruleset (Murray, 2003; Williams *et al.*, 2016). The basis for this line of modelling is that morphological behaviour at a given scale is primarily a function of the essential interactions occurring between variables at one scale level below (Werner, 1999). They are inherently different from physics-based models as they use rules that model the interactions between only neighbouring cells to solve more complex mass and momentum equations (Fonstad, 2013). As a result, the models are less computationally intensive, so smaller timesteps can be incorporated, allowing longer model timeframes to be studied quickly. With the emergence of increasing computational power, cellular automata models are constantly being updated with more detailed rulesets to enhance their simulations of morphological dynamics (Williams *et al.*, 2016). Models investigating braiding channels were initially developed by Murray and Paola (1994) and have since been extended by Thomas *et al.* (2007) and Nicholas *et al.* (2012) to improve flow representation and resulted in similar predictions to a 3D model and another focussing on shallow water equations, when simulating morphological change over a 30 km reach of the Rio Paraná, Argentina.

Although it enhances their computational efficiency, the main drawback to cellular automata models is their simplicity, wherein they do not include enough detail of complex flow and sediment processes to inform their simulations of landscape changes, and this may render them more suitable to qualitative projections of landform morphologies (Fonstad, 2013). This is especially prevalent with their simple flow routing algorithms, which struggle to distribute flow momentum correctly. To combat this, a novel approach has attempted to integrate the sediment components of reduced complexity cellular automata models with physics-based flow systems (Williams *et al.*, 2016). For example, CAESAR-Lisflood combines CAESAR, a cellular automata numerical model, with Lisflood-FP – a more complex flow model. Consequently, advancing a

cellular automata model to the next stage of model choice is deemed appropriate as they provide a viable alternative to a physics-based approach. Therefore, the next section will detail an example of a physics-based numerical model and a 2D reduced complexity cellular automata model to directly compare the options and, subsequently, decide on the most suitable morphological model for this research based on the selection criteria.

4.3.3 Choice of numerical model

Applying the criteria to the model types available resulted in shortlisting the physics-based morphodynamic model, Delft-3D, and the cellular automata model, CAESAR-Lisflood (Coulthard *et al.*, 2013). These models fulfil many, if not all, of the necessary criteria (Deltares, 2014; Millard *et al.*, 2017; Wong *et al.*, 2021). They also have user-friendly, intuitive interfaces and being commonly used software, generous support is available online (Caldwell and Edmonds, 2014; Valters, 2016).

Delft-3D has the ability to cope with the interactions of factors, including flood size, sediment transport, and morphology (Deltares, 2014), leading to accurate representations of the natural environment. This current research aims to run several hundred experiments, but the primary caveat to choosing Delft-3D is the computational intensity associated with physics-based morphodynamic models. This would potentially lead to prolonged run times - limiting the extent to which the environmental conditions could be explored in detail. For example, Millard *et al.* (2017) were limited to six models using Delft-3D. Furthermore, the complexity of solving shallow water equations within Delft-3D limits its applicability when dealing with short timescales (Vaz *et al.*, 2009).

CAESAR-Lisflood - a 2D flow and sediment transport model - is suitable for assessing the controls on the morphology of crevasse splays, as it is computationally efficient. Feeney *et al.* (2020) indicated that CAESAR-Lisflood allows the input of nine grain sizes during model runs and permits suspended sediment transport onto the floodplain through a user-defined parameter. Furthermore, this model can operate at high temporal resolutions (seconds and minutes) – allowing individual flood events to be simulated. It is recognised that because CAESAR-Lisflood is relatively simple compared to Delft-3D, the integration into CAESAR-Lisflood of the influences of ecological and anthropogenic components can be more challenging (Coulthard, 1999). Thus far, however, this view has been based mainly on qualitative rather than quantitative analysis of the validity of cellular automata models (Coulthard *et al.*, 2007). This research study provides an opportunity to undertake a thorough, quantitative assessment of the application of CAESAR-Lisflood in generating splays using various environmental conditions

and comparing them to real-world deposits – potentially yielding a required quantitative validation. The reduced complexity of CAESAR-Lisflood compared to physics-based numerical models is its primary advantage for its application within this thesis. This high computational efficiency will allow many experiments to be undertaken.

This assessment shows that of the two models, CAESAR-Lisflood allows the effects of morphological factors, such as storm size, grain size, floodplain roughness, and built obstacles, on crevasse splays to be studied in greater depth, and therefore it is chosen as the model for use in this research.

4.3.4 Detail of CAESAR-Lisflood

CAESAR-Lisflood (Coulthard *et al.*, 2013) is an open-source Cellular Automata model that was developed by incorporating the Lisflood-FP 2D flow model (Bates and De Roo, 2000; Bates *et al.*, 2010) into the CAESAR cellular LEM (Coulthard *et al.*, 2002). It can be described as a coupled hydrodynamic LEM – with the ability to model river channel and floodplain change and the evolution of a catchment (Feeney *et al.*, 2020). Fundamentally, CAESAR-Lisflood can forecast and test "What if?" situations (Coulthard and Van De Wiel, 2017; Ekeu-wei and Blackburn, 2020; Feeney *et al.*, 2020).

Independently, CAESAR (The Cellular Automation Evolutionary Slope and River Model) is a LEM geomorphological model which uses a topographic layer to drive erosion, transport, and deposition processes in river catchments. The model can replicate what will happen to a landscape over hours to thousands of years (Coulthard *et al.*, 2002), permitting a broad array of morphological scenarios to be explored. CAESAR simulates landscape change through fluvial and slope-driven erosion and deposition processes whilst water is transported across a raster grid, with movement dictated by the elevation of cells relative to their neighbours (Van De Wiel *et al.*, 2007). Erosion and deposition are then calculated cell-by-cell using the shear stress derived from flow depth and velocity. However, a limitation of CAESAR is its flow model, which characterises flow as a steady state and does not give a reliable representation of the mass of water or momentum. Therefore, an alternative flow model was sought for incorporation into CAESAR to increase the accuracy with which it can depict sediment movement and deposition.

To retain the computational efficiency of CAESAR, the integration of full 2D flow models was deemed unsuitable as it would dramatically slow the processing speeds of CAESAR - particularly when investigating morphological changes over extended periods. Lisflood-FP (Bates and De Roo, 2000), a reduced-complexity flow model, was seen as a viable option to improve the existing flow model (Coulthard *et al.,* 2013). Lisflood-FP calculates the continuity of the mass

within each cell and the momentum between cells, to work out the movement of flow. It comprises two components: a 1D channel flow part controlled by kinematic wave approximation and a 2D floodplain flow model designed using a diffusion wave representation (Bates and De Roo, 2000).

Typically, 2D reduced-complexity flow models require timesteps of less than two seconds to prevent numerical instability and, therefore, would not usually fit in with the long timescales commonly used in CAESAR, which was the case with the earlier versions of Lisflood-FP. This forms a considerable barrier to the general assimilation of more advanced 2D flow models into LEMs. However, Lisflood-FP introduced a new simple inertia term that dramatically decreased numerical instability (Bates *et al.*, 2010). With the increased computation speed associated with the new term, Lisflood-FP could be run in timesteps order of magnitudes higher than previously. Consequently, Coulthard *et al.* (2013) integrated the Lisflood-FP flow model into CAESAR by altering over 70% of the original CAESAR code to produce CAESAR-Lisflood.

CAESAR-Lisflood is a GUI (Graphical User Interface) LEM composed using the C# programming language – available to download at: https://sourceforge.net/projects/caesar-lisflood/. The model depicts a landscape as a grid of uniformly sized cells, enabling elevation rasters to be easily specified. Before running the model, the user can alter the elevation (as an input raster), grain size distribution and quantities, floodplain roughness, and define the specific input cells for discharge and sediment. The model runs on an iterative basis whereby after a timestep, the morphological alterations in flow, sediment movement, and cell elevation form the set-up for the next iteration. Sediment transport within CAESAR-Lisflood can occur as bed load and suspended load – with different mechanisms of deriving sediment transport and deposition. Bedload sediment is moved from cell to cell based on flow conditions, whereas suspended sediment transport is defined by fall velocities and sediment concentration within cells (Coulthard *et al.,* 2013). The model offers three sediment transport formulas: Meyer Peter and Müller (1948), Einstein-Brown (1950), and Wilcock and Crowe (2003), to drive the calculation of the movement of the bedload component.

Since its development, CAESAR-Lisflood has been used in various morphological studies examining landscape changes over various timeframes. It is most frequently utilised to simulate changes in river basins during individual events (Zellou and Rahali, 2017) and to simulate decadal dynamics of channels (Poeppl *et al.*, 2019; Feeney *et al.*, 2020; Ramirez *et al.*, 2020). It has also been used to investigate the stability of post-mining landscapes (Lowry *et al.,* 2013; Lowry *et al.*, 2019), to observe the impacts of land use change on channel response and sediment

yield (Walsh *et al.*, 2020), and to assess the effects of tectonic uplift and rainfall variability on sediment yields (Coulthard and Van de Wiel, 2013).

On account of its applicability in a wide range of morphological fields along with the strengths listed above, CAESAR-Lisflood provides a sound foundation to undertake an efficient and detailed investigation into the impacts of natural and built environments on crevasse splay formation.

4.3.5 CAESAR-Lisflood parameters

CAESAR-Lisflood includes approximately 50 user-defined parameters (Coulthard et al., 2013), ranging from sediment transport laws to Manning's N roughness to grass maturity rate (annual). Previous work that has utilised CAESAR-Lisflood have used a variety of values for the user-defined parameters to shape the model to accomplish the aims of their specific studies listed previously (Poeppl *et al.*, 2019; Lowry *et al.*, 2019; Walsh *et al.*, 2020).

Given the number of parameters and their applicability to different studies, Skinner et al., (2018) set out to undertake a sensitivity analysis of the morphological outcomes to parameters within CAESAR-:Lisflood. A sensitivity analysis of an LEM explores how variability in model outcomes is influenced by input parameters (Pianosi *et al.,* 2016). To investigate CAESAR-Lisflood's sensitivity, Skinner *et al.* (2018) employed the Morris method sensitivity analysis for model simulations in two contrasting catchments over a decade. This method is computationally efficient, and allows global variance to be calculated through multiple local sensitivity analyses completed across the full parameter space (Saltelli *et al.,* 2000; Norton, 2009). Their work used 15 parameters chosen due to their importance to the model known from previous work, or that the response of the model to a parameter was formerly poorly understood. These parameters included: sediment transport law, max erode limit, grass maturity rate, soil creep rate, Manning n roughness, and minimum and maximum Q values for flow depth calculation. Aside from the sediment transport law – where there were two options (Einstein-Brown, 1950; Wilcock and Crowe, 2003), the other 14 parameters were given five iterative step values. The mix of parameter values were tested against 4 core behaviours: sediment yield, internal geomorphology, catchment discharge, and model efficiency. Their findings suggested that the choice of sediment transport formula was ranked as most influential across all the core behaviours, with Manning's N, slope for edge cells, grain size, vegetation critical shear stress, and in channel lateral erosion rate scoring highly. However, they do note that the Morris method of sensitivity analysis only provides a ranking of each factor rather than an absolute value of sensitivity – so cannot observe the magnitude of differences between variables. Furthermore, they suggest the main limitation

of the work is that the two sediment transport laws are separated by a single step, whereas the other parameters are split over five iterative steps. As a result, this could distort the relative importance of this variable. In fact, they undertook additional analysis and found that placing the two sediment transport laws over the equivalent of four iterative steps substantially altered the results making the transport regime less important, with Manning's N and grain size increasing in influence. Despite this, the findings highlight the substantial impact changes in model parameters have on the potential outcomes of research.

In light of Skinner *et al's* sensitivity analysis, it was deemed appropriate to limit the number of variables used within this work to the main parameters being tested. As such, many of the model parameters can be seen as inapplicable and thus can be ignored allowing model efficiency to be maintained and reduce potential confounding variables. The work undertaken in this thesis focusses on an individual flood event, set over the course of six hours, trialling different discharges and grain sizes to assess their impact upon the morphology of depositional crevasse splays. Consequently, parameters that are commonly used during models with yearly/decadal time lengths can be omitted including the several variables within the dune, vegetation and soil development categories, as well as disregarding any in-channel erosional and slope processes due to the focus being solely on floodplain deposition.

The methodology set out in the next chapter will address the specific parametrisation of the model variables that are relevant to this work, including sediment transport model, grain sizes, and timesteps. There are additional tuning parameters, such as the courant number and minimum flow depth, which are defined in Chapter 5 based upon the chosen model resolution and the length and time steps of model runs.

4.4 Chapter summary and next steps

This chapter has provided a succinct overview of fluvial flood occurrence, the formation of crevasse splays, and known controls on their morphology. It highlights that controls on splay size and shape have not been fully quantified and are usually examined qualitatively, especially when they interact with built environments. A review of morphological models was completed, which deemed CAESAR-Lisflood, the most appropriate model for this work. The next chapter will apply CAESAR-Lisflood, on a deliberately simplified floodplain to determine the impacts of natural environmental conditions on crevasse splay morphology.

Chapter 5 Modelling controls on crevasse splay morphology on a deliberately simplified "natural" floodplain

5.1 Chapter objectives

This chapter addresses a gap in the quantitative understanding of the impacts of various natural environmental conditions on crevasse splay morphology. To do this, it will:

- Explore the impact of grain size, discharge and floodplain roughness on crevasse splay deposits using the CAESAR-Lisflood morphological model incorporating sediment dynamics with hydrology.

5.2 Introduction

Crevasse splays are overbank sediment deposits created by sediment being advected through levee breaches (Bristow *et al.,* 1999, Millard *et al.,* 2017) and are common in many fluvial and fluvio-deltaic systems (Rahman *et al.*, 2022). When propagated onto the fluvial floodplain, this sediment forms high sedimentation patches near the channel belt, wherein the flood flow slows, loses energy, and subsequently has a lower capacity to carry its sediment load (Shen *et al.*, 2015). Crevasse splays are vital in the morphological development of rivers by impacting levee growth (Bridge, 1984) and channel-avulsion processes (Stouthamer, 2001). In addition, sediment deposition on the floodplain near the river channel can elevate the landscape and provide sediment supply and nutrients to the broader morphological system, allowing connectivity between the channel and the surrounding area (Junk *et al.,* 1989, Heiler *et al.*, 1995).

Splay growth and terminal morphology are dictated by a combination of factors, with a principle component being discharge, which dictates the energy of the system and the subsequent sediment load (Williams, 1989; Rahman *et al.*, 2022; Li *et al.*, 2023). However, for a given discharge, splay morphology is controlled by characteristics of the sediment within the channel – needed for splay progradation, and the hydrology of the flood basin – which determines where sediment can accumulate (Millard *et al.,* 2017). Indeed, the distribution of grain sizes influences the pattern of sediment deposition (Mertes, 1997) and the availability of material to splay formation (Slingerland and Smith, 1998). Moreover, splay morphodynamics can also be influenced by the presence and density of vegetation on the floodplain, alongside flood size and the topography of the area affected (Hajek and Edmonds, 2014).

Even though there is a wealth of knowledge regarding sediment dynamics during overbank flow (Walling and He, 1998; Syvitski *et al.*, 2012), there remains little understanding of the quantitative impact flow and sediment characteristics have on crevasse splay morphology in terms of shape and size. Numerical models provide a solid foundation to unravel the complex behaviours associated with hydrological and sedimentary processes (Collins and Owens, 2006). As such, they are often used to simulate and visualise geomorphological processes in various applications (Hooke *et al.*, 2005; Temme and Veldkamp, 2009; Bastola *et al.*, 2018; Wong *et al.*, 2021). However, the validity of numerical models is often analysed qualitatively rather than quantitatively when replicating real-world morphological events. Therefore, this work can assess the application of CAESAR-Lisflood (Coulthard *et al.*, 2013) in generating splay deposits using a variety of environmental conditions by comparing these landforms to real-world deposits (Chapter 7) – allowing for quantitative validation, which is often challenging (Coulthard *et al.*, 2007).

To this end, under various environmental conditions, a 2-dimensional reduced-complexity morphological model - CAESAR-Lisflood - generates crevasse splay deposits on a deliberately simplified floodplain. The model inputs included a series of sediment grain sizes (five categories of sand grains – very fine, fine, medium, coarse, and very coarse), discharges (eleven values at even intervals between 10-30 cumecs) and surface roughness (ten Manning's N values from 0.01 to 0.1) – with each resulting splay deposit having their size components measured. The morphological parameters of length, perimeter, area, and volume are calculated, allowing for an examination and comparison of deposit size and shape (splay morphology).

5.3 Methods

The workflow for this chapter is conceptualised in Figure 5-1. This section runs through the elevation data sourced and how this was processed to develop a simplified floodplain. It then details the model setup, how discharge, grain size, and floodplain roughness were tested, and the decision regarding which sediment transport model to use. It finishes with an overview of the post-processing of the model outputs and how various morphometric data were ascertained.

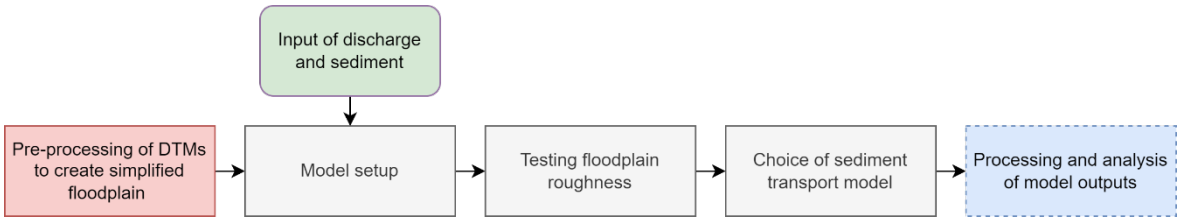

Figure 5-1 Framework of the natural fluvial method.

5.3.1 Data sources and study area

Light Detection and Ranging (LiDAR) is an active sensor used aboard airborne technology, which uses interactions between laser pulses and the Earth's surface to observe topography over large spatial study sites (Moorthy *et al.*, 2008; Muhadi *et al.*, 2020). DTM (Digital Terrain Model) refers to the bare ground terrain topography, whilst DSM (Digital Surface Model) is the first surface encountered by the laser pulses, e.g., buildings and vegetation (Chen *et al.*, 2017; Pfeifer and Mandlburger, 2017).

The LiDAR DTM dataset, sourced from the Environment Agency (https://environment.data.gov.uk/DefraDataDownload), comprises raster elevation files covering over 85% of England – made up of a series of surveys capturing the landscape between March 1998 and September 2019. DTMs with a spatial resolution of 2 m were sourced and specified as "LiDAR composite DTM 2019 – 2m". DTM rasters of this resolution were chosen to reduce each model's time to run for a given timeframe.

The DTM datasets sourced and downloaded for this research are located on the Somerset Flats in the southwest of the UK – a region prone to flooding (McEwen *et al.*, 2014). The low-lying, flat floodplains surrounding prominent levees parallel to the river channel provide a foundation for testing crevasse splay deposits created during a levee breach. Two DTMs were extracted from the 2020 dataset, named: a) "ST33sw_DTM_2m.tif" and b) "ST33se_DTM_2m.tif".

5.3.2 Data processing

All GIS and data processing was undertaken in ArcGIS Pro version 2.9, with river modelling implemented in CAESAR-Lisflood 1.9J. All data extracted from CAESAR-Lisflood was projected into the WGS 1984 World Mercator coordinate system when being analysed.

5.3.2.1 Pre-processing of floodplain raster

Figure 5-2 provides an overview of the procedure for generating the deliberately simplified floodplain used in CAESAR-Lisflood. It begins with the two 2 m resolution DTMs sourced and culminates with one floodplain raster.

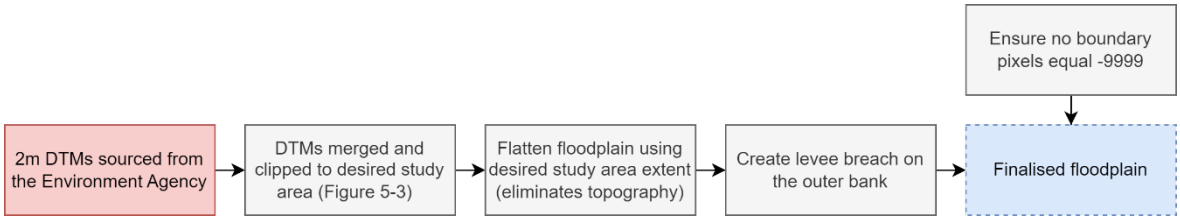

Figure 5-2 Flowchart of the creation of the deliberately simplified floodplain.

The 2 m DTMs downloaded from the Environment Agency were merged to create an unedited starting raster. This raster was then subset to include a section of the River Parrett located northeast of Northmoor Green, wherein the river channel flows directly northwards and then meanders to the west (Figure 5-3). The following DTM processing meant the floods modelled were not representative of a levee breach and subsequent sediment deposition at this specific real-world site. The floodplain was flattened to reduce the impact of topography on crevasse splays.

First, a shapefile was created, which comprised a digitised polygon depicting the extent of the floodplain to be studied, using the levees as an edge boundary. This polygon was then converted into a raster with the same spatial resolution as the DTM. Next, the floodplain study area was reclassified, so it was represented by a value of 1, with the rest of the study extent represented by a value of 0. Subsequently, the "Con" tool was used to create a new DTM layer where the pixels of the designated floodplain study area were given a constant value of 4.9 (a flat domain), and the rest of the DTM retained the values from the original elevation layer. Therefore, this rendered the floodplain lagoon-like –eliminating the influence of floodplain topography on the model results and allowing the impact of other variables to be isolated.

Using the raster pixel editor provided in ArcGIS Pro, a levee breach was artificially created between the river channel and the floodplain. The breach location was situated on the outer bank of where the River Parrett meanders to the West. It was determined that this breach position would be most effective as it promoted the movement of floodwaters out of the channel and onto the floodplain and, in turn, encouraged sediment to be transported and deposited as crevasse splays. In Rahman *et al.'s* (2022) investigation of 1556 crevasse splays, 70% of the landforms were located on the outer bend of sinuous channels – suggesting this is the dominant location of splay formation due to higher water flow velocity (Smith *et al.*, 1998). Therefore, the pixel editor's interpolation tool was utilised to create a 14 m wide breach on the outer bank of the meander. The tool allowed elevations from the river channel edge to be interpolated with pixels on the outside of the levee, producing a positive gradient towards the floodplain for water to exit. Furthermore, the pixels representing levees close to the discharge/sediment input cells were increased to prevent overtopping when higher discharges were input.

Finally, pixel editor software (RasterEdit) was used to ensure that the boundaries of the DTM were elevation values rather than NoData, as this prevents water and sediment from exiting the domain. Where edge cell values were -9999, they were assigned the elevation value of the

neighbouring cell. This final DTM layer (Figure 5-3) was then converted into ASCII format to make it compatible with CAESAR-Lisflood.

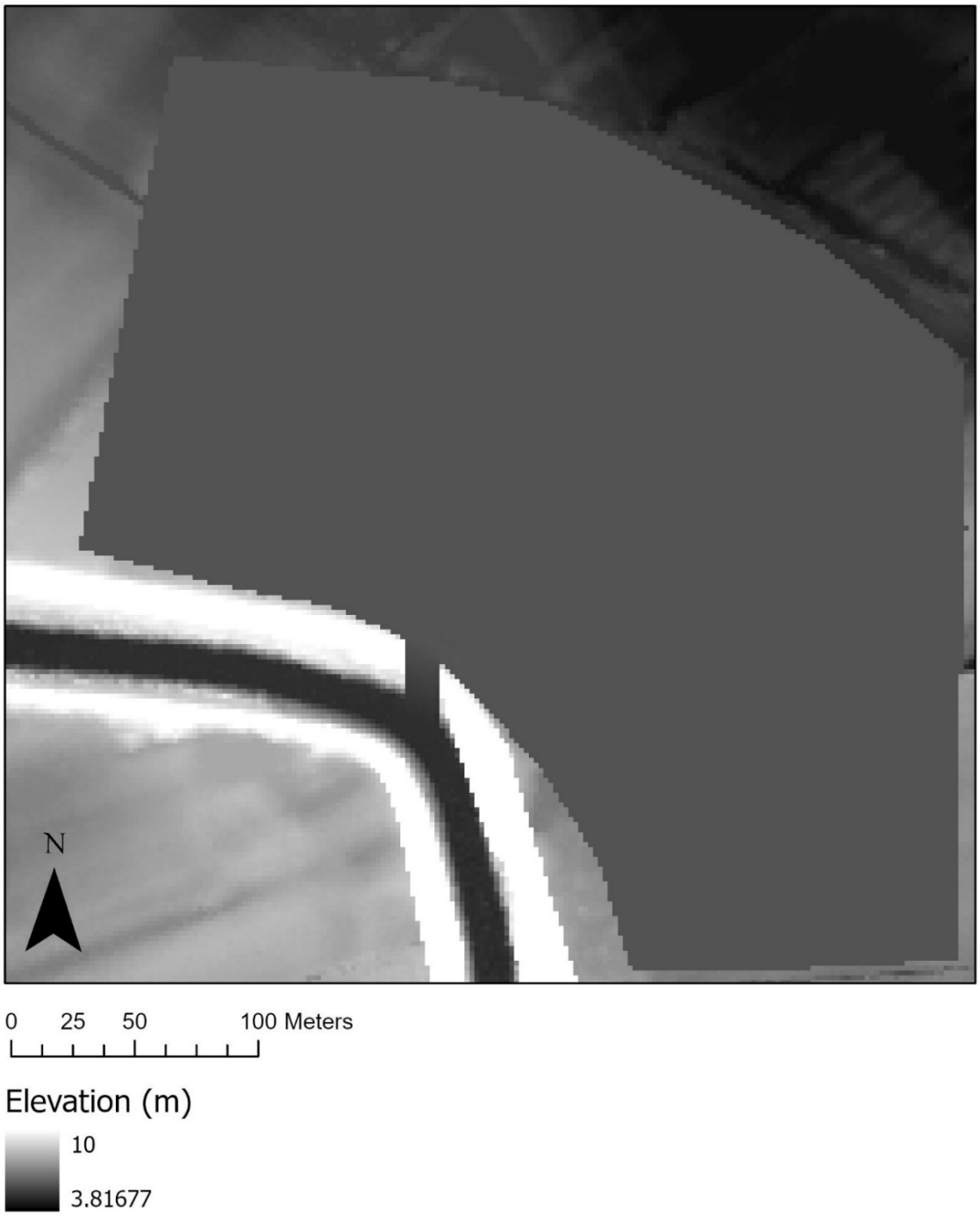

Figure 5-3 The final "deliberately simplified" floodplain for use in CAESAR-Lisflood.

5.3.2.2 Model setup to test discharge and sediment size

For CAESAR-Lisflood to operate, all input files must be in the same folder directory as the software. The model was run in reach mode, allowing river discharge to be input as the main driver of morphological processes. A default input text file allows the end user to specify the discharge (cumecs) and sediment quantity for all grain sizes required. Regarding the discharges tested, eleven values were chosen in increments of two from 10 to 30 cumecs. This allowed the morphology of splays created under small, medium, and large floods to be analysed. The model timesteps were set to 180 minutes to create a six hour flood event.

The sediment tab in CAESAR-Lisflood allows the necessary grain size information to be defined. This research used the Wentworth (1922) sediment classification chart to categorise and choose the sediment grain sizes to be sampled. The sediment size groups used were Very Fine Sand, Fine Sand, Medium Sand, Coarse Sand, and Very Coarse Sand. It is widely acknowledged that sand is commonly suspended during flood events and forms splay complexes when propagated onto floodplains (Florsheim and Mount, 2002; Nienhuis *et al.*, 2018; Rahman *et al.*, 2022). These classes were split into four representative sizes equally distributed in the size range within each category (proportions = 0.25), with the specific sizes provided in Table 5-1. The smallest in each sediment category was specified as the suspended fraction – with the respective fall velocity being estimated using Stokes' law.

The sediment quantities selected in this research were significant enough to ensure that during model runs, the system was not sediment-limited, which counterproductively would have resulted in widespread scouring of the floodplain. Instead, by providing a large quantity of sediment, splay deposits could form in the inundated areas close to the levee breach. These quantities were 10 cu m/3hrs, 10,000 cu m/3hrs, 1000 cu m/3hrs, and 10 cu m/3hrs, across the four proportions of each specified grain size. Moreover, the input cell locations can be specified. For all model runs, two input cells situated in the southernmost part of the river channel were chosen (98,201 and 100,201). Using two input cells prevented the model from scouring the domain at one point. Additionally, as the model limits how much sediment can be input into an individual cell, it was deemed appropriate to spread this over two cells, allowing the required quantity of sediment to be input without extensive erosion.

Lastly, in the flow model tab, the courant number was reduced to 0.3 to remove some numerical instability, whilst Manning's N value was specified as 0.04 across the model domain – previously described as characteristic of agricultural land or grassy vegetation (Chow, 1959).

Table 5-1 Sediment sizes used within each category of sand: very fine, fine, medium, coarse, and very coarse. The finest grain within each category is defined as the suspended load, with the estimated fall velocities provided.

Sand Category	Grain size (mm)	Fall Velocity (m/s)
Very Fine	0.06	0.002943
	0.08	N/A
	0.1	
	0.12	
Fine	0.13	0.011632
	0.17	N/A
	0.21	
	0.25	
Medium	0.26	0.03225
	0.34	N/A
	0.42	
	0.5	
Coarse	0.52	0.074902
	0.68	N/A
	0.84	
	1	
Very Coarse	1.01	0.146487
	1.34	N/A
	1.67	
	2	

5.3.2.3 Testing floodplain roughness

CAESAR-Lisflood allows an ASCII file to be input that spatially defines Manning's N coefficient across the floodplain, allowing the impact of floodplain roughness on splay morphology to be tested. This file allows various floodplain roughness values to be tested whilst keeping the levees and river channel roughness constant. Ten new rasters with different floodplain roughness values were created. In these rasters, the floodplain study areas were given values from 0.01 to 0.1 in increments of 0.01. Although Manning's N coefficient is used in many

studies to examine the influence of roughness on flow (Li and Zhang, 2001; Noarayanan *et al.*, 2012), it can be seen as reductionist as it groups multiple resistance factors into a single number. Importantly, roughness has been shown to vary at different flow depths during flume experiments (Västilä and Järvelä, 2014). Therefore, the roughness values used in this experiment were not seen to represent specific floodplain environments – as each individual N value may apply to a range of settings with varying vegetation types/presence, topography, and land use. Instead, it was seen as a non-dimensional input allowing the impact roughness to be assessed. Each grain size category was used for this investigation, but the input discharge was kept constant at 24 cumecs. Otherwise, the inputs were left the same as during the sediment size and discharge trials.

5.3.2.4 Choice of sediment transport model

The three sediment transport equations available for use in CAESAR-Lisflood are Meyer-Peter and Müller (MP-M) (1948), Einstein (1950), and Wilcock and Crowe (2003). All three are integrated into the software because they have the ability to calculate total sediment transport as a sum of the amount moved for each defined grain size. MP-M is a popular transport regime extensively used to ascertain sediment movement within open channels – derived from the surplus shear stress induced by water flow using a large experimental dataset (Wong and Parker, 2006). Einstein's (1950) theoretical approach is a probabilistic model incorporating the influences of turbulence and particle location on sediment entrainment and deposition (Gyr and Hoyer, 2006). Whilst, Wilcock and Crowe's (2003) bedload transport model for mixed-size sediment is a more modern equation. As a modern equation, it is constructed on the "similarity collapse" hypothesis, whereby the relationship between discharge and shear stress is independent of grain size (Parker and Klingeman, 1982; Gaeuman *et al.*, 2009). The formulas incorporated into the model were articulated using sediment data collected during flume experiments. The model is novel in that it utilises the full-size distribution of the bed surface and is derived from a comprehensive dataset comprising measurements of surface grain size during a series of flows and sediments. Moreover, it utilises a "hiding function", an exponential function that reflects how critical shear stress varies with grain size – which is absent from historic sediment transport laws (Parker, 2008).

It is worth noting that regardless of the choice of transport rules, there will be a degree of inaccuracy within the models outputs as transport laws are an acknowledged weakness within the fluvial geomorphological field. Given the laws are derived from limited experimental and field data, the transport formulae available in CAESAR-Lisflood do not, and were likely never meant to, demonstrate the true variability in actual river flow conditions (Skinner *et al.,* 2018)

and the sediment transport that occurs as a result. Consequently, no sediment transport formula is capable of consistently and accurately predicting transport rates unless standardised against measured data (Gomez and Church, 1989), with predictions within one order of magnitude often considered as reasonable performance (Recking *et al.,* 2012). Therefore, the application of any of the three transport equations currently available in CAESAR-Lisflood introduces an element of uncertainty into the results produced.

Nevertheless, these sediment transport functions can still prove beneficial when running fluvial experiments as they provide a solid basis to test the impacts of different discharges and grain sizes on morphological outcomes. This work will utilise the Wilcock and Crowe (2003) formulation in its model runs. Although it was designed using data produced during experiments with mixes of sand/gravel – it has previously been extrapolated to test finer sediments (Van de Wiel et al., 2008), wherein, it was deemed useful for investigative studies within the CAESAR LEM. During initial experiments, it was found that the Wilcock and Crowe transport law enabled a range of splay deposits, with variable morphologies, to be generated on the flattened floodplain across a range of discharges and grain sizes.

5.3.2.5 Other relevant model parameters

- Minimum time step
    - CAESAR-Lisflood automatically chooses an appropriate value based on the overall length of the model runs in order to maintain computational speed. Here, given the short timescale of the model runs, a minimum time step of 2 seconds was designated.
- Proportion of sediment to be re-circulated
    - In reach mode, this permits any sediment that exits the model domain to be re-inputted at the original input locations. This was defined as 1 (all sediment) to allow a continuous supply of sediment to the model.
- Minimum Q for depth calculation
    - The value specified acts as a threshold above which the model will calculate a flow depth. This avoids needless computational effort calculating miminal flow depths that are absent of erosion or deposition. The value suggested is 0.01 per metre cell size; consequently for a 2m DTM resolution, a value of 0.02 was utilised.
- Courant number

- This controls the numerical stability and speed of the model in CAESAR-Lisflood. Due to the high resolution of the study parameters, a courant value of 0.3 was selected.

5.3.2.6 Post-processing and analysis

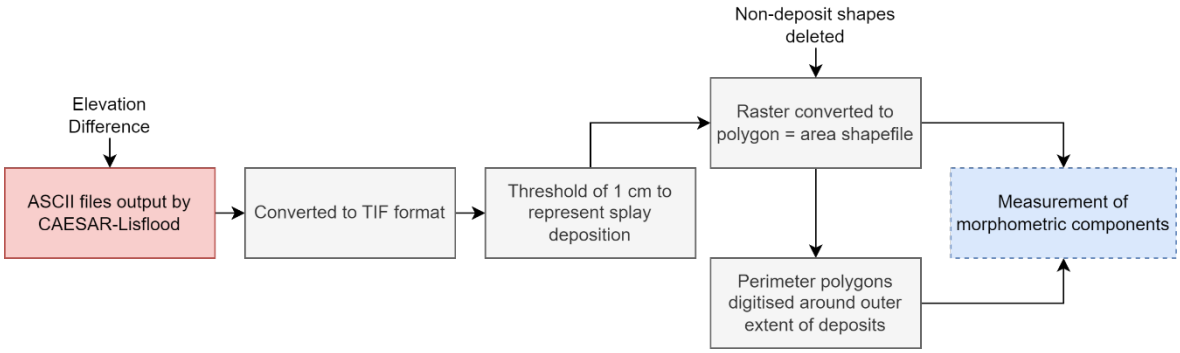

Figure 5-4 A workflow depicting the post-processing method of CAESAR-Lisflood outputs of natural crevasse splays.

Once the model runs were complete, data processing and analysis needed to be undertaken, visualised in Figure 5-4 as a flowchart and Figure 5-5 using a model output example. Using the "ASCII to Raster" tool in Python, the elevation difference outputs generated by CAESAR-Lisflood were converted into TIF format to be operational in ArcGIS. This elevation difference raster comprises values in metres representing the final output DTM by CAESAR-Lisflood subtracted from the input DTM. Therefore, negative numbers constitute deposition areas, and positive values show where scouring has occurred, with zero being no change (figure 5-4, panel A).

The first issue was determining the quantity of sediment deposition within an individual cell that constitutes a crevasse splay. A threshold is required as when separated by positive vs negative change, there was widespread deposition across the lagoonal floodplain, with the majority being insignificant. In response, a threshold of 1 cm of deposition was chosen to represent a crevasse splay in the elevation difference output. This process was applied in the raster calculator to create a binary raster with values of 1 illustrating areas that exceed this 1 cm threshold (Figure 5-5, panel B).

The new binary rasters were converted into shapefiles, which created polygons covering the entire model domain (Figure 5-5, panel C). Therefore, all polygons that did not represent the crevasse splay were deleted, leaving only the desired deposit shapes. Where the same splay polygon extended both onto the floodplain and into the levee breach, the polygons were split at the deposit throat, and breach deposition was deleted, so the only portion remaining was the

section on the floodplain. Not all areas of a given splay deposit were included in the same polygon, with some shapes independent of the main depositional body. These polygons were merged to form one master polygon for each deposit – labelled as the area shapefiles (Figure 5-5, panel D). Some area polygons had holes in the middle of the deposits that were erosional channels, wherein scouring, not deposition, was the most dominant process.

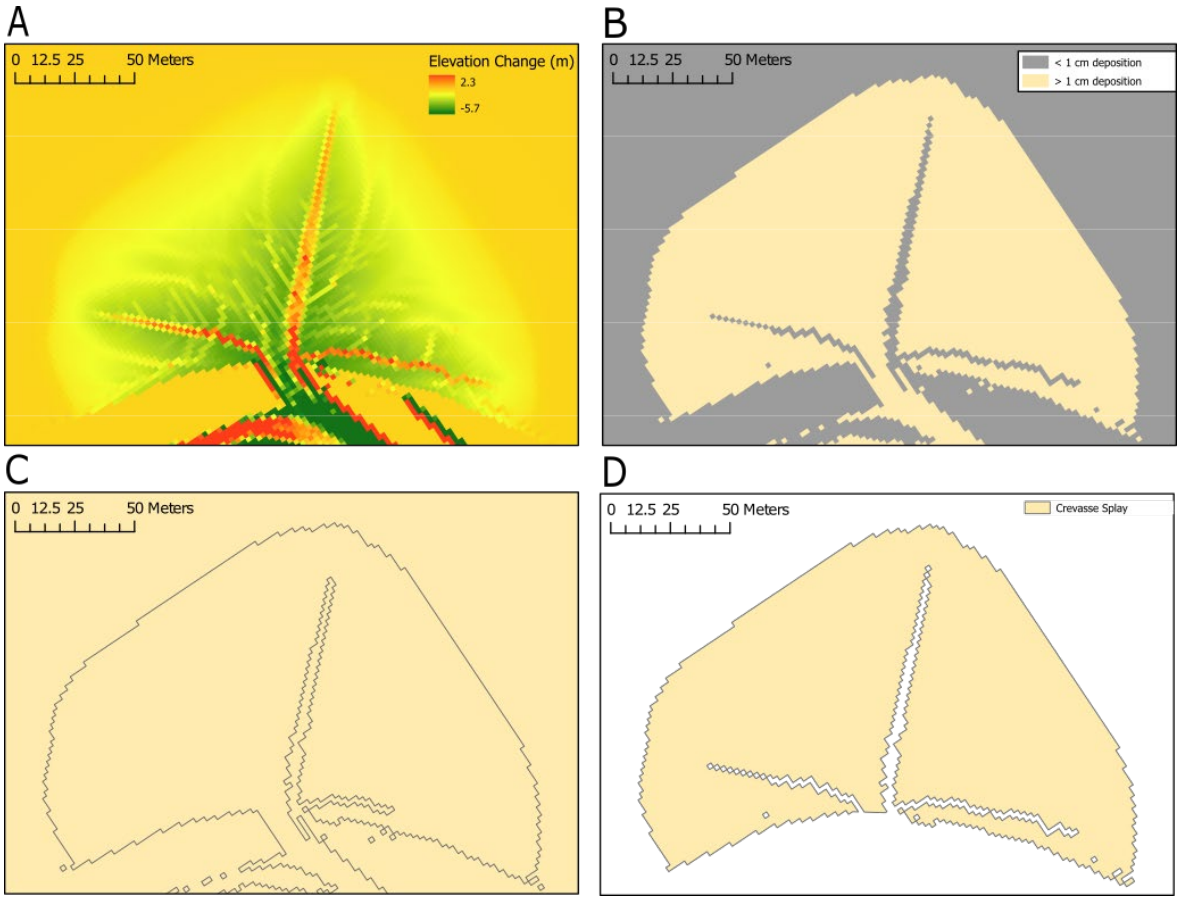

Figure 5-5 Illustration of the post-processing method of the natural model output.

Consequently, a new shapefile was generated for each model run to contain a digitised polygon of the outer perimeter of the whole sediment deposit. This digitisation was undertaken using the trace tool – allowing the deposit to be efficiently drawn around as it minimised user interaction.

Once all deposits were digitised, the physical attributes of the splays needed to be extracted, with an example provided in Figure 5-6. Measurements of length, width, perimeter, area, and volume were extracted for each splay. Length and widths were measured manually using the in-built ruler tool in ArcGIS. The splay length was taken as the longest perpendicular distance from the levee to an aligning deposit edge. Whilst, for width, a point was created in the centre of the deposit throat. Splay width was measured as the combined distances from the central point to the upstream and downstream deposit extents along the levee, providing an arc-like

representation of width. The deposit perimeters and areas were measured automatically using the calculate geometry feature. Finally, deposit volumes were calculated. To do this, the "zonal statistics as table" tool was used, which permitted the values within each elevation raster to be summed within the relevant area shapefile. An additional metric was calculated by dividing each deposit volume by its width – this provides width-averaged quantities of volume in m^3/m, as observed in Carruthers *et al.* (2013) and Rogers *et al.* (2015).

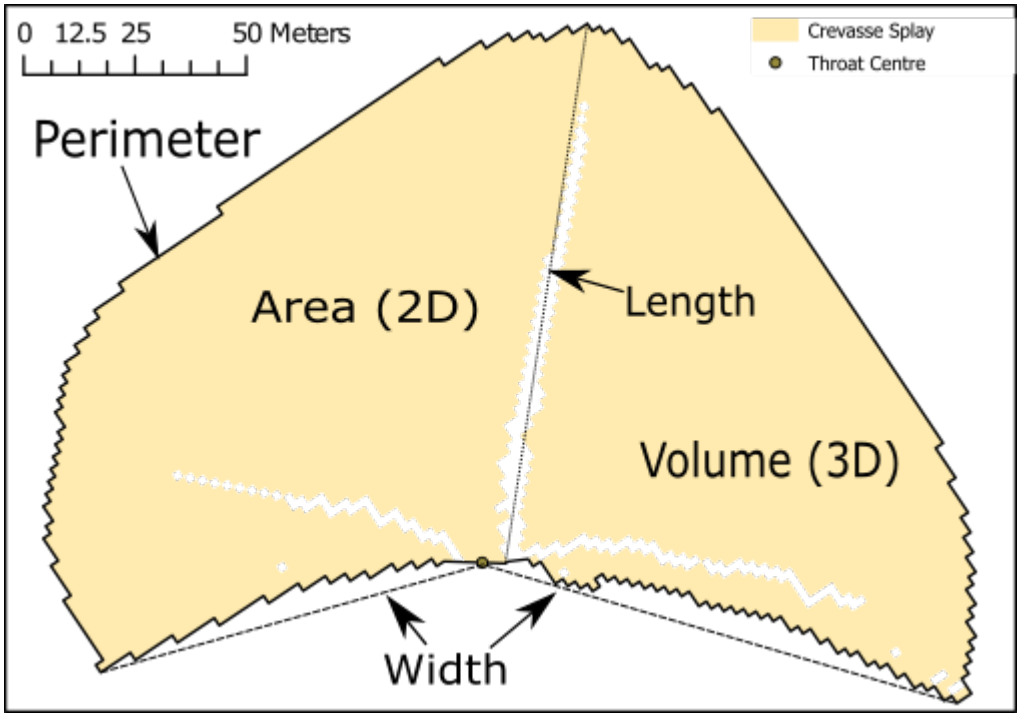

Figure 5-6 The morphometric measurements extracted from each natural crevasse splay.

5.4 Results

This section will present results that visually depict and quantify the morphology of crevasse splay deposits created under various flow and sediment conditions on a deliberately simplified floodplain.

5.4.1 Impacts of discharge and grain size on splay morphology

Analysis of the modelling results shows that the input parameters of grain size and discharge strongly impact the morphology of the crevasse splays formed in the 55 models run in CAESAR-Lisflood.

An initial visualisation of a subset of the deposits formed is provided in Figure 5-7. These are splays formed at a set discharge of 24 cumecs for each grain size. Panel A displays the extent of the five deposits, whilst panels B-F show deposit topographies, allowing a visual comparison of splay morphology under the five grain sizes. These examples highlight the variety of splays CAESAR-Lisflood created when environmental conditions were altered. In addition, they demonstrate a potential trend of deposit size decreasing as grain size becomes coarser, with the deposits comprising finer sand grains intruding further onto the floodplain than those created using the coarser sands.

Moreover, it is evident that as the distance from the levee increases, the deposits become thinner – with lighter shades of green at the furthest areas of deposition in all grain size examples. The very fine and fine sand deposits each have three distinct erosional channels, whilst the coarser sediments have one main channel with several others branching off it. It is palpable that the top of the very fine sand splays is more uniform and smoother, whereas the profile of the coarser sand deposits are rougher and variable.

Additionally, the coarser sand deposits have larger quantities of deposition concentrated closer to the levee breach than the finer examples. Because of this and their smaller extents, it is visible that steeper slopes typically characterise the coarser sediment splay deposits as splay elevation decreases whilst moving inland from the levee breach. In contrast, the slope of the finer sediment deposits appears gentler – with more distance between the changes in shades of green.

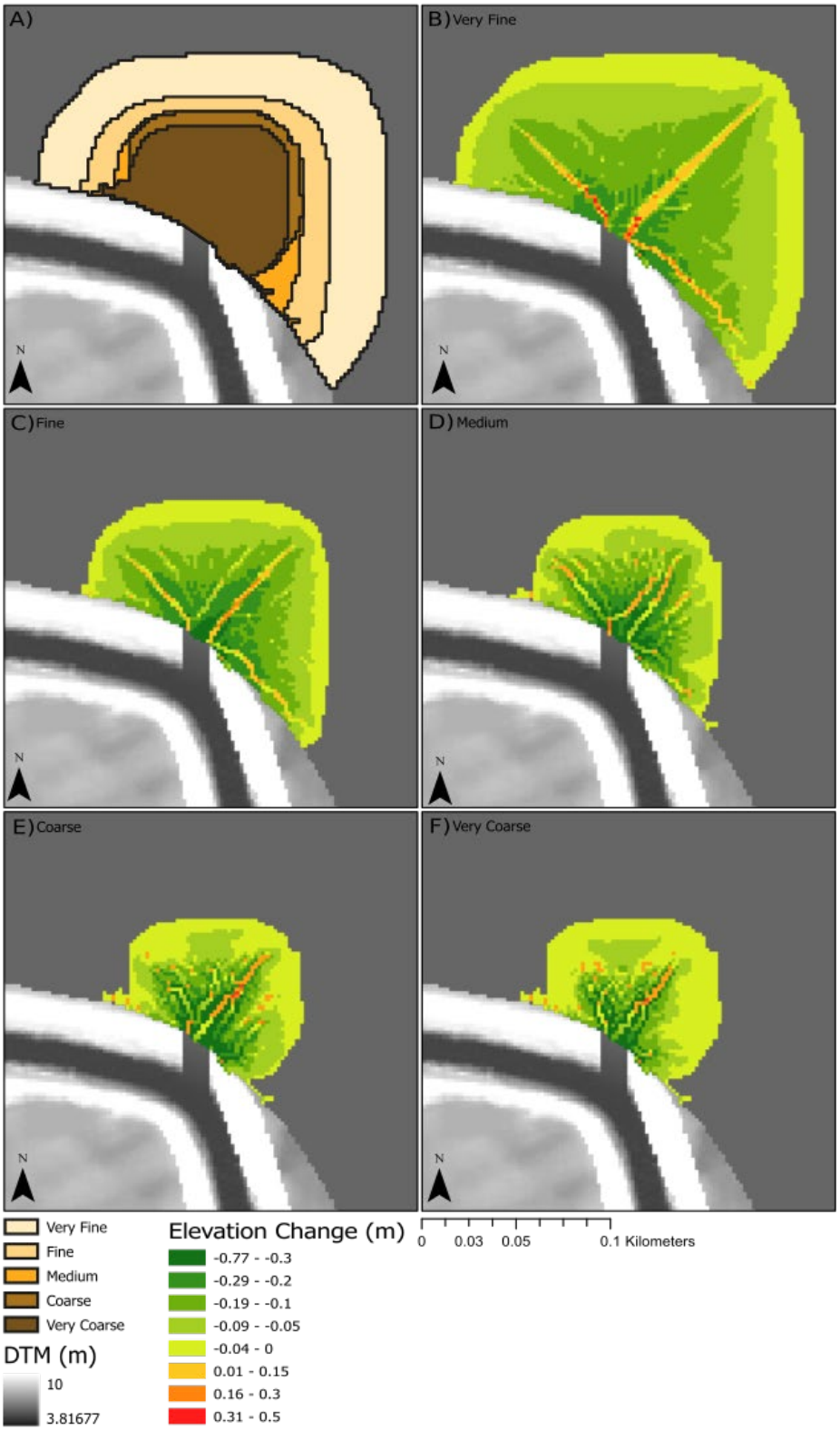

Figure 5-7 A series of maps showing natural deposit extents and elevation profiles for each grain size at a discharge of 24 cumecs. **A)** A map of the splay deposit extents for each grain size **B-F) V**isualisations of the elevation profiles from a planform viewpoint, with deposition shown as green (darker green = more deposition) and erosion as orange/red (red = more erosion).

Notably, there is a clear positive trend in the scatter plots (Figure 5-8a) and regime diagrams (Figure 5-8b) between the input discharges and the size of the splay created for a given grain size (for all size parameters). The calculated coefficients and p-values (all $p < 0.001$) suggest strong positive relationships and linear correlations between discharge and deposit size measures (Table 5-2). Furthermore, the universally high R-squared values (all exceeding 0.9) indicate that discharge can explain a substantial proportion of the variance in deposit size – for a fixed grain size.

Regarding the influence of grain size on splay size, qualitatively, the regime diagrams show two colour gradients in each plot (one horizontally and one vertically) moving from small deposits represented by light blue in the bottom left (deposits created under low discharge with coarser sediment) to more extensive deposits shown as dark blue cells in the top right (deposits produced under high discharge with finer sediment). This influence of grain size is replicated by a vertical gradient of dark to light brown in the scatter plots suggesting that the finer the sediment within the floodwater, the larger the deposit generated. This is further exemplified when considering the summary statistics for the deposits created. For example, the mean deposit area for very fine sand is 14719.31 m^2, which decreases for a rise in coarseness, reaching 3507.53 m^2 for very coarse sand. The minimum deposit area for very fine sand – 5111.8 m^2 at a discharge of 10 cumecs – exceeds the deposit area of fine sand at 16 cumecs (4409.24 m^2), medium sand at 18 cumecs (4277.3 m^2), coarse sand at 20 cumecs (4231.66 m^2) and very coarse sand at 24 cumecs (4915.88 m^2). In addition, the maximum deposit area for very fine sand is 25204.03 m^2, 9983.46 m^2 larger than the maximum created using fine sand and 18896.76 m^2 more considerable than the maximum of very coarse sand (all maximum deposit areas were generated during model runs where discharge was 30 cumecs). These patterns are replicated across all other attributes of deposit size.

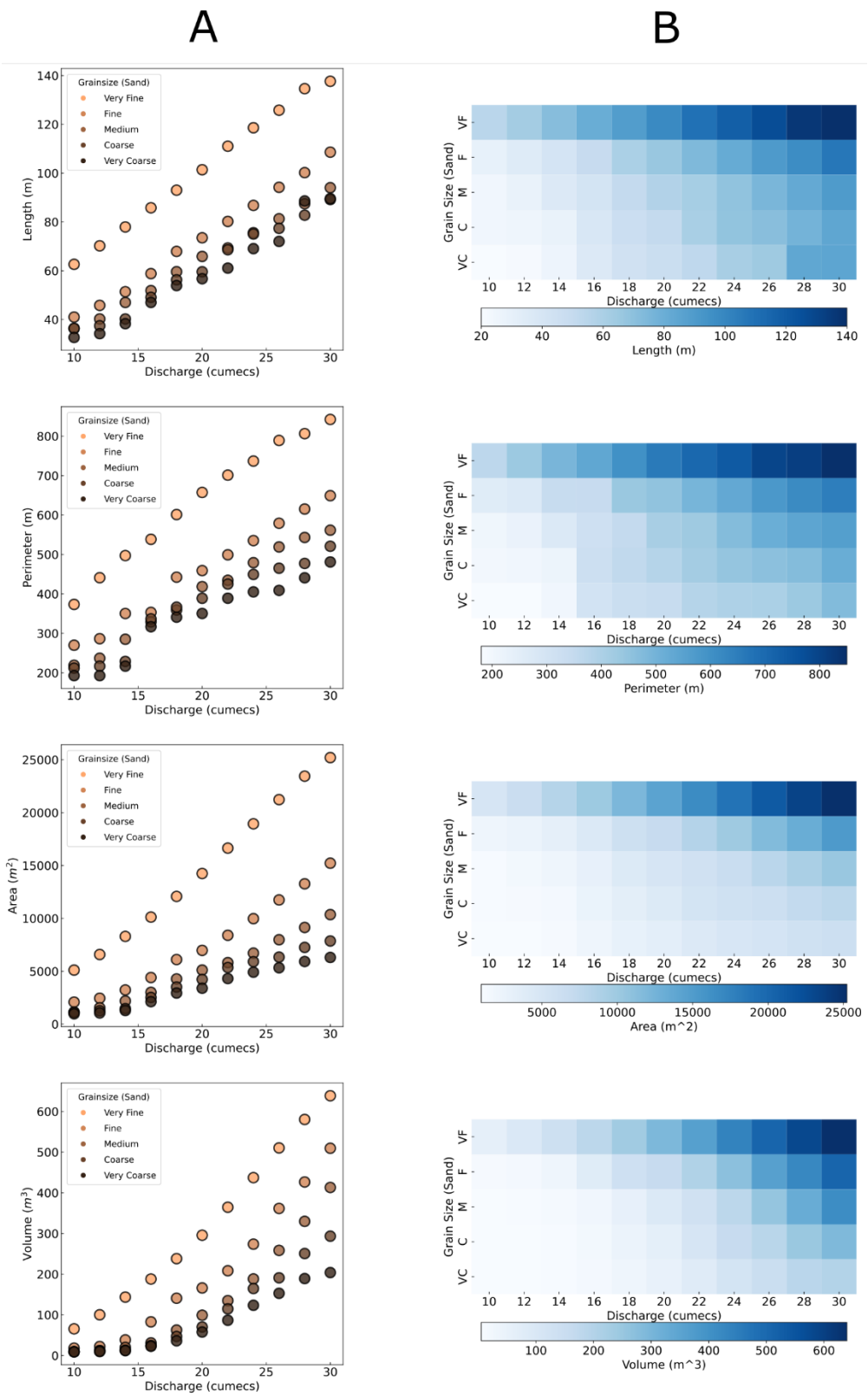

Figure 5-8 An illustration of how physical attributes of natural crevasse splay deposits change based on various grain sizes and discharges. A) scatter plots with physical parameters (length, perimeter, area, and volume) vs discharge, points coloured by grain size (light brown to deep brown). B) regime diagrams – each grid cell (an individual deposit) is coloured by a physical attribute of the deposits (light blue up to dark blue as size increases).

Table 5-2 Correlation statistics for discharge (cumecs) vs each deposit size metric for each sand grain size.

Grain size	Size Metric	Coefficient	Standard Error	R-Squared Value	P-Value
Very Fine Sand	Length	3.9	0.07	0.9973	p<0.001
	Perimeter	23.54	0.88	0.9876	p<0.001
	Area	1040.51	20.73	0.9964	p<0.001
	Volume	29.51	1.08	0.9883	p<0.001
Fine Sand	Length	3.42	0.05	0.9981	p<0.001
	Perimeter	19.63	0.65	0.9902	p<0.001
	Area	740.31	30.05	0.9823	p<0.001
	Volume	24.97	1.84	0.9534	p<0.001
Medium Sand	Length	2.9	0.04	0.998	p<0.001
	Perimeter	18.25	0.56	0.992	p<0.001
	Area	467.04	16.23	0.988	p<0.001
	Volume	19.95	2.19	0.902	p<0.001
Coarse Sand	Length	2.82	0.11	0.988	p<0.001
	Perimeter	16.27	1.23	0.951	p<0.001
	Area	367.9	15.03	0.985	p<0.001
	Volume	14.83	1.47	0.92	p<0.001
Very Coarse Sand	Length	2.98	0.16	0.975	p<0.001
	Perimeter	14.7	1.18	0.945	p<0.001
	Area	296.25	11.98	0.986	p<0.001
	Volume	10.76	0.98	0.93	p<0.001

The coefficients attained in the linear models (Table 5-2) reflect the amount that deposit size increases for a specific rise in discharge. These values provide a quantitative measure to observe the relationship between grain size and deposit size. It is shown that the finer the sediment, the higher the coefficient for each size metric. This suggests that the size of deposits comprising finer sands are more sensitive to a rise in discharge. For example, the coefficient for volume is 29.51 for very fine sand (for every increment of 1 in discharge, volume increases by 29.51 m^3), with the equivalents being: 24.97 (fine sand), 19.95 (medium sand), 14.83 (coarse sand), and 10.76 (very coarse sand).

5.4.2 Morphometric scaling relationships for natural crevasse splays

From the derivation of scaling relationships using natural log space, it is deduced that strong positive correlations exist between the physical parameters in each panel of Figure 5-9. A general trend in all four panels is that the higher the discharge, the larger the deposits. Within each grain size, the smaller circles are located towards the bottom left of each plot, with symbol size increasing as the morphometric measures on both axes increase. In addition, it is found that the crevasse splays created by all grain sizes are indistinguishable in the length vs area and the perimeter vs area scaling relationships in panels A and B. There is minor variation around the dominant gradient, irrespective of the grain size modelled.

The opposite is true when the splay volume is plotted, which is a more sensitive metric when examining the impact of sediment size on natural splay morphology. Positive correlations remain between the variables shown in panels C and D, with deposits created in low discharge and coarse sediment conditions located in the bottom left. However, each grain size appears to have an independent distribution perpendicular to the dominant gradient rather than collapsing into a single universal relationship. Indeed, panel C suggests that it requires a higher discharge in the coarser sand models to form the same splay area as that of a deposit comprising finer sands, yet these coarse sand splays then have a larger volume than finer sand deposits with the same area, implying that these coarse-grained deposits are thicker.

To analyse this further, panel D comprises width-averaged volumes of splays plotted against their intrusion length. This metric is commonly used to represent the mean thickness for a single slice through a deposit (Carruthers et al., 2013; Rogers et al., 2015). The plot demonstrates different linear relationships (plotted in natural log space) for the very fine and fine sand splays, with a linear dependence of splay volume on the splay extent. This indicates that regardless of the discharge used and the splay size created, the deposits composed of these finer sand grains retain their thickness relative to their length. Meanwhile, the relationships appear more muddled

for the medium to very coarse sand grains – particularly at low discharges where the deposits created were small. At higher discharges, width-averaged volumes of the coarse sand splays were greater than the finer sands for a given intrusion length. This corroborates the findings in panel C, wherein the coarser sand grains have the potential to create thicker deposits.

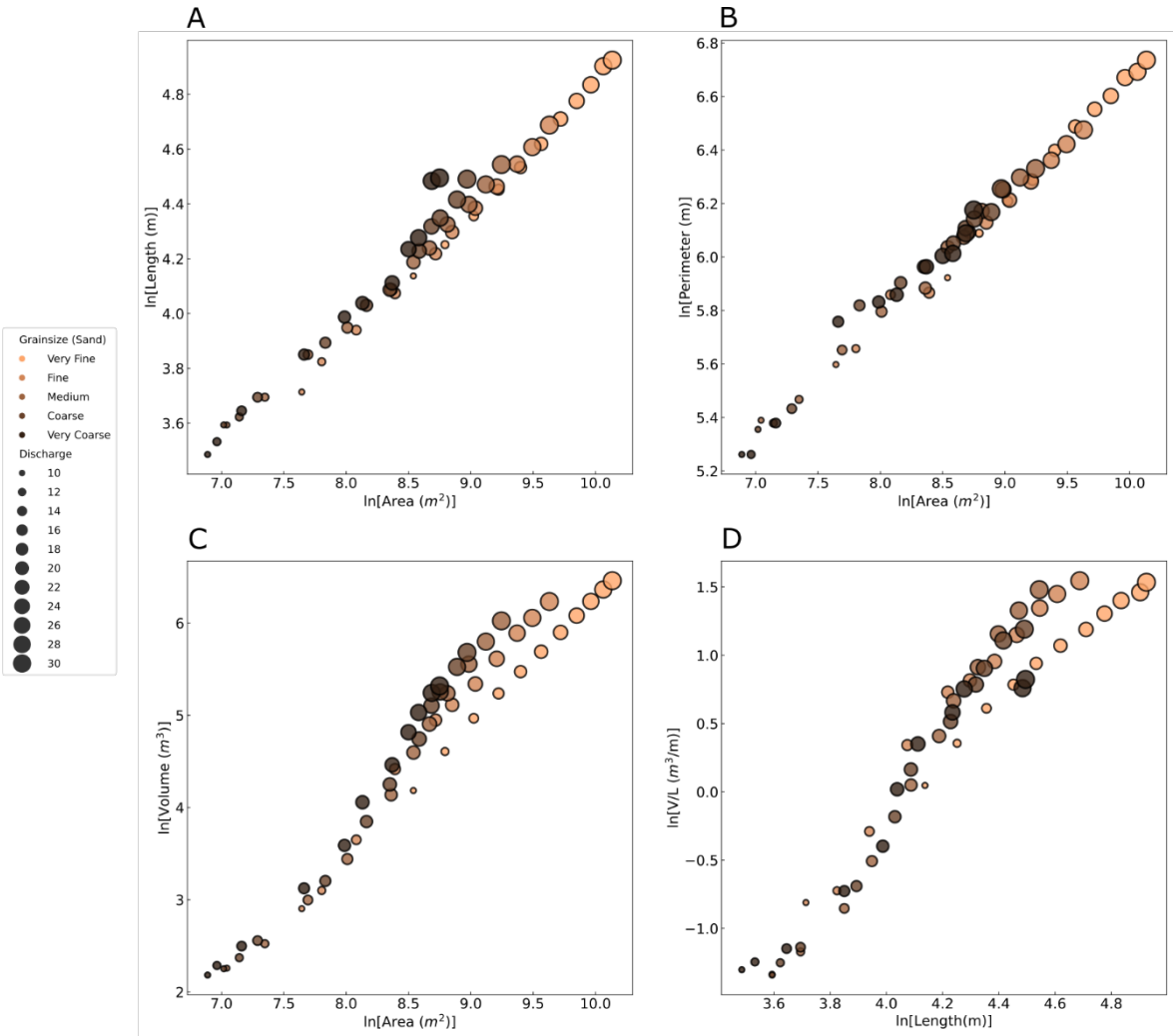

Figure 5-9 Morphometric scaling relationships for natural crevasse splay deposits with five parameters: length, perimeter, area, volume, and volume/width. For all panels, point colour represents the grain size modelled, whilst point size illustrates the input discharge for that experiment. These results are plotted in natural log space.

5.4.3 Influence of floodplain roughness on crevasse splay morphology

After analysing the effect of discharge and sediment size on crevasse splays, this section explores the impact of floodplain roughness on deposit morphology, using the five sediment classifications for a set discharge of 24 cumecs. Fundamentally, it was found that increasing the floodplain's roughness leads to the formation of larger splays (Figure 5-10).

The previous pattern of finer sand deposits being larger than coarser splays is replicated in these scatter plots. This demonstrates that the general impact of grain size on deposit size is not altered when floodplain roughness is changed. However, as floodplain roughness is increased towards the top end of the sampled Manning's N values, the size of the fine sand deposits is exceeded in some cases by splays formed using coarser sands. This pattern is present at a Manning's N of 0.1 for length (medium sand splay - 5.42 m longer), perimeter (medium sand splay - 36 m longer), area (medium sand splay - 255.89 m^2 larger) and volume (medium sand splay - 79.28 m^3 larger and very coarse sand splay - 42.32 m^3 larger).

For all grain sizes, the smoothest floodplain surface used (Manning's N = 0.01) induced the formation of the smallest crevasse splays. From this basepoint, there is a general trend of deposits growing as floodplain roughness increases. Nevertheless, when looked at in more detail, this trend varies between the different grain sizes and deposit size metrics. It appears that, universally, splay deposit size initially rises quickly for the first two increments of floodplain roughness, e.g. the area of the very fine sand deposit under a Manning's N value of 0.01 is 2107.78 m^2, growing to 11245.2 m^2 and 18472.37 m^2 for Manning's N values of 0.02 and 0.03, respectively. At this point in the Manning's N values tested, the steep upwards trend in deposit size for each roughness increment begins to stagnate for all grain sizes, with a much gentler positive gradient subsequently shown. When Manning's N reached 0.08 and above, there was a slight decrease in the very fine sand deposits' perimeter, area, and volume.

Meanwhile, the positive gradient between floodplain roughness and splay size tails off earlier in the fine sand sample. Here, whilst length, perimeter, and area remain stable from N = 0.04 onwards, deposit volume peaks at 303.76 m^3, at N = 0.05, decreasing to 275.51 m^3 and 255.48 m^3 at Manning's N values of 0.09 and 0.1, respectively. However, splay size increases for the coarsest three sand grains until the maximum roughness is used – but with a more gradual gradient. Lastly, the length scatterplot and regime diagram show a different pattern from that observed in the other size metrics. Here, an increase in splay length associated with rising roughness values appears to level off after a Manning's N value of 0.04. This suggests that whilst the intrusion distance remains relatively constant, the deposit's broadness and thickness change.

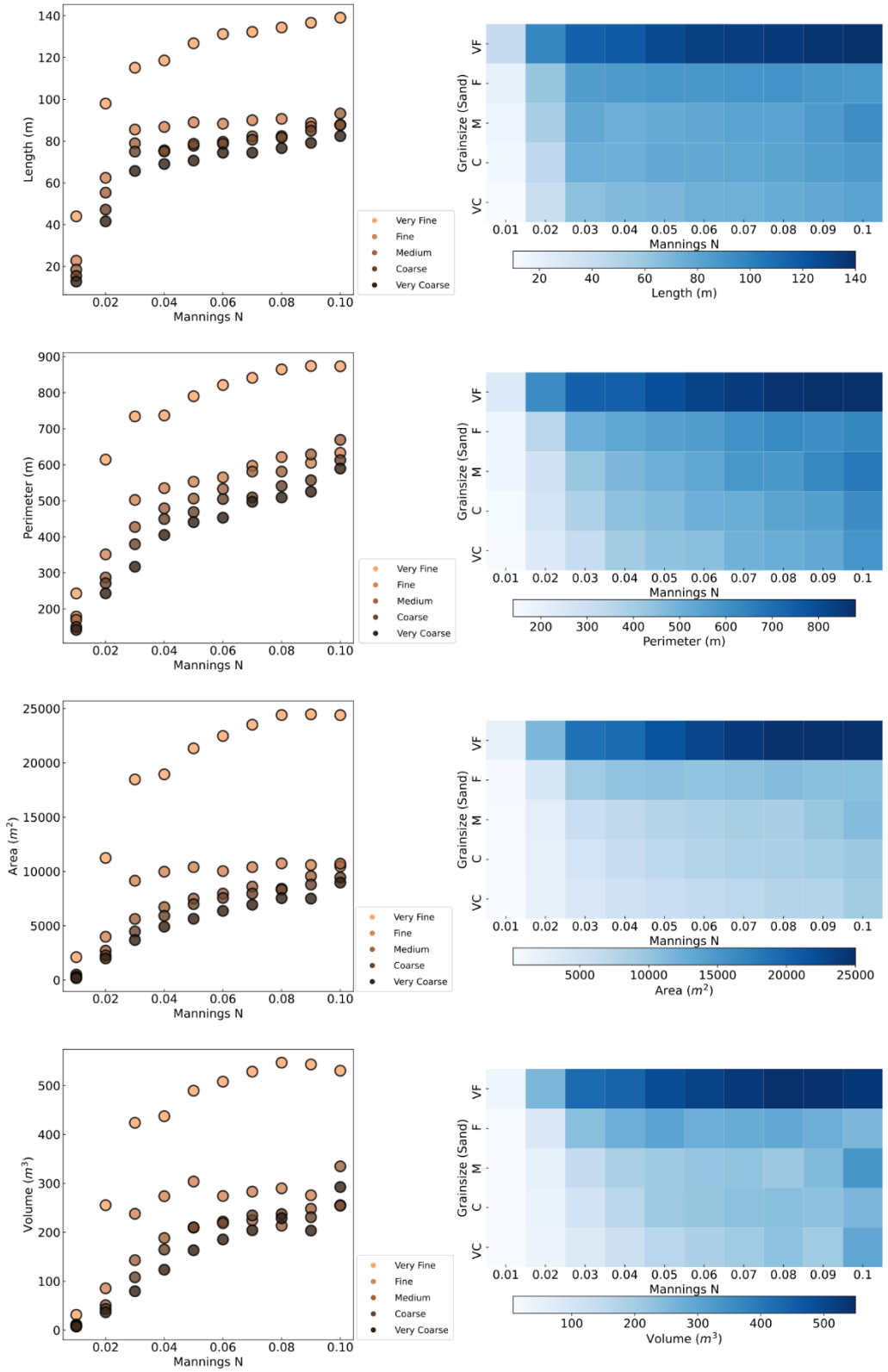

Figure 5-10 A depiction of floodplain roughness's impact on natural crevasse splay morphology. Left panel: scatter plots are provided with physical parameters (length, perimeter, area, and volume) vs Mannings N, with points coloured by grain size. Right panel: regime diagrams with roughness on the x-axis and grain size on the y-axis – each grid cell (an individual deposit) is coloured by a physical attribute of the deposits.

5.4.4 Impacts of discharge, grain size and floodplain roughness on deposit shape

This section focuses on splay shape rather than size and how this is affected by environmental conditions. The Distortion Index (DI) metric is used to compare the outer perimeter of each deposit to that of a semi-circle – a typical fan shape in hydrological environments - with the same area – measured perimeter (P_m) divided by the ideal perimeter (P_i). When examining the discharge figures, there is a discernible difference between the shapes of the deposits created using different grain sizes, as shown in Figure 5-11. Both the maximum DI and range of DI values increase as grain size coarsens. Indeed, the very fine sand deposits retain a DI of 1.3 to the nearest decimal place during all eleven discharges tested, with fine deposits reaching 1.5. Meanwhile, medium and coarse sand deposits attain a maximum DI of 1.6, with very coarse sand splays having the highest value of 1.7.

The higher DI values within each grain size occur when discharges are low, i.e. between 10 and 16 cumecs. In some cases, such as the coarse and very coarse sand model runs, DI begins lower at the minimum discharge (10 cumecs) with a value of 1.5. DI increases to 1.6 (coarse) and 1.7 (very coarse) once the input discharge reaches 16 cumecs. As discharge rises beyond 20 cumecs, DI decreases with the minimum DI values typically found between 26 and 30 cumecs for each grain size modelled.

When discharge was kept at a constant 24 cumecs, and instead the floodplain roughness was varied, each grain size followed a similar pattern, aside from very fine sand. As before, the very fine sand shows minimal fluctuation in its DI values from a Manning's N of 0.01 to 0.1, remaining at 1.3 and 1.4 – staying similar in their planform shape throughout. Meanwhile, the other four grain sizes begin with very high DI values when the N value is at the minimum of 0.01. At N = 0.01, DI increases as grain size coarsens - from 1.9 for fine sand to 2.7 for very coarse sand. These DI values then drop dramatically when floodplain roughness is increased. If the deposits created at N = 0.01 are ignored, the overall pattern is that, as roughness is increased, there is a gradual increase in DI values. For example, a medium sand deposit has a DI of 1.3 at N = 0.02, which rises to a DI of 1.6 at N = 0.1. This pattern is repeated across the trial runs consisting of the grain sizes: fine, coarse, and very coarse sand.

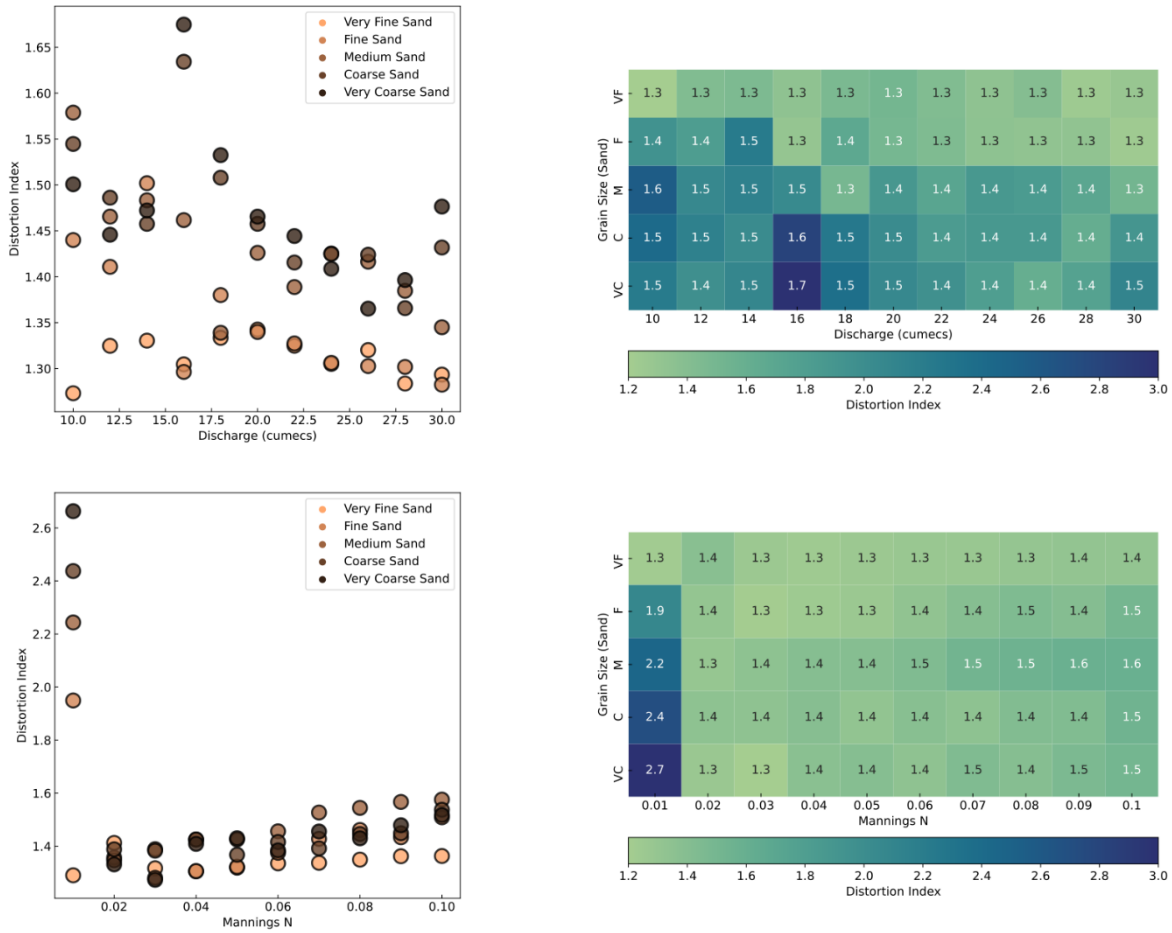

Figure 5-11 The impact of roughness on the planform shape of natural crevasse splays. Left: scatterplots with distortion index vs discharge and Mannings N, coloured by sediment size. Right: regime diagrams with grain size on both y-axes, coloured by distortion index, the top graph has discharge on the x-axis and the bottom graph has Mannings N on the x-axis.

Considering the results from the sand grain model runs and to allow a comparison to previous research (Millard *et al.,* 2017), a further nine experiments were run using three silt fractions (fine, medium, and coarse) across three discharges (10, 20 and 30 cumecs). The specific silt fraction grain sizes are detailed in Table 5-3. Figure 5-12 plots the physical parameters of the splays created in these silt models alongside those of the very fine sand and shows diverse relationships between grain size and deposit size, which are dictated by flood size. Firstly, at the lowest discharge of 10 cumecs, the largest deposits were formed using the finest silt fraction, with splays then decreasing in all size parameters as grain size was coarsened. This is highlighted by the volume of the coarse silt and very fine sand being ~2x and ~4x lower than that of the fine silt splays, respectively.

Table 5-3 Sediment sizes used within each grouping of silt: fine, medium, and coarse. The finest grain within each silt category is defined as the suspended load, with the fall velocities provided.

Silt Category	Grain size (mm)	Fall Velocity (m/s)
Fine	0.00078	0.0002
	0.00104	N/A
	0.0013	
	0.00156	
Medium	0.001561	0.0008
	0.00207	N/A
	0.00259	
	0.0031	
Coarse	0.00311	0.00187
	0.00415	N/A
	0.0052	
	0.00625	

When discharge was increased to 20 cumecs, all splays were more extensive than their counterparts at 10 cumecs, except the volume of the fine silt deposit, which decreased. The largest deposits were formed using the medium silt fraction, usurping the fine silt in all size metrics. Additionally, even though the splays derived from coarse silt and very fine sand remained smaller in length, perimeter, and area than the fine silt deposits, their volume exceeded that of the deposit composed of the finest grains.

Finally, the largest discharge of 30 cumecs instigated a reduction in the length and volume of the medium silt deposit compared to that produced in the 20 cumecs scenario, whilst perimeter and area both showed a minor increase. This, coupled with the considerable rise in the size of the splay composed of coarse silt, meant the deposit created in the coarse silt experiment at 30

cumecs was the most substantial. It is worth noting that although the very fine sand deposit has a lower length, perimeter, and area than fine and medium silt splays, its volume is over 220 m^3 higher than that of the medium silt and approximately 400 m^3 above that of the fine silt.

It has been shown that deposit size at 10 cumecs peaked at fine silt, medium silt for 20 cumecs and coarse silt for 30 cumecs. When the discharge is low, the fine silt splay is the largest, with a subsequent decreasing trend in deposit size as grain size coarsens. At a medium discharge of 20 cumecs, deposit size increases as grain size coarsens from fine silt to medium silt, an inverse of the previous trend. However, when grain size was increased beyond medium silt at this discharge, splay size decreased, as observed at 10 cumecs and within the sand results presented earlier. Meanwhile, at the highest discharge, deposit size continued to rise with increasing sediment coarseness until it peaked at coarse silt, with the trend inverting once again with a decrease in splay size for the very fine sand deposit.

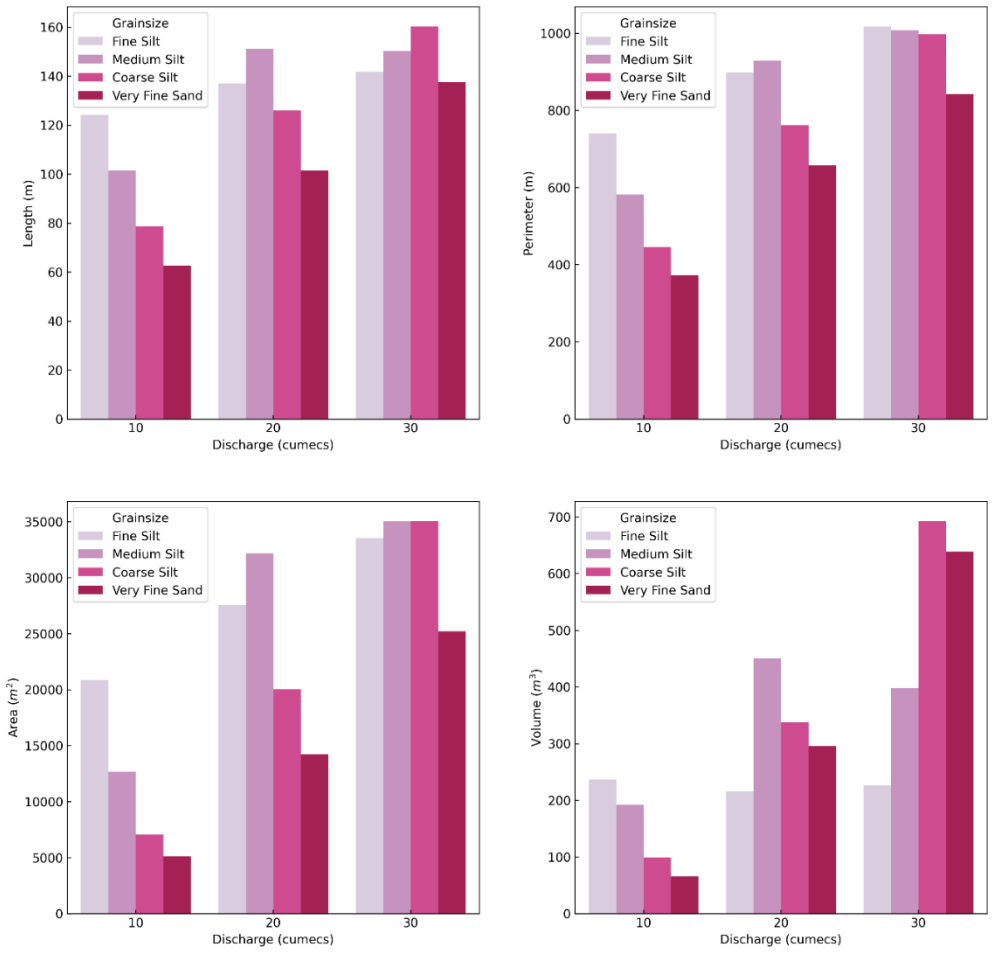

Figure 5-12 The size of natural crevasse splays created using three silt fractions and very fine sand.

5.5 Discussion

5.5.1 Applicability of CAESAR-Lisflood

Initially, it should be acknowledged that using the CAESAR-Lisflood software, along with the input parameters chosen, successfully allowed an array of splay deposits to be produced on the deliberately simplified floodplain - with a range of deposit shapes and sizes generated. This permitted the impact of various flow and sediment characteristics to be tested on splay morphology – and an observation of how the model acts under different environmental conditions.

A vital component of this study was whether the morphological processes implemented by the CAESAR-Lisflood software mirror theories set out in previous literature. Before examining the quantitative results, it is essential to note that during splay formation, the deposit closed off to additional floodwater and sediment, preventing further growth. This reflects the concept set out by both Roberts (1997) and Yuill *et al.* (2016) such that a deposits growth will cease once it reaches a certain thickness at the levee breach, caused by a reduction in energy slope and the consequent accretion in the breach channel blocking any further input. Moreover, it was immediately apparent that the deposits formed by CAESAR-Lisflood echoed the expectation that crevasse splays are fan-like in planform shape – brought about when the floodwaters move from a confined channel onto an unconfined floodplain (Iacobucci *et al.*, 2020), as illustrated in Figure 5-7. Once the waters reach the unconfined floodplain, they can move uniformly in each direction, depositing sediment as the flow decelerates – creating a semi-circular-shaped splay.

In addition, the observed phenomenon whereby the splay deposits were thickest near the levee breach, with a subsequent thinning pattern towards the deposit edges, matches established literature. For example, Pizzuto (1987) indicates that the thickness of sediment deposits on floodplains exponentially decreases as the distance from the channel increases – particularly for silt and sand grain sizes. Furthermore, in a study of the geometry of a natural crevasse splay on the banks of the Clarence River in New South Wales, Australia, O'Brien and Wells (1986) found the deposit was at its thickest next to the levee breach, with the deposit then thinning gradually towards its outermost edges. These findings, which coincide with existing theories concerning splay deposit morphology, imply that CAESAR-Lisflood is suitable for exploring the size and shape of crevasse splays under various environmental conditions.

5.5.2 Impact of discharge and grain size on splay morphology

5.5.2.1 Splay size and topography

In the case of discharge as an independent variable, there is no existing empirical morphometric data reflecting the impact of flow conditions on crevasse splay size. Hence, the results of this research provide a novel insight into the response of deposit morphology to flow size. As follows intuition, when the grain size is kept constant, higher discharges encourage the production of more extensive deposits than those created in low discharge conditions. This has been highlighted by the results of the linear model, which demonstrate strong positive correlations between discharge and each deposit size metric. Such findings reflect the notion that with increasing discharge comes the ability of the water to transport more sediment onto the floodplain through the levee breach (Millard *et al.,* 2017). Raising the discharge input into the model elevates the stream power (Bagnold, 1977; Gartner *et al.*, 2015), increasing the transport capacity of the flows within the river channel and those extending onto the floodplain. Such a rise in energy increases the sediment supply to the floodplain and consequently promotes the creation of larger splays. In addition, higher discharges lead to the entrained sediment being moved further onto the floodplain, leading to a broader extent of splay deposit (Yuill *et al.*, 2016).

The linear models used to develop correlation coefficients (Table 5-2), which depicted the relationship between discharge and deposit size, show an apparent disparity in the rate of deposit size increase between the five grain sizes sampled. As discharge was increased, the relative effect on deposit size differed for each grain size, with the finer sediment deposits growing faster than those composed of coarser sand. This has demonstrated that different flood discharges and grain sizes combine to generate a range of crevasse splay sizes. Therefore, implying discharge alone is not a sufficient predictor of crevasse splay size, with other environmental factors important to consider, as mentioned by Millard *et al.* (2017).

Here, it has been demonstrated that grain size impacts terminal deposit size, with the coarser the sand sediment, the smaller the deposit in all size metrics. A collective understanding substantiates these findings as grain size drives the quantity of sediment supplied to splay deposits (Asselman and Middelkoop, 1995; Slingerland and Smith, 1998). Stream power is often quantified using flow depth and discharge (Bagnold, 1977). It dictates the amount of sediment transport that can occur, with stream power needing to exceed a critical threshold for a specific grain size to be moved. The finer the sediment, the greater the amount of sediment transport for a given discharge – due to the lower amount of power necessary to move smaller sediment (Wilcock and Crowe, 2003; Ali *et al.*, 2013; Lammers and Bledsoe, 2018). Therefore justifying

that the finer sand models should result in more extensive splay deposits due to the sediment supply being higher through the levee breach than when sediment is coarser.

However, these results do not corroborate the conclusions of Millard *et al.* (2017), which indicate that splay size increases with coarsening grain sizes. This may be down to the grain sizes used in their Delft-3D experiments, which included three categories: a silt fraction, a coarse silt to fine sand fraction, and a coarse sand fraction. Therefore, an additional nine models were run in this research to allow a more thorough comparison with the data from Millard *et al.* (2017) data using three silt fractions.

The results have highlighted a more intricate relationship between grain size and deposit size than previously discovered. At the lowest discharge, the largest splay deposits were formed using the finest silt fraction, with splays decreasing in all size parameters as sediment was coarsened. In these experiments, the quantity of sediment transported through the levee breach and onto the floodplain is higher for the fine silt than the other grains, as this fraction requires the least energy to move. With discharge at 10 cumecs, the finest sediment can be deposited close to the levee breach as energy is low. However, the pattern became more complex when the storm size was increased. Firstly, the volume of the splays generated using the finer silt remains consistent with that created under low discharge conditions. Alongside this, the volume of the medium silt, the largest deposit at 20 cumecs, is reduced at the highest discharge (30 cumecs). This is because although the quantity of fine sediment being moved onto the floodplain is increased with higher discharges, a substantial proportion remains suspended due to the energy present. Indeed, silt-sized sediment typically makes up a river systems washload – staying suspended and not interacting with the bedload (van Gelder *et al.*, 1994; Yuill *et al.*, 2016). Thus, it can be inferred that, although the finer silts allow copious quantities of sediment to be transported onto the floodplain, the flood flows take much of the material out of the vicinity. This is particularly prevalent at larger storm sizes, with the increased energy preventing widespread deposition (Teeter, 2000; McCave, 2008).

When the sediment modelled was coarser than the fine and medium silts, the sediment supply to the floodplain became lower for a given flow size. However, when these experiments incorporated higher discharges, the crevasse splays formed using the coarse silt and very fine sand grains were composed of more sediment than those generated using finer silts. These coarser fractions require more energy to move, so even though the sediment supply to the floodplain is reduced, a more substantial proportion of the sediment load is deposited rather than being carried away from the deposit.

Succinctly, the greater the power, the more sediment is moved onto the floodplain for a given grain size, but this increase in energy can cause the finer grains to be transported away from the splay without being deposited. As such, the results generated by this sample of silt fractions have shown that the findings of Millard *et al.* (2017) can be reciprocated in some instances, in that the coarser the sediment, the larger the deposit. However, the conclusions of the models run in this research using an array of sand grain sizes suggest that their range of sampled grain sizes could not capture the complete picture of the relationship between grain size and the size of the splay produced. There appears to be a discharge threshold whereby increasing the grain size switches from encouraging the generation of more extensive deposits to inhibiting splay size. This pattern is indicative of an optimal grain size at which deposit size is largest - where the sediment supply to the floodplain is high, but the quantity being removed away from the floodplain as washload is reduced, highlighted by the bell-shaped curves illustrated in the silt results, at 20 and 30 cumecs (Figure 5-11).

Regarding deposit topography, the different grain sizes samples have produced a mix of splay deposit structures. From observation of the planform views of crevasse splays in Figure 5-7, it is evident that grain size has a dominant influence on the uniformness of splay elevation. The very fine and fine sand grain size deposits appear uniformly thin from the levee breach opening to the outer edge – with slight variance in topography. This is typified by each shade of green in the plan view of elevations being similar in shape to the deposit's outer perimeter. This pattern implies that as these flows move away from the breach, deceleration and energy loss occur at equal distances in all flow directions. As a result, transport capacity decreases uniformly, and these conditions produce an evenly spread crevasse splay.

Meanwhile, the topography of the splays composed of coarser sands looks rougher and more variable. Each green elevation class is an entirely different shape from the other, e.g., the extension of the -0.1 - -0.19 class to the north in the very coarse splay. Therefore, when flows laden with coarser sediment extended onto the floodplain, energy dissipation from the flows was more varied, causing uneven deposition across the study area. Such findings were expected given that established literature suggests that grain size has a direct impact on sediment deposition patterns (Cazanacli and Smith, 1998; Fedele and Paola, 2007).

5.5.2.2 Splay scaling laws

This section addresses the combined impact of grain size and discharge on crevasse splay morphometric scaling relationships. The scaling relationships developed have highlighted differences in how size metrics change in relation to each other when a variety of grain sizes and discharges are utilised. It was evident that the length and perimeter vs area scaling laws

remained consistent between grain sizes and at all discharges – with little deviation around a dominant gradient. As the deposit area grows, length and perimeter grow in tandem, regardless of grain size. This indicates that splays retain a similar planform shape as they grow with increasing discharge.

On the other hand, the scaling laws involving volume measurements are more varied. For example, when the splay volumes are plotted against their area, each grain size plots along its own dominant gradient rather than collapsing to one. These relationships have little variation and as such, it can be deduced that if one knew the main grain size that comprises the splay, and the area (2D) of land affected, the volume (3D) could be predicted. In this case, the coarser the sediment, the higher the volume for a given area. Coarser sediment requires a higher discharge to attain the same deposit area as the finer sands. With this increase in energy, more sediment can be entrained in the flood flows, and once the coarser sediment has been taken onto the floodplain, it requires more energy to keep moving than the finer grains. Therefore, for a given distance onto the floodplain, the flows would deposit greater quantities of coarse grains than the fine sediment due to its inability to transport a greater proportion of the coarser load. Overall, this pattern suggests that as discharge increases, deposits comprised of coarse sands accrete more vertically than laterally, as opposed to fine sand deposits, which retain their usual morphology and maintain their average thickness relative to length and area throughout. This is supported by the volume vs area and the volume/width vs length scaling relationships which provide insight into splay thickness.

There is a discrepancy in the width-averaged volume vs length scaling relationship. It is shown that two very coarse sand splays, formed under high discharge conditions, encroach upon the fine sand trendline. Here, the intrusion length of these splays is higher due to a small lobe extending from the deposit edge – a change in shape to the other very coarse sand deposits. This forces the deposits to have a longer length relative to their V/W value – even though volume has increased. This could result from the slight rise in discharge, inducing a variation in flow patterns on the edge of the deposit. Such variation creates a new scouring channel, with a new depositional lobe surrounding this. Therefore, when comparing the two scaling relationships that provide an insight into deposit thickness, volume vs area appears to provide a more consistent response than the width-averaged volume vs length. The latter is often used in studies of deposits (Carruthers *et al.*, 2013; Rogers *et al.*, 2015) and as such, they may not capture a true depiction of how volume scales and in turn, deposit thickness.

5.5.3 Impact of floodplain roughness on splay morphology

Floodplain roughness represents another variable which can alter the morphology of crevasse splays. Surface roughness is crucial in hydrodynamic models as it substantially impacts flow elevations and velocities (Mason *et al.*, 2003; Straatsma and Baptist, 2008). Roughness is a measure of the friction exerted by the surface upon the flows over it (Sellin *et al.*, 2003). Within hydrodynamic models, roughness causes the flow to lose momentum, which can be induced by obstacles, riparian vegetation, elevation changes, and bed characteristics (Baptist *et al.*, 2007). During extreme flooding, the principal component impacting flow dynamics is the quantity and density of riparian vegetation (Darby, 1999). Although Manning's N values do not necessarily provide an accurate representation of specific floodplain environments, including vegetation characteristics (Västilä and Järvelä, 2014), this research uses Manning's N as a proxy to investigate how smooth and rough surfaces influence splay deposit size.

As the only component altered was the roughness of the defined floodplain area outside the levee breach, it can be inferred that the potential sediment supply out of the channel from the floodwaters remained the same. During experiments where floodplain roughness was at its lowest (N = 0.01), the deposits created were at their smallest. Such a smooth surface allowed flows to travel over the floodplain with limited deceleration (Fernandes *et al.,* 2012). In these smooth drainage conditions, minimal friction is imparted on the sediment-laden flood flows by the underlying surface. Consequently, the flood flows were able to retain more of their energy, leading to a higher proportion of the sediment transported out of the levee breach being carried out of the studies domain as the transport capacity does not become exceeded (Asselman and Middelkoop, 1995). Therefore, although the sediment supply to the floodplain would be the same as within the other roughness values, the sediment available for deposit growth was at its lowest.

When floodplain roughness was increased from N = 0.01, in increments, deposit size increased as a result. This concurs with the findings from a study by Fraselle *et al.* (2010), which used flumes to test the distribution of sediment deposition on an artificial floodplain under different roughness conditions using steel sheeting and nets – which aimed to replicate vegetation presence. The increased roughness of the floodplain causes a reduction in flow velocity and, subsequently, lower energy. Such an energy reduction creates conditions which promote increased deposition in the crevasse splays, wherein the transport capacity of the flow is exceeded (Prosser and Rustomji, 2000; Lhomme *et al.*, 2008). Subsequently, areas with a higher level of roughness have the potential to trap more sediment by increasing drag (Fraselle *et al.,* 2010).

Another pattern discovered in this research was that once floodplain roughness reaches a certain roughness (N = 0.05 here), the gradient in splay size increase levels off for each grain size – but predominantly for the finer sediment. There are a couple of potential explanations for this, and they could work in conjunction. Firstly, the rise in floodplain roughness could act to make the deposit accrete near the levee breach opening. Once this accretion reaches a specific elevation, it would prevent additional sediment-laden flows from extending onto the floodplain. Therefore, the sediment supply to the crevasse splay could remain similar for all roughness values upwards from N = 0.05. Secondly, an equilibrium could exist between increasing floodplain roughness acting to trap more sediment at a wider extent and the impact it has on the deceleration of floodwaters. This suggestion would resonate with the different responses of each deposit size metric to increasing roughness. As N reaches 0.05, intrusion distance (length) becomes constant, whereas deposit volume and, inherently, thickness increase– at a more gradual rate. This implies that the low-velocity flows may have deposited a considerable proportion of the sediment before the maximum intrusion distance, and subsequently, the splay does not intrude further onto the floodplain. Instead, the sediment is deposited onto the existing crevasse splay. These findings reflect the theory by Nardin and Edmonds (2014), in that intermediate vegetation presence and density instigate the most deposition on floodplains – with the decrease in volume of very fine sand deposits once Manning's N reaches 0.08.

5.5.4 Impact of environmental conditions on the planform shape of splays

In previous studies, there has been a lack of investigation into the planform shape of crevasse splays. It is widely acknowledged that the topography of inundated areas can shape sediment deposition (Nicholas and Walling, 1997, Millard *et al.,* 2017), but depositional patterns on flat floodplains are unknown. Therefore, the distortion Index (DI) was used to interpret the planform shape of the crevasse splays generated using various discharges, grain sizes and floodplain roughness values. DI provides a quantitative measure of the degree to which the outer edge of a sediment deposit deviates from a perfect semi-circular arc. This study found that discharge, grain size and roughness influence deposit shape.

Typically, the coarser the sediment, the higher the DI for a given discharge, indicating that coarser deposits have uneven edges rather than a more-rounded shape. In contrast, deposits comprising finer sand are characterised by smoother, more uniform edges – closer to a semi-circular shape. This implies that flow containing coarser deposits decreases in velocity and thus transport capacity non-uniformly as the distance from the breach increases, creating different deposit shapes to that of finer sediment.

Moreover, the higher distortion values for each grain size occurred at the lower end of the sampled discharges. In these model runs, the deposits created are negligible due to the low sediment supply onto the floodplain, as the flows do not have the energy to transport much sediment out of the channel. Consequently, this causes scouring channels on the floodplain surface where the floodwaters do not need to drop the sediment they transport and instead erode. This creates small fan-shaped deposits with substantial gaps within them. As discharge and sediment supply increase, the deposits become more substantial with fewer gaps and erosional channels, reducing the DI values as the deposit area rises relative to the perimeter. When the discharge is higher, there is more sediment supply to the floodplain, meaning the transport capacity is exceeded quicker, creating deposits extending immediately from the levee breach.

Lastly, when the influence of roughness was isolated, there was a positive trend between Manning's N and DI. However, an outlier of this trend occurred at the lowest floodplain roughness value, N = 0.01, whereby DI was higher than in other model runs. In this situation, minimal deposition occurred for the fine to very coarse sand samples, resulting in small deposits with high perimeters relative to the area. As floodplain roughness increases, splay size increases, and the deposits become substantial, with the area growing relative to the perimeter.

5.6 Chapter Summary

This chapter has successfully tested the use and ability of the cellular automata model, CAESAR-Lisflood, in producing crevasse splay deposits on a flat floodplain following an artificial levee breach. A range of environmental conditions - grain size, discharge, and floodplain roughness - have been able to be tested extensively. In doing so, the two objectives in this chapter's introduction have been addressed.

1. Explore using a morphological model, which incorporates sediment dynamics and transport with hydrology, in assessing the impact of grain size, discharge and floodplain roughness on crevasse splay morphology.

The results generated in this chapter have extended to previous modelling research. The results produced here suggest that the response of deposit size to changing grain sizes is more complex than formerly thought. It has been illustrated that although increasing the grain size input from very fine to very coarse sand leads to a substantial incremental reduction in terminal splay size, the pattern is more complex when silt grains are utilised. This has enhanced the understanding of fluvial flood-induced sediment deposition patterns, alongside demonstrating that increasing discharge and floodplain roughness cause rises in deposit size.

2. Investigate whether CAESAR-Lisflood can generate crevasse splay deposits. Whether hydrodynamic morphological models can be reliably used to create landforms resulting from flood events is a question.

This chapter has highlighted that a morphological model can generate crevasse splays and has permitted the effect of different environmental conditions on splay morphology to be efficiently tested. Events witnessed during the model runs have reflected well-known morphological processes during levee breaches and splay formation. These include creating fan-like deposits and the levee breach's closing as sediment accretes, preventing continual flood flow and entrained sediment from reaching the floodplain.

Next, this thesis will study, using CAESAR-Lisflood, the impact of the built environment on the morphology of crevasse splay deposits and how the findings in this chapter are affected by a range of built setups.

Chapter 6 Modelling impacts of the built environment on crevasse splay morphology

6.1 Chapter objectives

This chapter addresses a gap in the quantitative understanding regarding how built environments impact crevasse splay morphology.

This chapter will:

1. Model a series of crevasse splay deposits in idealised built environment "fabrics" for various flood conditions using CAESAR-Lisflood (Coulthard *et al.,* 2013).
2. Investigate the effect of the built environment on the geometry and scaling of fluvial deposit morphology.

6.2 Introduction

Fluvial floods can transfer vast amounts of sediment from river channels onto neighbouring floodplains (Walling and He, 1998). Crevasse splays, a depositional landform, are produced when sediment-laden floodwaters propagate out of the river channel, usually through a levee breach, with sediment being released from the flows as energy dissipates on an unconfined surface, creating lobal fan-shaped deposits (Iacobucci *et al.*, 2020; Rahman *et al.*, 2022). Natural crevasse splays have been studied in a range of fluvial systems located across multiple continents (Aslan and Blum, 1999; Tye, 2004; Millard *et al.*, 2017; Nienhuis *et al.*, 2018; Rahman *et al.*, 2022), with their importance to landscapes accounted for in their ability for building land, i.e. floodplain upkeep and levee creation (Bridge, 1984; Stouthamer, 2001; Esposito *et al.*, 2017).

However, when sediment-laden flows enter built environments, they pose a hazard with the potential to cause damage to infrastructure (Sturm *et al.*, 2018) and disrupt road networks (Nordstrom and Jackson, 1995; Aldabet *et al.*, 2022). In addition, such damage can hinder emergency response (Kobayashi, 1995; USEPA, 2008) and halt the restoration of essential services such as electrical and water supply (Johansen and Tien, 2018). Despite this, the quantitative effect of built environments on the morphology of crevasse splays is unknown, with only qualitative observations existing (Nelson and Leclair, 2006).

To this end, CAESAR-Lisflood is utilised to explore the built environment's impact on crevasse splay deposits. This is tested using a constant floodplain roughness, various flow discharges and

five grain size distributions across a series of five built "fabrics" with differing densities of buildings. Following this, by setting discharge at 24 cumecs, two additional Manning's roughness values are used for each grain size and building setup. Overall, this produces 325 splay deposits in a variety of environmental conditions. The morphological parameters of length, perimeter, area, and volume are measured for each deposit, allowing for an examination and comparison of deposit size and shape.

6.2.1 Background

Fluvial floods are the most common natural disaster occurring globally, with more than 3000 floods recorded in the Emergency Event Database (EM-DAT) from 1990 to 2010 (Wang *et al.*, 2011). Although fluvial flooding is essential for natural landscapes and the ecosystems they support, when floods interact with urban areas, they can have devastating consequences on the human populations and infrastructure present (Koks and Thissen, 2016). Since 1980, floods from a fluvial source have caused approximately 200,000 deaths (Dottori *et al.*, 2018), with economic costs upwards of $1 trillion from 1980 – 2013. Despite this danger to livelihoods, low-lying floodplains are often densely populated as they provide a desirable location for human inhabitation due to their access to trade routes, water supply, and their attractiveness for recreation (De Stefano *et al.*, 2017), with over 50% of the global population living within 3 km of a freshwater body (Fang *et al.*, 2021) and approximately 800 million living in flood-prone zones (Peduzzi *et al.*, 2012). Recent estimations suggest that roughly 70 million people are affected by floods annually (Peduzzi *et al.,* 2012). However, projections indicate that the threat of floods will only rise because of socioeconomic development and ongoing climate change, making populations more vulnerable to more extreme and frequent hazards (Nirupama and Simonovic, 2007; Hirabayashi *et al.*, 2021).

Accompanying the inhabitation of river floodplains are substantial changes to land cover and the landscape. Flood management policies used on low-lying floodplains have led to significant changes to these landscapes, such as floodplain constriction through the building of embankments and discharge regulation (Hesselink *et al.*, 2003; Werner *et al.*, 2005). Deforestation, or at least the removal of smaller vegetation, is often necessary to make room for built environments. When this land conversion occurs, it has been shown that it is associated with increased annual discharges for the basin affected and a rise in sediment load annually – an estimated 8.7% rise in sediment supply for a 1% decrease in forest cover (Zhao *et al.*, 2022). In addition, the emergence of buildings and roads on floodplains has created widespread impermeable surfaces (Li *et al.*, 2020), impacting water flow dynamics and sediment sources, pathways, and sinks (Nordstrom, 2004; Syme, 2008; Monk *et al.*, 2019). Such development can

significantly impact peak discharges and, thus, the timing, duration, and amount of overbank flow (Verbeiren *et al.*, 2013). Therefore, this change in land cover directly impacts the morphological consequences of floods by altering natural sediment dynamics.

The only investigations into crevasse splays intruding into built settings have been purely qualitative. Nelson and Sinclair (2006) provide a planform map of a large crevasse splay extending into New Orleans following a levee breach during Hurricane Katrina. This, coupled with quantitative studies examining the morphology of deposits in built-up coastal environments (Rogers *et al.,* 2015; Lazarus *et al.,* 2022), has illustrated the disturbance human infrastructure can impart on sediment processes. It is understood that components of the built environment cause splay deposits to branch down streets and in-between buildings, meaning they are likely to diverge from the morphological norms characterising deposits created on natural floodplains. Built infrastructure manipulates the natural sediment flux by channelising material down streets, blocking pathways, and reducing sediment availability by covering the natural surface with concrete and tarmac (Nordstrom, 1994, 2004). Significantly, built environments are thought to disrupt the sediment supply in catchments leading to questions about how landscapes will evolve. It is essential to understand the impact of humans on natural processes – as this can help to influence informed policy decisions and provide helpful information for delivering recovery plans post-flood events.

Examples of sediment deposits extending into a range of built settings must be sampled, and their morphometric parameters measured to effectively assess the built environment's impact on crevasse splay morphology. Unfortunately, there is difficulty in acquiring high-resolution satellite or aerial imagery that captures crevasse splays within built environments, i.e. location and date, which, combined with the lack of an online repository of post-storm aerial imagery for fluvial floods (as provided by NOAA in the coastal research), necessitates an alternative source of splay deposits. Therefore, a morphological model can be utilised to generate the required dataset, which allows the observation of the impact of various built environments on splay morphology.

The morphological model used is the CAESAR-Lisflood software developed by Coulthard *et al.* (2013) to be consistent with the method implemented in the previous chapter, which looked at natural controls on sediment deposition on a deliberately simplified floodplain. Although this software has typically been used to examine various morphological systems in a natural context (Saynor *et al.*, 2018; Feeney *et al.*, 2020; Ramirez *et al.*, 2020), it provides the opportunity to add non-erodible surfaces into the study domain as bedrock. In addition, DTM (Digital Terrain Model) alterations allow built obstacles to be added in different densities as a raster grid.

Therefore, this chapter uses CAESAR-Lisflood to investigate the built environment's impact on crevasse splay morphology, using non-erodible obstacles in grid-like structures to represent buildings.

6.3 Methods

All GIS and data processing was undertaken in ArcGIS Pro version 2.9, with morphological modelling implemented in CAESAR-Lisflood 1.9J. Data output from the model was projected into the WGS 1984 World Mercator coordinate system.

The workflow below conceptualises the method used in this chapter (Figure 6-1). The starting point is the deliberately-simplified floodplain created in chapter 5. Subsequently, pre-processing is undertaken to develop the five built environments to test. The model parameters are then defined, culminating with detail of the post-processing and analysis techniques used on the model outputs.

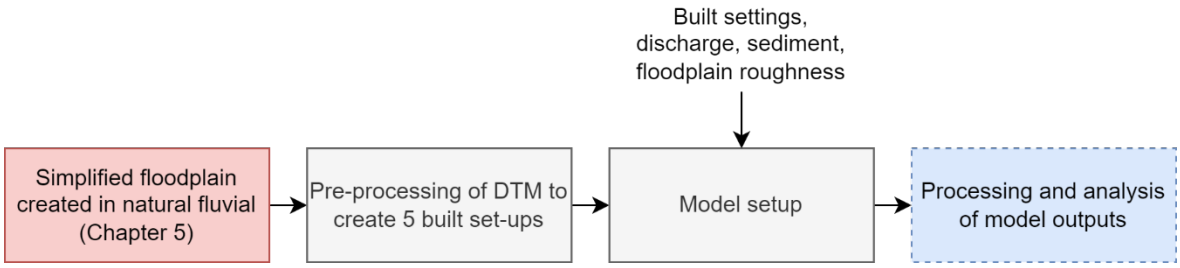

Figure 6-1 Framework for the method investigating crevasse splay morphology in built environments.

6.3.1 Pre-processing

This section details the processing measures undertaken to develop the five built environments from the simplified floodplain developed in Chapter 5, with an overview of the workflow provided in Figure 6-2.

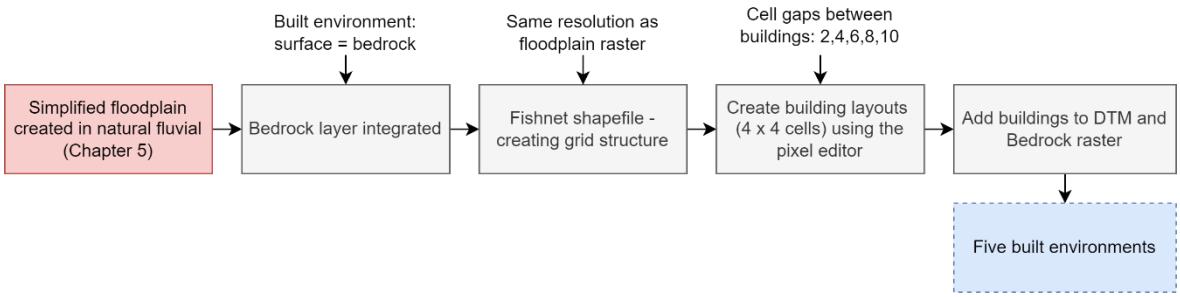

Figure 6-2 Framework for the pre-processing method to generate the five built environments.

To replicate a built environment, the floodplain must be altered to reflect the attributes of the non-erodible surfaces prevalent in built-up areas, i.e. tarmac and concrete. Therefore, developing a 'bedrock' layer as a DEM raster containing elevation below which the model cannot erode was deemed necessary. Firstly, 15 m was subtracted from all DTM values, producing an initial bedrock layer with each pixel depicting an elevation 15 m below the ground surface. However, as this was across the whole model domain, the bedrock elevation values must be aligned with the DTM values for the specified built environment study area.

To do this, the floodplain study area shapefile used to flatten the floodplain in the natural chapter was chosen to define the extent of the built environment. This shapefile was converted into a binary raster so the built environment pixels had a value of 1. This allowed the built environment pixels in the bedrock layer to be assigned the original DTM values (so the bedrock was at the surface), whilst the rest of the setting retained the DTM - 15 values.

The next stage involved integrating the buildings into the DTM so that CAESAR-Lisflood sees them as non-erodible blocks extending vertically above the surface. Therefore, buildings were manually drawn and imprinted onto the DTM and bedrock files. As all inputs to CAESAR-Lisflood must be in raster format, the buildings were limited to being grid-like with a straight orientation from north to south. It was decided that buildings would be made up of 4 x 4 grid cells (8 x 8m), and the street width (number of cells between each building – built spacing) would be altered between trials to test a variety of built fractions.

Firstly, a fishnet shapefile was created using the spatial resolution and extent of the DTM. This produced a red grid around each raster cell (Figure 6-3A). Next, the built environment on the

floodplain was reclassified, so the pixels were 50 and portrayed as white – this, alongside the fishnet, made it easy to delineate which pixels should be defined as buildings and streets. Subsequently, the pixel editor in ArcGIS Pro was used to specify pixel values. Before creating the building layouts, an 8m buffer was derived between the levee edge and the built environment to replicate an "access road" and ensure floodwater and sediment were not immediately blocked after passing through the breach. As the spatial resolution of the DTM was 2 m, pixels within four grid cells of the levee were assigned a value of 0 and prevented from accommodating built structures. Finally, five building setups were generated to test a range of built fractions and assess their relative effect on splay morphology. Each arrangement comprised the same initial building near the levee breach (Figure 6-3), with the rest of the buildings within each built environment extending from this reference point. The five built environments all had a set number of cells between each building – beginning at two cells (4 m street width) and rising at intervals of two until reaching a 10-cell gap (20 m street width). Where cells needed to be altered to represent buildings, these pixels were manually changed to 12. This process created five raster files of the different building setups depicted in Figure 6-3 (panels B-F).

The buildings were then added to the DTM and bedrock layers separately. Rasters were created with cell values of 12 where buildings were located, with the remaining cells retaining the elevation values from the original DTM and bedrock layers. This process produced five final DTM files with buildings, each with a corresponding bedrock layer with non-erodible surfaces of roads and buildings in the built environment. Finally, all ten files were converted into ASCII format to make the DTM and bedrock layers suitable for input into CAESAR-Lisflood.

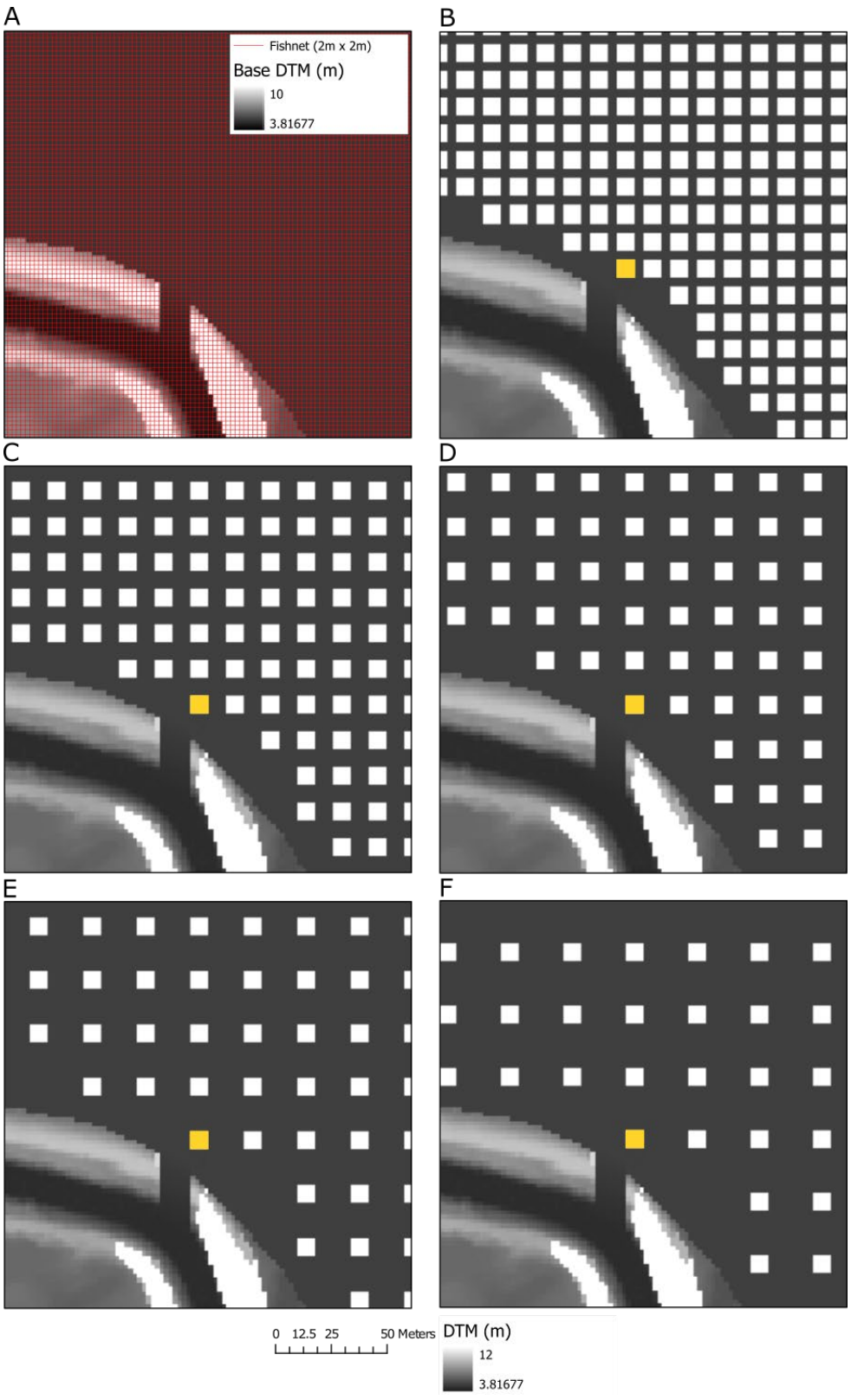

Figure 6-3 The fishnet grid system (A) set up to create the built settings and the five built environments (B-F) to use in CAESAR-Lisflood. These five setups have different numbers of cells between buildings which are 4 x 4 in shape (64 m^2). Panels B-F rely on the scale bar and legend at the bottom of the figure, with the orange highlighted building being the common starting point in each environment.

6.3.2 Model setup

A text file encapsulated the same parameters as the input text file created during the natural experiments. This inputted text file forms the flow and sediment conditions from which CAESAR-Lisflood functions. As per the natural experiments, the discharges used ranged from 10 to 30 cumecs in intervals of two to examine splay morphology in built environments during low, medium, and high-velocity flood conditions. The amount of sediment was consistent with the natural experiments, and ensured ensure the systems modelled were not sediment-limited, and splay deposits were encouraged to form. In the hydrology tab, two input cells were defined in the southernmost section of the river channel – cells 98, 201 and 100, 201. Defining two cells for the input of discharge and sediment prevents the model from eroding excessively at one point and allows more sediment to be input, as the software limits the quantity of sediment that can be input to one cell.

The grain size distributions used in the built environment experiments replicated those derived in the natural investigation in chapter 5 (table 5-1). Using Wentworth's (1922) classification, sediment size categories of very fine sand, fine sand, medium sand, coarse sand, and very coarse sand were selected. Each category was split into four subset sizes –the quantities of each respective sediment size were defined in the text file. The smallest grain size in each category was specified as the suspended fraction – with the individual fall velocities being estimated. For reasons provided in the natural fluvial chapter, the sediment transport laws used were Wilcock and Crowe's (2003) model for mixed-size sediment. Finally, the courant number was set to 0.3 to manage potential numerical instability.

Regarding the model runs, there were 275 initial built environment experiments. Each grain size category was tested with the five different built environments and eleven discharges (5 x 5 x 11), run with a universal Manning's roughness coefficient of 0.04. This provided the opportunity to examine the effect of various built environments on the morphology of crevasse splay deposits while accounting for different flood and sediment sizes.

Built environments can comprise surfaces with different degrees of roughness, ranging from smooth asphalt roads to vegetated surfaces. Consequently, it can prove tricky to quantify the Manning's value of a given urban setting due to the variability within the environment (Syme, 2008; Ozdemir *et al.,* 2013). Therefore, two rasters were generated to assess the impact of different surface roughness in a built environment on crevasse splay morphology. The shapefile previously used to delineate the urban floodplain extent in the initial set-up of the built environment allowed different Manning's N values to be assigned to non-urban and urban pixels, with the outputs used in CAESAR-Lisflood as spatially variable Manning's files. In both

new rasters, the non-urban pixels were assigned a Manning's N value of 0.04, whilst the urban pixels were given a Manning's N value of 0.02 in one raster and 0.03 in the other. Within this investigation into the effect of surface roughness, a set discharge of 24 cumecs was used for each grain size (five), each built environment (five), and the two new surface roughness domains, creating 50 new splays.

6.3.3 Analysis of the model outputs

The processing of the model outputs is illustrated in Figure 6-4, highlighting how the elevation difference raster (panel A) is manipulated to create the final crevasse splay extents (panel D). The elevation difference outputs generated by CAESAR-Lisflood were in ASCII format and converted to TIF. The threshold of 1 cm deposition defining a splay deposit was again used, with a conditional function used on the elevation difference rasters to create binary rasters with values of 1 representing the necessary deposition (panel B). These binary rasters were transformed into polygon files, and the shapes not part of the splay deposits were deleted. Moreover, the deposit polygon was split at the levee breach, so only the portion extending into the floodplain was present. The final deposits created via this process were saved as the area shapefiles – with holes inside the deposit for buildings and other areas of the built environment where deposition did not occur. Finally, separate shapefiles were created to store the outer perimeter polygons for each splay produced. These perimeter polygons were created by digitising the outline of the splay deposits – forming solid depictions of the furthest extent of the splays.

Length and widths were manually measured using the ruler tool. The splay length was the longest perpendicular distance from the levee to an aligning deposit edge. Whilst, for width, a point was created in the centre of the deposit throat. Splay width was measured as the combined distances from the central point to the upstream and downstream deposit extents along the levee, providing an arc-like representation of width. As the deposit was formed around the outer bend of a meander, measuring width as the crow flies from each deposit side would provide a smaller value than the base of the deposit takes up. Subsequently, the area and perimeter were automatically measured using the calculate geometry tool on the relevant shapefiles. Finally, deposit volumes were calculated using the "zonal statistics as table" tool, with the area shapefiles used as the extent raster and the corresponding elevation difference raster as the value raster. This calculates the sum of all elevation cells within each deposit area. Figure 6-5 demonstrates how all the morphometric measurements were extracted from an example deposit.

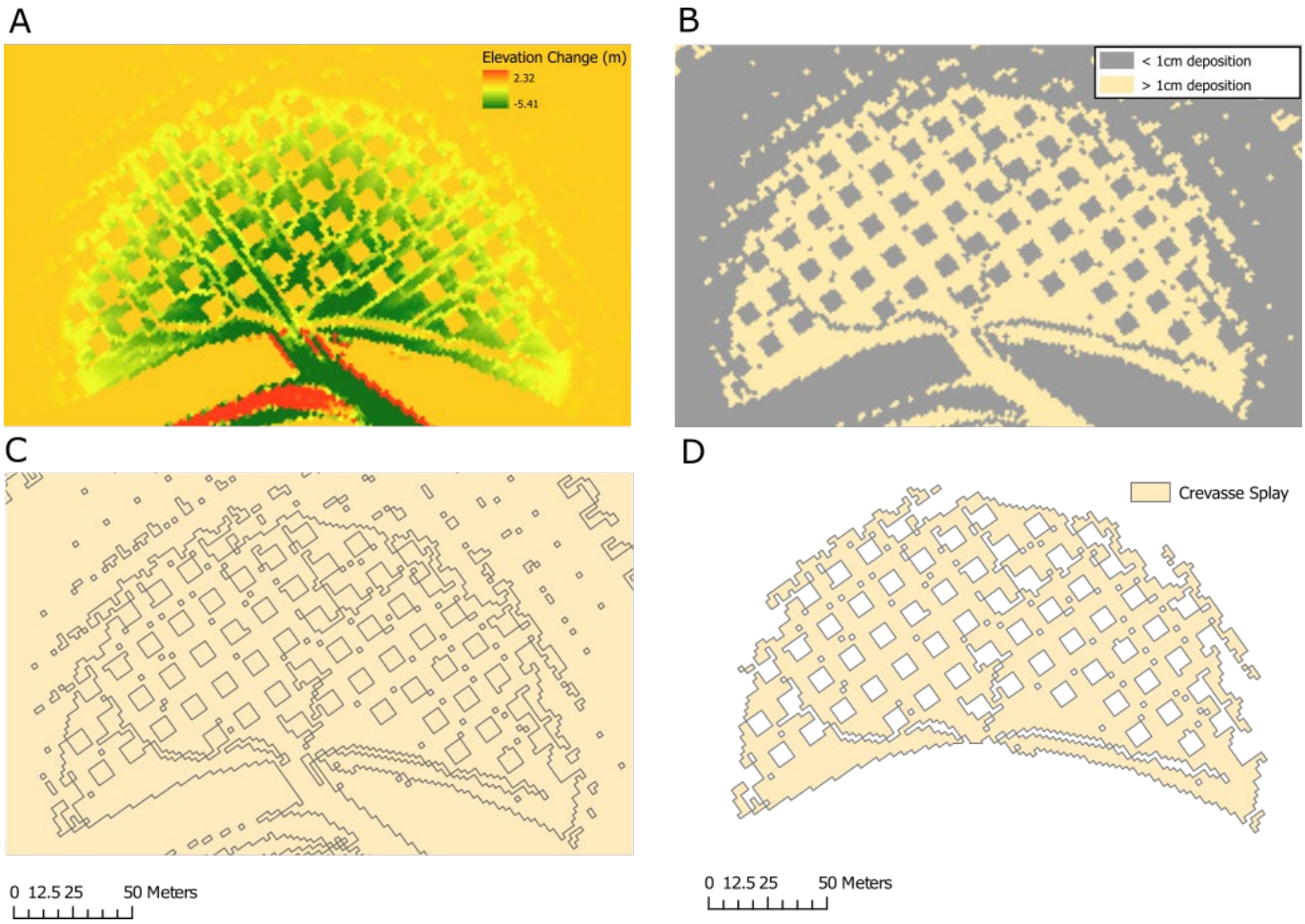

Figure 6-4 Post-processing of the built model output, using very fine sand, a discharge of 24 cumecs and 4 cell gaps between buildings. A) elevation change raster, B) binary raster, split by cells above and below 1cm of deposition, C) binary raster converted to polygon, and D) final depiction of crevasse splay.

A dimensionless "built fraction" was calculated for each deposit to quantify the built infrastructure interacting with the splays. To do this, convex hull bounding boxes (minimum bounding geometry tool) were created around each deposit polygon within the shapefile, spatially encompassing all buildings within the deposit footprint and those buildings shaping the deposit edges. A bounding box shapefile was produced for each built environment setup (5 in total) to compare each deposit to the correct builot environment. The urban floodplain extent was used to clip these convex hull shapefiles; otherwise, they encroached into the levee breach and over the levees due to the curve in the channel. Subsequently, the buildings were converted into polygons from the raster layers. An example of the convex hull and the interacting buildings it can capture is provided in Figure 6-5. The intersect tool was utilised with each convex hull shapefile, and the corresponding built fraction shapefile to provide the total area of buildings interacting with each convex hull. Finally, the built fraction was calculated by dividing the total building area within each deposit's convex hull by the area of the respective bounding box. As part of the analysis implemented, gridded regime diagrams were utilised to demonstrate the effect of the various built environment setups on measures of deposit size. To this end, the built fraction was replaced in these figures by built spacing, defined as the number of raster cells between each building, i.e. 2, 4, 6, 8, and 10, with 10 being the least dense urban fabric.

Multiple linear regression models are applied in two contexts within this chapter. Firstly, to test to what extent, on a flat floodplain, the combination of built fraction and discharge (a proxy for storm/flood size) can act as explanatory variables for different metrics of splay size when the grain size is controlled. The second application was to ascertain to what extent deposit shape (Distortion Index) could be predicted by a combination of built fraction, deposit area, and discharge when controlling for grain size and when not. The same methodology was utilised in both cases. The linear model function was used in R, with the outputs providing the significance of each variable and an adjusted R-squared value to assess how well the explanatory variables account for the variance in the dependent variable (deposit size and shape). It was then necessary to check that the models conformed to the assumptions needed. This involved looking at the VIF (Variance Inflation Factor) values to assess for collinearity between explanatory variables. Once it was observed that there was no collinearity between variables, the residuals and the raw data were normally distributed, and the residuals were uncorrelated, the results could be analysed.

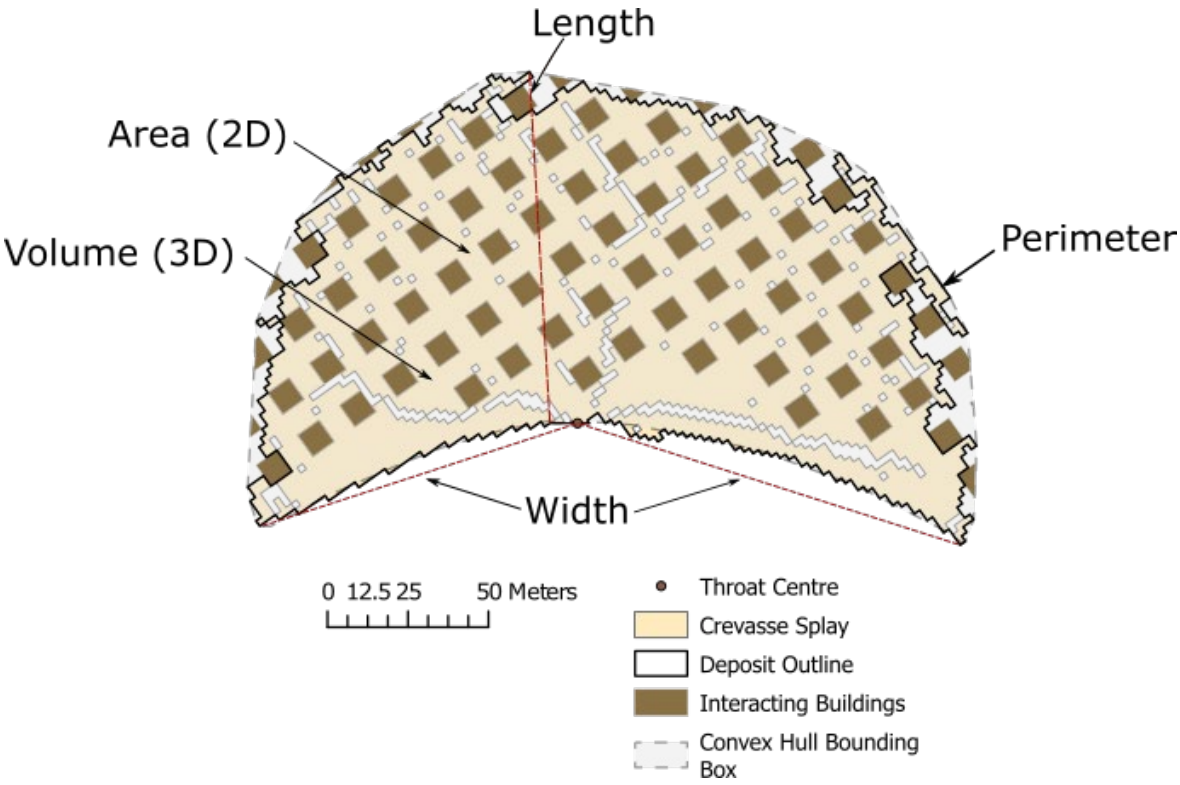

Figure 6-5 The morphometric sizes measured for the crevasse splays in built environments. The convex hull bounding box and the subsequent interacting buildings identified are illustrated.

6.4 Results

This section analyses the splays in built environments generated by CAESAR-Lisflood. It begins by examining how grain size, discharge, and built fraction combine to dictate the size of splays, moving to look at morphometric scaling relationships in these landscapes. It then inspects the built environment's impact on deposit shape before assessing how altering the surface roughness of the urban domain influences deposit morphology.

6.4.1 How does the built environment affect splay size in conjunction with discharge and grain size?

Analysis of the CAESAR-Lisflood results demonstrates the effect various built environments can induce on splays and shows how anthropogenic development works in conjunction with natural conditions, such as discharge and grain size, to dictate deposit morphology.

Firstly, planform visualisations of a subset of splays extending into the built environment are provided in Figure 6-6 (panels A-E), allowing for an initial qualitative examination of the impact of human development. These five deposits are derived from the very fine sand models at a discharge of 20 cumecs and incorporate the interactions with each built setup developed (2-cell to 10-cell gaps between buildings). In these panels, it is demonstrated that no erosion occurred on the built floodplain as expected, where the bedrock was defined to be at the surface, with only negative elevation change (deposition) present in the model's output. In all cases, the shades of green become lighter as distance increases from the breach with deposits thinning, and each splay has a similar intrusion length. Nevertheless, the change from dark green to lighter shades is more uniform for the deposits formed in low-density environments (panels D and E). In contrast, in panels A and B, there is more spatial variability in deposition patterns.

Furthermore, across all built settings, there exist channels of little deposition. These channels of minimal deposition branch from the breach opening outwards between built obstacles towards the splay edges, existing in all built environments illustrated in Figure 6-6. However, one pattern notable in panels A and B is that when the flood flows first encounter buildings (levee facing portion of the built obstacles), there are pixels where deposition is low. This can also occur in the grid cells along the buildings' sides. Meanwhile, the pixels on the buildings' leeward side show more substantial deposition.

Finally, it is demonstrated that where buildings are present on a splay's outer extent, it can cause uneven edges to occur. For example, in panel A (2 cell spacing), a sizeable proportion of the deposit edge appears irregular and uneven – particularly at the extent directly perpendicular to

the breach opening. This also occurs on the right-hand side of the splay featured in panel D (8-cell spacing). On the other hand, in panels C (6 cell spacing) and E (10 cell spacing), the deposit edge predominantly falls in the gaps between buildings, with less interaction taking place directly on the furthest extent. Where this happens – the deposit edges are smoother and less variable.

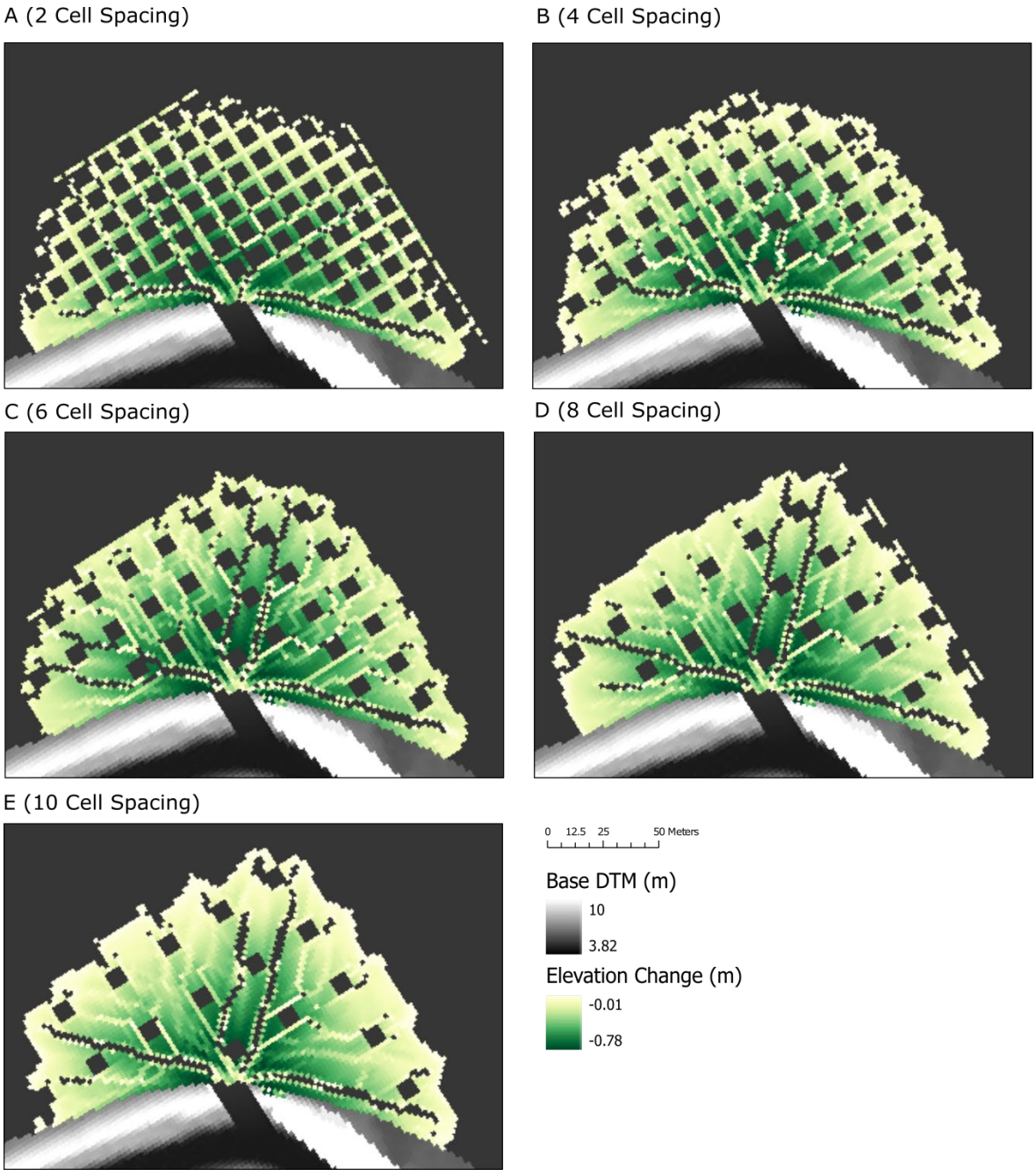

Figure 6-6 A series of maps depicting crevasse splay extents and topographies across the five built environments, created at 20 cumecs and with very fine sand. **A-E)** Visualisations of the elevation profiles from a planform viewpoint, with deposition elevations shown in green (dark green = more deposition).

6.4.1.1 Discharge and grain size

Before focusing solely on the built environment's impact, the influence of grain size and discharge on deposit size on built floodplains will be scrutinised. Firstly, there is a notable absence of splay deposits for the model runs comprising medium to very coarse sand grains between 10 and 14 cumecs. In these discharge conditions, only very fine and fine sand sediment produce deposits in the built domain. Once the input discharge reaches 16 cumecs, splays are universally produced for all sediment sizes and built fractions. Comparing the impact of the different grain sizes on the resultant splay size is most evident using the scatterplots in Figure 6-7, whilst the regime diagrams in Figure 6-8 provide greater insight into the trends within each grain size caused by the different built fractions and discharges. It is worth noting that the regime diagrams denote the density of the built environments as "Built Spacing", i.e. the number of cells between buildings. It is visible that the finer the sediment, the larger the deposit for a given discharge – with the very fine (star) and fine (circle) sand splays consistently above the coarser deposits for all size metrics.

Furthermore, there are positive correlations between discharge and each deposit size parameter. The gradient of this relationship is visually steeper in the finer sediment splays than in coarser ones. This is reflected in the multiple linear regression models that attempted to predict deposit size using discharge and built fraction. In all cases, the discharge had a significant positive impact on each metric of splay size.

Using volume as an example (Figure 6-7, panel D), at a discharge of 10 cumecs, the maximum splay volume was 59.04 m3, generated using the very fine sand class, whilst no deposits were created by those coarser than fine sand. Once all five grain sizes produce splay deposits at 16 cumecs, the very coarse sand exhibits the lowest volume at 9.22 m^3, with the maximum being 166.1 m^3 in the very fine sand runs. When discharge was increased to 30 cumecs, the maximum volume was 564 m^3 in the very fine sand parameter, while the minimum was 160.02 m^3 in the very coarse sand subset. These findings indicate that the range between the observed minimum and maximum volumes increases as the discharge increases. This is replicated across all size metrics measured. The volumes generated by the model runs comprising the middle three grain sizes fit the above pattern, wherein deposit volumes become sequentially smaller as sediment coarsens for a given discharge.

6.4.1.2 The built environment

Analysis into the influence of the built environment on splay morphology has demonstrated that the density of the built setup has juxtaposing effects on different size metrics – highlighted

by Figure 6-7 and Figure 6-8, alongside the multiple linear regression models utilised (Table 6-1). There are discrepancies in deposit sizes created using each sediment category, so the regression models were run on individual grain size datasets rather than the whole distribution. It is worth noting that each model run was statistically significant to $p < 0.001$.

In Figure 6-7 (panel A) and Figure 6-8, there is no clear relationship between splay length and built fraction within each grain size at the discharges tested. Using the very fine sand as an example, in some cases, such as the deposits generated by discharges of 26, 28, and 30 cumecs, the densest built fraction induces the longest length. However, with very fine sand splays created by 16, 20, and 24 cumecs discharges, the sparsest built environment generates the longest deposit lengths. The regression model corroborates this – suggesting that built fraction does not significantly impact deposit size for length at very fine, fine, and medium sand grain sizes. However, the regression models for the coarse, and very coarse sand indicate that built fraction has a negative impact on deposit length, although it is less significant than the impact of discharge.

A pattern is more apparent in the relationship between the density of the built environments and the deposit perimeters. When controlling for grain size and discharge, the higher the built fraction, the larger the perimeter. Figure 6-7 (panel B) shows that in the very fine sand distribution, there is a vertical gradient of light blue stars moving to dark blue as deposit size increases for a given discharge. This is replicated in the regime diagrams in figure 6-8 for all grain sizes – with the highest perimeters present in the deposits generated using the densest built environment (built spacing = 2). The multiple linear regression models support this with significant positive impacts ($p < 0.001$) from built fraction on deposit perimeter. However, the R-squared value of each perimeter model is lower than all the other size measures, suggesting it is the most difficult to predict, particularly for the coarser sediment, e.g. R-squared for very coarse sands is 0.449 compared to 0.95 for the fine sands.

However, as the built environment's density increases, the splays' area and volume decrease. This is highlighted clearly in both the area and volume plots whereby, for all grain sizes, the symbols become a lighter blue (Figure 6-7, panels C and D) and darker purple (figure 6-8) as deposit size increases - at each discharge. A mark of this impact from the built settings tested is that the volume of the fine sand splay deposit (482.63 m^3) at the lowest built fraction is higher than that of the very fine sand deposit (450.83 m^3) at the highest built fraction. The regression models reflect the observations from the plots. Discharge retains its significant positive influence on deposit size, whereas the impact of built fraction is significantly negative ($p <$

0.001) for both area and volume. Therefore, for a given discharge and grain size, increasing the built environment's density reduces the deposits' area and volume.

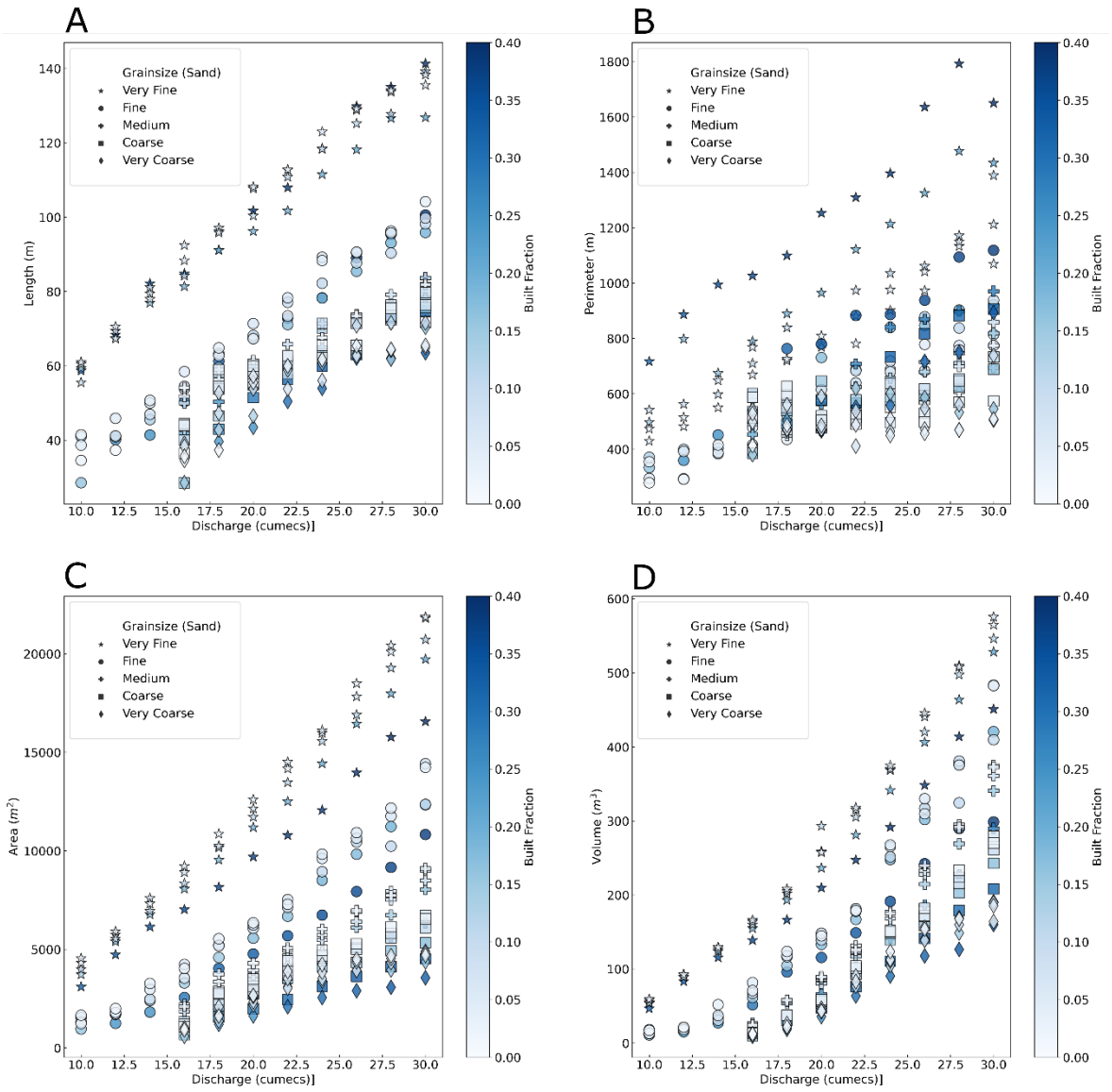

Figure 6-7 An illustration of the impact of natural and built factors on crevasse splay deposits. Four scatterplots are provided, each portraying different morphometric elements plotted against discharge. Data points are coloured by built fraction within the deposit convex hull bounding boxes (light blue to dark blue as built fraction increases) and shaped by grain size.

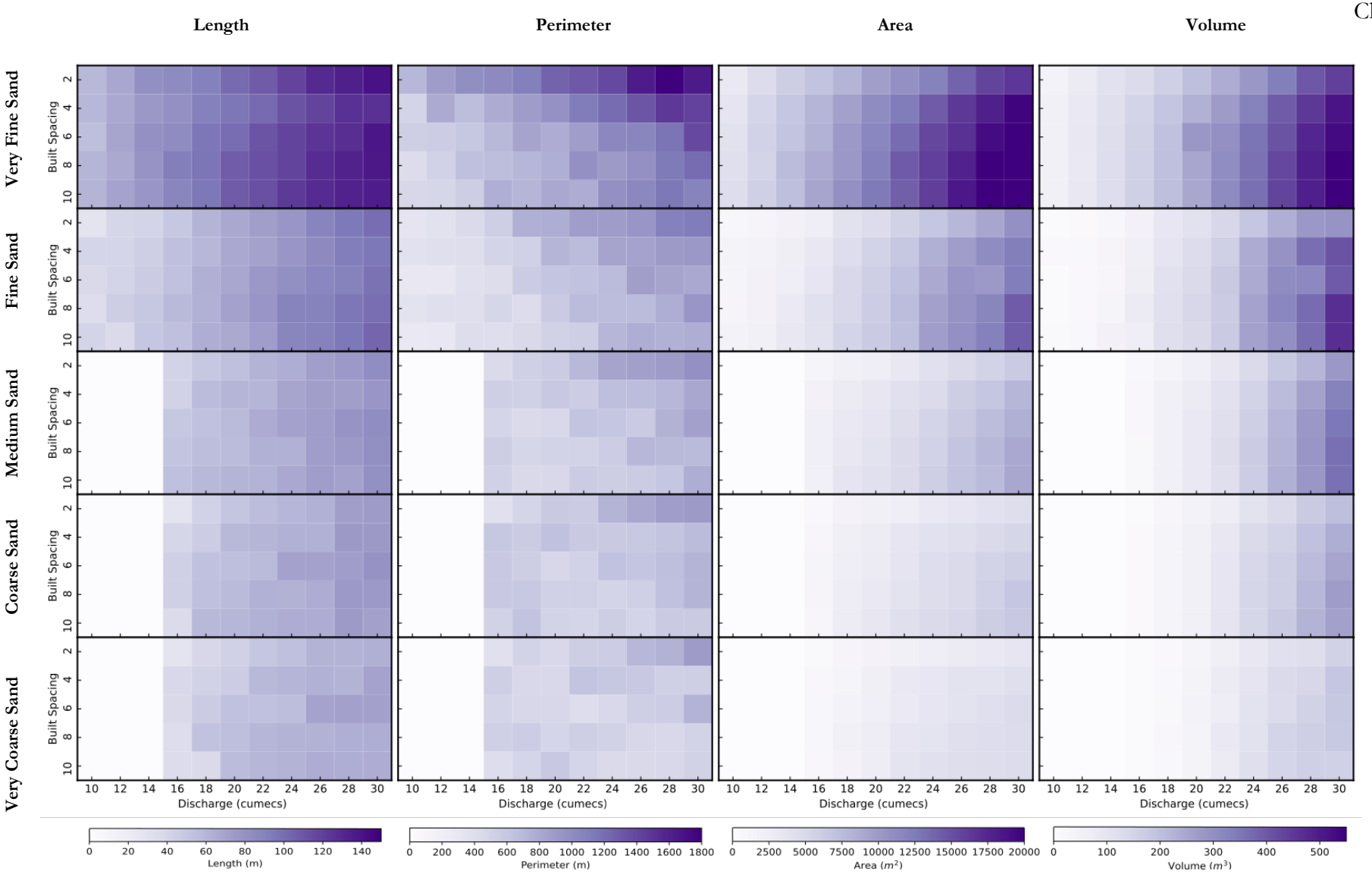

Figure 6-8 Regime diagrams which depict the size of deposits as a function of discharge and built spacing (Number of cell gaps between buildings, i.e. an analogy for street width), split into their respective grain size. Darker shades of purple demonstrate larger splays.

Table 6-1 Multiple linear regression model summary statistics predicting crevasse splay size using built fraction and discharge, within each grain size. Provided are the directions of the variable's impact (+ and -), with the p-value for each variable illustrated with star symbols (p> 0.001 = ***, 0.01 = **, * = 0.05). All models run, with variables combined, were significant to p > 0.001, and the respective adjusted R-squared values are present.

Grain size	Size Metric	Discharge	Built Fraction	R-squared
Very Fine Sand	Length	+ (***)		0.974
	Perimeter	+ (***)	+ (***)	0.956
	Area	+ (***)	- (***)	0.989
	Volume	+ (***)	- (***)	0.978
Fine Sand	Length	+ (***)		0.98
	Perimeter	+ (***)	+ (***)	0.95
	Area	+ (***)	- (***)	0.978
	Volume	+ (***)	- (***)	0.942
Medium Sand	Length	+ (***)		0.927
	Perimeter	+ (***)	+ (***)	0.818
	Area	+ (***)	- (***)	0.98
	Volume	+ (***)	- (***)	0.968
Coarse Sand	Length	+ (***)	- (*)	0.852
	Perimeter	+ (***)	+ (***)	0.509
	Area	+ (***)	- (***)	0.96
	Volume	+ (***)	- (***)	0.982
Very Coarse Sand	Length	+ (***)	- (*)	0.82
	Perimeter	+ (**)	+ (***)	0.449
	Area	+ (***)	- (***)	0.932
	Volume	+ (***)	- (***)	0.974

6.4.2 Morphometric scaling relationships of crevasse splays in built settings

Scaling relationships depict how one morphometric measure changes with another, using the natural log of the measurements, i.e. how a landforms perimeter changes in respect of its area (Lazarus, 2016). Here, the crevasse splay area is plotted against length, perimeter, and volume, whilst deposit length is plotted against volume/width (Figure 6-9). Each of these scaling relationships is plotted twice, once with the data points coloured by built fraction (panels A, C, E, G) and the other coloured by grain size (panels B, D, F, H), in order to observe how each environmental condition alters each scaling law. With discharge dictating the symbol size, it is shown that the higher the discharge, the more considerable the deposits for a given grain size.

In Figure 6-9, Panels A and B illustrate minor variation perpendicular to the dominant gradient within the length vs area relationship, regardless of built fraction or grain size. Panel B indicates that deposits composed of coarser sediment are smaller than those comprising finer sediment in both size metrics. Regarding the influence of built fraction in panel A, when built fraction is increased, it causes the deposits to have a longer length relative to their area, a trend particularly prevalent for deposits with finer sediment distributions.

Next, the perimeter vs area scaling relationship depicted in panels C and D indicates distinctive impacts from built fraction and grain size on the morphology of the splays. Whilst grain size primarily controls the size of the deposits with a clear trend of sediment fining towards the top right corner of the plot, built fraction acts to increase the perimeter of crevasse splays for a given area and grain size. The positive gradient of the scaling relationship between perimeter and area remains constant across the range of built fractions modelled. However, the data points are less clustered around a single dominant gradient, particularly when compared to the other scaling laws. Based on panel C, this pattern is controlled by the densities of the built environment. Moreover, some coarse and very coarse sand deposits formed in low discharge conditions buck this trend in the lower left of the plot, whereby they exhibit high perimeters relative to their area even in low built fraction conditions.

The volume vs area plots in panels E and F indicate that grain size is the principal control on this morphometric relationship despite the variety of built fractions used. Panel F shows that each grain size tested has an independent gradient of the rate at which crevasse splay volume rises relative to their area. At low discharges, all grain sizes initially follow a similar scaling relationship. However, as the discharge increases, only the very fine and fine sand distributions remain on this trajectory – both exhibiting a constant gradient. The model runs involving coarser sediment created splays with a higher volume for a given deposit area, suggesting that the coarser sand grains cause thicker deposits to be formed. Even though the built

environment's impact on this scaling law is minimal relative to grain size, within each sediment dataset, a higher built fraction causes higher volumes relative to the area. This is demonstrated by the light to dark blue colour gradient in each sampled grain size.

Lastly, the volume/width vs length scatterplots (panels G and H) again suggest that grain size plays the primary role in shaping this morphometric relationship. However, the built fraction controls the distribution within each grain size. This volume/width metric is commonly used to represent the mean thickness for a single slice through a deposit (Carruthers *et al.,* 2013; Rogers *et al.,* 2015). Initially, all grain sizes begin on a similar gradient, with the coarse sediment at low discharge matching that of the finer sediment at all discharges. The finest grains, therefore, retain their thickness relative to length as the deposit size increases. However, as discharge reaches ~18 cumecs, the medium, coarse, and very coarse sand assume a steeper gradient, whereby the volume/width grows faster relative to its length. This replicates the findings in panel F, wherein the coarser sand grains create deeper splays. In terms of built fraction, the influence is most evident in the very fine dataset. Here, the higher the built fraction, the lower the volume/width compared to length. This pattern is repeated for the fine sand splays but becomes more muddled in the other three grain sizes.

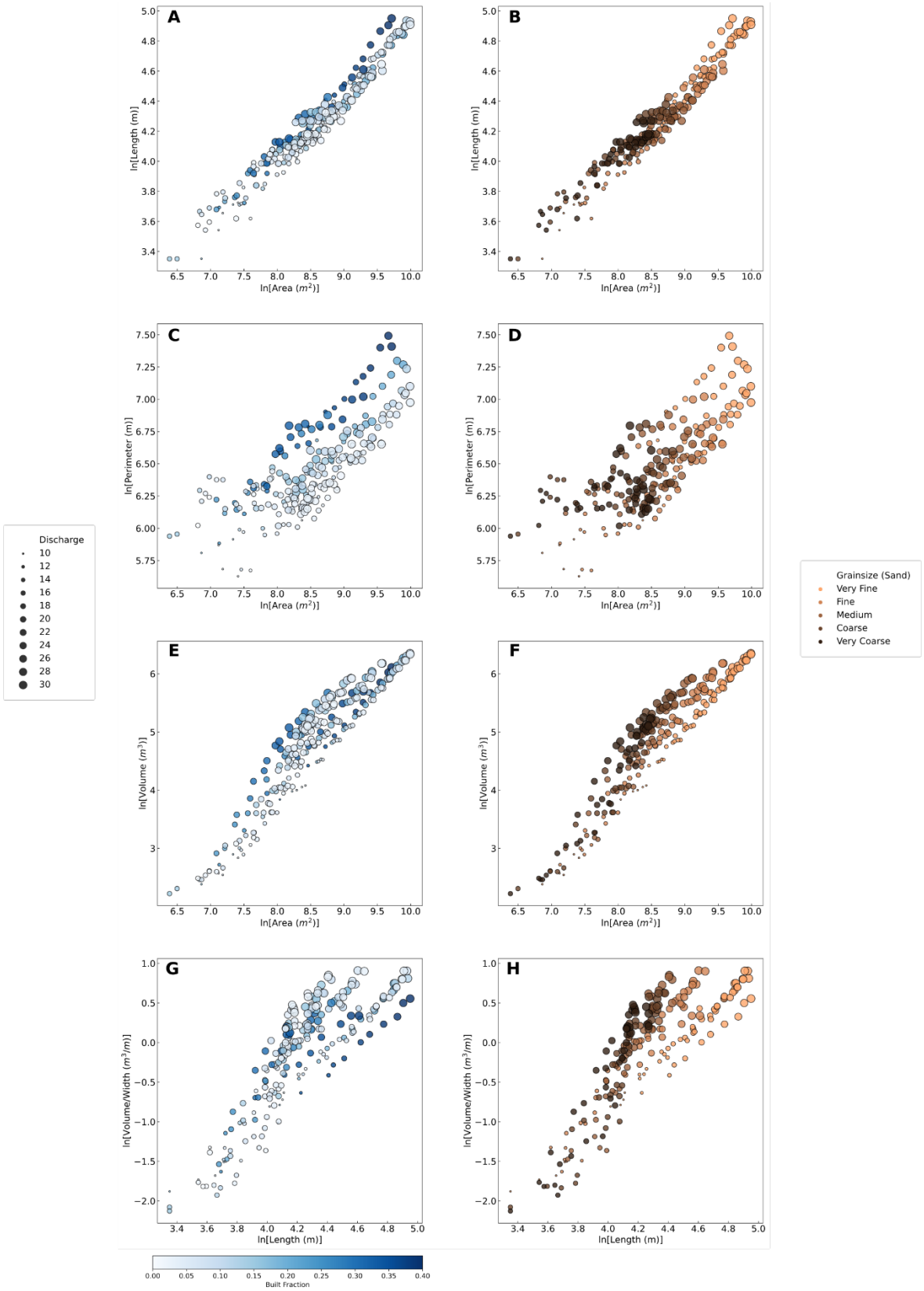

Figure 6-9 Morphometric scaling relationships for crevasse splay deposits in built environments, with five parameters: length, perimeter, area, volume, and volume/width. **Left Column (A, C, E, G):** Coloured by built fraction (light blue to dark blue as built fraction increases). **Right Column (B, D, F, H):** Coloured by grain size (light brown to deep brown in increasing coarseness).

6.4.3 Influence of the built environment on crevasse splay shape

The scatterplots in Figure 6-10 depict deposit distortion as a function of area, separated by grain size and coloured by built fraction. The Distortion Index (DI) metric is used to compare the outer perimeter of each deposit to that of a semi-circle – a typical fan shape in hydrological environments - with the same area – measured perimeter (P_m) divided by the ideal perimeter (P_i). Each of the five plots demonstrates that the DI is higher for deposits interacting with the denser built environments. As the built fraction is reduced, distortion decreases, meaning the splay deposits become more semi-circular in shape rather than branching between buildings and having irregular deposit edges. In the grain size range of fine sand to very coarse sand (discharge of 10-12 cumecs for fine sand and 16 cumecs for medium, coarse, and very coarse sand), there are deposits which exhibit high distortion values relative to the other deposits within their respective grain size and built fraction, whilst having small footprints. Here, the low discharge (small data points) causes elevated levels of distortion to occur independent of the density of the built environment. For example, in the coarse sand plot (panel D), there are small, light blue data points in the top left, with distortion index values ranging from 3.65 to 4.46 for a discharge of 16 cumecs. When the discharge is increased in this coarse sand model runs to between 26 and 30 cumecs, DI (Distortion Index) decreases to a minimum of 1.67 for the least dense urban framework and a maximum of 3.35 for the densest built environment.

Figure 6-11 plots DI against built fraction to visually scrutinise how various anthropogenic development structures govern distortion. The output depicts a strong positive correlation of 0.571 ($p < 0.001$) using Pearson's product-moment correlation, suggesting a strong relationship between built fraction and crevasse splay distortion. Nevertheless, some deposits do not follow this correlation, wherein, compared to many deposits, they have high distortion values relative to the built fraction. Such deposits can be explained using the scatterplots in Figure 6-10. These splays are created in low discharge conditions, characterised by small areas and high distortion values.

Multiple linear regression models were used to assess what extent deposit distortion can be predicted using built fraction and discharge as explanatory variables. Deposit area was initially touted as an input variable, but the VIF values produced in post-assessment of the model indicated that this metric had a large quantity of collinearity with discharge, thus skewing the overall model fit. Instead, the linear model suggested using the amalgamation of built fraction and discharge as there was no correlation between them, and they were able to combine to predict the distortion index in a significant manner.

The initial model included all the grain sizes, at one time, with the subsequent models run on the datasets split by their sediment size. The statistical outputs provided in Table 6-2 illustrate that all the models developed were classed as significant in their prediction of distortion index, with p-value's < 0.001. However, there was substantial variation between the six model runs. For example, the model incorporating the entire dataset exhibited the lowest R-squared (0.4), whereas the very fine sand produced the highest R-squared value (0.933). Therefore, in the very fine model, built fraction and discharge, when combined, accounted for 93.3% of the variation in the distortion index. In this model, the impact of both the input discharge ($p < 0.05$) and built fraction ($p < 0.001$) on deposit distortion are positive.

Aside from this, the general pattern is that as sediment becomes coarser, the ability of built fraction and discharge to predict distortion is reduced - illustrated by the decreasing R-squared values – even though the models remain statistically significant. In contrast to the very fine regression model, in the other four grain sizes, increasing the discharge has a significant negative impact on deposit distortion, whilst the effect of increasing built fraction remains positive – all of which at the $p < 0.001$ significance level.

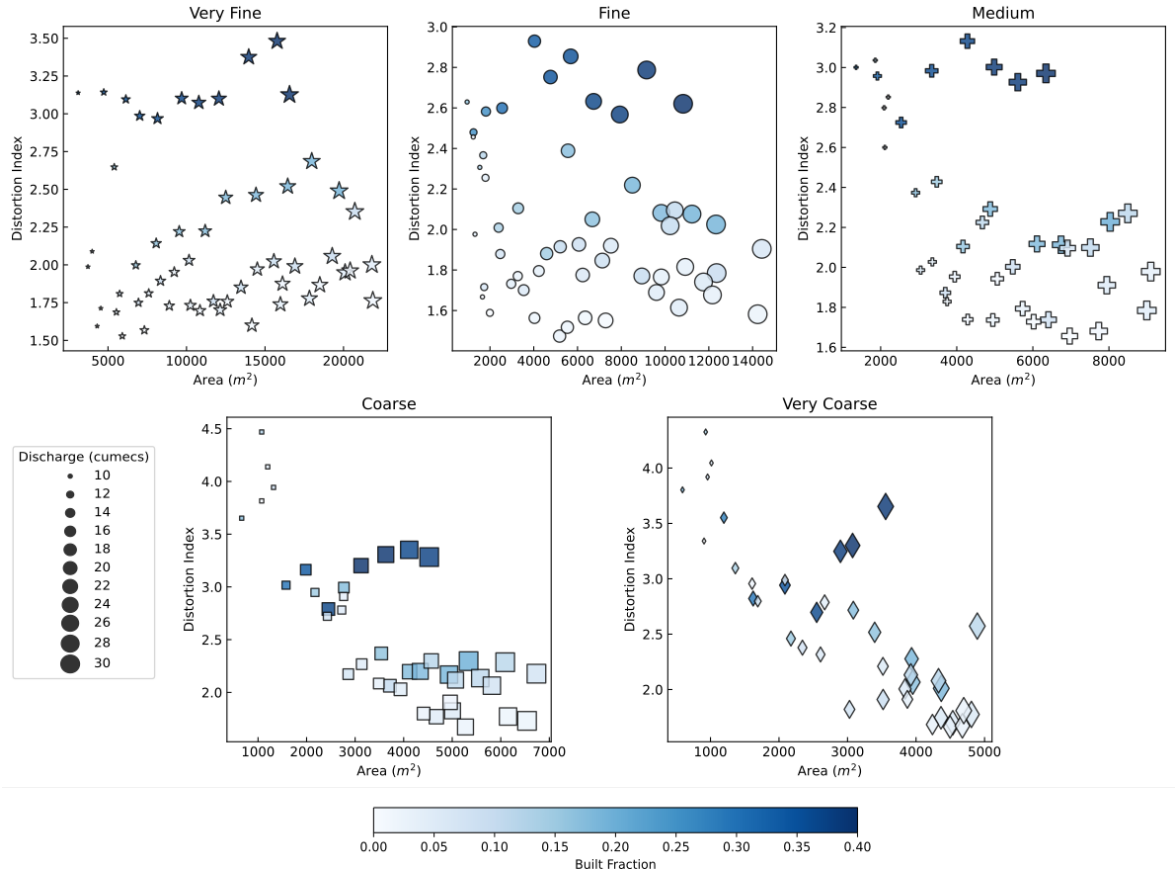

Figure 6-10 DI of crevasse splays as a function of area, coloured by built fraction. The plots are separated by grain size - very fine, moving to very coarse, as titled. Data points are sized according to the discharge which generated each crevasse splay.

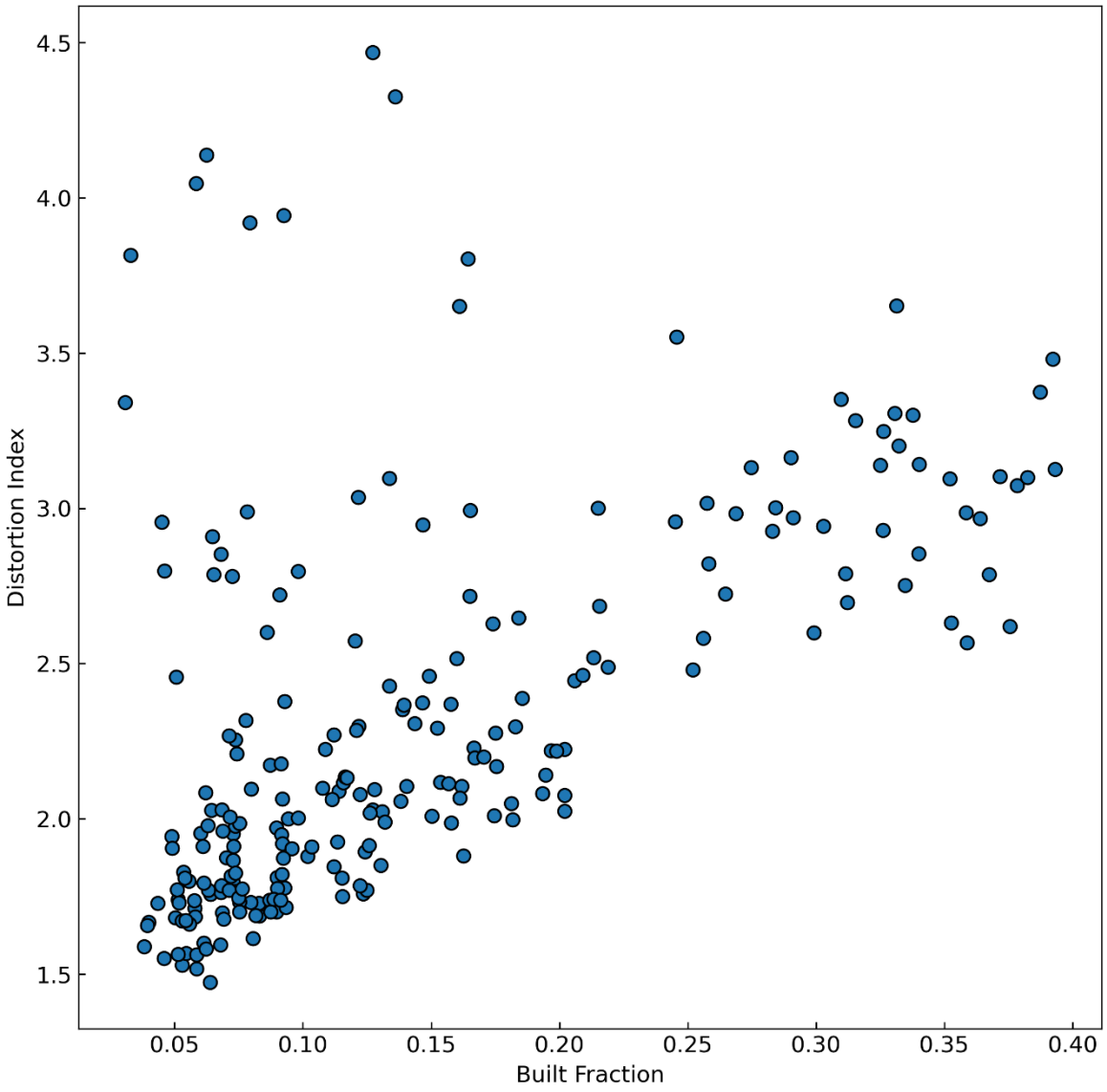

Figure 6-11 DI of crevasse splays, plotted as a function of built fraction.This plot includes splays created in all built environments, each grain size and every discharge – providing a universal measure of how building setup affects deposit morphology.

Table 6-2 Multiple linear regression model summary statistics predicting crevasse splay DI using built fraction and discharge, with one model for all deposits and then five when separating by grain size. This table includes the directions of the explanatory variables' impact (+ and -), with the p-value for each variable illustrated with star symbols (p < 0.001 = ***, 0.01 = **, * = 0.05). Each model was significant to p < 0.001, with adjusted R-squared values provided.

Grain size	**Discharge**	**Built Fraction**	**R-squared**
All	- (***)	+ (***)	0.4
Very Fine	+ (*)	+ (***)	0.933
Fine	- (***)	+ (***)	0.813
Medium	- (***)	+ (***)	0.731
Coarse	- (***)	+ (***)	0.548
Very Coarse	- (***)	+ (***)	0.615

6.4.4 The impact of roughness on crevasse splay size in a built environment

The analysis of the effect of floodplain roughness on deposit size centred on a static discharge allows a range of grain sizes, built fractions, and Manning's N values to be tested. This analysis produced a series of crevasse splay deposits, with the morphometric attributes illustrated in regime diagrams in Figure 6-12. Straight away, the usual trend of the finer grain sizes inducing the larger splays is visible. Darker colours of purple represent the largest deposits, typically found in the very fine sand distribution – the top row of the regime diagrams. Moving downwards through the plots, whereby the input grain size becomes coarser, each corresponding cell becomes progressively lighter relative to the plot above, demonstrating that for the same roughness and built fraction tested, the impact of sediment size on splay magnitude remains evident. Indeed, the only very fine splay deposits that are exceeded in size by any splays of coarser grain size are the deposits intruding into the smoothest built environment (N = 0.02), compared to fine sand splays in the rougher domains (N=0.03 and 0.04). For example, the very fine grain size volume at a building spacing of 8 at N = 0.02 is 258.78.64 m^3, compared to 266.34 m^3 and 265.17 m^3 at the same building spacing for fine grain size at 0.03 and 0.04 Manning's N,

respectively. This phenomenon ties in with the broader relationship between floodplain roughness and deposit size.

Each plot of a specific grain size and splay size metric has a clear gradient from left to right from lighter to darker cells. This pattern indicates that deposit size rises as roughness increases and other environmental conditions are controlled. Universally across the sediment sizes sampled, the built environments with Manning's N = 0.02 induce little sediment deposition compared to the other trialled roughness values. In all five grain size categories, the roughness of N = 0.03 makes deposit size (across all metrics and building spacing values) rise from the 0.02 baseline. However, for very fine and fine sand, this increase in deposit size stagnates when N = 0.03 is reached. Using deposit area at a building spacing of 8 to illustrate this, very fine deposits increase from 11513.09 m^2 (N = 0.02) to 15519.59 m^2 (N = 0.03) to 15979.22 m^2 (N = 0.04), whilst for the fine sediment the splay area rises from 3915.74 m^2 at N = 0.02 to 9711.237 m^2 and 9607.28 m^2 at Manning's N = 0.03 and N = 0.04, respectively.

On the other hand, for the coarser sand grain size deposits (medium, coarse, and very coarse), splay size appears to continue to rise between each Manning's N increment. This is shown by the continuous gradient of darkening shade from left to right - particularly in the area and volume plots. For example, using the mean crevasse splay areas and volumes for the coarse grain size model runs (average across all building spacing setups), deposit size increases from an average area of 1748.67 m^2 for N = 0.02 to 3578.36 m^2 at N = 0.03 and 4288.68 m^2 at N = 0.04, at the same time as average volume rises from 40.23 m^3 (N = 0.02) to 99.19 m^3 (N = 0.03) to 149.83 m^3 (N = 0.04). Such a trend is replicated in medium and very coarse sand grain sizes.

From this analysis and the visualisation within Figure 6-12, floodplain roughness and grain size govern the size of the deposits created and the available sediment to the splay. However, when only the density of the built environment is altered – the previously noted relationship between the density of the built setting and splay size remains when grain size and roughness are kept constant. The built environment's impact on crevasse splay size is most evident in the area and volume regime diagrams. Here, the least dense environments (8 – 10 built spacing) allow the deposits to be formed with a greater extent and quantity of sediment than the densest environments – portrayed by the darkening gradient as moving down through each plot within a floodplain roughness.

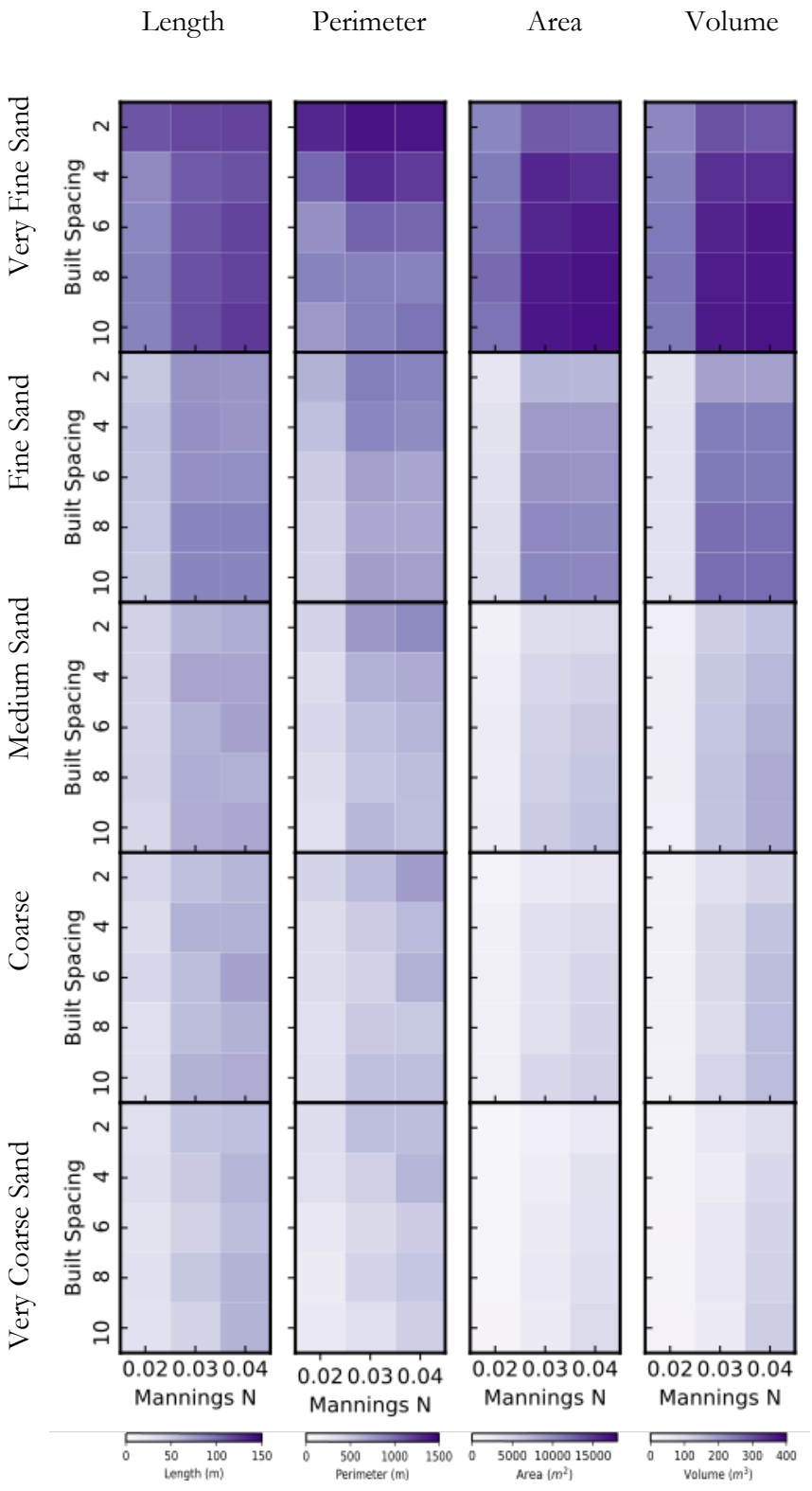

Figure 6-12 Regime diagrams which depict the size of crevasse splays as a function of floodplain roughness and built spacing, split into their respective grain sizes. The stacked figure is sorted by the morphometric parameter (columns) and grain size (rows). The light purple to dark purple colour gradient represents the transition from smaller to more extensive deposits.

6.5 Discussion

This section will evaluate the morphology of crevasse splays formed in a series of built environments in reference to the analysis undertaken and relevant literature. It is important to note that incorporating a non-erodible surface and vertical obstacles into CAESAR-Lisflood allowed the impact of anthropogenic development on splay size and shape to be quantified. Although the raster grid methodology used to create five different built setups can be seen as artificial and unrealistic in their depiction of built settings, these block-like inputs were necessitated by the structure of CAESAR-Lisflood. They also provided a simple platform to explore the effect of built structures, alongside other environmental conditions, on deposit morphology – with many environmental conditions able to be trialled efficiently.

6.5.1 The impact of the built environment on deposit size

This research has demonstrated that a non-erodible floodplain surface - mimicking concrete/tarmac surfaces alongside non-erodible vertical blocks - representing buildings, substantially impacts the morphology of the crevasse splays generated by CAESAR-Lisflood. Here, the impact of anthropogenic development on a deliberately simplified floodplain will be discussed concerning its influence on each size metric and, subsequently, how the infrastructure affects the morphometric scaling relationships between the physical parameters. Furthermore, the interactions between the variables of discharge, grain size, and built fraction will be examined because the environmental conditions set the baseline morphology from which the built domain can disrupt and cause variations in terminal splay size.

In terms of splay size, the magnitude of a deposit is often dependent on the system they develop in, with variances caused by factors such as climate, geomorphology, and hydrology (Millard *et al.*, 2017; Nienhuis *et al.*, 2018; Rahman *et al.*, 2022). Thus, when anthropogenic development alters the system in which crevasse splays form, the expected size will be disturbed due to disrupted geomorphological and hydrological processes. These changes in flow patterns and, subsequently, sediment pathways and sinks cause the built environment's impact to vary between the physical attributes of splays (length, perimeter, area, and volume).

The array of built obstacles engraved on the study's floodplain caused various impacts on deposit morphology. The effect of buildings comes down to two components: channelising and blocking, as expected from prior literature (Nordstrom, 2004; Syme, 2008). In the results concerning deposit length, there was a negligible impact from the built environment, with the major controls being the discharge of the input flows and grain size – although the regression

model suggested buildings had a blocking effect in the fine, coarse, and very coarse sand model runs, whereby building density had a negative impact on splay length.

It is noticeable that the relationship between built fraction and perimeter is inverse to the relationships between the built environment and the area and volume metrics. The positive impact imparted by built fractions on the deposit perimeter is characteristic of the branching effect that obstacles can cause. The setups of the densest arranged buildings incur the highest perimeters when discharge and grain size are controlled. In these model runs, the buildings drive the outer perimeter of the deposits to be longer as the edges of the splays extend into gaps between the obstacles, as seen by Nelson and Leclair (2006) during their qualitative study of a substantial splay formed in New Orleans during Hurricane Katrina. In contrast, the splays formed in less dense setups retain a smoother exterior as the deposit's border is less likely to interact with built infrastructure.

In contrast, increasing the density of the buildings significantly reduces the area and volume of crevasse splays under the same discharge and sediment conditions. This pattern is a testament to the buildings' blocking impact on flow velocity and direction, which induce deposition in the low-energy leeward side of obstacles, whilst also disrupting the flows exiting the levee breach – disrupting sediment supply. Also, channelisation through building gaps means the floodwater retains its transport capacity, and a lower proportion of sediment needs to be deposited. Furthermore, the non-erodible surface reduces sediment replenishment from erosional channels during crevasse splay formation. As a result, buildings disturb the characteristics of the flood flows and can act as sediment traps (Syme, 2008) and funnelling systems. Additionally, these results were found without all the components of built settings being incorporated. Other factors can include standing and collapsed fences, vegetation in gardens, debris blockages and cars, which all dissipate energy from flood flows and create eddies in the areas behind the obstacles (Syme, 2008) but cannot be captured using the coarse raster (2m x 2m) input into the models. As such, if these extra variables were included in the research as hard boundaries, the impact on deposit morphology would be more significant as they all would act as blocking features and, thus, sediment traps, further disrupting the size of crevasse splays.

It is difficult to corroborate these findings with evidence from fluvial studies due to the shortage of research. Instead, examples from flood-driven sediment deposits along coasts can complement these findings, such as Rogers *et al.* (2015), who found that coastal washover deposits formed during Hurricane Sandy along the Atlantic coast of the US were smaller in size in built environments compared to natural counterparts. These findings all support the theory set out by Nordstrom (1994) that anthropogenic development in flood-prone zones will directly

impact the morphology of the landforms produced during overflow events. A key issue with this is that sediment supply to floodplains is an essential source of sediment – useful for land building and maintenance (Nienhuis *et al.,* 2018), and nutrients – beneficial for the biodiversity of the ecosystems (Heiler *et al.,* 1995). By disrupting the natural norms and reducing the quantity of sediment transported from the channel to the surrounding floodplains, human pressure disturbs the long-term morphological development and longevity of historically natural environments.

6.5.2 The impact of the built environment on the 2D and 3D shape of splays

The shape of crevasse splays, intruding onto a deliberately simplified floodplain, were tested across various natural environmental conditions in chapter 5. To extend these findings, this chapter has introduced built obstacles to assess how anthropogenic development alters splay shape. Splay shape can be analysed using morphometric scaling relationships and the Distortion Index (DI) metric – quantitative tools to compare assess splay shapes. The morphometric scaling relationships produced from the size parameters of the crevasse splays allow intrinsic patterns to be analysed concerning deposits formed under different grain sizes, discharges, and built environment conditions.

6.5.2.1 Two-dimensional

A deposit's 2D shape is typically dictated by sediment size/supply, discharge, vegetation, and soil consolidation (Nienhuis *et al.,* 2018; Rahman *et al.,* 2022). In natural settings, splays are often described as elongated tongue-shaped or lobate – dependent on their length/width ratio (Rahman *et al.,* 2022). However, when deposits are formed in built environments, the natural norms of sediment movement are altered by the presence of impervious surfaces, the distribution of buildings, and the availability of street networks (Nordstrom, 2004; Syme, 2008). From the deposits produced here using CAESAR-Lisflood – the traditional lobe shapes are less obvious – especially when the built fraction is increased. The results expand on the work undertaken by Nelson and Sinclair (2006), who provided a qualitative assessment of how splay deposits follow new pathways by branching between buildings and down streets to find new sediment sinks in New Orleans following a levee breach during Hurricane Katrina.

The 2D scaling relationships, length vs area and perimeter vs area, have highlighted that built fraction, discharge, and grain size have different effects on the distribution of the size metrics relative to each other. Both these 2D relationships exhibit a common dominant gradient, regardless of the floodplain and environmental conditions that the splays are formed under. It has been demonstrated that grain size and discharge play a key role in dictating the overall 2D

size of splays, but do not cause variance in these scaling laws around the dominant gradient, consistent with the findings from the natural analysis in chapter 5. Therefore, it can be inferred that these environmental conditions dictate the amount of sediment supply being transported onto the floodplain and its deposition, rather than the planform shape of the deposits – which remains consistent. However, an exception to this are the small areal crevasse splays, which are typically comprised of coarser sand grains and formed in low discharge conditions, which can have a high perimeter for a given area regardless of the density of the built environment. These deposits are not well-formed and appear patchy due to the lower sediment supply that characterises these environmental parameters.

On the other hand, the built environment can disrupt these scaling relationships and create different magnitudes of perpendicular variation around the dominant gradient within the length vs area and perimeter vs area plots. The impact of built fraction on the length vs area relationship is minor, causing little variation around the dominant gradient. Nevertheless, higher built fractions do cause splays to have longer intrusion lengths for a given area, shown by the gradient of colour in panel A in Figure 6-9. This occurrence is a product of the area decreasing as built fraction rises, rather than intrusion length increasing, with splays retaining their length even when the built environments are at their most dense. This points to a balance between the channelling and blocking effects imparted by anthropogenic infrastructure, with the channelling of flows down paths between buildings allowing the deposits to extend a similar length onto a floodplain whether it has sparse or dense obstacles.

The perimeter vs area scaling relationship can be analysed using the plot in Figure 6-9, panels C and D, in combination with DI – a product of the perimeter and area measurements - calculated as a ratio of how a deposit perimeter differs from a semi-circle with the same area. Combining these two plots with the scatterplots in Figure 6-10 and Figure 6-11, alongside multiple linear regression results, provides insight into how much a deposit's 2D shape can change and the drivers of this.

Here, the higher the built fraction, the higher the perimeter for a given splay area, with this research finding that the density of the built environment primarily controls the splay shape on built floodplains, in conjunction with the discharge of the river flows. These interactions result in substantial perpendicular variations around the dominant gradient in Figure 6-9, panel C, with the clear blue gradient illustrating the impact of built fraction. This pattern due to an increasing built fraction imparting a significant positive impact on deposit perimeter, and a significant negative impact on deposit area. Therefore, as a deposit area decreases as built fraction rises, splay perimeter increases.

Before looking into the results of the regression models, a clear correlation between DI and built fraction was shown in Figure 6-11, which demonstrated a strong positive Pearson's coefficient of 0.571 ($p < 0.001$). The deposits not conforming to the relationship were the coarse grain models with low discharge, where high distortion was present independent of the built environment they encountered because of their small size. These deposits also had an impact during regression models, which were separated by grain size, with the r-square values of the coarser models being lower than those of the finer sand models. Despite this, the multiple linear regression models show that the combination of built fraction and discharge can account for a substantial proportion of the variance in DI. Therefore, it can be inferred that the built fabric strongly impacts the planform shape of crevasse splays, with the high-density built settings causing deposits to have a more extended perimeter relative to their area. This outcome was expected given the loss of the "lobal" splay shape amid sediment branching and material being channelised between built obstacles, particularly evident when buildings interact with a crevasse splays outer extent – an event more likely to occur in higher density built environments.

6.5.2.2 Three-dimensional

The scaling relationships used to depict 3D representations of flood-driven sediment deposits differ in literature. Many studies including Overbeck *et al.* (2015) and Rogers *et al.* (2015) have utilised a metric defined as a width-averaged volume often plotted against intrusion length, allowing them to observe deposit volume as if it were down an individual transect – a potential measure of thickness. Here, two measures of deposit thickness are shown using distinct scaling relationships, width-averaged volume vs length and volume vs area. Both plots disagree with Rogers *et al.* (2015) who suggested that the built environment disturb the scaling of deposit volumes. The effect of the built environment instead appears minimal, and the volume scaling relationships are more influenced by the grain size fraction trialled. The morphometric scaling relationships suggest that the deposits comprised of a coarser grain fraction are thicker than those created using finer sands – as demonstrated in the natural work.

Considering the plots are attempting to show a similar metric, there is a substantial difference between them. The width-averaged volume vs length shows a noisy relationship when compared to the volume vs area plot. When a measure of volume is plotted against length the relationship can become muddled (Lazarus *et al.,* 2022), as these transect-oriented scaling relationships can lose substantial detail of the three-dimensional properties of a deposit. Where these transect-oriented measures are used in depositional settings with the presence of built obstacles, it can lose the detail of the 3D components of landforms where they branch down streets and in between buildings. As such, the metrics utilised by Overbeck *et al.* (2015) and

Rogers *et al.* (2015) can be rendered insufficient in built environments. Therefore, the results of this chapter, combined with the findings of Lazarus *et al.* (2022), suggest that when representing the total sediment flux within built settings, it is vital to take into account the whole of the deposits – highlighted by the close fit of the volume vs area relationship. Here, there is little variation around the dominant gradient, with the steepness of the slope dictated by grainsize. Therefore, the volume vs area scaling law suggests that if the grain size and splay area is known, then volume can be estimated with some confidence - providing the ability to go from a 2D deposit depiction to a 3D characterisation.

6.5.3 The effect of roughness on crevasse splays on a floodplain with built infrastructure

To this point, the methodology implemented for the built environment analysis has used a set roughness of Manning's N = 0.04. In doing so, it matches the floodplain roughness in the previous chapter – to allow the impact of non-erodible surfaces and built obstacle presence to be compared without altering another variable. Another reason for this consistent value is that a wide range of surface roughness values has been used to represent built-up land within the literature. For example, Ozdemir *et al.* (2013) indicate that the surfaces commonly making up a built environment such as concrete and tarmac – have low Manning's N values (0.01 – 0.02), yet this is not representative of the built environment as a whole. This is because within built environments, small-scale features, i.e. kerbs and road cambers, can substantially impact floodplain roughness (Hunter *et al.*, 2008; Sampson *et al.*, 2012), which cannot be input in this work. Consequently, high-resolution DTMs obtained by terrestrial laser scanners are often sought after as they better represent the connectivity across a floodplain with more detailed features (Schubert *et al.*, 2008). In addition, vegetation is often present in built environments, and cars can act as obstacles – thus indicating that using the Manning's value of the smoothest surface in built settings would be inappropriate. As a result of this ambiguity surrounding what value of Manning's roughness is most representative, N = 0.04 was deemed most appropriate, alongside an analysis of the effect of using lower Manning's N values on splay size.

The impact of smoothing the built environment to Manning's N = 0.02 and 0.03 resulted in a reduction in deposit size (in all size metrics) when built fraction, discharge, and grain size were kept constant. Higher floodplain roughness, typically dictated by the presence and type of vegetation, increases sediment capture whilst also increasing surface friction and drag which reduces the energy within flood flows quicker, leading to more significant sediment deposition (Fraselle *et al.,* 2010). *Nienhuis et al.* (2018) suggest that when vegetation is highly dense, and soils are less prone to consolidation, the flood flows decelerate sharply once they exit the levee

breach, leading to smaller areal splays. Here, the smoother floodplains produced smaller splays due to the low surface friction not slowing the floodwaters sufficiently to cause widespread deposition (Fernandes *et al.,* 2012). Meanwhile, the rougher surfaces slow the flow and induce deposition. Through testing three separate roughness's on a built floodplain, it is highlighted that the surface's friction substantially impacts splay morphology, independent of the rest of the model setup. Indeed, where the density of built environments is the same, factors causing differences in roughness, such as vegetation and cars, will cause variances in terminal deposit size (Syme, 2008).

6.6 Chapter Summary

This chapter has utilised the CAESAR-Lisflood reduced-complexity morphological model to assess the impact of anthropogenic development on the size and shape of crevasse splays. By deriving 3D data from the urban deposits produced, this research has allowed a greater depth of analyses and permitted the objectives defined in this chapter's introduction to be achieved.

1. Generate a series of crevasse splay deposits within various urban environment setups and flood conditions using CAESAR-Lisflood (Coulthard *et al.,* 2013).

This work has successfully created 325 crevasse splay deposits intruding into a range of built environment setups with various flood sizes, grain sizes and floodplain roughness's.

2. Investigate the effect of the built environment on the geometry and scaling of fluvial deposit morphology.

The results have furthered the understanding of sediment deposits interacting with built environments areas and the subsequent effect on the sediment budgets. These results indicate that the built environment disrupts and alters the morphological processes driving crevasse splay formation and dictates their terminal morphology – when grain size and discharge are controlled. The reduction in sediment supply to denser built environments indicates the potential for issues in the future regarding the maintenance and upkeep of floodplains.

The next chapter will compare the data collected in the four depositional environments studied in this work: natural coastal, built coastal, natural fluvial, and built fluvial. Following this, the comparison will be extended to morphometric data sourced from flood-driven deposits in the literature.

Chapter 7 Synthesis of data

7.1 Overview

Sedimentary depositional landforms created during coastal and fluvial flood events are often studied independently with only occasional crossover, but efforts are being made to progress coupled models comprising coastline and fluvial dynamics (Ashton *et al.*, 2013). Beevers *et al.* (2016) utilised an established coastal morphodynamic model, X-Beach, in a fluvial environment and demonstrated that it could simulate sediment transport and morphological changes to good effect – but struggled with specific bedform processes. Therefore, the lack of studies comparing the morphology of flood-driven depositional landforms produced in either landscape occurs despite parallels between the energy of water flow and sediment transport and deposition mechanisms that occur on floodplains in both settings. The quantity of sediment moved onto the floodplain is controlled by sediment availability and transport capacity, which is valid for coastal and fluvial environments. When the composition or quantity of sediment delivered to these environments is altered, the stability of current landscapes becomes uncertain. Nevertheless, if the depositional landform morphology between different geomorphic settings is consistent, then the principles of their development can be applied between each setting and used to predict the resultant changes if sediment supply or transport conditions change.

Consequently, this chapter will synthesise the data produced in the three results chapters, comparing results with each other and against data published in the literature. It will accomplish this by first plotting and comparing the results from the natural and built fluvial research (**Chapters 5 and 6**). It will then compare the results generated in the coastal environment (**Chapter 3)** with those produced in the fluvial chapters – for natural and built domains. Here, natural settings are defined as floodplains without built infrastructure, whereas built environments are classed as any floodplain that has buildings/streets present. Following this, the data produced here will be combined with results from previous literature covering various depositional settings.

The results of this synthesis will provide essential information pertinent to answering the research questions set out in this thesis's introduction. Primarily, it will help answer research question 3: *"How are flood-driven deposits in coastal and fluvial settings morphologically similar? How do they compare to depositional landforms from broader literature?"*

This chapter will be separated into two distinct parts, a) a comparison of data within this study and b) a comparison of data collected in this work with broader research. Each section will plot

the physical attributes of the deposits against one another using various data sources. The second section will briefly outline each literature source of deposit morphology before the data comparison. The chapter will then finish with a summary of the synthesis's findings.

7.2 Natural vs built fluvial deposits

Chapters 5 and 6 used the CAESAR-Lisflood morphodynamic model to investigate the morphology of crevasse splays extending onto a deliberately simplified floodplain. Chapter 5 tested a range of natural environmental conditions, including grain size and discharge, whilst chapter 6 trialled a series of built environments of different densities to assess the impact of built obstacles on deposit shape and size. Although chapter 6 plotted the effects of increasing the density of the built environment on splay morphology, this section will directly compare the morphometric scaling relationships derived in both fluvial chapters.

Firstly, the natural and built fluvial results in all three plots of Figure 7-1 demonstrate consistent dominant gradients. This implies that a rise in a deposit size metric will lead to the same rise in another size metric in both environments. Thus, the splays formed in built environments scale similar to those in the natural setting. Panel A indicates no apparent difference between the distributions of the length vs area scaling relationship with considerable overlap of the data points. Also, the data from both depositional environments show a tight fit along the dominant gradient.

Panel B concurs with the findings presented in the coastal results of this thesis (chapter 3) in that the built environment causes a substantial amount of variation in the distribution of deposit perimeters that can occur for a given area. Here, it is shown that although both settings have a similar gradient, the natural dataset shows minor variation, whilst the built dataset shows considerable perpendicular variation around the dominant gradient. The investigation into the built environment's impact on flood-driven deposits in chapter 6 highlighted that increasing the built fraction resulted in higher deposit perimeters relative to the area. Finally, panel C highlights the close-knit relationship between deposit volume and area, consistent in the natural and built fluvial work. It has been demonstrated in chapters 5 and 6 that grain size has a degree of control over this relationship, whilst the relationship is largely insensitive to the density of the built environment – although there is more variation around the dominant gradient in the built environment.

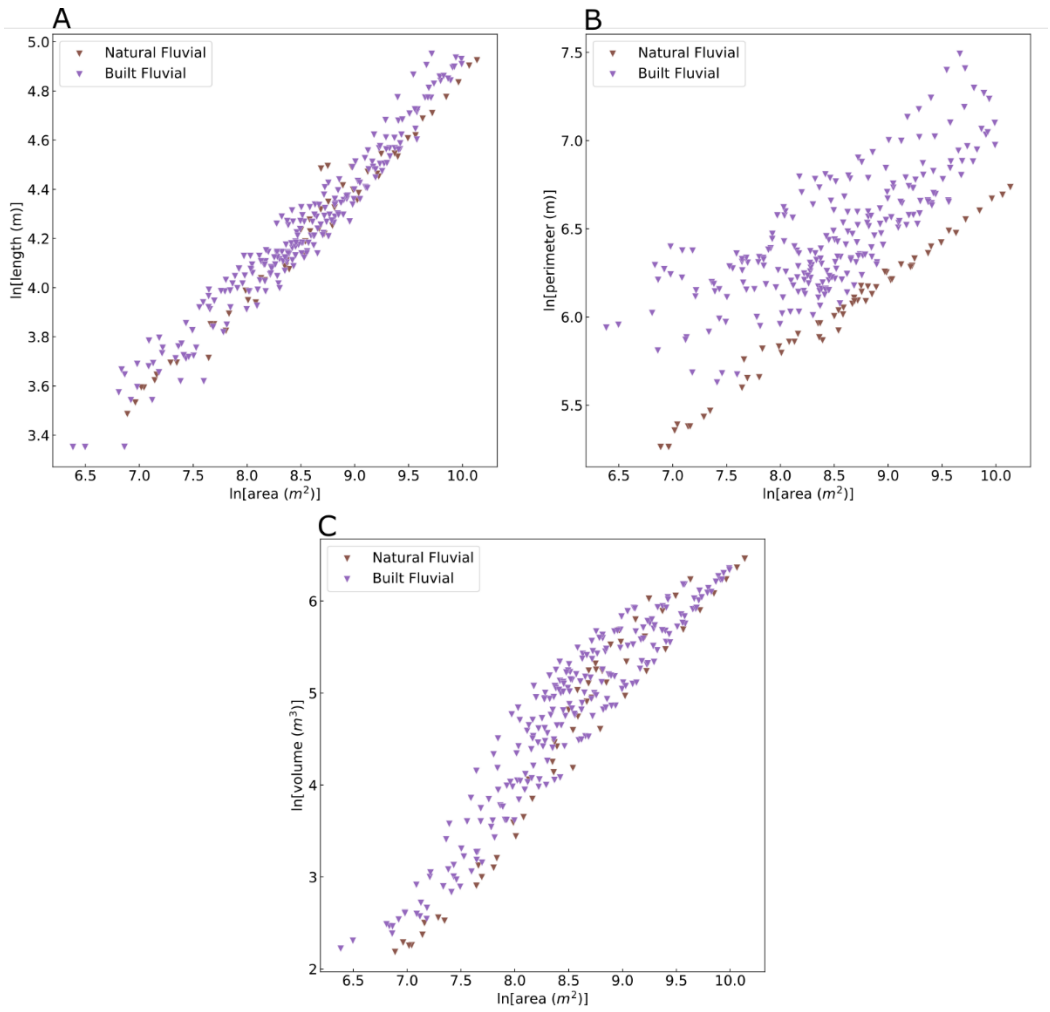

Figure 7-1 A comparison of the morphometric scaling relationships of the crevasse splays in natural and built environments. A) length vs area, b) perimeter vs area, and c) volume vs area. Brown triangles represent natural deposits, and deposits in built environments are purple triangles.

7.3 Coastal vs fluvial sediment deposits – how do they compare?

The results chapters in this thesis have focused on coastal sediment deposits in Chapter 3 (natural and built) and fluvial sediment deposits in Chapters 5 (natural) and 6 (built). Here, the data obtained will be directly compared between the four morphological environments, beginning with the scaling relationships in the natural and built settings and extending to the distortion index. Such a comparison will allow observation of similarities and differences between the environments. Subsequently, any differences in the scaling relationships can be discussed concerning data collection, depositional environments, and measurements extracted.

7.3.1 Scaling law comparison

Overall, this research has used 707 examples to study flood-driven sediment deposits in natural coastal, built coastal, natural fluvial, and built fluvial environments. For this comparison, 115 washover deposits from real-world natural coasts and 167 washover deposits from real-world built coasts are utilised (**Chapter 3**). These are accompanied by a series of crevasse splays generated by CAESAR-Lisflood under various user-defined floodplain conditions – here, only the splays formed under Manning's N = 0.04 will be utilised. The fluvial deposits are subset to the models that covered different discharge and grain size conditions at a fixed Manning's N value of 0.04. Therefore, the natural fluvial deposits are subset to 55 model examples (**Chapter 5**) and 275 fluvial deposits from built environments (**Chapter 6**). During this comparison of data from both natural and built settings in coastal and fluvial environments, the relationships between length, perimeter, and area will be investigated, as volume was not recorded in the coastal work.

The physical attributes of the deposits sampled from the real world and those generated in numerical models are plotted against one another in natural log form to assess whether they are morphologically similar. These visual comparisons, for both natural and built deposits, are provided in Figure 7-2, which includes Length vs Area (natural in panel A and built in panel B) and Perimeter vs Area (natural in panel C and built in panel D). In addition, the inset histograms provide the distribution of Length/Area (LA) and Perimeter/Area (PA) ratios, where relevant.

The coastal and fluvial datasets show a similarity within all four panels. Here, the positive gradients of the two scaling relationships in each scatterplot are comparable, with length and perimeter rising at the same rate with respect to area. For example, in panel C, the deposit perimeter rises alongside the deposit area at a comparable gradient for the coastal and fluvial natural landforms. Furthermore, the similarity in gradient is replicated across plots A, B, and D

– suggesting that the deposits produced in the CAESAR-Lisflood model scale similar to those sourced from the real-world coastal environment.

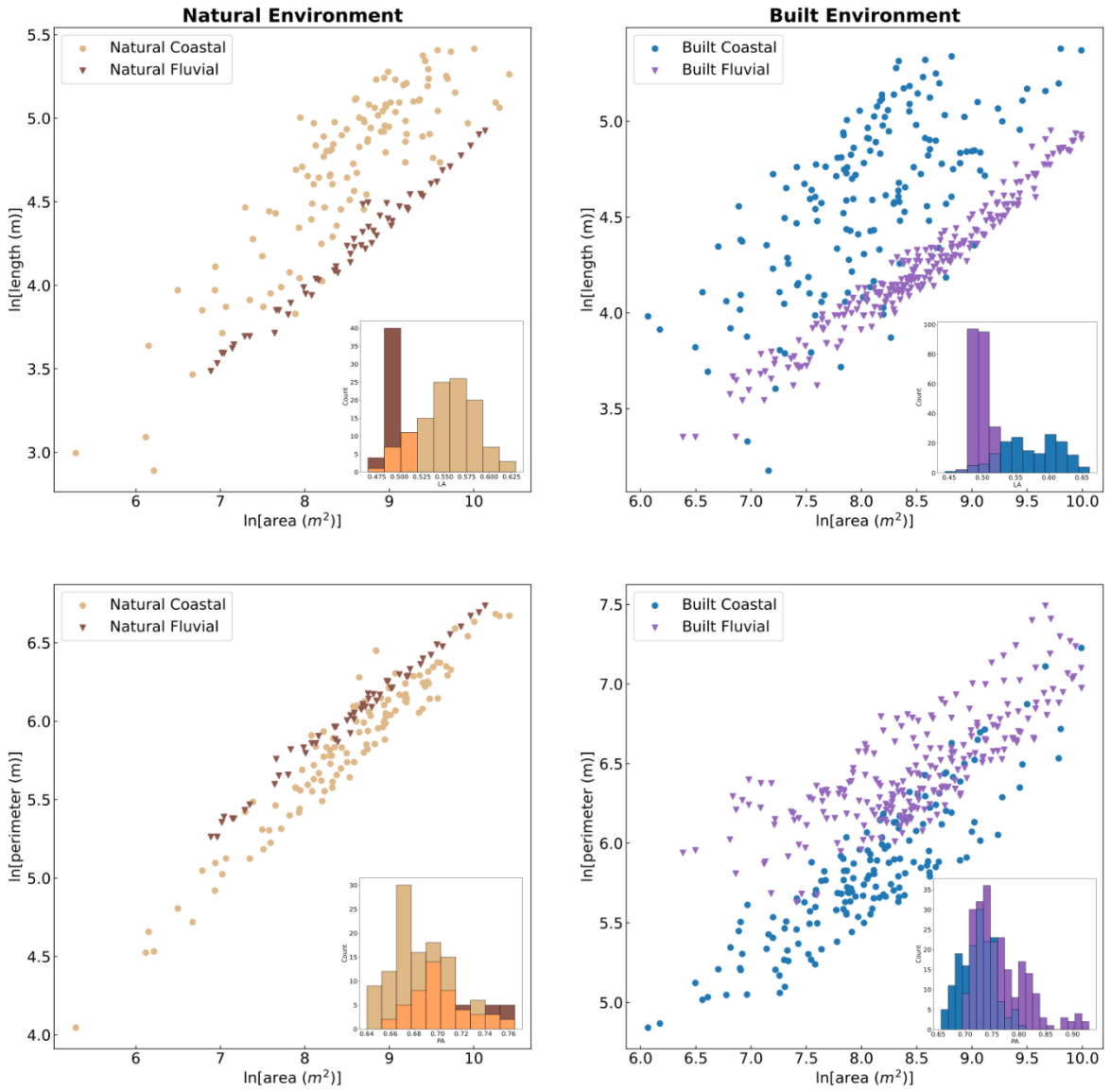

Figure 7-2 Morphometric scaling relationships comparing coastal and fluvial sediment deposits formed on natural and built floodplains, with inset histograms. The left panels (A and C) illustrate the natural environment, with natural coastal deposits symbolised by light brown circles and natural fluvial deposits as brown triangles. The right panels (B and D) show the built domain, with built coastal deposits as blue circles and built fluvial deposits as purple triangles. Panels A and B depict the Length vs Area scaling relationships, with inset histograms portraying each environment's Length/Area ratio distributions. Panels C and D show the Perimeter vs Area scaling relationships, and the histograms provide the Perimeter/Area ratio distributions.

However, there are discernible differences between the distributions in the four plots. From panel A (Figure 7-2), it is evident that the lengths of the natural fluvial deposits produced in Chapter 5 are typically lower for a given area than the length of the natural deposits in coastal environments. Such a pattern is replicated in the built environment for this scaling relationship in panel B. These patterns are further illustrated by the inset histograms plotting the L/A ratio for the respective datasets. Indeed, in natural and built settings, the L/A ratios for the fluvial deposits are condensed into a distribution dissimilar to most of the coastal dataset, with low lengths compared to areas. For example, the bulk of the natural fluvial dataset lies at a L/A ratio between 0.488 and 0.5 (mean = 0.493 and standard deviation = 0.009), peaking at 0.525. In contrast, most coastal natural deposits have a L/A ratio between 0.538 and 0.6 (mean = 0.553 and standard deviation = 0.031). From the scatterplots and histograms, it is evident that there is also a slight overlap between the coastal and fluvial settings, where the coastal deposits have low lengths relative to the area compared to the main distribution of the coastal deposits.

Regarding the perimeter vs area scaling relationship panels, it is immediately observable that more overlap occurs between the coastal and fluvial environments for deposits interacting with both natural and built floodplains than in the length vs area plots. In the natural environment, the P/A ratio peaks similarly for both the coastal and fluvial datasets. Furthermore, the distributions overlap substantially, with mean P/A ratios for coastal and fluvial natural settings of 0.687 and 0.708, respectively. Despite this, panels C and D (Figure 7-2) indicate that the opposite pattern occurs for the perimeter than that of length. This is because longer perimeters characterise fluvial deposits for a given area than coastal deposits. Such a pattern is discernible in the built deposits (panel D), where the coastal deposits reach a peak P/A of ~0.8 - yet there is a substantial number of fluvial splays with P/A values rising to exceed 0.9.

In addition, the scatterplots provided in panels A, B, C and D portray another element of variance between the coastal and fluvial datasets. There is a palpable difference between the distributions of the scatterplots presented from each depositional environment. Panels A and B suggest more variation in deposit length in the real-world coastal environment than from CAESAR-Lisflood derived fluvial deposits, i.e. a more extensive range of lengths occur for a particular area – shown by variation perpendicular to the dominant gradient. For example, at an area of 8 ln[area(m^2)] in panel A, natural coastal deposit length can range from 4 to 5 ln[area(m^2)], whereas the natural fluvial deposits are tightly packed around 4 ln[area(m^2). However, this is not as clear in the perimeter vs area scatterplots (panels C and D). In these panels, the scatterplots and histograms demonstrate substantial variation around the dominant gradient for coastal and fluvial data – particularly in the built environment. The purple triangles in plot D illustrate that

a large variety of deposit perimeters can be produced for a given area in CAESAR-Lisflood – mirroring the amount of variation in the coastal data.

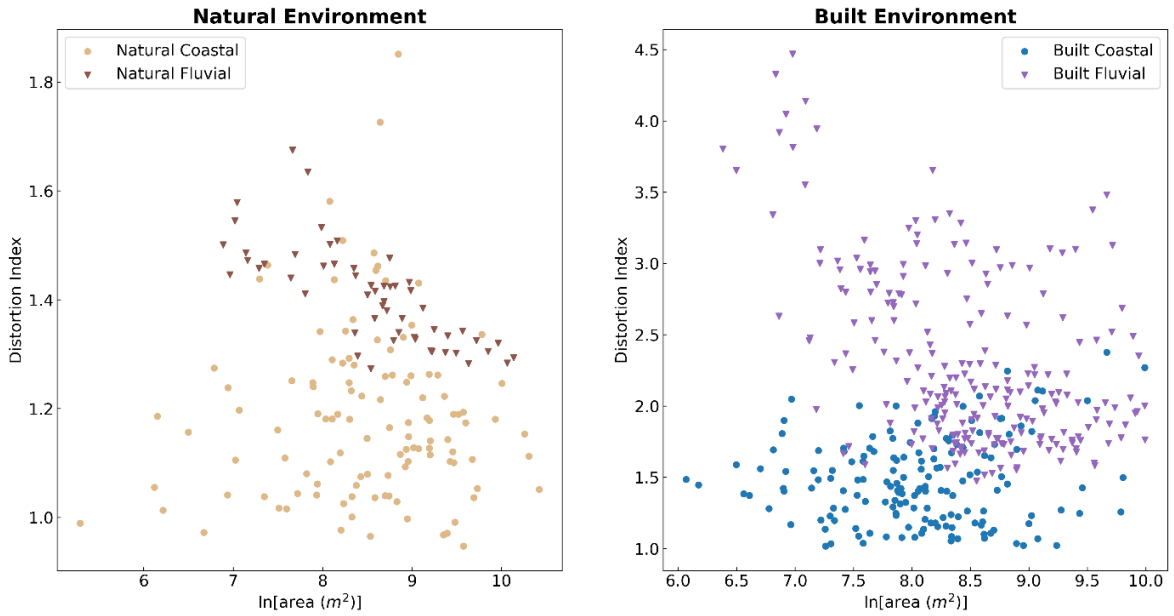

Figure 7-3 Two scatterplots depicting deposit area vs DI in natural and built environments. The natural environment consists of coastal deposits symbolised by light brown/beige circles and fluvial deposits as brown triangles. The right half shows the built domain, with coastal deposits as blue circles and fluvial deposits as purple triangles.

The plots in Figure 7-3 show the distribution of DI vs Area for the coastal and fluvial deposits. In natural and built environments, the fluvial deposits offer a different configuration to the coastal examples - especially in the built setting. The natural fluvial deposits are within the upper range of the coastal data, with no DI values below 1.25. Meanwhile, the natural coastal deposits exhibit an extensive range of DI values from below 1 to ~1.85. Moreover, it is observed that as the deposit area increases, the DI of the natural fluvial deposits shows a decreasing trend – moving towards the bulk of the coastal distribution.

A more discernible difference exists between the coastal and fluvial deposits within the built environment. Anthropogenically-developed floodplains cause an increase in DI from the natural environment. Despite this, as highlighted in previous chapters, a range of DI values can occur for deposits produced in the built environment – largely dependent on built fraction. The DI values produced in the built environment differ substantially between the coastal and fluvial work. In the real-world coastal dataset, DI ranges from ~1 to approximately 2.5, whereas in the CAESAR-Lisflood study, DI ranges from ~1.5 to 4.5. Therefore, although there is considerable overlap between the DI values within each depositional environment, much of the fluvial

deposits generated through modelling exceed the highest values in the coastal work. Many of the more distorted fluvial deposits in built environments (DI over 3.5) occur at the low deposit area in the upper left portion of the plot. As in the natural fluvial environment, the link between the area and DI shows evidence of a weak decreasing trend in the built equivalent, with more variability in DI than for a given area in the natural environment.

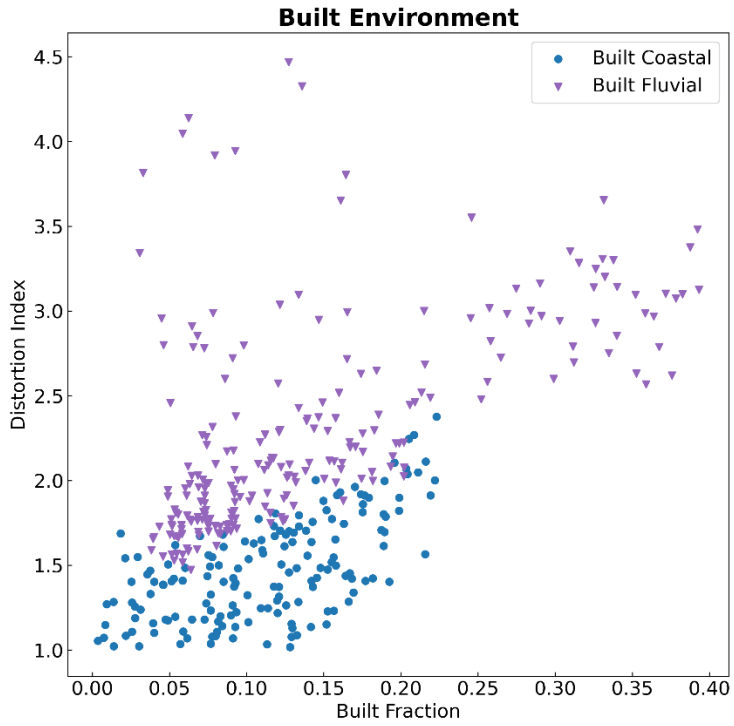

Figure 7-4 A scatterplot depicting the built environment's impact on deposit shape from the coastal and fluvial research. Here, Distortion Index is plotted against Built Fraction for both depositional environments. Blue circles represent coastal deposits, and purple triangles represent fluvial deposits.

Focussing on the built deposits from the coastal and fluvial chapters, Figure 7-4 plots Distortion Index against Built Fraction for the two morphological environments. The scatterplot illustrates that the DI is generally higher in the fluvial dataset than the coastal for the same built fraction, with a slight overlap between the settings. For example, at a built fraction of ~0.15, the coastal deposits range from a DI of 1.22 to 1.88, whilst the model-produced crevasse splays extend from 2.01 to 3.65.

As highlighted previously, the fluvial deposits with low areas that exhibit the highest DI values are formed at low-medium built fractions. These deposits do not interact with a substantial amount of the built environment. As such, they could occur in experiments with higher built fractions, thus inflating their DI values. These outliers occurred during the CAESAR-Lisflood model runs incorporating low discharges and coarse sand sediment characterised by low

sediment supply and transport capacity. Suppose these extremely high DI deposits are ignored for a given built fraction. In that case, the quantity of variation in DI is similar for both environments, just with the fluvial dataset beginning at a higher base DI value.

Furthermore, higher built fractions are tested in CAESAR-Lisflood than observed in the real-world coastal environment – extending from built fractions of approximately 0.223 to 0.393. These values of built fraction allow the relationship between built fraction and DI to be studied at a wide range of built environment densities. Consequently, the gradient between built fraction and DI continues beyond the pattern found in the coastal work – with a positive correlation present. Nevertheless, the similarities across lower built fraction values suggest that the same observations could be predicted to occur in denser-built environments.

7.3.2 Deciphering the similarities and differences between the coastal and fluvial datasets

Combining data from coastal and fluvial settings has highlighted several discrepancies in landform morphology between each environment for natural and built settings. Here, possible reasons for the differences will be investigated, such as the methods implemented and morphological factors not included in the fluvial models that are present in the real-world coastal environment.

Firstly, it has been observed that deposit lengths are lower in the fluvial datasets than the corresponding coastal data for a given area. A possible reason for this is the flat unconfined floodplain offered to the fluvial floods in CAESAR-Lisflood. As a result, the flows exiting the breach can retain their energy and thus keep the entrained sediment in many directions - leading to a broader deposit – with higher areas relative to length. On the other hand, the coastal deposits can experience channelling by the land's topography, with alongshore variances in topography restricting the spread of washover laterally. Another potential reason is that during coastal overwash events, sediment will likely be driven inland as this is the dominant flow direction, whereas, in the fluvial experiments, the levee breach is perpendicular to the dominant flow direction. Therefore, this potentially creates longer-length deposits for a given area in the coastal observations.

Secondly, the perimeters of the deposits formed in the fluvial research using CAESAR-Lisflood are characterised by high perimeters for a given area compared to the coastal data. An explanation for this is that the 2 m spatial resolution of the elevation layer being input into the morphological model causes the output deposits to be provided in 2 x 2 m blocks. These blocks cause the edge of the deposit to appear rougher than the typical smooth outer boundary of

deposits studied in the real-world coastal environment. As such, these more uneven edges increase the perimeter for a given deposit area. When raster-based models are utilised in modelling inundation and sediment movement, their spatial resolution is both a limiting factor and an advantage. Thus there is a balance in deciding upon the resolution to be used (Horritt and Bates, 2002). The spatial resolution restricts the detail of the resulting morphological outputs – as highlighted by the rougher edges. However, due to the greater computational efficiency, the resolution allows CAESAR-Lisflood to test a range of morphological conditions in many model runs (Avanzi *et al.*, 2013).

When considering the lengths, perimeters, and areas of the coastal deposits, some will also be due to spatial variability in transport capacity and sediment supply. For example, areas with a lower sediment supply for the same storm may find sediment carried the same distances, but the lower volume reduces the ability to detect the spread of a deposit. Conversely, heavily sediment-laden water may show the actual edge of the overwash more clearly. However, this is less of an issue in modelling results, as an elevation threshold rather than visual detection is used, identifying all areas that contain actual change. Furthermore, the perimeter values attained in the coastal work through manual digitising may be overly smoothed using this method across all resolution scales. This also makes comparing different digitised datasets from different users difficult, affecting a comparison between modelled data with a true perimeter and those obtained from imagery.

It is worth emphasising that despite the discrepancies in the spatial resolution of the deposit outlines produced in the coastal and fluvial research, and the lack of topographic variance in the DTM used, the gradients of the scaling relationships remain aligned. Therefore, although there are differences in the distributions of deposit length and perimeter relative to deposit area between the two environments, the physical parameters still scale in accordance with one another. Furthermore, even though deposit lengths are relatively low for a given area and the perimeters relatively high in the fluvial dataset - they still reside within the distribution of the real-world coastal deposits – as illustrated by the inset histograms and the scatterplots themselves. This suggests that despite limitations with spatial resolution and a lack of topographic variation, the morphological results from CAESAR-Lisflood are consistent with the findings obtained in the coastal work.

The natural research shows an extensive range of DI values within the coastal environment, demonstrated by this dataset containing both the minimum and maximum DI values observed in the natural dataset. Such a range in DI results from the low-lying coasts' variable topography, which can alter the morphology of washover deposits (Fisher and Stauble, 1977; Donnelly *et al.,*

2006), forcing divergence from a semi-circular shape. Some coastal floodplains will be relatively flat, allowing deposits to spread evenly in an idealised fan-like body. Other topography could be uneven, causing channelisation and pooling of sediment deposits. The DIs of the natural fluvial deposits overlap with the more distorted washover deposits at a given area – likely to be an artefact of the spatial resolution of the DTM used as no surface variation in topography was present.

On the other hand, it has been observed that within the built environment dataset, DI is high for the deposits created using CAESAR-Lisflood, compared to the coastal built deposits, with some overlap in the deposits with a larger area. As detailed in Chapter 6, the small deposits exhibiting high DI values are formed during low-discharge, coarse grain size conditions whereby the sediment supply to the floodplain is insufficient to generate substantial deposits. No such trend has occurred in the coastal work, as all the deposits were well-formed.

The DI for the built fluvial splays at higher deposit areas typically remains above that of equivalent coastal deposit areas. Indeed, to some degree, this is likely to be a consequence of the spatial resolution of the DTM. However, as shown in the DI vs Built Fraction scatterplot, many of the fluvial deposits characterised by higher DIs are produced during model runs with higher built fraction values than those found in the real-world coastal dataset. The built fractions of the coastal work in the real-world reached ~0.22, whilst a substantial number of crevasse splays generated during the fluvial experiments had built fractions ranging from 0.25 to 0.4. Notably, where these higher built fractions occur, the DI values extend from the DI vs built fraction relationship found at lower built fractions. As such, the rise in DI follows the same gradient as for the lower built fraction deposits, reflecting the positive relationship between built fraction and deposit distortion and suggesting that the fluvial experiments reflect the morphological patterns found in the coastal work.

7.4 How does the data collected here compare to previous work?

Next, the morphometric data created throughout this research is plotted against deposit measurements sourced from previous literature in various morphological environments. Most of the external data focus on sedimentary landforms produced in natural settings. These include examples from natural coastal floodplains (Hudock *et al.*, 2014; Lazarus, 2016; Rodriguez *et al.*, 2020; Williams and Rains, 2022), natural fluvial floodplains (Guzzetti *et al.*, 1997; Millard *et al.*, 2017), as well as some sampled from Mars (Kraal *et al.*, 2008). Meanwhile, for the built environment, data from Lazarus *et al.* (2022) provides size measurements of washover deposits generated in the Total Environment Simulator (TES) at the University of Hull (UK). Indeed,

the physical parameters measured vary from study to study, with length and area measurements common and data concerning perimeter and volume less frequent. Where possible, the external data is plotted alongside the scaling relationships composed of the data produced in this research. Before plotting the results against each other, a brief description of the datasets utilised is provided.

7.4.1 The natural environment

This section plots the data obtained from the natural research within this thesis, alongside deposit measurements from various other studies. The external data for the natural comparison derives from multiple data sources. The only study to provide data for length, perimeter, area and volume - and thus contribute to the comparison between all three scaling laws, was undertaken by Lazarus *et al.* (2022). Their research comprised an experimental barrier island set up in the TES, with water and sediment run through the flume mimicking the overwash process – generating 3-D results. Millard *et al.* (2017) is the only other study to provide deposit perimeter data, along with length and area. To do this, they undertook a meta-analysis of 114 previously measured natural crevasse splays formed during levee breaches.

Most studies investigating sediment deposit morphology looked primarily at length and area, with no other size metrics measured. These include real-world coastal washover deposits (Hudock *et al.*, 2014; Williams, 2015; Jamison-Todd *et al.*, 2020; Rodriguez *et al.*, 2020; Williams and Rains, 2022), flume experiments imitating coastal inundation (Lazarus, 2016), large-scale floodplain deposits in Italy (Guzzetti *et al.,* 1997), and sediment deposits in Death Valley (Bull, 1962; Denny, 1965) and on Mars (Moore and Howard, 2005; Kraal *et al.*, 2008). All of these deposits exist across a spectrum of size scales, from millimetres in the flume experiments to thousands of metres in length in the observations on extensive Italian floodplains and alluvial fans on Mars. Notably, only the lobe deposit measurements were included from data generated by Lazarus (2016), as the throat measurements referred to scouring.

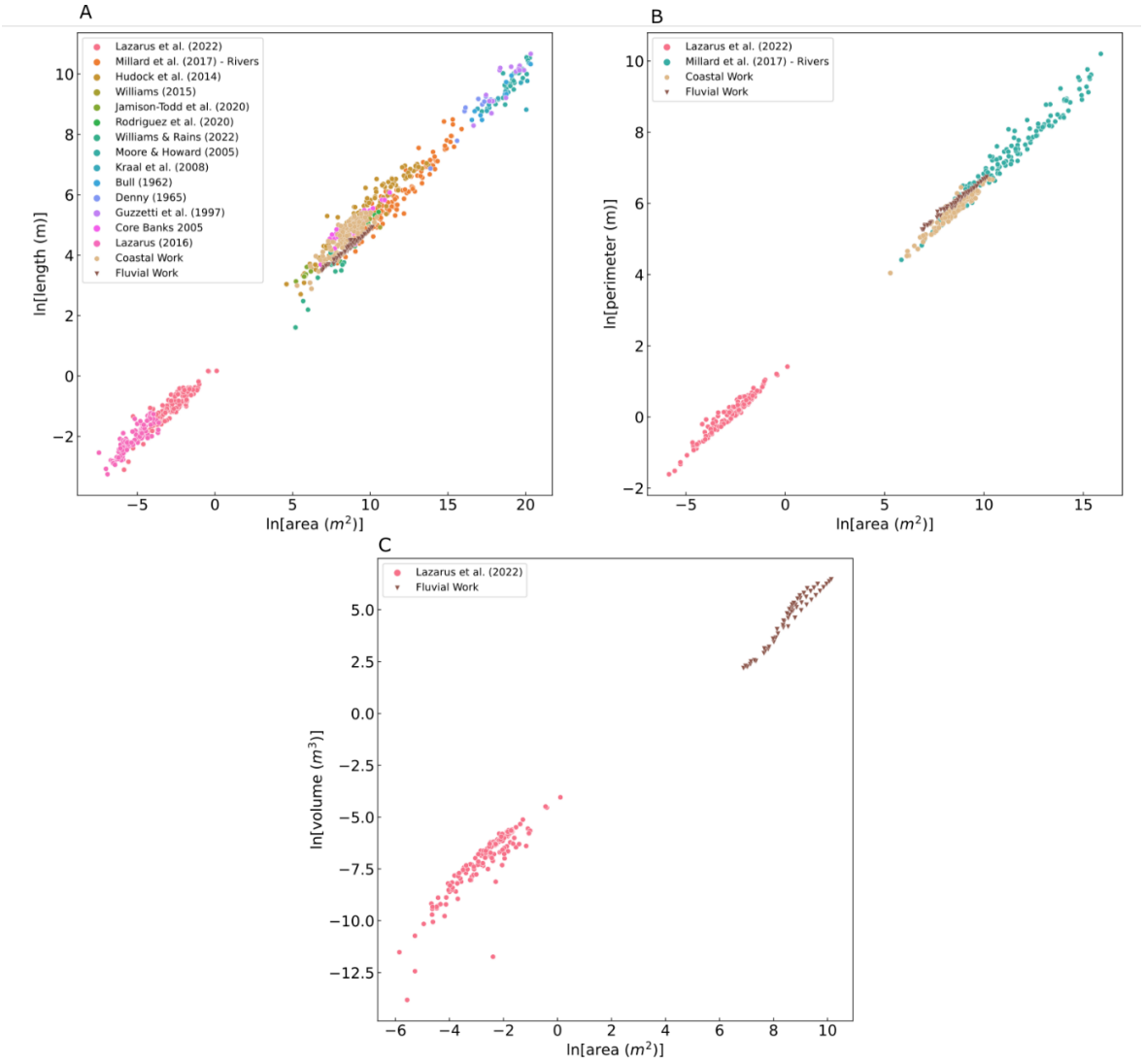

Figure 7-5 Scaling relationships between a) Length and Area, b) Perimeter and Area, and c) Volume vs Area for the natural sediment deposit measurements within this research and various literature Different colours represent each dataset – as provided in the respective legends. The natural coastal work undertaken in this research remains as light brown circles, whilst the natural fluvial data stay as brown triangles.

The graphs produced suggest that the work undertaken in this thesis, in both the natural environments, fits well with the scaling relationships observed in the wider literature. The plots in Figure 7-5 show the light brown coastal deposits and the dark brown fluvial deposits aligning with the distributions from other depositional research. For example, in the length vs area plot, the natural coastal deposits sourced from the east and gulf coasts of the US, fall in the centre of the variety of deposit lengths that can occur for a given area. Furthermore, although the length of the model-generated crevasse splays has been lower at a specific area than most of the washover deposits digitised in Chapter 3, they still reside in the distribution of the sampled deposits globally. In addition, the length vs area graph highlights that the deposits within this

research are mid-range in size compared to deposits sampled from flumes (small-scale) and Mars (large-scale), with the vast deposits only having their lengths and areas measured. Within the other two plots in Figure 7-5, the morphometric data extracted from the methods used in this thesis exhibit a similar scaling gradient to that found in Millard *et al.'s* (2017) meta-analysis of crevasse splays, and the flume results from Lazarus *et al.* (2022). The small-scale deposits created by Lazarus *et al.* (2022) provided the only comparison for the volume metric – which could be directly compared to the splays formed using CAESAR-Lisflood. Both datasets fall on the same scaling relationship gradient; however, the lack of comparison to observed natural volumes makes it harder to apply these findings to real-world studies.

Fundamentally, this indicates that the natural deposits measured in the real-world coastal environment, and those generated using CAESAR-Lisflood, demonstrate the typical scaling relationships of natural deposits in a range of previous studies. This implies that the scaling relationships observed are likely to apply in various morphological environments, benefitting research and preparedness in various coastal and fluvial landscapes prone to flooding.

7.4.2 The built environment

When considering the deposits formed in the built environments, fewer external studies examine their morphology. Herein, the data comparison focuses on the results of Lazarus *et al.* (2022) – who used bricks to represent built obstacles in their coastal overwash experiments using the HES facilities at the University of Hull. Their work mimicked two of the overwash regimes defined by Morton and Sallenger (2003), waves and inundation. The deposits from each overwash regime are plotted independently in Figure 7-6 alongside the data generated in this thesis. The study by Lazarus *et al.* (2022) of washover in replica-built environments extracted the length, perimeter, area, and volume measurements from the resultant washover – matching the size metrics retrieved from the CAESAR-Lisflood model runs.

The scatterplots provided in Figure 7-6 illustrate that the results obtained in this work align with the findings of Lazarus *et al.* (2022). The scaling law for length vs area shows greater variability among the data from this research than that of Lazarus *et al.* (2022), however, this is similar to the variability also seen in natural environments. Moreover, the variation between wave and inundation regimes used by Lazarus *et al.* (2022) is not dissimilar to the variation seen in the coastal (wave) and fluvial (flood) regimes, with the greatest variability seen in coastal/wave scenarios for both datasets. Moving to the perimeter vs area and volume vs area scaling relationships, the results from the research here align well with the findings from Lazarus *et al.* (2022). The scaling laws here are more closely followed and fit the patterns observed in the

natural environments where variability around these trends was reduced compared to area vs length.

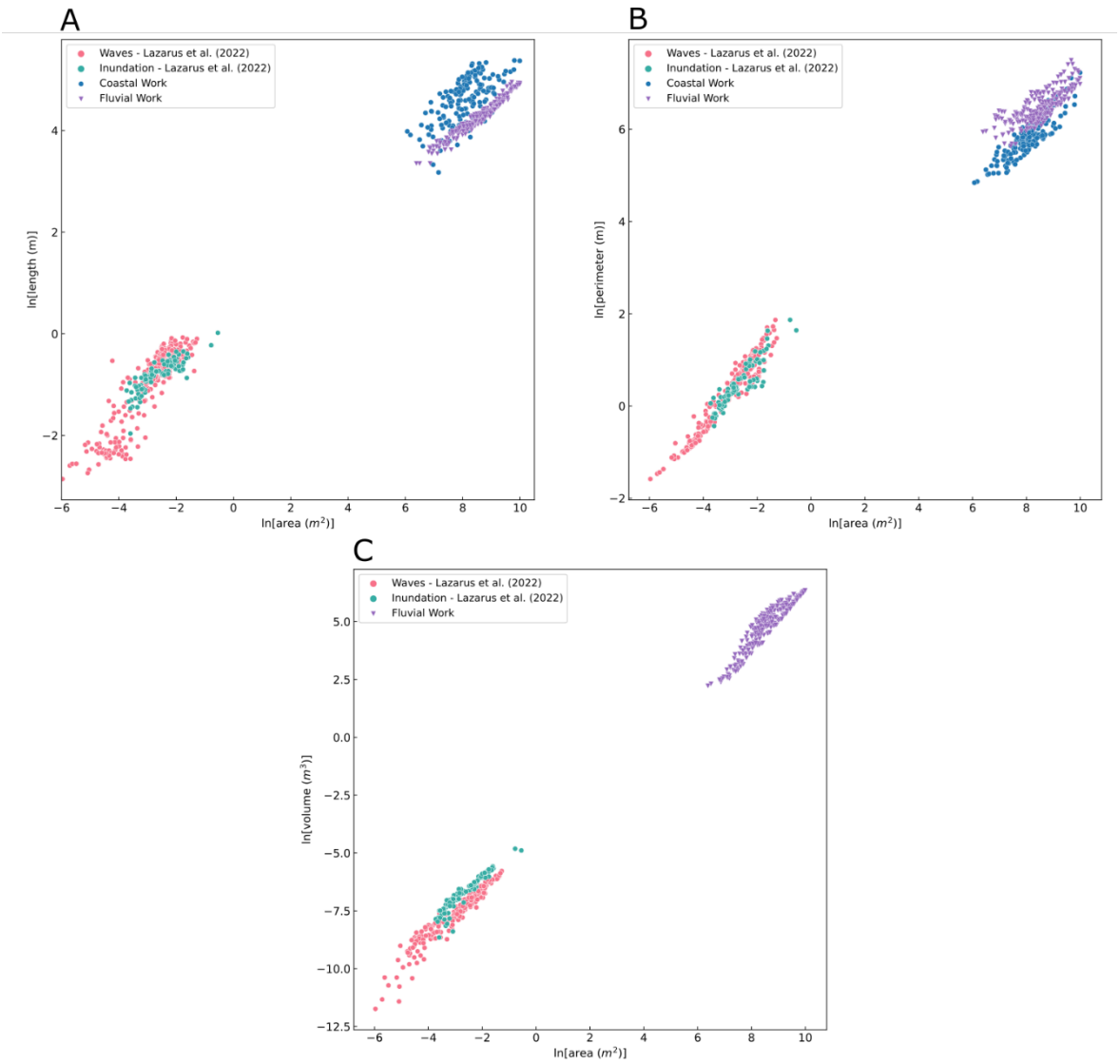

Figure 7-6 Scaling relationships between a) Length and Area, b) Perimeter and Area, and c) Volume vs Area for the built environment sediment deposit measurements within this research and data from Lazarus *et al.* (2022) – split into wave and inundation regimes. Different colours represent each dataset – as provided in the respective legends. The coastal work undertaken in this research remains blue circles, whilst the fluvial data remain purple triangles.

7.5 Chapter Summary

This chapter has synthesised the data collected from coastal and fluvial environments in this research, alongside a comparison with data from published literature for both natural and built environments.

Natural and built fluvial

This plot highlighted that the length vs area, and the volume vs area scaling relationships showed minor variation between the two depositional environments. Meanwhile, the perimeter vs area relationship showed substantial variation despite the datasets displaying the same dominant gradient – similar to the coastal results in chapter 3.

Coast and fluvial (Natural and Built)

There is considerable overlap between the scaling relationships derived from the coastal and fluvial research. In both the natural and built comparisons, three patterns are evident. Firstly, the lengths are relatively low for a given deposit area in the fluvial splays than in the coastal washover. Secondly, the deposit perimeter is higher in the fluvial domain for a given deposit area. Thirdly, and most importantly, despite the variance in deposit lengths and perimeters relative to areas between coastal and fluvial domains, the gradients of the scaling relationships are well-aligned for each depositional environment for both natural and built settings. That is, length and perimeter rise at the same rate for an increase in the deposit area.

Furthermore, it has been shown that although there is an overlap between the DI in coastal and fluvial deposits, the DI of the crevasse splays is typically higher for a given area, especially within the built environment. Here, the CAESAR-Lisflood experiments comprise built fractions up to double that found in the real-world coastal dataset, allowing the positive correlation between built fraction and DI to be extended to denser built environments.

Comparison with external data

When plotting the data collected in this research against results from previous literature from various depositional settings, it has been observed that the scaling relationships observed within this research are consistent with those found elsewhere. Furthermore, these findings were similar across all three scaling relationships in both natural and built environments – suggesting that the results from CAESAR-Lisflood can be effectively used to model observed flood-driven depositional landforms.

Chapter 8 Discussion

8.1 Overview

In this chapter, I combine the key results and the subsequent advancements in understanding flood-driven sediment deposit morphology in coastal and fluvial environments. I will cover the morphology of coastal washover in natural and built settings (**Chapter 3**), the novel use of CAESAR-Lisflood to investigate the impact of environmental conditions on natural crevasse splay morphology (**Chapter 5**), and the use of a morphological model to examine the effect of built environments on crevasse splays (**Chapter 6**). First, I discuss these concerning the research questions defined in the introduction. Following this, I address the implications and importance of the research in their applicability to disaster impact prediction and broader morphological understanding. Lastly, I assess the opportunities for future research, using the limitations of this work, alongside the thesis's implications, as a basis.

8.2 Discussion of key findings

The terminal morphology of flood-driven sediment deposits is the function of various environmental conditions. However, the quantitative impact of individual factors is not fully understood, mainly where deposits interact with anthropogenically-altered floodplains. To this end, the introduction of this thesis set out three broad questions, which, when combined, would allow the overall research aim to be sufficiently addressed in detail. This overarching aim was to quantitatively investigate flood-driven sediment deposition on natural and built coastal and fluvial floodplains to gain physical insight into their comparative morphometry and explore how such understanding may inform forward-looking models of landscape dynamics for risk assessment and management. Here, the key results of this work are discussed concerning the research questions set out.

8.2.1 Research Question 1

What is the morphometry of flood-driven deposits in natural - coastal and fluvial floodplains? What natural environmental conditions control sediment deposit morphology?

Natural sediment deposits have been studied in coastal (**chapter 3**) and fluvial (**chapter 5**) settings, where they are termed washover (Morton and Sallenger, 2003; Donnelly *et al.,* 2006) and crevasse splays (Millard *et al.,* 2017; Nienhuis *et al.* 2018), respectively. Chapter 3 extends

upon previous literature (Hudock *et al.,* 2014; Lazarus, 2016) by measuring the size, and subsequently the shape, of 115 natural washover deposits produced by five hurricane events (Irene, Matthew, Michael, Nate and Sandy) along the Atlantic and Gulf coasts of the US. However, the main drawback to the method comprising post-storm aerial imagery was the absence of information regarding the environmental conditions under which each sediment deposit was formed. Therefore, the fluvial research, which utilised a hydrodynamic morphological model, investigated the effect of various natural environmental factors on deposit morphology.

Chapter 5 used CAESAR-Lisflood to generate crevasse splays on a deliberately simplified floodplain encapsulating various discharges, grain sizes and floodplain roughness values. Here, the discharge input into each experiment acted as a proxy for storm size. Through utilising eleven discharges (10 - 30 cumecs), five sand grain size distributions (very fine sand - very coarse sand) - supplemented by several experiments using silt fractions - and ten Manning's N values (0.01 - 0.1) to represent different floodplain roughness's, this chapter provided a detailed insight into the effect of these conditions on crevasse splay morphology.

The results obtained within the natural fluvial research indicate that two distinct phases dictate deposit size: A) the amount of sediment transported onto the floodplain (sediment supply), and B) the amount of sediment deposited as part of the landform. Both phases are driven by discharge and grain size, working in conjunction. Phase A, the sediment supply, is governed by the amount of energy present and the quantity of sediment it can subsequently transport through the levee breach. For a given grain size, the higher the discharge used, the greater the quantity of sediment that can be entrained and carried onto the floodplain. This reflects the principles of sediment transport mechanics, as a higher discharge ultimately leads to a rise in stream power (Bagnold, 1977). As such, more significant storms instigate higher transport capacities and heightened potential for substantial quantities of material to be entrained as suspended load and bedload (Gartner *et al.*, 2015; Millard *et al.*, 2017) – increasing the sediment supply to the floodplain. Also, grain size is a first-order control governing the amount of sediment extending onto a floodplain to be provided to crevasse splay formation (Asselman and Middelkoop, 1995). Finer sediment requires less stream power to move, and thus the sediment supply to the floodplain is higher during these experiments (Ali *et al.*, 2013). Consequently, using the sand grain distributions, it was shown that the higher discharges, combined with the finest sands, generated the largest crevasse splays. When discharge was decreased, crevasse splay size was reduced – with the same trend found when grain size was coarsened.

However, these findings contradict Millard *et al.* (2017), who concluded that the size of crevasse splays increased as the sediment fraction trialled was coarsened. Yet, using one set discharge, this conclusion was based on results obtained from only six model runs, limited to three distinct sediment sizes (fine silt, coarse silt and sand). Therefore, this research extended the sampled grain size distributions to encompass three silt fractions. Indeed, during the silt fraction experiments, the sediment supply to the floodplain is highest for a given discharge. The morphometry of the deposits generated highlighted that although phase A plays a crucial role in dictating the quantity of sediment available, it does not encapsulate the dynamic processes on the floodplain. Instead, once the sediment supply to the floodplain is defined, the amount of sediment deposited as part of the crevasse splay varies under different discharge and grain size conditions (Phase B). Deposition on the floodplain is determined by changes in flow velocities and, thus, the transport capacity of the floodwater (Hairsine *et al.*, 2002; Polyakov and Nearing, 2003).

On the floodplain, the higher flow velocities associated with stronger storms can retain a higher proportion of the entrained sediment for longer distances than lower-intensity floods which have to deposit most of the suspended sediment closer to the river channel (Yuill *et al.,* 2016). When the entrained sediment consists of coarser grains, the deposit extends a smaller distance due to the higher transport capacity required to carry this sediment fraction. These additional experiments showed that fine silts create the largest splays at low discharges due to the increased sediment supply compared to the sand grains, and the consequent low energy on the floodplain allows deposition. Whereas at high discharges, when this silt supply reaches the floodplain, it is transported away as washload, and thus the coarser silt distribution is shown to instigate the largest splays, with a decreasing trend in both grain size directions from this peak. At high discharges, the increasing trend in crevasse splay size from fine silt to very fine sand mirrors the conclusions of Millard *et al.* (2017) - which indicates that deposits get more extensive for a specific subset of coarsening grain sizes. Such findings suggest that the relationships between grain size, discharge, and deposit size are more intricate than previously thought, with a dynamic equilibrium existing wherein an optimum grain size exists to generate the largest splays, with this grain size shifting depending on storm size.

CAESAR-Lisflood also allowed the alteration of floodplain roughness to analyse its impact on crevasse splay morphology because surface friction influences flow elevations and velocities (Mason *et al.*, 2003). Floodplain roughness is primarily governed by riparian vegetation's presence, type and density (Darby, 1999). Such vegetation can considerably influence splay size by acting as sediment traps, reducing floodwater energy, and inducing deposition (Liu and Nepf,

2016). Floodplain roughness can also be driven by obstacles extending above the ground, changing flow momentum (Baptist *et al.*, 2007).

Here, floodplain roughness was defined using Manning's N, which provided a simple and effective mechanic to test the impact of surface friction on splay morphology. Notably, a roughness value did not constitute a specific floodplain environment, e.g. shrubland vs agricultural land, but was seen as a quantitative measure to test smooth vs rough depositional environments. This work has highlighted that when the floodplain is smoother, the deposit formed is less substantial than under conditions with higher surface friction. Smoother drainage conditions allow the flow to travel across the floodplain unconstrained. Consequently, the transport capacity is less likely to be exceeded and less sediment is deposited (Asselman and Middelkoop, 1995). Meanwhile, higher floodplain roughness values induce elevated levels of drag, which causes higher quantities of sediment to be released from the floodwater – corresponding with findings from flume experiments (Fraselle *et al.* 2010).

However, upwards of N = 0.05, the gradient in splay size increase levelled off, with the size parameters remaining relatively constant, aside from deposit volume, which still grew gradually. Firstly, increased roughness causes the deposits to accrete substantially near the breach opening, which can then block additional sediment being supplied to the splay as it becomes blocked off. Secondly, there could be a point in the roughness values wherein the friction imparted on the flood flows such that a higher proportion of the sediment fraction is deposited closer to the breach opening, and simultaneously, there is a maximum extent on the floodplain that the flow does not have the energy to move the sediment past. This explanation compliments the different responses of deposit extents and volume to increasing roughness values. The low velocities at the deposit edge mean the material is deposited onto the existing splay, thus increasing the volume but not the splay extent.

These findings have highlighted that the three natural factors tested: storm size (discharge), grain size, and floodplain roughness, substantially impact deposit morphology. However, these are not the only drivers of flood-driven deposit morphology within natural environments. When comparing the natural morphometric scaling laws (length vs area and perimeter vs area) between the coastal and fluvial work in Figure 7-2, it was evident that there was more variation around a dominant gradient in the real-world coastal results. This indicates that some natural factors influencing deposit morphology are absent in the CAESAR-Lisflood experiments (chapter 5). Each washover deposit sourced from the post-storm aerial imagery would be affected by the unique elevation profile of the barrier/shoreline they encountered during the flood event. The topography of the floodplain on which the deposit forms can alter the expected terminal

morphology (Morton and Sallenger, 2003; Millard *et al.,* 2017). Elevation changes can alter flow speeds and energy – directly influencing the capability of the floodwaters to transport sediment (Soria *et al.*, 2017), which can cause variations in deposit size and shape. Further, surface depressions can result in slow-moving sediment-laden flood waters where deposition must occur due to lower transport capacity and thus, landforms are restricted by local topography (Donnelly *et al.,* 2006). Therefore, this demonstrates that the impact of the natural environment on flood-driven deposit morphology is not limited to being a function of storm size, grain size and roughness, the factors quantitatively assessed in this research.

8.2.2 Research Question 2

How does the morphometry of flood-driven deposits differ between natural (unbuilt) and built floodplains? How might the spatial characteristics of built environments determine the size and distribution of flood-driven deposits?

Research question 2 has been addressed through the analysis of flood-driven sediment deposits in built environments within **chapter 3** (Coastal) **and chapter 6** (Fluvial), providing novel information regarding the impact of built infrastructure on the shape and size of these landforms.

Previously, little quantitative research has examined anthropogenic development's effect on morphological landforms. The development of quantitative data has illustrated how the built environment can disrupt natural norms of deposit morphology whilst also highlighting the relative influence of specific urban characteristics, including the urban fabric density (here termed built fraction) and street length (Boeing, 2017). This analysis has built upon work by Roger *et al.* (2015), who demonstrated the blocking effect that a range of urban areas in the US have on coastal washover formation. It has also extended on early theory developed by Nordstrom (1994), who suggested that humans can alter natural landforms through changing sediment sources, pathways and sinks.

Regarding deposit size, the fluvial work allowed regression models to be run within each grain size distribution to assess how size-related measures such as area and volume can be predicted using storm size and built fraction. Storm size had a significant positive impact on each size metric – consistent with the natural work in Research Question 1, yet the models showed built fractions to have varying directions of effects and significance. Alongside this, morphometric scaling relationships were developed to observe the quantitative difference of deposits between natural and built environments in coastal (Figure 3-4) and fluvial (Figure 7-1) landscapes.

Comparatively to the other size metrics, the effect of built environments on deposit length was relatively minor. The very fine, fine, and medium sand regression models showed that increasing built fraction has no significant impact on intrusion length, whereas there was a negative impact in the coarse and very coarse sands. Such a pattern is likely a testament to the various impacts the built environment can impart on the intrusion distance of deposits. It is suggested that there is a balance between the amounts of blocking and channelling that can occur as the built fraction increases, with both processes countering each other. The roads and pathways between buildings provide conduits for channelised deposition, whereas the buildings can reduce flow energy and induce deposition (Hall and Halsey, 1991; Houser, 2013; Rogers *et al.*, 2015). This is reflected within the length vs area scaling relationships derived from the coastal and fluvial datasets, indicating no difference between the natural and built environments.

However, the impact of built environments on the planform shape of the landforms was evident when using the deposit perimeters. The perimeter of the landforms produced in built settings is typically higher than those formed on natural floodplains for a given deposit area. This was highlighted in the morphometric scaling laws (coastal and fluvial), as well as a significant positive impact of the built fraction on perimeters (fluvial). The Distortion Index (DI) was developed to analyse this relationship in greater detail, which calculates the extent a deposit's perimeter diverges from that expected for a given semi-circle area – noted to be representative of an undisturbed natural depositional fan (Donnelly *et al.*, 2006; Hoyal and Sheets, 2009; Yuill *et al.*, 2016). The DI results added detail to the difference in deposit shape between those formed in natural and built environments. Deposits extending into built domains typically have higher DI values than those in natural landscapes, with increasing built fraction having a significant positive impact ($p < 0.001$) on DI (coastal and fluvial). Therefore, the planform shape of depositional sediment landforms in natural and built settings is distinct, with the natural norms being disrupted by anthropogenic development. This corresponds with Nordstrom (1994, 2004), who suggested that built infrastructure can substantially impact landform morphology.

However, other factors affect deposit shape in built environments other than the density of buildings, given the discrepancy between the explanatory power within the real-world deposit samples in **chapter 3** (R-squared = 0.51) and those generated by models in **chapters 3 and 6** (R-squared > 0.8). These can include the presence of fronting dunes in the coastal domain, which can alter the quantity of mobile sediment (Nott, 2006), as well as factors affecting deposition in both coastal and fluvial environments, such as variations in local topography which can channel and disrupt flows (Kain *et al.*, 2014), and the presence of vegetation within the built domain which increases the friction present, in turn, causing reductions in energy.

The built environment had similar effects on deposit area and volume. When the built fraction was increased, there was a universally strong negative impact on deposit areas and volumes ($p < 0.001$) for a given storm size and grain size distribution. Here, built environments disrupt sediment pathways, meaning areas of the floodplain that previously would have experienced sedimentation remain devoid of sediment supply. The blocking effect of the buildings close to the levee breach can alter the quantity of material extending further onto the floodplain and disrupt the velocity and direction of flows within the breach. Where the density of buildings is higher, there is more opportunity for blocking, as shown on barrier islands by Rogers *et al.* (2015), with fewer routes the floodwater laden with sediment can move through. In addition, during the natural model runs, the floodwaters created erosional channels on the floodplain, an element not permitted in the non-erodible built experiments – negating an additional facet of sediment supply. Fundamentally, these findings imply a substantial impact by the built environment, extenuated as the infrastructure becomes denser, on sediment budgets within a landscape by instigating a change in deposit extent and size.

Despite the detrimental effect of the built environment on deposit area and volume, the morphometric scaling relationship between the two size parameters in the natural setting is shown to be preserved in the built environment - consistent with findings from Lazarus *et al.* (2022). This indicates that the reduction in area and volume are similar in magnitude, so the relationship is retained. Such findings contradict Rogers *et al.* (2015), who indicated that the scaling of washover deposit volume is affected by buildings. However, to conclude this, they plotted volume as a transect-oriented quantity against intrusion length which can ignore 3-Dimensional components of deposits (Lazarus *et al.,* 2022), including where sediment branches down streets and in between buildings and where thickness varies spatially. Therefore, this study's findings suggest that the whole of a deposit should be considered to derive accurate reflections of sediment flux and allow the volume to be estimated from the area.

8.2.3 Research Question 3

How are flood-driven deposits in coastal and fluvial settings morphologically similar? How do they compare to depositional landforms from broader literature?

Flood-driven sediment deposits produced in coastal and fluvial environments are often studied separately, despite the parallels between the energy of water flow and the mechanisms of sediment transport and deposition (Beever *et al.,* 2016). At present, coastal washover is seen as a distinct morphological landform to fluvial crevasse splays. However, if shown to be similar, it allows for studying the sediment deposits in tandem. Therefore, the knowledge of the landforms

produced in one environment could be vital in developing a substantial understanding of morphological processes in both settings, efficiently and in detail.

The data synthesis in **chapter 7** brought together the quantitative results from the coastal and fluvial research. It was demonstrated that there was some overlap between the morphometric scaling relationships derived from the two datasets – in both natural and built environments. However, the lengths of the crevasse splays produced using CAESAR-Lisflood were lower for a given area than the coastal deposits sampled. Reasons for such differences have been provided in chapter 7. These include the lack of topography in the model experiments – which can cause channelling and reduced lateral spread in the coastal environments – leading to narrower, elongated deposits and the dominant flow direction of overwash being directly inland. It was also shown that the perimeters of the crevasse splays were higher for a given area than the coastal deposits. The primary reason for this is the input raster's 2 m spatial resolution, which limits the output deposits to be displayed as 2 x 2 m blocks – causing longer perimeters than if the edge of the landforms were smooth. The effect of this could be exaggerated by the digitising method used to extract the outlines of coastal deposits from high-resolution aerial imagery - where manual digitising can overly smooth the deposit edges.

Despite these variances in the coastal and fluvial scaling relationship distribution, the most important similarity was their gradient. Thus, as the deposit area increases, deposit length and perimeter rise at the same rate in the coastal and fluvial work. Moreover, regardless of the length measurements being low and perimeters high relative to the area in the modelled crevasse splays, the deposits still fit within the distribution of the washover deposits. Therefore, it can be deduced that the real-world washover and modelled splays are morphologically similar, notwithstanding the slight variation in length and perimeter measurements – caused by the different methodologies used to generate the datasets.

The synthesis also combined the results obtained in this work with data extracted from previous literature. The dataset compiled from literature included deposits formed on natural coastal floodplains (Hudock *et al.,* 2014; Lazarus, 2016; Rodriguez *et al.,* 2020; Williams and Rains, 2022), natural fluvial floodplains (Guzzetti *et al.,* 1997; Millard *et al.* 2017), fan deposits on Mars (Kraal *et al.* 2008), and natural and built environment coastal floodplains in a flume experiment (Lazarus *et al.* 2022). From this comparative analysis, it was acknowledged that the natural and built results from the coastal environment (**Chapter 3**) and those created by CAESAR-Lisflood from the fluvial domain (**Chapters 5 and 6**) closely correlate with the morphometric data extracted from literature – consisting of a large number of deposits across many environments and scales. Such findings indicate that the CAESAR-Lisflood generated splay deposits reflect the genuine

morphometric scaling relationships observed in real-world scenarios and experimental work. Therefore, as well as the 2-dimensional reduced-complexity model gaining qualitative validity in its ability to reflect realistic morphological patterns, including how deposits close off to additional sediment, CAESAR-Lisflood is shown to be quantitatively accurate in its depictions of flood-driven deposits.

8.3 Implications

With floods in both morphological systems likely to continue rising in intensity and frequency because of global climate change (Lim, 2022), coupled with the urbanisation of hazard-prone floodplains (Monk *et al.,* 2019), improving our understanding of the impacts such extreme events on natural and built environments is crucial. This work has begun to improve our knowledge of such hazards by delivering new data concerning depositional landforms in floodplain environments, enriching the understanding of elements that drive variations in their morphology. Moreover, it has enhanced the knowledge of the impact anthropogenic development on floodplains can have on deposit size, shape, and consequently, the sediment budget of landscapes.

Understanding the controls on the development of natural sediment deposits can help manage floodplains, reconstruct paleoenvironmental conditions, and forecast sand-body connectivity below the surface (Bridge, 1984; Millard *et al.,* 2017). Some key findings replicated and extended upon morphological patterns observed in other work regarding the natural domain. For example, it has been shown that storm size, grain size and floodplain roughness play a first-order role in determining the terminal morphology of sediment deposits and floodplain sedimentation patterns. From the results obtained, alongside previous research, it is highlighted that two distinct phases ultimately decide the size of splays:

A. The quantity of sediment delivered to the floodplain
B. The quantity of this sediment then deposited on the floodplain

The model results indicate that storm size is dominant in driving the quantity of sediment supply – the higher the energy, the higher the supply. However, it has been clear that independent of storm size, grain size is a significant component controlling terminal splay size by influencing sediment availability and the distribution of sedimentation on the floodplain – as suggested by Slingerland and Smith (1998) and Dingle *et al.* (2020). The grain size findings are novel because they extend on Millard *et al.* (2017), who indicated that splays become larger as grain size coarsens. However, here it is demonstrated that there is a more intricate pattern wherein a dynamic equilibrium appears where an optimum grain size exists to generate the largest splays,

which shifts depending on storm size. Fine silts create the largest splays at low discharges due to the increased sediment supply compared to coarser grains and the consequent low energy on the floodplain. Whereas at high discharges, when this silt supply reaches the floodplain, it is transported away as washload, and thus very fine sand is shown to instigate the largest splays, with a decreasing trend in both grain size directions from this peak. Furthermore, floodplain conditions can alter the morphodynamics and induce varied depositional patterns once the sediment has exited the breach. For example, where floodplain roughness is low, flows can retain their energy and transport capacity, whereas high friction environments induce drag and cause substantial deposits to form. These findings contribute to understanding where various fluvial landscapes will fall regarding their potential depositional features and strengthen the ability to predict morphodynamic behaviours – seen in modern systems and those that have created ancient deposits (Millard *et al.,* 2017).

Moving to the built environment, it is clear that anthropogenic development profoundly impacts landforms produced during coastal and fluvial floods. These findings indicate the principle theory set out by Nordstrom (1994): humans can alter the morphological environment by changing the sources, pathways and sinks of sediment and, consequently, the size and shape of sedimentary landforms produced. Consequently, landscapes that have been transformed by human activity, whether that be roads, buildings, or even flood defences such as sea walls and groynes (Nordstrom, 1994), represent distinct depositional systems to the natural domain. Thus, to fully comprehend and plan for managing morphological events extending into anthropogenically developed environments, one must understand the role of the built environment.

The results obtained from CAESAR-Lisflood show that built environments considerably impact the quantity of sediment transported onto floodplains, thus impacting the abundance and distribution of sediment deposition in landscapes. The quantity of sediment moved onto floodplains, a major component of the sediment budget, is a significant facet of landscape development in the environments found directly alongside coasts and rivers (Croke *et al.,* 2013; Plomaritis *et al.,* 2018). When the amount of sediment delivered to the system is altered, it can harm the long-term viability of these landscapes both morphologically and ecologically (Rogers *et al.,* 2015; Lazarus *et al.,* 2022). In this research, it has been demonstrated that when the built fraction was increased, area and volume measurements decreased, highlighting the detrimental impact of built infrastructure on sediment influx. On top of this, post-storm clean-up efforts often remove the sediment from the affected area to elsewhere (Lazarus and Goldstein, 2019) – further decreasing the sediment supply.

A reduction in sediment supply to built-up floodplains points towards future issues for these inhabited areas – particularly in the coastal environment. For example, barrier islands rely on sediment input in order to retain their elevation relative to sea level. Therefore, where these shorelines receive less sediment from its principal source – overwash delivery – the barrier system is unlikely to retain its elevation relative to projected sea level rise. In the US specifically, where the population of barrier islands is more than 1.4 million (Zhang and Leatherman, 2011) and continuously growing, there is a hotspot of sea level rise with rates 3 -4 times the global average (Sallenger, 2012). Due to consistent sediment supply, natural shorelines will likely persist via landward migration over time (Timmons *et al.*, 2010; Rogers *et al.*, 2015), yet built settings will lack this process, and, as such, there is potential that these built-up barrier islands may become inundated under projected rising sea levels. In the meantime, with it estimated that by the year 2100, the global sea levels will rise in the range of 28 – 61 cm (Swapna *et al.*, 2020), causing infrastructure and human populations to experience considerably more exposure during large storms, with associated amplified damage and recovery costs. As a result of the increased risk to populations inhabiting flood-prone environments, the morphological outcomes of flood events must be understood to allow suitable mitigation mechanisms to be put in place to reduce the impact of such events.

Despite the negative impact on deposit area and volume associated with increasing built environment densities, the morphometric scaling laws concerning volume measurements and area are preserved, corresponding with findings from Lazarus *et al.* (2022). Such findings counter the argument of Rogers *et al.* (2015), which indicated that built environments disturb the scaling of washover volume. As replicated in this research, they plotted a width-averaged volume as a function of intrusion length, which creates a noisy relationship – even when the volume is not normalised (Lazarus *et al.* 2022). By default, these transect-oriented scaling relationships can lose substantial detail of the three-dimensional properties of a deposit. For example, a transect may represent a thin slice of a deposit close to the margin or through the thickest part – causing an exaggerated volume to be calculated. Further, it is not applicable in a built environment where the deposits branch down streets and between buildings – where the detail would be lost. Therefore, it is essential to consider the whole of the deposits as a function of their volume and area to accurately represent sediment flux in natural and built depositional settings.

The primary influence on the volume vs area scaling relationship is grain size, with the coarser sands exhibiting steeper gradients and thus thicker deposits than finer sands, with the gradients insensitive to the density of the built environments. Whilst the built environment can cause the planform shape of deposits to become distorted from natural norms, as highlighted by the perimeter vs area scaling relationship and the subsequent Distortion Index metric, volume as a

function of the area remains undisturbed. Therefore, it implies there is potential to take 2D data - derived from aerial imagery (such as that provided by NOAA for post-hurricane information) - and convert it into 3D information. Indeed, obtaining data regarding deposit area and grain size can facilitate the estimation of a deposit's volume because the area can be viewed as a powerful predictor of landform volume across a range of built environments.

The ability to ascertain deposit volumes from 2D size metric can be beneficial in two ways. Firstly, it offers the chance to look at aerial imagery of historic flood events and determine the quantity of sediment offloaded onto the environment during overwash/levee breaching. From this, it would be possible to estimate sediment supply during these events and thus observe and quantify how sediment budgets – driven by extreme events – have changed with the increasing presence of humans and their associated infrastructure. Additionally, predicting sediment deposit volume from area measurements allows land managers and policymakers to make more informed decisions in management and resourcing. For example, if the deposit area is known within a built environment or across a road network, the estimated volume would allow clean-up tasks to be more time and cost-efficient, such as permitting suitable resourcing of an appropriate number of bulldozers to clear the land. Furthermore, estimating volumes of sediment deposits from aerial imagery – a common resource immediately post-storm – allows the impacts on infrastructure, including roads and communication networks, to be assessed rapidly, enabling improved information to be available for authorities to undertake post-event emergency management.

With anthropogenic development and pressures increasing in an array of hazard-prone regions worldwide (Chang *et al.*, 2012; Brown *et al.*, 2015; Odiase *et al.*, 2019), it is important to note that the observed human impact on natural deposition patterns is unlikely to be limited to the low-lying coastal and fluvial floodplain domains. Other hydrological events which instigate water to enter and flow through built environments, such as tsunamis, follow the same transportation and deposition laws, whilst it can be assumed that there would be some degree of replication in other geomorphic fields, e.g. landslides, avalanches, and volcanic eruptions, wherein built infrastructure also impacts on flow patterns (Gurioli *et al.,* 2005; Bricker *et al.,* 2015). Therefore, expanding the knowledge and understanding of flood-driven deposits in natural and built environments can aid in developing the resilience of other built environments to cope with the effects of natural disasters.

A crucial part of building this resilience is to predict the impact such events will have in the future. With changing weather patterns, sea level rise, and increasing anthropogenic pressures, being able to model the impacts these factors have on our current understanding of risk is

essential. Our ability to trust that models used to predict impacts represent real-world conditions is essential (Baart *et al.*, 2016). CAESAR-Lisflood (Coulthard *et al.,* 2013), which is a two-dimensional reduced-complexity morphodynamic model (cellular automata), has proven a valuable tool for studying the drivers of deposit morphology. The results suggest that CAESAR-Lisflood can qualitatively reflect real-world morphological norms while generating crevasse splays. Firstly, the termination of crevasse splay growth within the model runs mirror reality in how deposits close off to continued sediment supply (Roberts, 1997; Yuill *et al.,* 2016). Once the accretion of material within the levee breach reaches a certain thickness, the deposit is closed off to additional sediment. During the experiments, it was observed that the breach became blocked after some time, and floodwaters no longer propagated onto the floodplain. Secondly, the splay deposits created by CAESAR-Lisflood show a thinning pattern from the deepest part of the landform close to the levee breach opening, moving outwards to the deposit edge. Such a pattern mirrors natural crevasse splays in New South Wales, Australia (O'Brien and Wells, 1986) and overbank sedimentation on Brandywine Creek, Pennsylvania (Pizzuto, 1987).

However, it is challenging to quantifiably validate cellular automata models against real-world individual landforms (Coulthard *et al.,* 2007; Fonstad, 2013). Nevertheless, the work undertaken in this thesis has allowed the crevasse splays generated to be compared quantitatively to flood-driven sediment deposits studied in other work from a range of experiments and real-world observations (e.g. Lazarus, 2016; Millard *et al.,* 2017; Rahman *et al.,* 2022), including the washover sampled in chapter 3. It has been shown that the splays generated by CAESAR-Lisflood fit within the distributions of the morphometric scaling relationships of the other landform examples, as well as matching the scaling gradients – indicating a rise in one metric causes the same increase in another. Such an assessment adds quantitative validity in using reduced complexity models, particularly CAESAR-Lisflood, with its assimilation of a more advanced flow model, to study morphological landforms and the controls on their size and shape. This provides confidence to those using such model outputs in the future to prepare for, and respond to, events in which large quantities of sediment are deposited on the floodplain.

8.4 Future research avenues

The methodology used in this research has successfully obtained a substantial amount of quantitative data, significantly enhancing the understanding of the size and shape of flood-driven sediment deposits in coastal and fluvial settings, along with the impact of humans on natural norms. However, when considering the method's limitations and this thesis's findings, potential opportunities for future research present themselves.

The coastal research into washover deposits has focused solely on sandy barrier islands and low-lying coasts along the Atlantic and Gulf coasts of the US. This can be extended two-fold. Firstly, washover deposits can be studied within other sandy coasts worldwide. Accounts of the sediment budgets in these landscapes, including atoll islands in the Pacific and Maldives, can provide important information regarding the future of these vulnerable settings during sea level rise. Forecasts based on simple hydrodynamic models indicate that these islands will be uninhabitable due to sea level rise (Storlazzi *et al.*, 2018) – but these consider the islands to be immobile. Instead, if the dynamic processes of repeated overwash, and the intertwined sediment delivery, are reflected, these landscapes could retain their height relative to sea level (Masselink *et al.*, 2020).

Secondly, this work could be extended to gravel deposits because this coarser sediment dominates many coastal and fluvial settings. This includes the coasts of Northern Europe, Japan, and New Zealand (Buscombe and Masselink, 2006; Almeida *et al.*, 2017), where the sediment supply and wave energy causes coarse-grained sediment to accumulate along the shore (Orford *et al.*, 2002). Gravel barriers also rely on overwash occurrence and the creation of washover deposits in their rollover mechanism to retain their heights relative to sea level and migrate landwards (Carter and Orford, 1993; Matias *et al.*, 2014). Therefore, it would be beneficial to understand better the washover produced in these gravel-dominated landscapes to assess and project future responses to rising sea levels and allow a comparison with sandy shores. On top of this, a numerical morphological model specific to coasts, such as XBeach (Roelvink *et al.*, 2009), could be used to explore whether the deposits generated conform to scaling relationships observed here and with wider literature, using a broad range of sediment size distributions – to assess sandy and gravel-based systems. The locations and conditions under which the scaling relationships are broken can be identified by generating a comprehensive dataset of morphometric components of flood deposits in a range of environments.

This thesis has investigated the effect of various natural environmental conditions whilst retaining a deliberately flattened floodplain. Nevertheless, it is widely understood that the

antecedent topography of landscapes considerably impacts the morphology of flood-driven sediment deposits by altering the flow directions of overwash (Kain *et al.*, 2014). Variable elevation on floodplains could account for a large proportion of the differences between the explanatory powers deposit shape in the real-world and model regression models. The effect of simple topographies comprising a drained and ponded floodplain has previously been tested in crevasse splay formation (Millard *et al.,* 2017). However, there is room for an in-depth investigation into the quantitative impact of more complex elevation profiles on sediment deposits and to what degree the shape and size of the depositional landforms can be affected.

For efficiency, the CAESAR-Lisflood results in this research were limited to a 2 x 2 m raster grid to allow many depositional environments and conditions to be tested. Therefore, the key caveat to this work is its restriction to the spatial resolution necessary for the work to be undertaken and the simplistic built environments required to be utilised in the CAESAR-Lisflood software to explore the impact of anthropogenic development on deposit morphology. However, it is essential to note that despite this potential issue, the morphometric scaling relationships developed here closely reflected those observed in the real world and laboratory experiments. Regardless, due to the ongoing technological advances, the availability of high-resolution data will only increase, as well as an increase in computational power, resulting in morphological processes being studied in greater detail. For example, in a built environment, this could include the ability to incorporate barrier features such as fences and pavements and high-resolution spatially variable roughness values to illustrate gardens and parks. Although it has been shown to replicate morphometric scaling relationships within many other studies, the next stage could be to test the morphological outcomes of CAESAR-Lisflood, regarding crevasse splays, to a real-world flood event that induced splay formation. Using parameters reflecting the flood conditions that occurred, including discharge, quantities of sediment load and grain size distributions, and an elevation layer representing pre-flood conditions, it could be investigated to what extent the morphological model reflects the event's outcomes.

An opportunity to explore the effect of built environments on sediment budgets over a period of time has presented itself. In this work, as well as in Lazarus *et al.* (2022), it has been indicated that the volume vs area morphometric scaling relationship is preserved between natural and built environments irrespective of the density of the built fabric. Therefore, there is the possibility to use historical flood events to observe how deposits have changed through time with increasing built development. By georeferencing historical imagery or using previous measurements of deposits, a time series analysis could be completed investigating the impact of a built environment on a coast over time – assessing changes in sediment flux as humans alter the landscape.

Finally, the morphometric scaling relationships derived in this work are constructed using depictions of depositional landforms captured at a specific point in time – providing quantitative data concerning a snapshot of deposits (Bull, 1975). Indeed, they are a result of physical processes rather than a direct measure of morphodynamics which occur during flood events (Mackin, 1963; Lazarus *et al.,* 2020). Consequently, they do not address the impacts of natural conditions and built environments on the underlying flow dynamics, and how landforms form and develop. Therefore, future research could aim to explore the underpinning processes driving the disturbance effect of built structures on flow velocities and directions, and the subsequent impacts on sediment deposition. As technology advances, the ability to investigate overwash processes and morphology during storm events is enhanced. This additional research could be undertaken in high-spec laboratory experiments, or using sensor platforms which can be placed in floodplains during a storm event. For example, the novel MeOW equipment developed by Reeves *et al.,* (2021) can capture high-resolution water and sediment elevations once per minute during flood events (Borrell and Puleo, 2019). Such work would provide in-depth understanding of the morphodynamics which drive landform formation in natural and built environments.

List of References

Abdelfatah, N. *et al.* (2022) 'Experimental investigation of wind impact on low-rise elevated residences', *Engineering Structures*, 257, p. 114096. Available at: https://doi.org/10.1016/j.engstruct.2022.114096.

Abebe, Y.A. *et al.* (2019) 'Flood risk management in Sint Maarten – A coupled agent-based and flood modelling method', *Journal of Environmental Management*, 248, p. 109317. Available at: https://doi.org/10.1016/j.jenvman.2019.109317.

Adams, P.N., Opdyke, N.D. and Jaeger, J.M. (2010) 'Isostatic uplift driven by karstification and sea-level oscillation: Modeling landscape evolution in north Florida', *Geology*, 38(6), pp. 531–534. Available at: https://doi.org/10.1130/G30592.1.

Adams, P.N., Slingerland, R.L. and Smith, N.D. (2004) 'Variations in natural levee morphology in anastomosed channel flood plain complexes', *Geomorphology*, 61(1–2), pp. 127–142. Available at: https://doi.org/10.1016/j.geomorph.2003.10.005.

Aldabet, S., Goldstein, E.B. and Lazarus, E.D. (2022) 'Thresholds in Road Network Functioning on US Atlantic and Gulf Barrier Islands', *Earth's Future*, 10(5). Available at: https://doi.org/10.1029/2021EF002581.

Ali, M. *et al.* (2013) 'A unit stream power based sediment transport function for overland flow', *CATENA*, 101, pp. 197–204. Available at: https://doi.org/10.1016/j.catena.2012.09.006.

Almeida, L.P. *et al.* (2017) 'Storm overwash of a gravel barrier: Field measurements and XBeach-G modelling', *Coastal Engineering*, 120, pp. 22–35. Available at: https://doi.org/10.1016/j.coastaleng.2016.11.009.

Andreadis, K.M. *et al.* (2022) 'Urbanizing the floodplain: global changes of imperviousness in flood-prone areas', *Environmental Research Letters*, 17(10), p. 104024. Available at: https://doi.org/10.1088/1748-9326/ac9197.

Ashton, A.D. *et al.* (2013) 'Progress in coupling models of coastline and fluvial dynamics', *Computers & Geosciences*, 53, pp. 21–29. Available at: https://doi.org/10.1016/j.cageo.2012.04.004.

Aslan, A., Autin, W.J. and Blum, M.D. (2005) 'Causes of River Avulsion: Insights from the Late Holocene Avulsion History of the Mississippi River, U.S.A.', *Journal of Sedimentary Research*,

75(4), pp. 650–664. Available at: https://doi.org/10.2110/jsr.2005.053.

Aslan, A. and Blum, M.D. (1999) Contrasting styles of Holocene avulsion, Texas Gulf Coastal Plain, USA. In:Fluvial Sedimentology VI(Eds N.D. Smith and J. Rogers),*Int. Assoc. Sedimentol. Spec. Publ.,*28, 193–209.

Aslan, A. and Blum, M.D. (2009) 'Constrasting Styles of Holocene Avulsion, Texas Gulf Coastal Plain, USA', in *Fluvial Sedimentology VI*. Oxford, UK: Blackwell Publishing Ltd., pp. 193–209. Available at: https://doi.org/10.1002/9781444304213.ch15.

Asselman, N.E.M. and Middelkoop, H. (1995) 'Floodplain sedimentation: Quantities, patterns and processes', *Earth Surface Processes and Landforms* [Preprint]. Available at: https://doi.org/10.1002/esp.3290200602.

Avanzi, J.C. *et al.* (2013) 'Spatial distribution of water erosion risk in a watershed with eucalyptus and Atlantic Forest', *Ciência e Agrotecnologia*, 37(5), pp. 427–434. Available at: https://doi.org/10.1590/S1413-70542013000500006.

Avila, L. A., and Cangialosi, J. (2012) Tropical cyclone report: Hurricane Irene (AL092011), 21–28 August 2011. *NHC Tech. Rep.*, 45 pp., http://www.nhc.noaa.gov/data/tcr/AL092011_Irene.pdf.

Baart, F. *et al.* (2016) 'Morphological impact of a storm can be predicted three days ahead', *Computers & Geosciences*, 90, pp. 17–23. Available at: https://doi.org/10.1016/j.cageo.2015.11.011.

Bagnold, R.A. (1977) 'Bed load transport by natural rivers', *Water Resources Research*, 13(2), pp. 303–312. Available at: https://doi.org/10.1029/WR013i002p00303.

Di Baldassarre, G. *et al.* (2013) 'Socio-hydrology: Conceptualising human-flood interactions', *Hydrology and Earth System Sciences*, 17(8), pp. 3295–3303. Available at: https://doi.org/10.5194/HESS-17-3295-2013.

Baldwin, D.S. and Mitchell, A.M. (2000) 'The effects of drying and re-flooding on the sediment and soil nutrient dynamics of lowland river-floodplain systems: a synthesis', *Rivers: Res. Mgmt*, 16, pp. 457–467. Available at: https://doi.org/10.1002/1099-1646(200009/10)16:5.

Baptist, M.J. *et al.* (2007) 'On inducing equations for vegetation resistance', *Journal of Hydraulic Research*, 45(4), pp. 435–450. Available at: https://doi.org/10.1080/00221686.2007.9521778.

Bastola, S. *et al.* (2018) 'The role of vegetation on gully erosion stabilization at a severely

degraded landscape: A case study from Calhoun Experimental Critical Zone Observatory', *Geomorphology*, 308, pp. 25–39. Available at: https://doi.org/10.1016/j.geomorph.2017.12.032.

Bates, P.D., Horritt, M.S. and Fewtrell, T.J. (2010) 'A simple inertial formulation of the shallow water equations for efficient two-dimensional flood inundation modelling', *Journal of Hydrology*, 387(1–2), pp. 33–45. Available at: https://doi.org/10.1016/j.jhydrol.2010.03.027.

Bates, P.D. and De Roo, A.P.J. (2000) 'A simple raster-based model for flood inundation simulation', *Journal of Hydrology* [Preprint]. Available at: https://doi.org/10.1016/S0022-1694(00)00278-X.

Beevers, L. *et al.* (2016) 'Applicability of a coastal morphodynamic model for fluvial environments', *Environmental Modelling & Software*, 80, pp. 83–99. Available at: https://doi.org/10.1016/j.envsoft.2016.02.016.

Bendoni, M. *et al.* (2019) 'Numerical modelling of the erosion of marsh boundaries due to wave impact', *Coastal Engineering*, 152, p. 103514. Available at: https://doi.org/10.1016/j.coastaleng.2019.103514.

Best, J. (2019) 'Anthropogenic stresses on the world's big rivers', *Nature Geoscience*, 12(1), pp. 7–21. Available at: https://doi.org/10.1038/s41561-018-0262-x.

Bevacqua, E. *et al.* (2020) 'More meteorological events that drive compound coastal flooding are projected under climate change', *Communications Earth & Environment 2020 1:1*, 1(1), pp. 1–11. Available at: https://doi.org/10.1038/s43247-020-00044-z.

Beven II, J.L., Berg, R., and Hagen, A. (2019) Tropical Cyclone Report Hurricane Michael, National Hurricane Center (AL142018) 19 April 2019

Beven, J. L., and Berg, R. (2018) National Hurricane Center tropical cyclone report: Hurricane Nate. NOAA/NWS Rep. AL162017, 45 pp., https://www.nhc.noaa.gov/data/tcr/AL162017_Nate.pdf.

Blake, E. S., *et al.* (2013) Tropical Cyclone Report Hurricane Sandy (AL182012) -22–29 October 2012

Blenkinsopp, C.E. *et al.* (2016) 'Wave runup and overwash on a prototype-scale sand barrier', *Coastal Engineering*, 113, pp. 88–103. Available at: https://doi.org/10.1016/j.coastaleng.2015.08.006.

Blum, M.D. and Roberts, H.H. (2009) 'Drowning of the Mississippi Delta due to insufficient

sediment supply and global sea-level rise', *Nature Geoscience 2009 2:7*, 2(7), pp. 488–491. Available at: https://doi.org/10.1038/ngeo553.

Boeing, G. (2017) 'OSMnx: New methods for acquiring, constructing, analyzing, and visualizing complex street networks', *Computers, Environment and Urban Systems* [Preprint]. Available at: https://doi.org/10.1016/j.compenvurbsys.2017.05.004.

Bookhagen, B. (2010) 'Appearance of extreme monsoonal rainfall events and their impact on erosion in the Himalaya', *Geomatics, Natural Hazards and Risk*, 1(1), pp. 37–50. Available at: https://doi.org/10.1080/19475701003625737.

Booth, A.M., Roering, J.J. and Rempel, A.W. (2013) 'Topographic signatures and a general transport law for deep-seated landslides in a landscape evolution model', *Journal of Geophysical Research: Earth Surface*, 118(2), pp. 603–624. Available at: https://doi.org/10.1002/jgrf.20051.

Borrell, S. and Puleo, J. (2019) 'In situ hydrodynamic and morphodynamic measurements during extreme storm events', *Shore & Beach*, pp. 23–30. Available at: https://doi.org/10.34237/1008743.

Bouwer, L.M. and Jonkman, S.N. (2018) 'Global mortality from storm surges is decreasing', *Environmental Research Letters*, 13(1), p. 014008. Available at: https://doi.org/10.1088/1748-9326/AA98A3.

Brakenridge, G.R. *et al.* (2013) 'Global mapping of storm surges and the assessment of coastal vulnerability', *Natural Hazards: Journal of the International Society for the Prevention and Mitigation of Natural Hazards*, 66(3), pp. 1295–1312. Available at: https://doi.org/10.1007/S11069-012-0317-Z.

Bricker, J.D. *et al.* (2015) 'On the need for larger Manning's roughness coefficients in depth-integrated tsunami inundation models', *Coastal Engineering Journal*, 57(2). Available at: https://doi.org/10.1142/S0578563415500059.

Bridge, J. (2003) *Rivers and Floodplains: Forms, Processes, and Sedimentary Record*. 1st edn. Hong Kong: Blackwell Publishing Ltd.

Bridge, J.S. (1984) 'Large-scale Facies Sequences In Alluvial Overbank Environments', *SEPM Journal of Sedimentary Research*, Vol. 54. Available at: https://doi.org/10.1306/212F8477-2B24-11D7-8648000102C1865D.

Bristow, C.S., Skelly, R.L., and Ethridge, F.G. (1999) Crevasse splays from the rapidly aggrading sand-bed braided Niobrara River, Nebraska: effect of base-level rise: *Sedimentology*, v. 46, p. 1029–1047

Britter, R.E. and Hanna, S.R. (2003) 'Flow and Dispersion in Urban Areas', *Annual Review of Fluid Mechanics* [Preprint].

Brown, C., Milke, M. and Seville, E. (2011) 'Disaster waste management: A review article', *Waste Management*, 31(6), pp. 1085–1098. Available at: https://doi.org/10.1016/J.WASMAN.2011.01.027.

Brown, S.. *et al.* (2015) *Global volcanic hazards and risk*. 1st edn. Edited by S.. Loughlin et al. Cambridge: Cambridge University Press. Available at: https://doi.org/10.1017/CBO9781316276273.004.

Brunner, M.I. *et al.* (2021) 'Challenges in modeling and predicting floods and droughts: A review', *WIREs Water*, 8(3). Available at: https://doi.org/10.1002/wat2.1520.

Bull, W. B. (1962) Relations of alluvial-fan size and slope to drainage-basin size and lithology in western Fresno County, *California U.S. Geol. Surv. Prof. Pap.* 450-B.

Bull, W. B. (1975) Allometric change of landforms, *Geol. Soc. Am. Bull.*, 86, 1489, https://doi.org/10.1130/0016-7606(1975)86<1489:ACOL>2.0.CO;2

Bulti, D.T. and Abebe, B.G. (2020) 'A review of flood modeling methods for urban pluvial flood application', *Modeling Earth Systems and Environment*, 6(3), pp. 1293–1302. Available at: https://doi.org/10.1007/s40808-020-00803-z.

Burns, C.E. *et al.* (2017) 'Anatomy and dimensions of fluvial crevasse-splay deposits: Examples from the Cretaceous Castlegate Sandstone and Neslen Formation, Utah, U.S.A.', *Sedimentary Geology*, 351, pp. 21–35. Available at: https://doi.org/10.1016/j.sedgeo.2017.02.003.

Buscombe, D. and Masselink, G. (2006) 'Concepts in gravel beach dynamics', *Earth-Science Reviews*, 79(1–2), pp. 33–52. Available at: https://doi.org/10.1016/j.earscirev.2006.06.003.

Caldwell, R.L. and Edmonds, D.A. (2014) 'The effects of sediment properties on deltaic processes and morphologies: A numerical modeling study', *Journal of Geophysical Research: Earth Surface*, 119(5), pp. 961–982. Available at: https://doi.org/10.1002/2013JF002965.

Carruthers, E.A. *et al.* (2013) 'Quantifying overwash flux in barrier systems: An example from Martha's Vineyard, Massachusetts, USA', *Marine Geology*, 343, pp. 15–28. Available at:

https://doi.org/10.1016/J.MARGEO.2013.05.013.

Carter, R.W.G. and Orford, J.D. (1993) 'The Morphodynamics of Coarse Clastic Beaches and Barriers: A Short- and Long-term Perspective', *Journal of Coastal Research*, pp. 158–179. Available at: http://www.jstor.org/stable/25735728.

Cazanacli, D. and Smith, N.D. (1998) 'A study of morphology and texture of natural levees—Cumberland Marshes, Saskatchewan, Canada', *Geomorphology*, 25(1–2), pp. 43–55. Available at: https://doi.org/10.1016/S0169-555X(98)00032-4.

Chang, S.E. *et al.* (2012) 'Urban Growth and Long-Term Changes in Natural Hazard Risk':, *http://dx.doi.org/10.1068/a43614*, 44(4), pp. 989–1008. Available at: https://doi.org/10.1068/A43614.

Chen, Z., Gao, B. and Devereux, B. (2017) 'State-of-the-Art: DTM Generation Using Airborne LIDAR Data', *Sensors*, 17(12), p. 150. Available at: https://doi.org/10.3390/s17010150.

Chomiak, L. (2020) 'Crevasse splays within a lignite seam at the Tomisławice opencast mine near Konin, central Poland: architecture, sedimentology and depositional model', *Geologos*, 26(1), pp. 25–37. Available at: https://doi.org/10.2478/logos-2020-0002.

Chow, V.T. (1959) Open-channel hydraulics: New York, McGraw-Hill Book Co., 680 p.

Chuang, S.C. *et al.* (2009) 'Increase in basin sediment yield from landslides in storms following major seismic disturbance', *Engineering Geology*, 103(1–2), pp. 59–65. Available at: https://doi.org/10.1016/J.ENGGEO.2008.08.001.

Collins, A.J. and Owens, P.N. (2006) 'Introduction to soil erosion and sediment redistribution in river catchments: measurement, modelling and management in the 21st century.', in *Soil erosion and sediment redistribution in river catchments: measurement, modelling and management*. UK: CABI, pp. 3–9. Available at: https://doi.org/10.1079/9780851990507.0003.

Costanza, R. *et al.* (1997) 'The value of the world's ecosystem services and natural capital', *Nature*, 387(6630), pp. 253–260. Available at: https://doi.org/10.1038/387253a0.

Costanza, R., Sklar, F.H. and White, M.L. (1990) 'Modeling Coastal Landscape Dynamics', *BioScience*, 40(2), pp. 91–107. Available at: https://doi.org/10.2307/1311342.

Coulthard, T.J. (1999) Modelling upland catchment response to Holocene environmental change, PhD Thesis, University of Leeds.

Coulthard, T.J. *et al.* (2013) 'Integrating the LISFLOOD-FP 2D hydrodynamic model with the CAESAR model: Implications for modelling landscape evolution', *Earth Surface Processes and Landforms* [Preprint]. Available at: https://doi.org/10.1002/esp.3478.

Coulthard, T.J., Hicks, D.M. and Van De Wiel, M.J. (2007) 'Cellular modelling of river catchments and reaches: Advantages, limitations and prospects', *Geomorphology*, 90(3–4), pp. 192–207. Available at: https://doi.org/10.1016/j.geomorph.2006.10.030.

Coulthard, T.J., Macklin, M.G. and Kirkby, M.J. (2002) 'A cellular model of Holocene upland river basin and alluvial fan evolution', *Earth Surface Processes and Landforms* [Preprint]. Available at: https://doi.org/10.1002/esp.318.

Coulthard, T.J. and Van de Wiel, M.J. (2013) 'Climate, tectonics or morphology: what signals can we see in drainage basin sediment yields?', *Earth Surface Dynamics*, 1(1), pp. 13–27. Available at: https://doi.org/10.5194/esurf-1-13-2013.

Coulthard, T.J. and Van De Wiel, M.J. (2017) 'Modelling long term basin scale sediment connectivity, driven by spatial land use changes', *Geomorphology*, 277, pp. 265–281. Available at: https://doi.org/10.1016/j.geomorph.2016.05.027.

Croke, J., Fryirs, K. and Thompson, C. (2013) 'Channel-floodplain connectivity during an extreme flood event: implications for sediment erosion, deposition, and delivery', *Earth Surface Processes and Landforms*, 38(12), p. n/a-n/a. Available at: https://doi.org/10.1002/esp.3430.

Crosato, A. and Saleh, M.S. (2011) 'Numerical study on the effects of floodplain vegetation on river planform style', *Earth Surface Processes and Landforms*, 36(6), pp. 711–720. Available at: https://doi.org/10.1002/esp.2088.

Culliton T. (1998) Population: distribution, density, and growth. NOAA's State of the coast report. NOAA

Dadson, S.J. *et al.* (2004) 'Earthquake-triggered increase in sediment delivery from an active mountain belt', *Geology*, 32(8), pp. 733–736. Available at: https://doi.org/10.1130/G20639.1.

Dahl B.E. *et al.* (1983) Posthurricane Survey of Experimental Dunes on Padre Island, Texas. Ft. Belvoir, Virginia: U.S. Army Corps of Engineers, Coastal Engineering Research Center.

Darby, S.E. (1999) 'Effect of Riparian Vegetation on Flow Resistance and Flood Potential', *Journal of Hydraulic Engineering*, 125(5), pp. 443–454. Available at: https://doi.org/10.1061/(ASCE)0733-9429(1999)125:5(443).

Davis, R.A. (Ed.) (1985) Coastal Sedimentary Environments. Springer-Verlag, New York, NY, 663 pp.

Dawson, F.H. (1988) 'Water Flow and the Vegetation of Running Waters', in *Vegetation of inland waters*. Dordrecht: Springer Netherlands, pp. 283–309. Available at: https://doi.org/10.1007/978-94-009-3087-2_9.

Deltares (2014) Delft3D-WAVE Simulation of short-crested waves with SWAN, User Manual, version: 3.05.34160, Deltares, The Netherlands.

Denny, C. S. (1965) Alluvial fans in the Death Valley region, *California and Nevada U.S. Geol. Surv. Prof. Pap.* 466.

Diffenbaugh, N.S. (2020) 'Verification of extreme event attribution: Using out-of-sample observations to assess changes in probabilities of unprecedented events', *Sci. Adv*, 6(12). Available at: https://www.science.org (Accessed: 23 March 2022).

Dingle, E.H. *et al.* (2020) 'Sediment dynamics across gravel-sand transitions: Implications for river stability and floodplain recycling', *Geology*, 48(5), pp. 468–472. Available at: https://doi.org/10.1130/G46909.1.

Van Dinter, M., & Van Zijverden, W. (2010). Settlement and land use on crevasse splay deposits; geoarchaeological research in the Rhine-Meuse Delta, the Netherlands. *Netherlands Journal of Geosciences, 89*(1), 21-34. doi:10.1017/S0016774600000792

Dodds, P.S. and Rothman, D.H. (2000) 'Scaling, Universality, and Geomorphology', *Annual Review of Earth and Planetary Sciences*, 28(1), pp. 571–610. Available at: https://doi.org/10.1146/annurev.earth.28.1.571.

Dolan, R. and Godfrey, P. (1973) 'Effects of Hurricane Ginger on the Barrier Islands of North Carolina', *GSA Bulletin*, 84(4), pp. 1329–1334. Available at: https://doi.org/10.1130/0016-7606(1973)84<1329:EOHGOT>2.0.CO;2.

Donnelly, C., Kraus, N. and Larson, M. (2006) 'State of Knowledge on Measurement and Modeling of Coastal Overwash', *Journal of Coastal Research*, 224(4 (224)), pp. 965–991. Available at: https://doi.org/10.2112/04-0431.1.

Donnelly, C., Kraus, N.C. and Larson, M. (2004) *Coastal Overwash: Part 1, Overview of Processes.*

Donnelly, C., Larson, M. and Hanson, H. (2009) 'A numerical model of coastal overwash', *Proceedings of the Institution of Civil Engineers: Maritime Engineering*, 162(3), pp. 105–114. Available

at: https://doi.org/10.1680/MAEN.2009.162.3.105.

Donnelly, C. and Sallenger, A.H. (2007) 'Characterisation and Modeling of Washover Fans', in *Coastal Sediments '07*. Reston, VA: American Society of Civil Engineers, pp. 2061–2073. Available at: https://doi.org/10.1061/40926(239)162.

Doronzo, D.M. and Dellino, P. (2011) 'Interaction between pyroclastic density currents and buildings: Numerical simulation and first experiments', *Earth and Planetary Science Letters* [Preprint]. Available at: https://doi.org/10.1016/j.epsl.2011.08.017.

Dottori, F. *et al.* (2018) 'Increased human and economic losses from river flooding with anthropogenic warming', *Nature Climate Change 2018 8:9*, 8(9), pp. 781–786. Available at: https://doi.org/10.1038/s41558-018-0257-z.

Douben, K.J. (2006) 'Characteristics of river floods and flooding: A global overview, 1985-2003', *Irrigation and Drainage*, 55(SUPPL. 1). Available at: https://doi.org/10.1002/IRD.239.

Douben N, Ratnayake RMW. (2005) Characteristic data on river floods; facts and figures. In Floods, from Defence to Management, Symposium Papers, van Alphen J, van Beek E, Taal M (eds). Taylor & Francis Group: London, UK; 11–27.

Du, H. *et al.* (2019) 'Precipitation From Persistent Extremes is Increasing in Most Regions and Globally', *Geophysical Research Letters*, 46(11), pp. 6041–6049. Available at: https://doi.org/10.1029/2019GL081898.

Edmonds, D.A. *et al.* (2011) 'Quantitative metrics that describe river deltas and their channel networks', *Journal of Geophysical Research*, 116(F4), p. F04022. Available at: https://doi.org/10.1029/2010JF001955.

Einstein, H.A. and Brown, C.B. (1950) Bedload function for sediment transportation, In: Rouse Hunter (ed.) Engineering Hydraulics, John Wiley and Sons, New York.

Eisma, D. (1998) Intertidal Deposits: River Mouths, Tidal Flats, and Coastal Lagoons. New York: CRC Press, 525.

Ekeu-wei, I.T. and Blackburn, G.A. (2020) 'Catchment-Scale Flood Modelling in Data-Sparse Regions Using Open-Access Geospatial Technology', *ISPRS International Journal of Geo-Information*, 9(9), p. 512. Available at: https://doi.org/10.3390/ijgi9090512.

Engelstad, A. *et al.* (2017) 'Observations of waves and currents during barrier island inundation', *Journal of Geophysical Research: Oceans*, 122(4), pp. 3152–3169. Available at:

https://doi.org/10.1002/2016JC012545.

Environment Agency (2018) Estimating economic costs of the 2015/16 winter floods, LIT10736

Esposito, C.R. *et al.* (2017) 'Efficient retention of mud drives land building on the Mississippi Delta plain', *Earth Surface Dynamics*, 5(3), pp. 387–397. Available at: https://doi.org/10.5194/esurf-5-387-2017.

Ezer, T. and Atkinson, L.P. (2014) 'Accelerated flooding along the U.S. East Coast: On the impact of sea-level rise, tides, storms, the Gulf Stream, and the North Atlantic Oscillations', *Earth's Future*, 2(8), pp. 362–382. Available at: https://doi.org/10.1002/2014EF000252.

Fagherazzi, S. *et al.* (2020) 'Salt Marsh Dynamics in a Period of Accelerated Sea Level Rise', *Journal of Geophysical Research: Earth Surface*, 125(8). Available at: https://doi.org/10.1029/2019JF005200.

Fang, Y. *et al.* (2021) 'Chinese Built-up Land in Floodplains Moving Closer to Freshwaters', *International Journal of Disaster Risk Science*, 12(3), pp. 355–366. Available at: https://doi.org/10.1007/S13753-021-00343-9/FIGURES/4.

Farrell, K.M. (2001) 'Geomorphology, facies architecture, and high-resolution, non-marine sequence stratigraphy in avulsion deposits, Cumberland Marshes, Saskatchewan', *Sedimentary Geology*, 139(2), pp. 93–150. Available at: https://doi.org/10.1016/S0037-0738(00)00150-0.

Feagin, R.A. *et al.* (2015) 'Going with the flow or against the grain? The promise of vegetation for protecting beaches, dunes, and barrier islands from erosion', *Frontiers in Ecology and the Environment*, 13(4), pp. 203–210. Available at: https://doi.org/10.1890/140218.

Fedele, J.J. and Paola, C. (2007) 'Similarity solutions for fluvial sediment fining by selective deposition', *Journal of Geophysical Research*, 112(F2), p. F02038. Available at: https://doi.org/10.1029/2005JF000409.

Feeney, C.J. *et al.* (2020) 'Modelling the decadal dynamics of reach-scale river channel evolution and floodplain turnover in CAESAR-Lisflood', *Earth Surface Processes and Landforms*, 45(5), pp. 1273–1291. Available at: https://doi.org/10.1002/esp.4804.

FEMA (2007) Debris Management Guide. Public Assistance

Fernandes, J. N., Leal, J. B. and Cardoso, A. H. (2012) Flow structure in a compound channel with smooth and rough floodplains. *European Water*, 38(1), 3–12.

Feyen, L. *et al.* (2012) 'Fluvial flood risk in Europe in present and future climates', *Climatic Change*, 112(1), pp. 47–62. Available at: https://doi.org/10.1007/s10584-011-0339-7.

Field, C.B., *et al.* (2012) Managing the risks of extreme events and disasters to advance climate change adaptation. *Special Report of Working Groups I and II of the Intergovernmental Panel on Climate Change (IPCC)*. Cambridge: Cambridge University Press

Figlus, J. *et al.* (2011) 'Wave Overtopping and Overwash of Dunes', *Journal of Waterway, Port, Coastal, and Ocean Engineering*, 137(1), pp. 26–33. Available at: https://doi.org/10.1061/(ASCE)WW.1943-5460.0000060.

Fisher, J.S., Leatherman, S.P. and Perry, F.C. (1974) 'Overwash Processes on Assateague Island', in *Coastal Engineering 1974*. New York, NY: American Society of Civil Engineers, pp. 1194–1212. Available at: https://doi.org/10.1061/9780872621138.073.

Fisher, J.S. and Stauble, D.K. (1977) 'Impact of Hurricane Belle on Assateague Island washover', *Geology*, 5(12), pp. 765–768. Available at: https://doi.org/10.1130/0091-7613(1977)5<765:IOHBOA>2.0.CO;2.

Fisher, R. V. (1979) 'Models for pyroclastic surges and pyroclastic flows', *Journal of Volcanology and Geothermal Research*, 6(3–4), pp. 305–318. Available at: https://doi.org/10.1016/0377-0273(79)90008-8.

Fitzgerald, D.M. *et al.* (2008) 'Coastal Impacts Due to Sea-Level Rise', *Annual Review of Earth and Planetary Sciences*, 36, pp. 601–647. Available at: https://doi.org/10.1146/annurev.earth.35.031306.140139.

FitzGerald, D.M., Heteren, S. van and Montello, T.M. (1994) 'Shoreline Processes and Damage Resulting from the Halloween Eve Storm of 1991 along the North and South Shores of Massachusetts Bay, U.S.A.', *Journal of Coastal Research*, 10(1), pp. 113–132. Available at: http://www.jstor.org/stable/4298197.

Fletcher, C.H. *et al.* (1995) 'Marine Flooding on the Coast of Kaua'i during Hurricane Iniki: Hindcasting Inundation Components and Delineating Washover', *Journal of Coastal Research*, 11(1), pp. 188–204. Available at: http://www.jstor.org/stable/4298321.

Florsheim, J.L. and Mount, J.F. (2002) 'Restoration of floodplain topography by sand-splay complex formation in response to intentional levee breaches, Lower Cosumnes River, California', *Geomorphology*, 44(1–2), pp. 67–94. Available at: https://doi.org/10.1016/S0169-555X(01)00146-5.

Foley, J.A. *et al.* (2005) 'Global consequences of land use', *Science*, 309(5734), pp. 570–574. Available at: https://doi.org/10.1126/SCIENCE.1111772/SUPPL_FILE/FOLEY_SOM.PDF.

Fonstad, M.A. (2013) '2.9 Cellular Automata in Geomorphology', in J.F. Shroder (ed.) *Treatise on Geomorphology*. San Diego: Academic Press, pp. 117–134. Available at: https://doi.org/https://doi.org/10.1016/B978-0-12-374739-6.00035-X.

Forzieri, G. *et al.* (2011) 'Satellite multispectral data for improved floodplain roughness modelling', *Journal of Hydrology*, 407(1–4), pp. 41–57. Available at: https://doi.org/10.1016/j.jhydrol.2011.07.009.

Fraselle, Q., Bousmar, D. and Zech, Y. (2010) 'Diffusion and dispersion in compound channels: The role of large scale turbulent structures', First IAHR European Congress, 1-6.

Frattini, P. and Crosta, G.B. (2013) 'The role of material properties and landscape morphology on landslide size distributions', *Earth and Planetary Science Letters*, 361, pp. 310–319. Available at: https://doi.org/10.1016/J.EPSL.2012.10.029.

Gaeuman, D. *et al.* (2009) 'Predicting fractional bed load transport rates: Application of the Wilcock-Crowe equations to a regulated gravel bed river', *Water Resources Research*, 45(6). Available at: https://doi.org/10.1029/2008WR007320.

Galloway, W.E. and Hobday, D.K. (1996) Terrigenous clastic depositional systems: applications to fossil fuel and groundwater resources: Springer-Verlag, Berlin, 489 p

Gartner, J.D. *et al.* (2015) 'Gradients in stream power influence lateral and downstream sediment flux in floods', *Geology*, 43(11), pp. 983–986. Available at: https://doi.org/10.1130/G36969.1.

van Gelder, A. *et al.* (1994) 'Overbank and channelfill deposits of the modern Yellow River delta', *Sedimentary Geology*, 90(3–4), pp. 293–305. Available at: https://doi.org/10.1016/0037-0738(94)90044-2.

Givoni, B. (1994) 'Building design principles for hot humid regions', *Renewable Energy*, 5(5–8), pp. 908–916. Available at: https://doi.org/10.1016/0960-1481(94)90111-2.

Glenn, N.F. *et al.* (2006) 'Analysis of LiDAR-derived topographic information for characterizing and differentiating landslide morphology and activity', *Geomorphology*, 73(1–2), pp. 131–148. Available at: https://doi.org/10.1016/J.GEOMORPH.2005.07.006.

Godfrey, P.J. and Godfrey, M.M. (1974) The role of overwash and inlet dynamics in the formation of salt marshes on North Carolina barrier islands. In: REINOLD, R.A. (ed.), *Ecology of Halophytes*. New York: Academic Press, pp. 407-427.

Goldstein, E.B. and Moore, L.J. (2016) 'Stability and bistability in a one-dimensional model of coastal foredune height', *Journal of Geophysical Research: Earth Surface*, 121(5), pp. 964–977. Available at: https://doi.org/10.1002/2015JF003783.

Gomez, B. and Church, M. (1989) 'An assessment of bed load sediment transport formulae for gravel bed rivers', *Water Resources Research*, 25(6), pp. 1161–1186. Available at: https://doi.org/10.1029/WR025i006p01161.

González-Hidalgo, J.C., de Luis, M. and Batalla, R.J. (2009) 'Effects of the largest daily events on total soil erosion by rainwater. An analysis of the USLE database', *Earth Surface Processes and Landforms*, 34(15), pp. 2070–2077. Available at: https://doi.org/10.1002/esp.1892.

Gulliford, A.R., Flint, S.S. and Hodgson, D.M. (2017) 'Crevasse splay processes and deposits in an ancient distributive fluvial system: The lower Beaufort Group, South Africa', *Sedimentary Geology*, 358, pp. 1–18. Available at: https://doi.org/10.1016/j.sedgeo.2017.06.005.

Gurioli, L. *et al.* (2005) 'Interaction of pyroclastic density currents with human settlements: Evidence from ancient Pompeii', *Geology* [Preprint]. Available at: https://doi.org/10.1130/G21294.1.

Gurnell, A.M., Bertoldi, W. and Corenblit, D. (2012) 'Changing river channels: The roles of hydrological processes, plants and pioneer fluvial landforms in humid temperate, mixed load, gravel bed rivers', *Earth-Science Reviews*, 111(1–2), pp. 129–141. Available at: https://doi.org/10.1016/j.earscirev.2011.11.005.

Guzzetti, F., Marchetti, M. and Reichenbach, P. (1997) 'Large alluvial fans in the north-central Po Plain (Northern Italy)', *Geomorphology*, 18(2), pp. 119–136. Available at: https://doi.org/10.1016/S0169-555X(96)00015-3.

Gyr, A., and Hoyer, K. (2006) Sediment Transport, a Geophysical Phenomenon. Fluid Mechanics and its Applications Series, 82. *Springer-Verlag*, Dordrecht. 279 pp

Hairsine, P.B., Beuselinck, L. and Sander, G.C. (2002) 'Sediment transport through an area of net deposition', *Water Resources Research*, 38(6), pp. 22-1-22–7. Available at: https://doi.org/10.1029/2001WR000265.

Hajek, E.A. and Edmonds, D.A. (2014) 'Is river avulsion style controlled by floodplain

morphodynamics?', *Geology*, 42(3), pp. 199–202. Available at: https://doi.org/10.1130/G35045.1.

Hajek, E.A. and Wolinsky, M.A. (2012) 'Simplified process modeling of river avulsion and alluvial architecture: Connecting models and field data', *Sedimentary Geology*, 257–260, pp. 1–30. Available at: https://doi.org/10.1016/j.sedgeo.2011.09.005.

Hall, M.J. and Halsey, S.D. (1991) 'Comparison of Overwash Penetration from Huricane Hugo and Pre-Storm Erosion Rates for Myrtle Beach and North Myrtle Beach, South Carolina, U.S.A.', *Journal of Coastal Research*, pp. 229–235. Available at: http://www.jstor.org/stable/25735417.

Hallegatte, S. *et al.* (2013) 'Future flood losses in major coastal cities', *Nature Climate Change 2013 3:9*, 3(9), pp. 802–806. Available at: https://doi.org/10.1038/nclimate1979.

Hallegatte, S., *et al.* (2017) Unbreakable: building the resilience of the poor in the face of natural disasters. (World Bank Publications, 2017).

Halverson, J.B. and Rabenhorst, T. (2013) 'Hurricane Sandy: The Science and Impacts of a Superstorm', *Weatherwise*, 66(2), pp. 14–23. Available at: https://doi.org/10.1080/00431672.2013.762838.

Hancox, G.T. *et al.* (2005) 'The October 1999 Mt Adams rock avalanche and subsequent landslide dam-break flood and effects in Poerua river, Westland, New Zealand', *New Zealand Journal of Geology and Geophysics*, 48(4), pp. 683–705. Available at: https://doi.org/10.1080/00288306.2005.9515141.

Hanson, Susan *et al.* (2011) 'A global ranking of port cities with high exposure to climate extremes', *Climatic Change*, 104, pp. 89–111. Available at: https://doi.org/10.1007/s10584-010-9977-4.

Heiler, G. *et al.* (1995) 'Hydrological connectivity and flood pulses as the central aspects for the integrity of a river-floodplain system', *Regulated Rivers: Research & Management*, 11(3–4), pp. 351–361. Available at: https://doi.org/10.1002/RRR.3450110309.

Hesselink, A.W. *et al.* (2003) 'Inundation of a Dutch river polder, sensitivity analysis of a physically based inundation model using historic data', *Water Resources Research*, 39(9). Available at: https://doi.org/10.1029/2002WR001334.

Hirabayashi, Y. *et al.* (2013) 'Global flood risk under climate change', *Nature Climate Change*, 3(9), pp. 816–821. Available at: https://doi.org/10.1038/nclimate1911.

Hirabayashi, Y. *et al.* (2021) 'Global exposure to flooding from the new CMIP6 climate model projections', *Scientific Reports*, 11(1), p. 3740. Available at: https://doi.org/10.1038/s41598-021-83279-w.

Hodge, J. and Williams, H. (2016) 'Deriving spatial and temporal patterns of coastal marsh aggradation from hurricane storm surge marker beds', *Geomorphology*, 274, pp. 50–63. Available at: https://doi.org/10.1016/j.geomorph.2016.09.005.

Holden, J. (2012) *An Introduction to Physical Geography and the Environment*, *Pearson*. Available at: https://doi.org/10.1038/nrrheum.2014.109.PTPN22.

Hooke, J.M. *et al.* (2005) 'A simulation model of morphological, vegetation and sediment changes in ephemeral streams', *Earth Surface Processes and Landforms*, 30(7), pp. 845–866. Available at: https://doi.org/10.1002/esp.1195.

Horritt, M.S. and Bates, P.D. (2002) 'Evaluation of 1D and 2D numerical models for predicting river flood inundation', *Journal of Hydrology* [Preprint]. Available at: https://doi.org/10.1016/S0022-1694(02)00121-X.

Houghton, B. and Carey, R.J. (2015) 'Pyroclastic Fall Deposits', *The Encyclopedia of Volcanoes*, pp. 599–616. Available at: https://doi.org/10.1016/B978-0-12-385938-9.00034-1.

Houser, C. (2009) 'Synchronization of transport and supply in beach-dune interaction', *Progress in Physical Geography: Earth and Environment*, 33(6), pp. 733–746. Available at: https://doi.org/10.1177/0309133309350120.

Houser, C. (2012) 'Feedback between ridge and swale bathymetry and barrier island storm response and transgression', *Geomorphology*, 173–174, pp. 1–16. Available at: https://doi.org/10.1016/j.geomorph.2012.05.021.

Houser, C. (2013) 'Alongshore variation in the morphology of coastal dunes: Implications for storm response', *Geomorphology*, 199, pp. 48–61. Available at: https://doi.org/10.1016/j.geomorph.2012.10.035.

Hoyal, D.C.J.D. and Sheets, B.A. (2009) 'Morphodynamic evolution of experimental cohesive deltas', *Journal of Geophysical Research*, 114(F2), p. F02009. Available at: https://doi.org/10.1029/2007JF000882.

Hoyt, J.H. (1968) 'Barrier island formation: Reply', *Bulletin of the Geological Society of America*, 79(7), pp. 947–948. Available at: https://doi.org/10.1130/0016-7606(1968)79[947:BIFD]2.0.CO;2.

Hu, M. *et al.* (2018) 'Flood Mitigation by Permeable Pavements in Chinese Sponge City Construction', *Water*, 10(2), p. 172. Available at: https://doi.org/10.3390/w10020172.

Huang, D., Wang, S. and Liu, Z. (2021) 'A systematic review of prediction methods for emergency management', *International Journal of Disaster Risk Reduction*, 62, p. 102412. Available at: https://doi.org/10.1016/J.IJDRR.2021.102412.

Hudock, J.W., Flaig, P.P. and Wood, L.J. (2014) 'Washover Fans: A Modern Geomorphologic Analysis and Proposed Classification Scheme To Improve Reservoir Models', *Journal of Sedimentary Research* [Preprint]. Available at: https://doi.org/10.2110/jsr.2014.64.

Hunter, N.M. *et al.* (2008) 'Benchmarking 2D hydraulic models for urban flooding', *Proceedings of the Institution of Civil Engineers: Water Management* [Preprint]. Available at: https://doi.org/10.1680/wama.2008.161.1.13.

Iacobucci, G. *et al.* (2020) 'Combining Satellite Multispectral Imagery and Topographic Data for the Detection and Mapping of Fluvial Avulsion Processes in Lowland Areas', *Remote Sensing*, 12(14), p. 2243. Available at: https://doi.org/10.3390/rs12142243.

Izumida, A., Uchiyama, S. and Sugai, T. (2017) 'Application of UAV-SfM photogrammetry and aerial lidar to a disastrous flood: Repeated topographic measurement of a newly formed crevasse splay of the Kinu River, central Japan', *Natural Hazards and Earth System Sciences* [Preprint]. Available at: https://doi.org/10.5194/nhess-17-1505-2017.

Jackson, N.L. and Nordstrom, K.F. (2011) 'Aeolian sediment transport and landforms in managed coastal systems: A review', *Aeolian Research*, 3(2), pp. 181–196. Available at: https://doi.org/10.1016/J.AEOLIA.2011.03.011.

Jamal, M.H., Simmonds, D.J. and Magar, V. (2014) 'Modelling gravel beach dynamics with XBeach', *Coastal Engineering*, 89, pp. 20–29. Available at: https://doi.org/10.1016/j.coastaleng.2014.03.006.

Jamison-Todd, S. *et al.* (2020) 'Hurricane Deposits on Carbonate Platforms: A Case Study of Hurricane Irma Deposits on Little Ambergris Cay, Turks and Caicos Islands', *Journal of Geophysical Research: Earth Surface*, 125(8). Available at: https://doi.org/10.1029/2020JF005597.

Johansen, C. and Tien, I. (2018) 'Probabilistic multi-scale modeling of interdependencies between critical infrastructure systems for resilience', *Sustainable and Resilient Infrastructure*, 3(1), pp. 1–15. Available at: https://doi.org/10.1080/23789689.2017.1345253.

Johnson, J.P.L. *et al.* (2009) 'Transport slopes, sediment cover, and bedrock channel incision in

the Henry Mountains, Utah', *Journal of Geophysical Research: Earth Surface*, 114(F2). Available at: https://doi.org/10.1029/2007JF000862.

Jongman, B., Ward, P.J. and Aerts, J.C.J.H. (2012) 'Global exposure to river and coastal flooding: Long term trends and changes', *Global Environmental Change* [Preprint]. Available at: https://doi.org/10.1016/j.gloenvcha.2012.07.004.

Julien, P.Y. and Simons, D.B. (1985) Sediment transport capacity of overland flow. *Transactions of the American Society of Agricultural Engineers*, 28 (3), 755–762.

Junk, W.J., Bayley, P.B. and Sparks, R.E. (1989). The flood pulse concept in river-floodplain systems. *Canadian special publication of fisheries and aquatic sciences*, *106*(1), pp.110-127.

Kain, C.L. *et al.* (2014) 'Assessing topographic controls on flow direction in washover deposits using measurements of Magnetic Fabric', *Marine Geology*, 350, pp. 16–26. Available at: https://doi.org/10.1016/j.margeo.2014.01.010.

Kennedy, A. *et al.* (2020) 'Hurricane Michael in the Area of Mexico Beach, Florida', *Journal of Waterway, Port, Coastal, and Ocean Engineering*, 146(5). Available at: https://doi.org/10.1061/(ASCE)WW.1943-5460.0000590.

Kennish, M.J. (2001) 'Coastal Salt Marsh Systems in the U.S.: A Review of Anthropogenic Impacts', *Journal of Coastal Research*, 17(3), pp. 731–748. Available at: http://www.jstor.org/stable/4300224.

Kirchner, J.W. (1993) 'Statistical inevitability of Horton's laws and the apparent randomness of stream channel networks', *Geology*, 21(7), pp. 591–594. Available at: https://doi.org/10.1130/0091-7613(1993)021<0591:SIOHSL>2.3.CO;2.

Kirkpatrick, J.I.M. and Olbert, A.I. (2020) 'Modelling the effects of climate change on urban coastal-fluvial flooding', *Journal of Water and Climate Change*, 11(S1), pp. 270–288. Available at: https://doi.org/10.2166/wcc.2020.166.

Kirwan, M.L. *et al.* (2016) 'Sea level driven marsh expansion in a coupled model of marsh erosion and migration', *Geophysical Research Letters*, 43(9), pp. 4366–4373. Available at: https://doi.org/10.1002/2016GL068507.

Klemas, V. V. (2009) 'The Role of Remote Sensing in Predicting and Determining Coastal Storm Impacts', *Journal of Coastal Research*, 25(6 (256)), pp. 1264–1275. Available at: https://doi.org/10.2112/08-1146.1.

Kobayashi, Y. (1995) Disasters and the problems of wastes – institutions in Japan and issues raised by the Great Hanshin-Awaji earthquake. In: *Earthquake Waste Symposium*, 12–13 June 1995, 12–13 June 1995, Osaka.

Kobayashi, N., Gralher, C. and Do, K. (2013) 'Effects of Woody Plants on Dune Erosion and Overwash', *Journal of Waterway, Port, Coastal, and Ocean Engineering*, 139(6), pp. 466–472. Available at: https://doi.org/10.1061/(ASCE)WW.1943-5460.0000200.

Kochel, R.C. and Wampfler, L.A. (1989) 'Relative Role of Overwash and Aeolian Processes on Washover Fans, Assateague Island, Virginia-Maryland', *Journal of Coastal Research*, 5(3), pp. 453–475. Available at: http://www.jstor.org/stable/4297556.

Koi, T. *et al.* (2008) 'Prolonged impact of earthquake-induced landslides on sediment yield in a mountain watershed: The Tanzawa region, Japan', *Geomorphology*, 101(4), pp. 692–702. Available at: https://doi.org/10.1016/J.GEOMORPH.2008.03.007.

Koks, E.E. and Thissen, M. (2016) 'A Multiregional Impact Assessment Model for disaster analysis', *Economic Systems Research*, 28(4), pp. 429–449. Available at: https://doi.org/10.1080/09535314.2016.1232701/SUPPL_FILE/CESR_A_1232701_SM3178.DOCX.

Kooistra, L. *et al.* (2003) 'The potential of field spectroscopy for the assessment of sediment properties in river floodplains', *Analytica Chimica Acta*, 484(2), pp. 189–200. Available at: https://doi.org/10.1016/S0003-2670(03)00331-3.

Korup, O. (2012) 'Earth's portfolio of extreme sediment transport events', *Earth-Science Reviews*, 112(3–4), pp. 115–125. Available at: https://doi.org/10.1016/J.EARSCIREV.2012.02.006.

Kraal, E.R. *et al.* (2008) 'Catalogue of large alluvial fans in martian impact craters', *Icarus*, 194(1), pp. 101–110. Available at: https://doi.org/10.1016/j.icarus.2007.09.028.

Kraft, J.C., Biggs, R.B., and Halsey, S.D. (1973) Morphology and vertical sedimentary sequence models in Holocene transgressive barrier systems, coastal geomorphology. In: Coates, D.R. (Ed.), *Publications in Geomorphology*. State University of New York, Binghamton, New York, pp. 321–354.

Kraus, N. C., and Wamsley, T. V. (2003). "Coastal barrier breaching, Part 1: Overview of breaching processes," Coastal and Hydraulics Engineering Technical Note ERDC/CHL CHETN-IV-56, U.S. Army Engineer Research and Development Center, Vicksburg, MS

Kundzewicz, Z.W. *et al.* (2019) 'Flood risk in a range of spatial perspectives – from global to local scales', *Natural Hazards and Earth System Sciences*, 19(7), pp. 1319–1328. Available at: https://doi.org/10.5194/nhess-19-1319-2019.

Lammers, R.W. and Bledsoe, B.P. (2018) 'Parsimonious sediment transport equations based on Bagnold's stream power approach', *Earth Surface Processes and Landforms*, 43(1), pp. 242–258. Available at: https://doi.org/10.1002/esp.4237.

Lane, S.N. and Thorne, C.R. (2007) River processes. In: Thorne, C.R., Evans, E.P.and Penning-Rowsell, E. (eds) *Future Flooding and Coastal Erosion Risks*. Thomas Telford, London, pp. 82–99.

Langley, J.A. *et al.* (2009) 'Elevated CO_2 stimulates marsh elevation gain, counterbalancing sea-level rise', *Proceedings of the National Academy of Sciences*, 106(15), pp. 6182–6186. Available at: https://doi.org/10.1073/pnas.0807695106.

Larson, M., Wise, R.A., and Kraus, N.C. (2004) "Coastal Overwash. Part 2: Upgrade to SBEACH," Regional Sediment Management Demonstration Technical Note, ERDC/RSM-TN-15, U.S. Army Engineer Research and Development Center, Vicksburg, MS

Lazarus, E.D. (2016) 'Scaling laws for coastal overwash morphology', *Geophysical Research Letters*, 43(23), pp. 12,113-12,119. Available at: https://doi.org/10.1002/2016GL071213.

Lazarus, E.D. and Armstrong, S. (2015) 'Self-organized pattern formation in coastal barrier washover deposits', *Geology* [Preprint]. Available at: https://doi.org/10.1130/G36329.1.

Lazarus, E.D., Davenport, K.L. and Matias, A. (2020) 'Dynamic allometry in coastal overwash morphology', *Earth Surface Dynamics*, 8(1), pp. 37–50. Available at: https://doi.org/10.5194/esurf-8-37-2020.

Lazarus, E.D. and Goldstein, E.B. (2019) 'Is There a Bulldozer in your Model?', *Journal of Geophysical Research: Earth Surface*, 124(3), pp. 696–699. Available at: https://doi.org/10.1029/2018JF004957.

Lazarus, E.D., Williams, H.E. and Goldstein, E.B. (2022) 'Volume Estimation From Planform Characteristics of Washover Morphology', *Geophysical Research Letters*, 49(22). Available at: https://doi.org/10.1029/2022GL100098.

Leatherman, S. P. (1976) Quantification of overwash processes. Ph.D. Thesis, University of Virginia, U.S.A

Leatherman, S. P. (1977) Overwash hydraulics and sediment transport. *Proceedings Coastal Sediments 1977* (Charleston, South Carolina, ASCE), pp. 135–148.

Leatherman, S. P. (1988) Barrier Island Handbook Baltimore, Maryland Coastal Publications Series, Laboratory for Coastal Research, University of Maryland, 92p.

Leatherman, S.P., Williams, A.T. and Fisher, J.S. (1977) Overwash sedimentation associated with a large-scale northeaster. *Marine Geology*, *24*(2), pp.109-121.

Leatherman, S.P. and Zaremba, R.E. (1986) 'Dynamics of a northern barrier beach: Nauset Spit, Cape Cod, Massachusetts', *GSA Bulletin*, 97(1), pp. 116–124. Available at: https://doi.org/10.1130/0016-7606(1986)97<116:DOANBB>2.0.CO;2.

Leonardi, N. *et al.* (2018) 'Dynamic interactions between coastal storms and salt marshes: A review', *Geomorphology*, 301, pp. 92–107. Available at: https://doi.org/10.1016/j.geomorph.2017.11.001.

Lhomme, J. *et al.* (2008) 'Recent development and application of a rapid flood spreading method', in *Flood Risk Management: Research and Practice*. Available at: https://doi.org/10.1201/9780203883020.ch2.

Li, J. *et al.* (2023) 'Crevasse splay morphodynamics near a non-vegetated, ephemeral river terminus: Insights from process-based modelling', *Journal of Hydrology*, 617, p. 129088. Available at: https://doi.org/10.1016/j.jhydrol.2023.129088.

Li, Y. *et al.* (2020) 'An approximation method for evaluating flash flooding mitigation of sponge city strategies – A case study of Central Geelong', *Journal of Cleaner Production*, 257, p. 120525. Available at: https://doi.org/10.1016/j.jclepro.2020.120525.

Li, Z. and Zhang, J. (2001) 'Calculation of field manning's roughness coefficient', *Agricultural Water Management*, 49(2), pp. 153–161. Available at: https://doi.org/10.1016/S0378-3774(00)00139-6.

Lim, J.R. (2022) 'Why People Adopt Climate Change Adaptation and Disaster Risk Reduction Behaviors: Integrated Model of Risk Communication and Results from Hurricanes, Floods, and Wildfires', *Bulletin of the American Meteorological Society* [Preprint]. Available at: https://doi.org/10.1175/BAMS-D-21-0087.1.

Lin, G.-W. *et al.* (2008) 'Effects of earthquake and cyclone sequencing on landsliding and fluvial sediment transfer in a mountain catchment', *Earth Surf. Process. Landforms*, 33, pp. 1354–1373. Available at: https://doi.org/10.1002/esp.

Little, C.M. *et al.* (2015) 'Joint projections of US East Coast sea level and storm surge', *Nature Climate Change 2015 5:12*, 5(12), pp. 1114–1120. Available at: https://doi.org/10.1038/nclimate2801.

Liu, C. and Nepf, H. (2016) 'Sediment deposition within and around a finite patch of model vegetation over a range of channel velocity', *Water Resources Research*, 52(1), pp. 600–612. Available at: https://doi.org/10.1002/2015WR018249.

Liu, K. and Fearn, M.L. (2000) 'Reconstruction of Prehistoric Landfall Frequencies of Catastrophic Hurricanes in Northwestern Florida from Lake Sediment Records', *Quaternary Research*, 54(2), pp. 238–245. Available at: https://doi.org/10.1006/qres.2000.2166.

Lorenzo-Trueba, J. and Ashton, A.D. (2014) 'Rollover, drowning, and discontinuous retreat: Distinct modes of barrier response to sea-level rise arising from a simple morphodynamic model', *Journal of Geophysical Research: Earth Surface*, 119(4), pp. 779–801. Available at: https://doi.org/10.1002/2013JF002941.

Lowry, J. B. C., Coulthard, T. J., and Hancock, G. R. (2013) 'Assessing the long-term geomorphic stability of a rehabilitated landform using the CAESAR-Lisflood landscape evolution model', in M Tibbett, AB Fourie & C Digby (eds), *Mine Closure 2013: Proceedings of the Eighth International Seminar on Mine Closure*, Australian Centre for Geomechanics, Cornwall, pp. 611-624

Lowry, J.B.C. *et al.* (2019) 'Understanding post-mining landforms: Utilising pre-mine geomorphology to improve rehabilitation outcomes', *Geomorphology*, 328, pp. 93–107. Available at: https://doi.org/10.1016/j.geomorph.2018.11.027.

Mackin, J. H. (1963) Rational and empirical methods of investigation in geology, in: The fabric of geology, edited by: Albritton, C. C., Freeman, Cooper, Stanford, California, USA, 135–163.

Magliocca, N.R., McNamara, D.E. and Murray, A.B. (2011) 'Long-Term, Large-Scale Morphodynamic Effects of Artificial Dune Construction along a Barrier Island Coastline', *Journal of Coastal Research*, 276, pp. 918–930. Available at: https://doi.org/10.2112/JCOASTRES-D-10-00088.1.

Manfreda, S., Di Leo, M. and Sole, A. (2011) 'Detection of Flood-Prone Areas Using Digital Elevation Models', *Journal of Hydrologic Engineering*, 16(10), pp. 781–790. Available at: https://doi.org/10.1061/(ASCE)HE.1943-5584.0000367.

Manh, N. V. *et al.* (2014) 'Large-scale suspended sediment transport and sediment deposition

in the Mekong Delta', *Hydrology and Earth System Sciences*, 18(8), pp. 3033–3053. Available at: https://doi.org/10.5194/HESS-18-3033-2014.

Martin, J.F. *et al.* (2000) 'PROFILE: Evaluation of Coastal Management Plans with a Spatial Model: Mississippi Delta, Louisiana, USA', *Environmental Management*, 26(2), pp. 117–129. Available at: https://doi.org/10.1007/s002670010075.

Martin, J.F. *et al.* (2002) 'Landscape Modeling of the Mississippi Delta: Using a series of landscape models, we examined the survival and creation of Mississippi Delta marshes and the impact of altered riverine inputs, accelerated sea-level rise, and management proposals on these marshes', *BioScience*, 52(4), pp. 357–365. Available at: https://doi.org/10.1641/0006-3568(2002)052[0357:LMOTMD]2.0.CO;2.

Martínez, P. *et al.* (2021) 'Wind Speed Analysis of Hurricane Sandy', *Atmosphere*, 12(11), p. 1480. Available at: https://doi.org/10.3390/atmos12111480.

Mason, C.H. and Perreault, W.D. (1991) 'Collinearity, Power, and Interpretation of Multiple Regression Analysis', *Journal of Marketing Research*, 28(3), p. 268. Available at: https://doi.org/10.2307/3172863.

Mason, D.C. *et al.* (2003) 'Floodplain friction parameterization in two-dimensional river flood models using vegetation heights derived from airborne scanning laser altimetry', *Hydrological Processes*, 17(9), pp. 1711–1732. Available at: https://doi.org/10.1002/HYP.1270.

Masselink, G., Beetham, E. and Kench, P. (2020) 'Coral reef islands can accrete vertically in response to sea level rise', *Science Advances*, 6(24). Available at: https://doi.org/10.1126/sciadv.aay3656.

Matias, A. *et al.* (2008) 'Classification of washover dynamics in barrier islands', *Geomorphology*, 97(3–4), pp. 655–674. Available at: https://doi.org/10.1016/j.geomorph.2007.09.010.

Matias, A. *et al.* (2016) 'Measurements of morphodynamic and hydrodynamic overwash processes in a large-scale wave flume', *Coastal Engineering*, 113, pp. 33–46. Available at: https://doi.org/10.1016/j.coastaleng.2015.08.005.

Matias, A. *et al.* (2019) 'Field measurements and hydrodynamic modelling to evaluate the importance of factors controlling overwash', *Coastal Engineering*, 152, p. 103523. Available at: https://doi.org/10.1016/j.coastaleng.2019.103523.

Matias, A., Blenkinsopp, C.E. and Masselink, G. (2014) 'Detailed investigation of overwash on a gravel barrier', *Marine Geology*, 350, pp. 27–38. Available at:

https://doi.org/10.1016/j.margeo.2014.01.009.

Matias, A. and Masselink, G. (2017) 'Overwash Processes: Lessons from Fieldwork and Laboratory Experiments', *Coastal Storms: Processes and Impacts*, pp. 175–194. Available at: https://doi.org/10.1002/9781118937099.CH9.

Mayer-Schönberger, V. and Cukier, K. (2013) 'Big data. [electronic resource] : a revolution that will transform how we live, work, and think', *RESEARCH-TECHNOLOGY MANAGEMENT* [Preprint].

McCall, R.T. *et al.* (2010) 'Two-dimensional time dependent hurricane overwash and erosion modeling at Santa Rosa Island', *Coastal Engineering*, 57(7), pp. 668–683. Available at: https://doi.org/10.1016/j.coastaleng.2010.02.006.

McCave, I.N. (2008) 'Chapter 8 Size Sorting During Transport and Deposition of Fine Sediments: Sortable Silt and Flow Speed', in M. Rebesco and A. Camerlenghi (eds) *Developments in Sedimentology*. Elsevier, pp. 121–142. Available at: https://doi.org/https://doi.org/10.1016/S0070-4571(08)10008-5.

McEwen, L., Jones, O. and Robertson, I. (2014) '"A glorious time?" Some reflections on flooding in the Somerset Levels', *The Geographical Journal*, 180(4), pp. 326–337. Available at: http://www.jstor.org/stable/43870926.

McGranahan, G., Balk, D. and Anderson, B. (2007) 'The rising tide: assessing the risks of climate change and human settlements in low elevation coastal zones', *Environment and Urbanization*, 19(1), pp. 17–37. Available at: https://doi.org/10.1177/0956247807076960.

McKee, K.L. and Cherry, J.A. (2009) 'Hurricane Katrina sediment slowed elevation loss in subsiding brackish marshes of the Mississippi River delta', *Wetlands*, 29(1), pp. 2–15. Available at: https://doi.org/10.1672/08-32.1.

McNamara, D.E. and Lazarus, E.D. (2018) 'Barrier Islands as Coupled Human–Landscape Systems', in L.J. Moore and A.B. Murray (eds) *Barrier Dynamics and Response to Changing Climate*. Cham: Springer International Publishing, pp. 363–383. Available at: https://doi.org/10.1007/978-3-319-68086-6_12.

McNamara D.E. and Werner B.T., (2008) Coupled barrier island–resort model: 2. Tests and predictions along Ocean City and Assateague Island National Seashore, Maryland: Journal of Geophysical Research , v. 113, F01017, doi:10.1029/2007JF000841.

Mendelssohn, I.A. and Kuhn, N.L. (2003) 'Sediment subsidy: effects on soil–plant responses

in a rapidly submerging coastal salt marsh', *Ecological Engineering*, 21(2–3), pp. 115–128. Available at: https://doi.org/10.1016/j.ecoleng.2003.09.006.

Merkens, J.L. *et al.* (2016) 'Gridded population projections for the coastal zone under the Shared Socioeconomic Pathways', *Global and Planetary Change*, 145, pp. 57–66. Available at: https://doi.org/10.1016/J.GLOPLACHA.2016.08.009.

Mertes, L.A.K. (1997) 'Documentation and significance of the perirheic zone on inundated floodplains', *Water Resources Research*, 33(7), pp. 1749–1762. Available at: https://doi.org/10.1029/97WR00658.

Middelkoop, H. and Van der perk, M. (1998) 'Modelling spatial patterns of overbank sedimentation on embanked floodplains', *Geografiska Annaler: Series A, Physical Geography*, 80(2), pp. 95–109. Available at: https://doi.org/10.1111/j.0435-3676.1998.00029.x.

Mignot, E., Paquier, A. and Haider, S. (2006) 'Modeling floods in a dense urban area using 2D shallow water equations', *Journal of Hydrology* [Preprint]. Available at: https://doi.org/10.1016/j.jhydrol.2005.11.026.

Millard, C., Hajek, E. and Edmonds, D.A. (2017) 'Evaluating controls on crevasse-splay size: Implications for floodplain-basin filling', *Journal of Sedimentary Research*, 87(7), pp. 722–739. Available at: https://doi.org/10.2110/JSR.2017.40.

Mitsch, W. J., and Gosselink, J. G. (2015) Wetlands. 5th ed. Hoboken, NJ: John Wiley & Sons, Inc

Monk, W.A. *et al.* (2019) 'Urbanisation of floodplain ecosystems: Weight-of-evidence and network meta-analysis elucidate multiple stressor pathways', *Science of The Total Environment*, 684, pp. 741–752. Available at: https://doi.org/10.1016/j.scitotenv.2019.02.253.

Montgomery, D.R. and Dietrich, W.E. (1988) 'Where do channels begin?', *Nature*, 336(6196), pp. 232–234. Available at: https://doi.org/10.1038/336232a0.

Montreuil, A.L. *et al.* (2020) 'Post-storm recovery assessment of urbanized versus natural sandy macro-tidal beaches and their geomorphic variability', *Geomorphology*, 356, p. 107096. Available at: https://doi.org/10.1016/J.GEOMORPH.2020.107096.

Moore, J.M. and Howard, A.D. (2005) 'Large alluvial fans on Mars', *Journal of Geophysical Research*, 110(E4), p. E04005. Available at: https://doi.org/10.1029/2004JE002352.

Moorthy, I. *et al.* (2008) 'Retrieving crown leaf area index from an individual tree using

ground-based lidar data', *Canadian Journal of Remote Sensing*, 34(3), pp. 320–332. Available at: https://doi.org/10.5589/m08-027.

Morales de Luna, T., Castro Díaz, M.J. and Parés Madroñal, C. (2011) 'A Duality Method for Sediment Transport Based on a Modified Meyer-Peter & Müller Model', *Journal of Scientific Computing*, 48(1–3), pp. 258–273. Available at: https://doi.org/10.1007/s10915-010-9447-1.

Morton, R.A. *et al.* (2000) 'Frequent Non-Storm Washover of Barrier Islands, Pacific Coast of Colombia', *Journal of Coastal Research*, 16(1), pp. 82–87. Available at: http://www.jstor.org/stable/4300013.

Morton, R.A., Paine, J.G. and Gibeaut, J.C. (1994) 'Stages and Durations of Post-Storm Beach Recovery, Southeastern Texas Coast, U.S.A.', *Journal of Coastal Research*, 10(4), pp. 884–908. Available at: http://www.jstor.org/stable/4298283.

Morton, R.A. and Paine, J.G. (1985) Beach and vegetation-line changes at Galveston Island, Texas, erosion, deposition, and recou- ery from Hurricane Alicia. The University of Texas at Austin, Bureau of Economic Geology, Geological Circular 85-5, 39p.

Morton, R.A. and Sallenger, A.H. (2003) 'Morphological Impacts of Extreme Storms on Sandy Beaches and Barriers', *Journal of Coastal Research*, 19(3), pp. 560–573. Available at: http://www.jstor.org/stable/4299198.

Muhadi, N.A. *et al.* (2020) 'The Use of LiDAR-Derived DEM in Flood Applications: A Review', *Remote Sensing*, 12(14), p. 2308. Available at: https://doi.org/10.3390/rs12142308.

Muis, S. *et al.* (2019) 'Spatiotemporal patterns of extreme sea levels along the western North-Atlantic coasts', *Scientific Reports*, 9(1), p. 3391. Available at: https://doi.org/10.1038/s41598-019-40157-w.

Murray, A. B. (2003) Contrasting the goals, strategies, and predictions associated with simplified numerical models and detailed simulations. In: Wilcock, P. R. and Iverson, R. M. (eds) *Prediction in geomorphology*. Washington, DC: American Geophysical Union, pp.151–165

Murray, A.B. and Paola, C. (1994) 'A cellular model of braided rivers', *Nature*, 371(6492), pp. 54–57. Available at: https://doi.org/10.1038/371054a0.

Nardin, W. and Edmonds, D.A. (2014) 'Optimum vegetation height and density for inorganic sedimentation in deltaic marshes', *Nature Geoscience*, 7(10), pp. 722–726. Available at: https://doi.org/10.1038/ngeo2233.

National Geodetic Survey. (2020). Emergency response imagery. NOAA. Retrieved from: https://storms.ngs.noaa.gov/

Nelson, S.A. and Leclair, S.F. (2006) 'Katrina's unique splay deposits in a New Orleans neighborhood', *GSA Today*, 16(9), pp. 4–10. Available at: https://doi.org/10.1130/GSAT01609A.1.

Nepf, H.M. and Koch, E.W.K. (1999) 'Vertical secondary flows in submersed plant-like arrays', *Limnology and Oceanography*, 44(4), pp. 1072–1080. Available at: https://doi.org/10.4319/lo.1999.44.4.1072.

Nersesian, G.K., Kraus, N.C., and Carson, F.C. (1992) Functioning of Groins at Westhampton Beach, Long Island, NY. In: Proceedings of the 23rd International Coastal Engineering Conference (Venice, Italy), pp. 3357-3370.

Nguyen, X.T., Donnelly, C., and Larson, M. (2006) A new empirical formula for coastal overwash volume. *Proceedings Vietnam-Japan Estuary Workshop*, Water Resources University, Vietnam, 60-65

Nicholas, A.P. *et al.* (2012) 'Modelling hydrodynamics in the Rio Paraná, Argentina: An evaluation and inter-comparison of reduced-complexity and physics based models applied to a large sand-bed river', *Geomorphology*, 169–170, pp. 192–211. Available at: https://doi.org/10.1016/j.geomorph.2012.05.014.

Nicholas, A.P. (2013) 'Modelling the continuum of river channel patterns', *Earth Surface Processes and Landforms*, 38(10), pp. 1187–1196. Available at: https://doi.org/10.1002/esp.3431.

Nicholas, A. P., and Walling, D. E. (1997) Modelling flood hydraulics and overbank deposition on river floodplains. *Earth Surface Processes and Landforms*, 22(1), 59–77. https://doi.org/10.1002/(SICI)1096-9837(199701)22:1<59::AID-ESP652>3.0.CO;2-R

Nickling, W.G. and Neuman, C.M.K. (2009) 'Aeolian Sediment Transport', *Geomorphology of Desert Environments*, pp. 517–555. Available at: https://doi.org/10.1007/978-1-4020-5719-9_17.

Nienhuis, J.H. and Lorenzo-Trueba, J. (2019) 'Can Barrier Islands Survive Sea-Level Rise? Quantifying the Relative Role of Tidal Inlets and Overwash Deposition', *Geophysical Research Letters*, 46(24), pp. 14613–14621. Available at: https://doi.org/10.1029/2019GL085524.

Nienhuis, J.H., Törnqvist, T.E. and Esposito, C.R. (2018) 'Crevasse Splays Versus Avulsions: A Recipe for Land Building With Levee Breaches', *Geophysical Research Letters*, 45(9), pp. 4058–

4067. Available at: https://doi.org/10.1029/2018GL077933.

Nirupama, N. and Simonovic, S.P. (2007) 'Increase of flood risk due to urbanisation: A Canadian example', *Natural Hazards* [Preprint]. Available at: https://doi.org/10.1007/s11069-006-0003-0.

Noarayanan, L., Murali, K. and Sundar, V. (2012) 'Manning's "n" co-efficient for flexible emergent vegetation in tandem configuration', *Journal of Hydro-environment Research*, 6(1), pp. 51–62. Available at: https://doi.org/10.1016/j.jher.2011.05.002.

Noe, G.B. and Hupp, C.R. (2005) 'Carbon, nitrogen, and phosphorus accumulation in floodplains of Atlantic coastal plan rivers USA', *Ecological Applications*, 15(4), pp. 1178–1190. Available at: https://doi.org/10.1890/04-1677.

Nordstrom, K.F. (1994) 'Beaches and dunes of human-altered coasts', *Progress in Physical Geography*, 18(4), pp. 497–516. Available at: https://doi.org/10.1177/030913339401800402.

Nordstrom, K.F. (2004) 'Beaches and dunes of developed coasts', *Cambridge University Press* [Preprint]. Available at: https://doi.org/10.1029/01EO00262.

Nordstrom, K.F. and Jackson, N.L. (1995) 'Temporal scales of landscape change following storms on a human-altered coast, New Jersey, USA', *Journal of Coastal Conservation*, 1(1), pp. 51–62. Available at: https://doi.org/10.1007/BF02835562.

Nordstrom, K.F. and McCluskey, J.M. (1984) 'Considerations for control of house construction in coastal dunes', *Coastal Zone Management Journal*, 12(4), pp. 385–402. Available at: https://doi.org/10.1080/08920758409361972.

Norton, J.P., (2008) Algebraic sensitivity analysis of environmental models. Environmental Modelling & Software, 23(8), pp.963-972.

Nott, J. (2006) 'Tropical Cyclones and the Evolution of the Sedimentary Coast of Northern Australia', *Journal of Coastal Research*, 221, pp. 49–62. Available at: https://doi.org/10.2112/05a-0005.1.

Notti, D. *et al.* (2018) 'Potential and Limitations of Open Satellite Data for Flood Mapping', *Remote Sensing*, 10(11), p. 1673. Available at: https://doi.org/10.3390/rs10111673.

O'Connor, J.. and Costa, J.. (2004) *The World's Largest Floods, Past and Present: Their Causes and Magnitudes*. 1st edn. U.S. Geological Survey.

Odiase, O., Wilkinson, S. and Neef, A. (2019) 'Urbanisation and disaster risk: the resilience of

the Nigerian community in Auckland to natural hazards', *https://doi.org/10.1080/17477891.2019.1661221*, 19(1), pp. 90–106. Available at: https://doi.org/10.1080/17477891.2019.1661221.

Olde Venterink, H. *et al.* (2006) 'Importance of sediment deposition and denitrification for nutrient retention in floodplain wetlands', *Applied Vegetation Science*, 9(2), pp. 163–174. Available at: https://doi.org/10.1111/j.1654-109x.2006.tb00665.x.

Orford, J.D., Forbes, D.L. and Jennings, S.C. (2002) 'Organisational controls, typologies and time scales of paraglacial gravel-dominated coastal systems', *Geomorphology*, 48(1–3), pp. 51–85. Available at: https://doi.org/10.1016/S0169-555X(02)00175-7.

Orford, J.; Jennings, S., and Pethick, J. (2003) Extreme storm effect on gravel dominated barriers. In: *Proceedings Coastal Sediments '03*. Corpus Christi, Texas: World Scientific Press and East Meets West Productions, 14p.

Overbeck, J.R. *et al.* (2015) 'Enhancing evaluation of post-storm morphologic response using aerial orthoimagery from Hurricane Sandy', in *The Proceedings of the Coastal Sediments 2015*. WORLD SCIENTIFIC. Available at: https://doi.org/10.1142/9789814689977_0250.

Ozdemir, H. *et al.* (2013) 'Evaluating scale and roughness effects in urban flood modelling using terrestrial LIDAR data', *Hydrology and Earth System Sciences*, 17(10), pp. 4015–4030. Available at: https://doi.org/10.5194/hess-17-4015-2013.

O'Brien, P. T and Wells, A. T. (1986) 'A Small, Alluvial Crevasse Splay', *SEPM Journal of Sedimentary Research*, Vol. 56. Available at: https://doi.org/10.1306/212F8A71-2B24-11D7-8648000102C1865D.

Papathoma-Köhle, M. *et al.* (2017) 'Matrices, curves and indicators: A review of approaches to assess physical vulnerability to debris flows', *Earth-Science Reviews*, 171, pp. 272–288. Available at: https://doi.org/10.1016/J.EARSCIREV.2017.06.007.

Park, H. *et al.* (2013) 'Tsunami inundation modeling in constructed environments: A physical and numerical comparison of free-surface elevation, velocity, and momentum flux', *Coastal Engineering*, 79, pp. 9–21. Available at: https://doi.org/10.1016/j.coastaleng.2013.04.002.

Park, S.C. and Chu, K.S. (1991) 'Dispersal Patterns of River-Derived Fine-Grained Sediments on the Inner Shelf of Korea Strait', in, pp. 231–240. Available at: https://doi.org/10.1016/S0422-9894(08)70098-9.

Park, Y.H. and Edge, B.L. (2010) 'An Empirical Model to Estimate Overwash', *Journal of*

Coastal Research, 26, pp. 1157–1167. Available at: https://doi.org/10.2112/JCOASTRES-D-09-00017.1.

Parker, G. (2008) Transport of Gravel and Sediment Mixtures. In: García, M. (ed). Sedimentation Engineering: Processes, Measurements, Modeling, and Practice. Manual and Reports in Engineering Practice No. 110, American Society of Civil Engineers: Reston, VA, 165-264.

Parker, G. and Klingeman, P.C. (1982) 'On why gravel bed streams are paved', *Water Resources Research*, 18(5), pp. 1409–1423. Available at: https://doi.org/10.1029/WR018i005p01409.

Peduzzi, P. *et al.* (2012) 'Global trends in tropical cyclone risk', *Nature Climate Change* [Preprint]. Available at: https://doi.org/10.1038/nclimate1410.

Pendergrass, A.G. *et al.* (2017) 'Precipitation variability increases in a warmer climate', *Scientific Reports*, 7(1), p. 17966. Available at: https://doi.org/10.1038/s41598-017-17966-y.

Periathamby, A., Hamid, F.S. and Sakai, S.I. (2012) 'Disaster waste management challenges', *Waste Management and Research*, 30(2), pp. 113–114. Available at: https://doi.org/10.1177/0734242X11434630.

Petak, W.J. (1985) 'Emergency Management: A Challenge for Public Administration', *Public Administration Review*, 45, p. 3. Available at: https://doi.org/10.2307/3134992.

Pfahl, S., O'Gorman, P.A. and Fischer, E.M. (2017) 'Understanding the regional pattern of projected future changes in extreme precipitation', *Nature Climate Change 2017 7:6*, 7(6), pp. 423–427. Available at: https://doi.org/10.1038/nclimate3287.

Pfeifer, N. and Mandlburger, G. (2017) LiDAR data filtering and DTM generation. In *Topographic Laser Ranging and Scanning* (pp. 307-334). CRC Press.

Pianosi, F., Beven, K., Freer, J., Hall, J.W., Rougier, J., Stephenson, D.B. and Wagener, T., (2016) Sensitivity analysis of environmental models: A systematic review with practical workflow. Environmental Modelling & Software, 79, pp.214-232.

Pizzuto, J.E. (1987) 'Sediment diffusion during overbank flows', *Sedimentology*, 34(2), pp. 301–317. Available at: https://doi.org/10.1111/j.1365-3091.1987.tb00779.x.

Plant, N.G. and Griggs, G.B. (1992) 'Interactions between Nearshore Processes and Beach Morphology Near a Seawall', *Journal of Coastal Research*, 8(1), pp. 183–200. Available at: http://www.jstor.org/stable/4297962.

Plomaritis, T.A., Ferreira, Ó. and Costas, S. (2018) 'Regional assessment of storm related overwash and breaching hazards on coastal barriers', *Coastal Engineering*, 134, pp. 124–133. Available at: https://doi.org/10.1016/j.coastaleng.2017.09.003.

Poeppl, R.E. *et al.* (2019) 'Modeling the impact of dam removal on channel evolution and sediment delivery in a multiple dam setting', *International Journal of Sediment Research*, 34(6), pp. 537–549. Available at: https://doi.org/10.1016/j.ijsrc.2019.06.001.

Polyakov, V.. and Nearing, M.. (2003) 'Sediment transport in rill flow under deposition and detachment conditions', *CATENA*, 51(1), pp. 33–43. Available at: https://doi.org/10.1016/S0341-8162(02)00090-5.

Prosser, I.P. and Rustomji, P. (2000) 'Sediment transport capacity relations for overland flow', *Progress in Physical Geography: Earth and Environment*, 24(2), pp. 179–193. Available at: https://doi.org/10.1177/030913330002400202.

Purvis, M.J., Bates, P.D. and Hayes, C.M. (2008) 'A probabilistic methodology to estimate future coastal flood risk due to sea level rise', *Coastal Engineering*, 55(12), pp. 1062–1073. Available at: https://doi.org/10.1016/j.coastaleng.2008.04.008.

Rahman, M.M., Howell, J.A. and MacDonald, D.I.M. (2022) 'Quantitative analysis of crevasse-splay systems from modern fluvial settings', *Journal of Sedimentary Research*, 92(9), pp. 751–774. Available at: https://doi.org/10.2110/jsr.2020.067.

Rajib, A. *et al.* (2020) 'Towards a large-scale locally relevant flood inundation modeling framework using SWAT and LISFLOOD-FP', *Journal of Hydrology*, 581, p. 124406. Available at: https://doi.org/10.1016/j.jhydrol.2019.124406.

Ralston, D.K. *et al.* (2013) 'Sediment transport due to extreme events: The Hudson River estuary after tropical storms Irene and Lee', *Geophysical Research Letters*, 40(20), pp. 5451–5455. Available at: https://doi.org/10.1002/2013GL057906.

Ramirez, J.A. *et al.* (2020) 'Modeling the geomorphic response to early river engineering works using CAESAR-Lisflood', *Anthropocene*, 32, p. 100266. Available at: https://doi.org/10.1016/j.ancene.2020.100266.

Recking, A., Liébault, F., Peteuil, C. and Jolimet, T., (2012) Testing bedload transport equations with consideration of time scales. Earth Surface Processes and Landforms, 37(7), pp.774-789.

Reeves, I.R.B. *et al.* (2021) 'Dune Dynamics Drive Discontinuous Barrier Retreat', *Geophysical*

Research Letters, 48(13). Available at: https://doi.org/10.1029/2021GL092958.

Reyes, E. *et al.* (2000) 'Landscape Modeling of Coastal Habitat Change in the Mississippi Delta', *Ecology*, 81(8), p. 2331. Available at: https://doi.org/10.2307/177118.

Roberts, H.H. (1997) Dynamic changes of the Holocene Mississippi River delta plain: the delta cycle: *Journal of Coastal Research*, v. 13, p. 605–627.

Rodriguez, A.B. *et al.* (2020) 'Long-term washover fan accretion on a transgressive barrier island challenges the assumption that paleotempestites represent individual tropical cyclones', *Scientific Reports*, 10(1), p. 19755. Available at: https://doi.org/10.1038/s41598-020-76521-4.

Roelvink, D. *et al.* (2009) 'Modelling storm impacts on beaches, dunes and barrier islands', *Coastal Engineering*, 56(11–12), pp. 1133–1152. Available at: https://doi.org/10.1016/j.coastaleng.2009.08.006.

Roelvink, J. A., and van Banning. G. K. F. M. (1995) Design and development of DELFT3D and application to coastal morphodynamics. *Oceanogr. Lit. Rev.* 11:925

Rogers, L.J. *et al.* (2015) 'Anthropogenic controls on overwash deposition: Evidence and consequences', *Journal of Geophysical Research F: Earth Surface* [Preprint]. Available at: https://doi.org/10.1002/2015JF003634.

Rudorff, C.M., Melack, J.M. and Bates, P.D. (2014) 'Flooding dynamics on the lower Amazon floodplain: 1. Hydraulic controls on water elevation, inundation extent, and river-floodplain discharge', *Water Resources Research*, 50(1), pp. 619–634. Available at: https://doi.org/10.1002/2013WR014091.

Ruggiero, P. *et al.* (2001) 'Wave Runup, Extreme Water Levels and the Erosion of Properties Backing Beaches', *Source: Journal of Coastal Research*, 17(2), pp. 407–419.

Sadeghi, F. *et al.* (2022) 'Assessing the Performance of LISFLOOD-FP and SWMM for a Small Watershed with Scarce Data Availability', *Water*, 14(5), p. 748. Available at: https://doi.org/10.3390/w14050748.

Sallenger, J. (2000) 'Storm impact scale for barrier islands', *Journal of Coastal Research*, 16(3), pp. 890–895. Available at: https://about.jstor.org/terms (Accessed: 3 June 2020).

Saltelli, A., Chan, K., and Scott, E. M (2000) Sensitivity Analysis, John Wiley, New York

Samela, C., Troy, T.J. and Manfreda, S. (2017) 'Geomorphic classifiers for flood-prone areas delineation for data-scarce environments', *Advances in Water Resources*, 102, pp. 13–28. Available

at: https://doi.org/10.1016/j.advwatres.2017.01.007.

Sampson, C.C. *et al.* (2012) 'Use of terrestrial laser scanning data to drive decimetric resolution urban inundation models', *Advances in Water Resources*, 41, pp. 1–17. Available at: https://doi.org/10.1016/j.advwatres.2012.02.010.

Saynor, M.J., Lowry, J.B.C. and Boyden, J.M. (2018) 'Assessment of rip lines using CAESAR-Lisflood on a Trial Landform at the Ranger Uranium Mine', *Land Degradation & Development*, p. ldr.3242. Available at: https://doi.org/10.1002/ldr.3242.

Schubert, J.E. *et al.* (2008) 'Unstructured mesh generation and landcover-based resistance for hydrodynamic modeling of urban flooding', *Advances in Water Resources*, 31(12), pp. 1603–1621. Available at: https://doi.org/10.1016/j.advwatres.2008.07.012.

Schuerch, M. *et al.* (2018) 'Changing Sediment Dynamics of a Mature Backbarrier Salt Marsh in Response to Sea-Level Rise and Storm Events', *Frontiers in Marine Science*, 5. Available at: https://doi.org/10.3389/fmars.2018.00155.

Schumann, G. *et al.* (2009) 'Progress in integration of remote sensing-derived flood extent and stage data and hydraulic models', *Reviews of Geophysics* [Preprint]. Available at: https://doi.org/10.1029/2008RG000274.

Schumm, S., & Lichty, R. (1963) Channel widening and flood-plain construction along Cimarron River in southwestern Kansas. *Geological Survey Professional Paper*, 352(D), 71–88.

Schuurman, F., Marra, W.A. and Kleinhans, M.G. (2013) 'Physics-based modeling of large braided sand-bed rivers: Bar pattern formation, dynamics, and sensitivity', *Journal of Geophysical Research: Earth Surface*, 118(4), pp. 2509–2527. Available at: https://doi.org/10.1002/2013JF002896.

Schwartz, R.K. (1982) 'Bedform and stratification characteristics of some modern small-scale washover sand bodies', *Sedimentology*, 29(6), pp. 835–849. Available at: https://doi.org/10.1111/j.1365-3091.1982.tb00087.x.

Seavey, J.R., Gilmer, B. and McGarigal, K.M. (2011) 'Effect of sea-level rise on piping plover (Charadrius melodus) breeding habitat', *Biological Conservation*, 144(1), pp. 393–401. Available at: https://doi.org/10.1016/j.biocon.2010.09.017.

Sedgwick, P.E., and Davis, R.A., Jr. (2003) Stratigraphy of washover deposits in Florida: Implications for recognition in the stratigraphic record: *Marine Geology*, v. 200, p. 31–48, doi:10.1016 /S0025-3227(03)00163-4.

Sellin, R.H.J., Bryant, T.B. and Loveless, J.H. (2003) 'An improved method for roughening floodplains on physical river models', *Journal of Hydraulic Research*, 41(1), pp. 3–14. Available at: https://doi.org/10.1080/00221680309499924.

Shen, Z. *et al.* (2015) 'Episodic overbank deposition as a dominant mechanism of floodplain and delta-plain aggradation', *Geology*, 43(10), pp. 875–878. Available at: https://doi.org/10.1130/G36847.1.

Sherwood, C.R. *et al.* (2014) 'Inundation of a barrier island (Chandeleur Islands, Louisiana, USA) during a hurricane: Observed water-level gradients and modeled seaward sand transport', *Journal of Geophysical Research: Earth Surface*, 119(7), pp. 1498–1515. Available at: https://doi.org/10.1002/2013JF003069.

Shi, Z.H. *et al.* (2012) 'Soil erosion processes and sediment sorting associated with transport mechanisms on steep slopes', *Journal of Hydrology*, 454–455, pp. 123–130. Available at: https://doi.org/10.1016/J.JHYDROL.2012.06.004.

Silveira, T.M. *et al.* (2016) 'Assessing the extreme overwash regime along an embayed urban beach', *Geomorphology*, 274, pp. 64–77. Available at: https://doi.org/10.1016/j.geomorph.2016.09.007.

Skinner, C.J., Coulthard, T.J., Schwanghart, W., Van De Wiel, M.J. and Hancock, G., (2018) Global sensitivity analysis of parameter uncertainty in landscape evolution models. Geoscientific Model Development, 11(12), pp.4873-4888.

Slingerland, R. and Smith, N.D. (1998) 'Necessary conditions for a meandering-river avulsion', *Geology*, 26(5), pp. 435–438. Available at: https://doi.org/10.1130/0091-7613(1998)026<0435:NCFAMR>2.3.CO;2.

Smith, A.B. and Matthews, J.L. (2015) 'Quantifying uncertainty and variable sensitivity within the US billion-dollar weather and climate disaster cost estimates', *Natural Hazards*, 77(3), pp. 1829–1851. Available at: https://doi.org/10.1007/s11069-015-1678-x.

Smith, K. (2013) *Environmental Hazards: Assessing Risk and Reducing Disaster*. 6th edn. London: Routledge. Available at: https://doi.org/10.4324/9780203805305.

Smith, N.D. *et al.* (1998) 'The 1870s avulsion of the Saskatchewan River', *Canadian Journal of Earth Sciences*, 35(4), pp. 453–466. Available at: https://doi.org/10.1139/e97-113.

Smith, N.D. and Perez-Arlucea, M. (1994) 'Fine-Grained Splay Deposition in the Avulsion Belt of the Lower Saskatchewan River, Canada', *SEPM Journal of Sedimentary Research*, Vol. 64B.

Available at: https://doi.org/10.1306/D4267F7D-2B26-11D7-8648000102C1865D.

Soria, J.L.A. *et al.* (2017) 'Typhoon Haiyan overwash sediments from Leyte Gulf coastlines show local spatial variations with hybrid storm and tsunami signatures', *Sedimentary Geology*, 358, pp. 121–138. Available at: https://doi.org/10.1016/j.sedgeo.2017.06.006.

Spasojevic, M. and Holly, F.M. (2008) 'Two- and Three-Dimensional Numerical Simulation of Mobile-Bed Hydrodynamics and Sedimentation', in *Sedimentation Engineering*. Reston, VA: American Society of Civil Engineers, pp. 683–761. Available at: https://doi.org/10.1061/9780784408148.ch15.

De Stefano, L. *et al.* (2017) 'Assessment of transboundary river basins for potential hydro-political tensions', *Global Environmental Change*, 45, pp. 35–46. Available at: https://doi.org/10.1016/J.GLOENVCHA.2017.04.008.

Steiger, J. and Gurnell, A.M. (2003) 'Spatial hydrogeomorphological influences on sediment and nutrient deposition in riparian zones: observations from the Garonne River, France', *Geomorphology*, 49(1–2), pp. 1–23. Available at: https://doi.org/10.1016/S0169-555X(02)00144-7.

Stewart, S.R. (2017) National hurricane center tropical cyclone report: Hurricane Matthew. *National Hurricane Center*.

Storlazzi, C.D. *et al.* (2018) 'Most atolls will be uninhabitable by the mid-21st century because of sea-level rise exacerbating wave-driven flooding', *Science Advances*, 4(4). Available at: https://doi.org/10.1126/sciadv.aap9741.

Stouthamer, E. (2001) 'Sedimentary products of avulsions in the Holocene Rhine–Meuse Delta, The Netherlands', *Sedimentary Geology*, 145(1–2), pp. 73–92. Available at: https://doi.org/10.1016/S0037-0738(01)00117-8.

Straatsma, M.W. and Baptist, M.J. (2008) 'Floodplain roughness parameterization using airborne laser scanning and spectral remote sensing', *Remote Sensing of Environment*, 112(3), pp. 1062–1080. Available at: https://doi.org/10.1016/J.RSE.2007.07.012.

Sturm, M. *et al.* (2018) 'Understanding impact dynamics on buildings caused by fluviatile sediment transport', *Geomorphology*, 321, pp. 45–59. Available at: https://doi.org/10.1016/j.geomorph.2018.08.016.

Stutz, M.L. and Pilkey, O.H. (2001) 'A review of global barrier island distribution', *Journal of Coastal Research*, (Special Issue 34), pp. 15–22. Available at: https://doi.org/10.2307/25736270.

Stutz, M.L. and Pilkey, O.H. (2011) 'Open-Ocean Barrier Islands: Global Influence of Climatic, Oceanographic, and Depositional Settings', *Journal of Coastal Research*, 272(2), pp. 207–222. Available at: https://doi.org/10.2112/09-1190.1.

Suter, J.R. *et al.* (1982) 'A Process-Response Model for Hurricane Washovers', *Coastal Engineering 1982*, pp. 1459–1478. Available at: https://doi.org/10.1061/9780872623736.089.

Swain, D.L. *et al.* (2020) 'Increased Flood Exposure Due to Climate Change and Population Growth in the United States', *Earth's Future*, 8(11), p. e2020EF001778. Available at: https://doi.org/10.1029/2020EF001778.

Swapna, P. *et al.* (2020) 'Sea-Level Rise', in *Assessment of Climate Change over the Indian Region*. Singapore: Springer Singapore, pp. 175–189. Available at: https://doi.org/10.1007/978-981-15-4327-2_9.

Syme, W. J. (2008) Flooding in Urban Areas - 2D Modelling Approaches for Buildings and Fences. 9th National Conference on Hydraulics in Water Engineering. Darwin: Engineers Australia.

Syvitski, J.P.M. *et al.* (2012) 'Floods, floodplains, delta plains — A satellite imaging approach', *Sedimentary Geology*, 267–268, pp. 1–14. Available at: https://doi.org/10.1016/j.sedgeo.2012.05.014.

Tahvildari, N. and Castrucci, L. (2021) 'Relative Sea Level Rise Impacts on Storm Surge Flooding of Transportation Infrastructure', *Natural Hazards Review*, 22(1). Available at: https://doi.org/10.1061/(ASCE)NH.1527-6996.0000412.

Takagi, H. *et al.* (2016) 'Storm surge and evacuation in urban areas during the peak of a storm', *Coastal Engineering*, 108, pp. 1–9. Available at: https://doi.org/10.1016/j.coastaleng.2015.11.002.

Tariq, M.A.U.R. and van de Giesen, N. (2012) 'Floods and flood management in Pakistan', *Physics and Chemistry of the Earth, Parts A/B/C*, 47–48, pp. 11–20. Available at: https://doi.org/10.1016/j.pce.2011.08.014.

Teeter, A.M. (2000) 'Clay-silt sediment modeling using multiple grain classes', in, pp. 157–171. Available at: https://doi.org/10.1016/S1568-2692(00)80119-9.

Temme, A.J.A.M. and Veldkamp, A. (2009) 'Multi-process Late Quaternary landscape evolution modelling reveals lags in climate response over small spatial scales', *Earth Surface Processes and Landforms*, 34(4), pp. 573–589. Available at: https://doi.org/10.1002/esp.1758.

Thomas, A. *et al.* (2019) 'Influence of storm timing and forward speed on tides and storm surge during Hurricane Matthew', *Ocean Modelling*, 137, pp. 1–19. Available at: https://doi.org/10.1016/j.ocemod.2019.03.004.

Thomas, R., Nicholas, A.P. and Quine, T.A. (2007) 'Cellular modelling as a tool for interpreting historic braided river evolution', *Geomorphology*, 90(3–4), pp. 302–317. Available at: https://doi.org/10.1016/j.geomorph.2006.10.025.

Timmons, E.A. *et al.* (2010) 'Transition of a regressive to a transgressive barrier island due to back-barrier erosion, increased storminess, and low sediment supply: Bogue Banks, North Carolina, USA', *Marine Geology*, 278(1–4), pp. 100–114. Available at: https://doi.org/10.1016/j.margeo.2010.09.006.

Tomsett, C. and Leyland, J. (2019) 'Remote sensing of river corridors: A review of current trends and future directions', *River Research and Applications*, 35(7), pp. 779–803. Available at: https://doi.org/10.1002/rra.3479.

Tomsett, C. and Leyland, J. (2022) Exploring the 4D scales of eco-geomorphic interactions along a river corridor using repeat UAV Laser Scanning (UAV-LS), multispectral imagery, and a functional traits framework, *Earth Surf. Dynam. Discuss.* [preprint], https://doi.org/10.5194/esurf-2021-102, in review.

Toonen, W.H.J. *et al.* (2016) 'Depositional development of the Muskeg Lake crevasse splay in the Cumberland Marshes (Canada)', *Earth Surface Processes and Landforms*, 41(1), pp. 117–129. Available at: https://doi.org/10.1002/esp.3791.

Tye, R.S. (2004) 'Geomorphology: An approach to determining subsurface reservoir dimensions', *AAPG Bulletin*, 88(8), pp. 1123–1147. Available at: https://doi.org/10.1306/02090403100.

United Nations Office for Disaster Risk Reduction (UNDRR) (2020), The Human Cost of Disasters: An Overview of the Last 20 Years 2000–2019. At: https://reliefweb.int/report/world/human-cost-disasters-overview-last-20-years-2000-2019.

USEPA (2008) Planning for natural disaster debris. In: Office of Solid Waste and Emergency Response and Office of Solid Waste (Eds.).

Uyanık, G.K. and Güler, N. (2013) 'A Study on Multiple Linear Regression Analysis', *Procedia - Social and Behavioral Sciences*, 106, pp. 234–240. Available at: https://doi.org/10.1016/j.sbspro.2013.12.027.

Valters, D. (2016) Modelling geomorphic systems: Landscape evolution. In *Geomorphological techniques*. British Society for Geomorphology.

VanDusen, B.M. *et al.* (2016) 'Monitoring overwash using water-level loggers resolves frequent inundation and run-up events', *Geomorphology*, 254, pp. 32–40. Available at: https://doi.org/10.1016/j.geomorph.2015.11.010.

Västilä, K. and Järvelä, J. (2014) 'Modeling the flow resistance of woody vegetation using physically based properties of the foliage and stem', *Water Resources Research*, 50(1), pp. 229–245. Available at: https://doi.org/10.1002/2013WR013819.

Vaz, N., Miguel Dias, J. and Chambel Leitão, P. (2009) 'Three-dimensional modelling of a tidal channel: The Espinheiro Channel (Portugal)', *Continental Shelf Research*, 29(1), pp. 29–41. Available at: https://doi.org/10.1016/j.csr.2007.12.005.

Vázquez-Tarrío, D. and Menéndez-Duarte, R. (2015) 'Assessment of bedload equations using data obtained with tracers in two coarse-bed mountain streams (Narcea River basin, NW Spain)', *Geomorphology*, 238, pp. 78–93. Available at: https://doi.org/10.1016/j.geomorph.2015.02.032.

Venter, O. *et al.* (2016) 'Sixteen years of change in the global terrestrial human footprint and implications for biodiversity conservation', *Nature Communications 2016 7:1*, 7(1), pp. 1–11. Available at: https://doi.org/10.1038/ncomms12558.

Verbeiren, B. *et al.* (2013) 'Assessing urbanisation effects on rainfall-runoff using a remote sensing supported modelling strategy', *International Journal of Applied Earth Observation and Geoinformation*, 21(1), pp. 92–102. Available at: https://doi.org/10.1016/J.JAG.2012.08.011.

Viero, D.P. *et al.* (2019) 'Floods, landscape modifications and population dynamics in anthropogenic coastal lowlands: The Polesine (northern Italy) case study', *Science of The Total Environment*, 651, pp. 1435–1450. Available at: https://doi.org/10.1016/J.SCITOTENV.2018.09.121.

Viles, H. and Spencer, T. (1995) *Coastal Problems: Geomorphology, Ecology and Society at the Coast*. 1st edn. London: Routledge. Available at: https://doi.org/10.4324/9781315832586.

Visser, H., Petersen, A.C. and Ligtvoet, W. (2014) 'On the relation between weather-related disaster impacts, vulnerability and climate change', *Climatic Change* [Preprint]. Available at: https://doi.org/10.1007/s10584-014-1179-z.

Walker, H.J. (1984) 'Man's impact on shorelines and nearshore environments: a

geomorphological perspective', *Geoforum*, 15(3), pp. 395–417. Available at: https://doi.org/10.1016/0016-7185(84)90047-2.

Walling, D.E. and He, Q. (1998) 'The spatial variability of overbank sedimentation on river floodplains', *Geomorphology*, 24(2–3), pp. 209–223. Available at: https://doi.org/10.1016/S0169-555X(98)00017-8.

Walsh, P., Jakeman, A. and Thompson, C. (2020) 'Modelling headwater channel response and suspended sediment yield to in-channel large wood using the Caesar-Lisflood landscape evolution model', *Geomorphology*, 363, p. 107209. Available at: https://doi.org/10.1016/j.geomorph.2020.107209.

Walters, D. *et al.* (2014) 'Interactions between barrier islands and backbarrier marshes affect island system response to sea level rise: Insights from a coupled model', *Journal of Geophysical Research: Earth Surface*, 119(9), pp. 2013–2031. Available at: https://doi.org/10.1002/2014JF003091.

Wang, P. and Horwitz, M.H. (2007) 'Erosional and depositional characteristics of regional overwash deposits caused by multiple hurricanes', *Sedimentology*, 54(3), pp. 545–564. Available at: https://doi.org/10.1111/j.1365-3091.2006.00848.x.

Wang, Y. *et al.* (2011) 'A GIS-Based Spatial Multi-Criteria Approach for Flood Risk Assessment in the Dongting Lake Region, Hunan, Central China', *Water Resources Management* [Preprint]. Available at: https://doi.org/10.1007/s11269-011-9866-2.

Wentworth, C.K. (1922) 'A Scale of Grade and Class Terms for Clastic Sediments', *The Journal of Geology*, 30(5), pp. 377–392. Available at: http://www.jstor.org/stable/30063207.

Werner, B.T. (1999) 'Complexity in Natural Landform Patterns', *Science*, 284(5411), pp. 102–104. Available at: https://doi.org/10.1126/science.284.5411.102.

Werner, M.G.F., Hunter, N.M. and Bates, P.D. (2005) 'Identifiability of distributed floodplain roughness values in flood extent estimation', *Journal of Hydrology*, 314(1–4), pp. 139–157. Available at: https://doi.org/10.1016/j.jhydrol.2005.03.012.

Wernette, P. *et al.* (2020) 'Investigating the Impact of Hurricane Harvey and Driving on Beach-Dune Morphology', *Geomorphology*, 358, p. 107119. Available at: https://doi.org/10.1016/J.GEOMORPH.2020.107119.

Van De Wiel, M.J. *et al.* (2007) 'Embedding reach-scale fluvial dynamics within the CAESAR cellular automaton landscape evolution model', *Geomorphology* [Preprint]. Available at:

https://doi.org/10.1016/j.geomorph.2006.10.024.

Wilcock, P.R. and Crowe, J.C. (2003) 'Surface-based transport model for mixed-size sediment', *Journal of Hydraulic Engineering* [Preprint]. Available at: https://doi.org/10.1061/(ASCE)0733-9429(2003)129:2(120).

Wilcock, P.R, Pitlick, J. and Cui, Y. (2009) Sediment transport primer: estimating bed-material transport in gravel-bed rivers. Gen. Tech. Rep. RMRS-GTR-226. Fort Collins, CO: U.S. Department of Agriculture, Forest Service, Rocky Mountain Research Station. 78 p

Williams, G.P. (1989) 'Sediment concentration versus water discharge during single hydrologic events in rivers', *Journal of Hydrology*, 111(1–4), pp. 89–106. Available at: https://doi.org/10.1016/0022-1694(89)90254-0.

Williams, H.F.L. (2015) 'Contrasting styles of Hurricane Irene washover sedimentation on three east coast barrier islands: Cape Lookout, North Carolina; Assateague Island, Virginia; and Fire Island, New York', *Geomorphology*, 231, pp. 182–192. Available at: https://doi.org/10.1016/J.GEOMORPH.2014.11.027.

Williams, H.F.L. and Rains, B.J. (2022) 'Effect of Barrier Height on Magnitude and Character of Hurricane Harvey Washover Fans, Matagorda Peninsula, Texas, U.S.A.', *Journal of Coastal Research*, 38(1). Available at: https://doi.org/10.2112/JCOASTRES-D-21-00043.1.

Williams, R.D., Brasington, J. and Hicks, D.M. (2016) 'Numerical Modelling of Braided River Morphodynamics: Review and Future Challenges', *Geography Compass*, 10(3), pp. 102–127. Available at: https://doi.org/10.1111/gec3.12260.

Wing, O.E.J. *et al.* (2018) 'Estimates of present and future flood risk in the conterminous United States', *Environmental Research Letters*, 13(3), p. 034023. Available at: https://doi.org/10.1088/1748-9326/AAAC65.

Wing, O.E.J. *et al.* (2019) 'A flood inundation forecast of Hurricane Harvey using a continental-scale 2D hydrodynamic model', *Journal of Hydrology X*, 4, p. 100039. Available at: https://doi.org/10.1016/j.hydroa.2019.100039.

Wolman, M. G., and Leopold, L. B. (1957) River flood plains: some observations on their formation. *US Geol. Survey Prof Pap.*, 282-C, 87-107.

Wong, J.S. *et al.* (2021) 'Assessing the hydrological and geomorphic behaviour of a landscape evolution model within a limits-of-acceptability uncertainty analysis framework', *Earth Surface Processes and Landforms*, 46(10), pp. 1981–2003. Available at: https://doi.org/10.1002/esp.5140.

Wong, M. and Parker, G. (2006) 'Reanalysis and Correction of Bed-Load Relation of Meyer-Peter and Müller Using Their Own Database', *Journal of Hydraulic Engineering*, 132(11), pp. 1159–1168. Available at: https://doi.org/10.1061/(ASCE)0733-9429(2006)132:11(1159).

Wright, D.B., Bosma, C.D. and Lopez-Cantu, T. (2019) 'U.S. Hydrologic Design Standards Insufficient Due to Large Increases in Frequency of Rainfall Extremes', *Geophysical Research Letters*, 46(14), pp. 8144–8153. Available at: https://doi.org/10.1029/2019GL083235.

Wu, Z. *et al.* (2020) 'Study on the Improved Method of Urban Subcatchments Division Based on Aspect and Slope- Taking SWMM Model as Example', *Hydrology*, 7(2), p. 26. Available at: https://doi.org/10.3390/hydrology7020026.

Xian, S., Lin, N. and Hatzikyriakou, A. (2015) 'Storm surge damage to residential areas: a quantitative analysis for Hurricane Sandy in comparison with FEMA flood map', *Natural Hazards*, 79(3), pp. 1867–1888. Available at: https://doi.org/10.1007/S11069-015-1937-X/TABLES/4.

Yuill, B.T. *et al.* (2016) 'Morphodynamics of the erosional phase of crevasse-splay evolution and implications for river sediment diversion function', *Geomorphology*, 259, pp. 12–29. Available at: https://doi.org/10.1016/j.geomorph.2016.02.005.

Zellou, B. and Rahali, H. (2017) 'Assessment of reduced-complexity landscape evolution model suitability to adequately simulate flood events in complex flow conditions', *Natural Hazards* [Preprint]. Available at: https://doi.org/10.1007/s11069-016-2671-8.

Zhang, B. *et al.* (2021) '3D numerical modelling of asynchronous propagation characteristics of flood and sediment peaks in three gorges reservoir', *Journal of Hydrology*, 593, p. 125896. Available at: https://doi.org/10.1016/j.jhydrol.2020.125896.

Zhang, K. and Leatherman, S. (2011) 'Barrier Island Population along the U.S. Atlantic and Gulf Coasts', *Journal of Coastal Research*, 27(2), p. 356. Available at: https://doi.org/10.2112/JCOASTRES-D-10-00126.1.

Zhang, Y.J. *et al.* (2016) 'Seamless cross-scale modeling with SCHISM', *Ocean Modelling*, 102, pp. 64–81. Available at: https://doi.org/10.1016/j.ocemod.2016.05.002.

Zhao, B. *et al.* (2022) 'Runoff and sediment response to deforestation in a large Southeast Asian monsoon watershed', *Journal of Hydrology*, 606, p. 127432. Available at: https://doi.org/10.1016/J.JHYDROL.2022.127432.

Zhu, T. and Kobayashi, N. (2021) 'Rock mound to reduce wave overwash and crest lowering

of a sand barrier', *Coastal Engineering Journal*, 63(4), pp. 504–516. Available at: https://doi.org/10.1080/21664250.2021.1957550.

Zope, P.E., Eldho, T.I. and Jothiprakash, V. (2016) 'Impacts of land use–land cover change and urbanization on flooding: A case study of Oshiwara River Basin in Mumbai, India', *CATENA*, 145, pp. 142–154. Available at: https://doi.org/10.1016/J.CATENA.2016.06.009.